Novel Immune Biomarkers for Pulmonary Tuberculosis Treatment Monitoring : a Multicentered study in Moderate- and High-Incidence Settings

Carole Chedid

Numéro National de Thèse : 2021LYSEN049

THÈSE DE DOCTORAT DE L'UNIVERSITÉ DE LYON

opérée par

l'École Normale Supérieure de Lyon

École doctorale N°341
Écologie, Évolution, Microbiologie, Modélisation

Discipline : Sciences de la vie et de la santé
Spécialité de doctorat : Immunologie

Soutenue publiquement le 18/10/2021 par :

Carole CHEDID

Novel Immune Biomarkers for Pulmonary Tuberculosis Treatment Monitoring: a Multicentered Study in Moderate- and High-Incidence Settings

De nouvelles perspectives sur le suivi immunologique du traitement de la tuberculose pulmonaire : une étude multicentrique internationale pour l'évaluation de biomarqueurs immunologiques.

Devant le jury composé de :

TATTEVIN, Pierre, PU-PH, CHU de Rennes	Rapporteur
VENET, Fabienne, PU-PH, Hospices Civils de Lyon	Rapporteure
BRODIN, Priscille, DR, Institut Pasteur de Lille	Examinatrice
DUMITRESCU, Oana, MCU-PH, Hospices Civils de Lyon	Examinatrice
HOFFMANN, Jonathan, Attaché de Recherche, Fondation Mérieux	Examinateur
ADER, Florence, PU-PH, Hospices Civils de Lyon	Directrice de thèse
BANU, Sayera, DR, icddr,b, Bangladesh	Co-directrice de thèse

Remerciements

En premier lieu, j'adresse mes sincères remerciements au Pr. Pierre Tattevin, au Pr. Fabienne Venet, au Dr. Priscille Brodin, et au Dr. Oana Dumitrescu pour avoir accepté de participer au jury de ma thèse. C'est un plaisir pour moi de vous présenter l'ensemble des résultats obtenus au cours de ces années de recherche.

Je tiens ensuite à adresser mes remerciements aux membres du réseau GABRIEL avec qui j'ai pu collaborer au long de ce projet de recherche. Merci en particulier au Dr. Niaina Rakotosamimanana qui m'a accueillie avec patience et gentillesse au sein de son équipe à l'Institut Pasteur de Madagascar, à Antananarivo. My heartfelt thanks also go to Dr. Sayera Banu for welcoming me in her team at icddr,b in Dhaka as well. I would like to thank Dr. Arjoo for mentoring me during that stay, showing me around beautiful Dhaka, and keeping me involved in great projects long afterwards. Je souhaite également remercier les Pr. Delia Goletti et Pr. Giovanni Delogu pour cette collaboration enrichissante que nous avons initiée au cours de ma thèse et qui, je l'espère, se poursuivra dans les projets à venir.

J'adresse des remerciements particuliers à toute l'équipe du LPE et à mes amis du CIRI pour votre bonne humeur et votre soutien sans faille pendant ma thèse. Merci à Juliet de m'avoir accueillie avec bienveillance dans l'équipe, et Marie, Emilie, Alex, Stéphane M (c'est bien parce que je suis polie), Stéphane P, Marie-Charlotte, Rim, Mame, Letitia, Jean-Luc, Milen, Alain, et Florence (Pradel). Merci pour ces belles années ponctuées de précieux apéros et pique-niques. Merci à Charlotte et Albin pour votre gentillesse, votre bonne humeur, et nos bons moments intensément caféinés passés ensemble à la Croix-Rousse. Merci à Joris pour ta patience face à mes problèmes pour dompter le CyTOF !

Un merci ému à Thibault pour ta présence tout au long de ma thèse, dans la bonne humeur, et toujours pour me tirer vers le haut scientifiquement, que ce soit par des congrès, de nouveaux appareils, ou de nouvelles méthodes d'analyse. Non seulement on a bien rigolé, mais en plus tu as grandement contribué à faire de moi la scientifique que je suis aujourd'hui.

Bien sûr, un grand merci à Jonathan ; je ne sais même pas où faire commencer les remerciements qui te sont destinés. Cette thèse et ses voyages si enrichissants n'auraient pas existé sans toi, tout comme la plupart de mes capacités professionnelles d'ailleurs. Travailler avec toi sur nos différents projets a été un plaisir, et en jetant un regard en arrière sur les trois et quelques dernières années, je suis très fière de notre travail ensemble !

Et évidemment, merci du fond du cœur à Flo d'avoir accepté d'assurer la direction de ma thèse, et de l'avoir fait avec autant de bienveillance, de patience, et de compétence. Tu es une source d'inspiration inépuisable pour moi, et je serai contente si ma carrière et mon caractère ressemblent un jour aux tiens, ne serait-ce que de loin.

Place maintenant à mes proches et au soutien précieux qu'ils m'ont fourni. Mes remerciements les plus essentiels vont à mes parents sans qui je serais vraisemblablement dénutrie d'abord, et déscolarisée ensuite. Merci Charlotte pour ta présence apaisante et nos conversation de cinéphiles, et merci Jade de tolérer patiemment mes efforts dans mon précieux rôle de nouvelle Khalto.

Un grand merci à mes amis qui m'ont soutenue sans faille durant ces dernières années. Merci à Chris pour nos beaux moments partagés d'abord suite à une jolie rencontre à Madagascar, puis entre calanques marseillaises et promenades lyonnaises. Obvious thanks to my bro Cesare who made my stays across Mada and Italy way better, although I now suffer from chronically excessive pasta consumption and liver failure. Heaps of love to Sam who made my visit in Dhaka infinitely cooler: I'm proud of our long distance friendship, and I miss our iftars every year.

En particulier, merci à mes irréductibles Gab et Manon – nous étions dans le même bateau, et heureusement (beep boop beep boop). Merci à Sofia et Gus pour votre crème de marrons principalement, et accessoirement pour votre présence bienveillante pendant ma dernière année de thèse. Merci à Esther pour tes recommandations littéraires de qualité et imitations incroyables, et à Ea et Clément pour vos aprèms goûter, jeux, badminton, fripes... Merci à Julia pour ta douceur, ton soutien irremplaçable, et ton sens de l'humour qui égaye toujours mes visites parisiennes. Un grand merci à Shanis d'être sorti du chapeau de manière impromptue à la fin de ma thèse pour augmenter significativement ma qualité de vie entre deux rouleaux de jambon à la mayo. Et merci à Mélie, Coco, Quentin, Lozéa, Chris et toute l'équipe – je suis ravie d'avoir fait enfin votre connaissance, bien trop tardivement à mon goût !

Polite and moderate thanks to the small Emiches, nothing excessive. I hope you will think that's lovely. My tent is neatly packed and awaits the next adventure. My stomach awaits your next fried eggs.

Un évident merci à Valentine d'assurer ma survie physique et émotionnelle depuis maintenant presque une décennie (sourire crispé) à grands renforts de brioches et autres crêpes, de photos de bébés chiens, et d'anecdotes croustillantes.

Le merci le plus doux à My Sweet Strawberry Plantain pour avoir spawné près de chez moi par chance, et avoir rendu ces derniers mois à la fois moelleux et Bass Boosted © [TATA03] (Brutal Remix EXTENDED 7h) pls DM for collab.

Thank you Ryan for sticking around, reading my stuff, nodding appreciatively at my paintings, listening to my rants, generally tolerating me, and for keeping my head above all rough waters. Unfortunately, half of my personality is now built after your personality; but luckily, all of my film taste is copied after your film taste.

Enfin, merci Mathilde, grand cru 2020, pour ton infinie gentillesse, ton humour de haute volée, et tes notes vocales sans queue ni tête (dans l'ordre d'importance). Les mots me manquent.

Quand à mon frère, si un jour vous nous cherchez, nous aurons probablement tous deux changé d'identité et enfin fini par ouvrir une crêperie, quelque part en Amérique centrale.

Table of contents

Abstract

Context: Tuberculosis (TB) is one of the most deadly infectious diseases in the world, with more than one million deaths by 2020. Neglected in international health policies, it mainly affects developing countries. Its treatment requires antibiotic multi-therapies with toxic side effects. Concerning pulmonary TB in particular, there is a clinical need for new tests to monitor treatment more rapidly, using samples that are more consistently accessible than sputum. In this context, immunological blood biomarkers represent promising options.

Objectives: The main objective was to evaluate the clinical relevance of selected blood-based immunological tests for anti-TB treatment monitoring, in relation *Mycobacterium tuberculosis* (Mtb) culture conversion. For this purpose, we conducted a prospective multicentered translational study in five high-TB incidence countries (Bangladesh, Georgia, Lebanon, Madagascar, Paraguay). We adopted a hybrid research approach including an on-site evaluation of two point-of-care tests (complete blood counts and interferon-gamma (IFN-γ) release assays), and an exploratory component using high-dimensional single-cell techniques for signature discovery (mass cytometry and full spectrum flow cytometry, in Lyon).

Findings: We enrolled 152 adult patients with culture-confirmed drug-susceptible (DS) or drug-resistant (DR) pulmonary TB. Peripheral whole blood and sputum samples were collected at inclusion, after two months (T1), and at the end of treatment (6 to 24 months). At inclusion, high total white blood cell counts and low lymphocyte counts – measured by routine complete blood counts – were predictive of treatment failure. Then, a combination of two plasma-based IFN-γ release assays (QuantiFERON-TB Gold Plus and heparin-binding hemagglutinin; HBHA) was evaluated. In a subgroup of patients whose sputum cultures remained positive at T1, a common clinical pattern at inclusion was observed (neutrophilia, lymphopenia, low body mass index, low QFT-P IFN-γ responses) as well as a low IFN-γ response to HBHA during treatment. Finally, in a subgroup of 22 patients, the phenotypic diversity of peripheral T-cells was characterized by mass and full spectrum flow cytometry. At T1, T-cell immune-profile comparison distinguished negative- from positive-sputum culture patients at two months, whether infected with a DS- or DR-Mtb strain. In-depth analyses revealed an under-representation of differentiated cytotoxic $CD8^+$ T-cells and an over-representation of naive $CD4^+$ T-cells in positive-sputum culture patients at two months. This suggests a link between the T-cell differentiation and mycobacterial clearance during treatment.

Perspectives: In this work, we have documented the clinical relevance of two simple monitoring tests, adapted to lower-income, high-TB incidence settings. We have generated new data on T-cell immunobiology during TB treatment in patients representative of the most affected populations. These results may have direct applications to other major issues in TB management, including latent TB infection screening, identification of patients most likely to progress to active TB, and prediction of post-treatment relapse risk.

PART A: BACKGROUND

Introduction

Tuberculosis (TB) is one of the leading causes of death by a single infectious agent in the world. It is caused by the bacillus *Mycobacterium tuberculosis* (*M. tuberculosis*; Mtb), which preferentially infects the lungs, but also causes a diversity of extrapulmonary disease forms. In 2020, one-fourth of the world population was estimated to latently carry Mtb, and active TB disease was responsible for over 1 million deaths and an estimated 10 million new infections. Although the sole existing vaccine (the *Bacille de Calmette et Guérin* (BCG) vaccine) has been administered to over 3.5 billion people since its discovery in the early twentieth century, the control of the TB epidemic remains a vastly unmet public health goal. Simultaneously, the rising incidence of multi-drug resistant (MDR) and extensively drug resistant (XDR) TB cases, and the emergence of totally-drug resistant (TDR) Mtb strains have become a major public health concern as they require significantly heavier therapeutic options and mobilize important funds.

Comprehensively understanding the immune response to Mtb infection remains a challenging task despite decades of work. Mtb is a thick layered, slow-growing bacterium which can survive a long time in a reversible latent state, is naturally tolerant to numerous antibacterial chemotherapies, and displays highly effective immune escape mechanisms. Immune responses to Mtb are hence only partly effective, leading to a vast reservoir of asymptomatic, non-contagious latent infections in the general population. For these reasons, the treatment of active TB requires combined antibiotic therapies that last six months at least[1,2] and are associated with toxic side effects ranging from nausea to peripheral nerve damage and hepatotoxicity, requiring consistent patient follow-up during treatment. However, adherence to anti-TB treatment is notoriously low, in particular in primary care settings[3,4]. This is a risk factor for treatment failure and relapse as well as for further selection of drug-resistant strains[5–7]. Efficient monitoring of anti-TB treatment adherence and efficacy is critical to provide adequate patient care and curb relapse episodes and acquired drug resistance.

As per the current WHO recommendations, anti-TB treatment monitoring relies on bacilli detection by sputum smear microscopy and *M. tuberculosis* culture when possible[8]. These microbiology-based methods have been in use for over a century and their experimental limitations take a toll on clinical TB management. Smear microscopy has poor sensitivity and specificity for outcome prediction in patients with pulmonary TB because it is impacted by the bacterial load and immunological state of patients, and the quality of results is highly

operator-dependent[9,10]. *M. tuberculosis* culture is considered the gold standard for TB treatment monitoring as it provides good outcome predictions, but slow mycobacterial growth often causes results to arrive too late. It requires high biosafety laboratory environments (BSL-3) and therefore has limited availability in primary care settings[11].

There is a clinical and public health need for new anti-TB treatment monitoring tests adapted to primary care settings and that would provide quicker outcome predictions. To meet the clinical needs for TB follow-up, the novel tests detecting biomarkers of interest would need to be conductible on accessible samples (blood, urine, feces) and to require limited laboratory expertise and equipment[12]. As the TB epidemic keeps outgrowing our current bacteria-centered diagnostic and therapeutical options, and as their limitations have become more apparent over the years, novel developments on immune biomarkers of TB have showcased a host-centered view as a promising alternative[13].

Chapter 1. Historical perspective on the fight against TB: from a bacterium-centered to a host-centered approach.

1.1 From prehistorical times to modern history: TB, the eternal plague

1.1.1 Evidence of TB disease from Prehistorical and Antique times

TB is one of the oldest infectious diseases recorded in human history. Archeological, paleontological, and genotyping evidence indicate that TB is intricately linked with the history of human development. Historically, the first archeological discoveries of TB-characteristic lesions in human remains were made in the early XXth century on Ancient Egyptian mummies dating back to 3,400 B.C. through the uncovering of bones showing typical TB-caused abscess cavities (Figure 1.A.) or lesions evocative of Pott's disease, a TB infection of the spine which may cause spectacular spinal deformities (Figure 1.B.)[14].

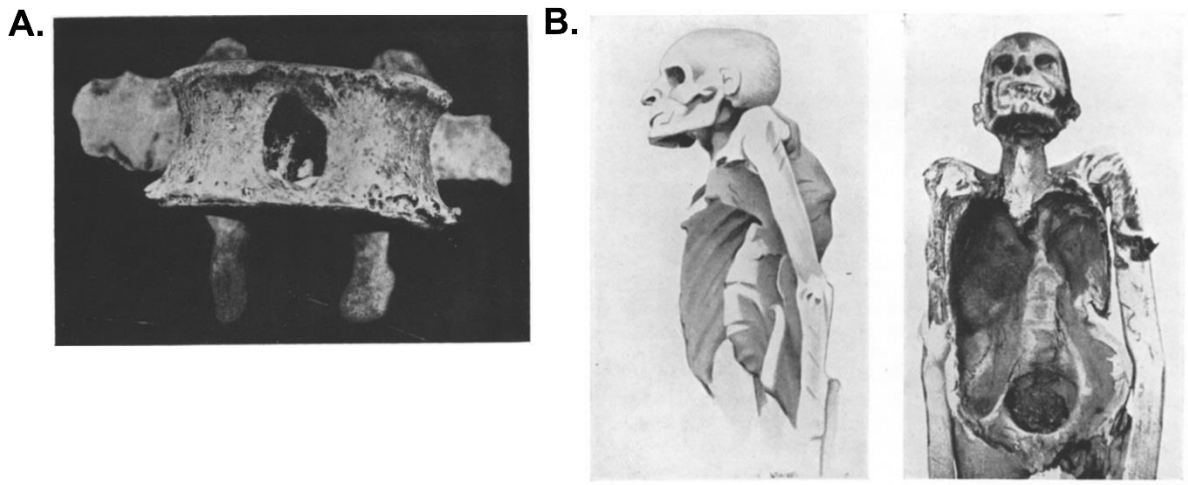

Figure 1. Paleontological evidence of bone TB infection in Ancient Egyptian mummies.
A. TB abscess cavity in a lumbar vertebra from a Middle Kingdom Egyptian mummy (c. 1975 – 1640 B.C.). **B.** Spinal deformities evocative of TB infection (Pott's disease) on the mummy of the priest Nesperehân (c. 1069 – 945 B.C.). Source: A.J.E. Cave, 1941[14].

Nowadays, however, modern genotyping methods have revealed the presence of Mtb DNA in human remains as ancient as 9,000 to 8,000 years, in a Neolithic settlement located in the Eastern Mediterranean, south of Haifa (Occupied State of Palestine)[15]. In animals, Mtb DNA was detected in 17,000 year old remains of an extinct *Bison antiquus* species found in Natural Trap Cave (Wyoming, USA)[16]. Erosive lesions of the articular surface of metacarpal bones were deemed as characteristic of Mtb-like granulomatous infection, as confirmed by PCR[17]; over a decade later, lipidic Mtb virulence factors were even detected in the same remains[18]. Such paleomicrobiology discoveries were consistent with the anthropological hypothesis that TB arose along with human settlement and with the development of agriculture and cattle domestication (c. 9,000 – 8,000 B.C.). This led to initial theories that TB was a zoonotic disease, passed on by cattle to humans, and that *M. tuberculosis* originated from *Mycobacterium bovis*. However, over the last 20 years, whole genome sequencing (WGS) studies along with extensive phylogenetics works have challenged these theories and generated debate over the historical evolution of the *M. tuberculosis* complex (MTBC) genus, which includes seven human-adapted *M. tuberculosis* lineages and nine animal-adapted ecotypes which may infect humans as well and are found in diverse animal reservoirs, from bovids (*M. bovis)* to poultry *(M. avium*) or pinnipeds (*M. pinnipedii*). Phylogenetic analyses within the MTBC rely on the detection of genomic insertions or deletions of regions of difference (RD), which are unique large sequence polymorphisms that occurred only once in the phylogeny of each MTBC species, and help identify each species and their phylogenetic relationships[19]. Based on this, WGS studies now suggest that *M. tuberculosis*, *M. bovis,* and other animal ecotypes share a common ancestor which would be genetically closer to *M. tuberculosis* (Figure 2). In addition, phylogeny evidence indicates that MTBC emerged at least 70,000 years ago – well before cattle domestication – and has constantly followed human migrations out of Africa, spreading faster as population density increased during the Neolithic period, with very little genetic diversification[20].

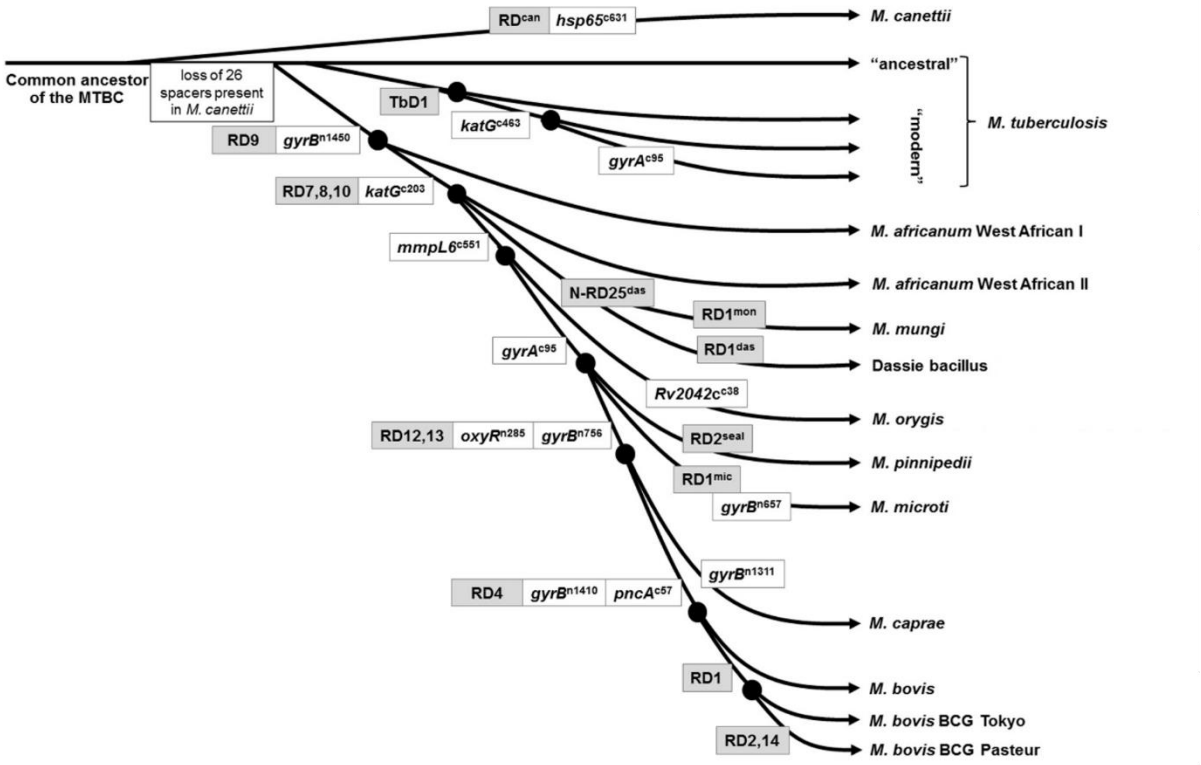

Figure 2. Phylogeny of the MTBC complex.
Phylogenetic relationships were based on the absence of regions of difference (RD; grey boxes) and the detection of single nucleotide polymorphisms (SNPs; white boxes) with superscripts indicating the position of the mutation at the nucleotide (n) or the codon (c) of each gene. BCG: Bacille Calmette Guérin strains. Adapted from Rodriguez-Campos et al., 2014[21].

1.1.2 Medical depictions of TB from Antiquity to the XVIIth century

The earliest written evidence referencing TB disease was discovered in India and dates back to over 3,000 years[22]. Interestingly, some of these texts already advise patients to "move to higher altitudes", which is reminiscent of the XIXth-XXth sanatorium movement. Pictural references to TB disease were present in ancient Egyptian art as well, although found mostly on funerary portraits with evocative depictions of Pott's disease rather than on papyrus[14]. Later on, in Ancient Greece, TB became known as *phtisis* (φθίσις), derived from root words meaning "to waste away", "to decay". Hippocrates (460–370 B.C.) was one of the first physicians to accurately describe clinical symptoms of pulmonary TB as we know them today in his *Of the Epidemics* (Book I), citing "a state of consumption", "constant sweats", and a "weakness of the lung" along with descriptions of cough, hemoptysis, and nocturnal fever[23]. However, he thought the disease to be hereditary; it is Aristotle (384-322 B.C.) who is credited as the first Antiquity scholar to suspect the contagious nature of TB, as he writes: "in approaching the consumptive, one breathes [his] pernicious air"[24]. He described occurrences of TB-like disease in pigs and oxes[22], likely corresponding to depictions of *Mycobacterium bovis* infection. After the fall of the Roman Empire (Vth century) and on to the Middle Ages, TB had spread throughout Europe, where the first records of TB cervical lymphadenitis were found. It was then referred to as *scrofula* or "écrouelles" in French, derived from the latin word for "sow", evocative of the disgust physicians and patients alike felt for the spectacular symptoms of the disease[25]. It was known as "the King's Evil" in France and England, and thought to be healed by the touch of a royal person endorsed with divine power. In the late XVIIth century, the first anatomically accurate characterizations of pulmonary TB pathology were published by the physician Franciscus Sylvius de la Boe, who first introduced the notion of "tubercles" in his "Opera Medica" (1679)[22]. These tubercles were considered the origin of the *phtisis* and were later illustrated consistently by other pathologists (Figure 3). Later on, at the end of the XVIIIth century, some scientists such as Benjamin Marten had formulated hypotheses about the infectious nature of TB, but the majority of the physicians at the time believed in its hereditary transmission. But by then, TB had started morphing into a deadly epidemic, which expanded with the increasing urbanization of Europe and boomed throughout the Industrial Revolution and its assorted cortege of precarious living conditions. As the "white plague" tore through European cities with a mortality rate of over 900 per 100,000 people per year, physicians and scientists started investigating the infectious origin of TB[26].

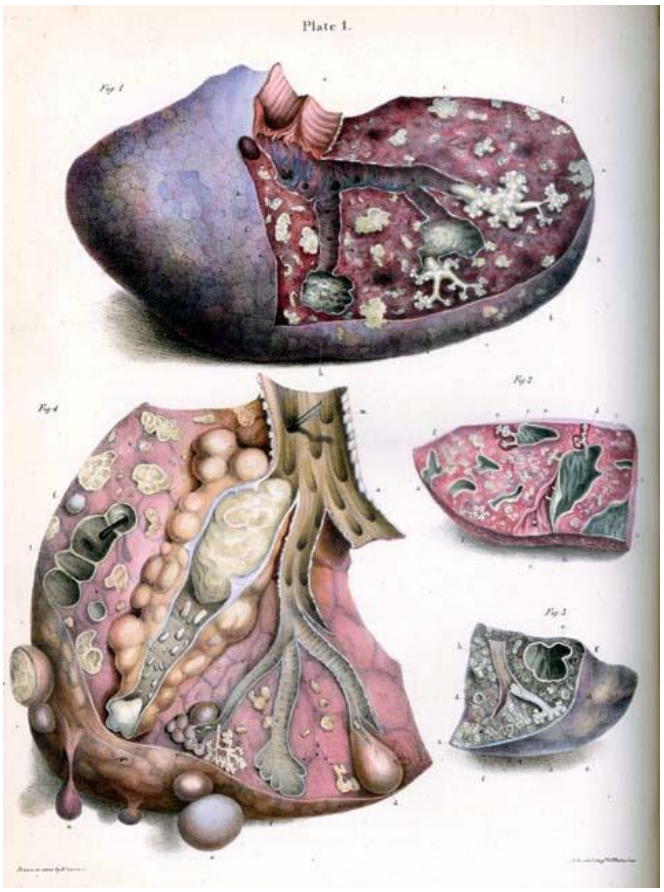

Figure 3. "Tubercle" illustration showing advanced lung lesions and caseous granuloma caused by pulmonary TB.
Colored plate published in "Illustrations of the Elementary Forms of Disease" (1837) by the Scottish pathologist Sir Robert Carswell. Source: University of Edimburgh.

1.2 From the XIXth century to modern days: TB in the landscape of microbiology and immunology research

1.2.1 Discovery of the etiological agent

As Europe and North America scrambled through the raging TB epidemic which would remain responsible for over 20% of all their human deaths until the XIXth century[20], the German and French scientific communities extensively searched for its etiological agent. In 1865, the French surgeon Jean-Antoine Villemin demonstrated the infectious nature of TB by infecting a rabbit with liquid sampled from a TB cavity collected from a human dissection, and showing TB symptoms upon sacrifice of the rabbit three months later[26]. Then, in 1882, the German microbiologist Robert Koch used methylene blue staining to isolate, stain, and characterize the tubercle bacillus, to which he gave the name *Mycobacterium tuberculosis*. He received the Nobel Prize in Medicine or Physiology in 1905 partly for this research. Koch is also credited for the discovery of tuberculin or purified protein derivative (PPD), a combination of Mtb proteins used for diagnostic purposes.

1.2.2 Early TB treatment strategies and advances in antibiotic research

For centuries, the only available therapeutic options for TB were formulated along recommendations by the Greek physician Galen (133 – 201 A.D.) who recommended rest, fresh air, and consumption of milk[26]. If some early descriptions of surgery for scrofula were documented during the XIVth century, and later led to pneumothorax surgeries for upper lung cavity lesions (Figure 4), the first therapeutic regimens which improved the quality of life of TB patients were sanatorium cures, introduced in the mid-XIXth century. As they gained popularity from the end of the XIXth until the mid-XXth century, sanatoria multiplied in mountain towns throughout Europe and North America, enabling TB patients to rest in less crowded areas and breathe cleaner air. In retrospect, this regimen is likely to have induced an immune restauration caused by the improvement of living conditions in sanatoria compared to cramped XXth century European urban centers; but its clinical efficacy is difficult to document accurately[27]. In 1908, the French scientists Albert Calmette and Camille Guérin developed an attenuated strain of *M. bovis* by growing and passaging it on fresh plates of bile-potato media for over 11 years to decrease its virulence. The resulting strain, termed Bacille Calmette Guérin (BCG), was first used in humans as a live attenuated vaccine in 1921; it is still the vaccine used nowadays even though its efficacy is under 50% for adult TB patients.

Figure 4. Pneumonolysis performed to collapse an underlying TB cavity.
Here, ping pong balls were used to create space under the ribcage and keep the lung separated from the pleura. Source: Pezzella, 2019[27].

In contrast, the true turning point in the history of TB treatment was the discovery of the first antibiotics. If penicillin, discovered in 1929, was one of the first drugs routinely implemented for antibacterial chemotherapy throughout the 1940s, it had no effect on *M. tuberculosis*, which exhibited natural resistance due in part to its thick mycobacterial cell wall. In contrast, streptomycin, discovered in 1944, was the first antibiotic agent shown to efficiently kill Mtb in clinical trials[28]. However, these spectacular results were challenged by the drug's limited availability and the significant side effects, as well as by the quick rise in streptomycin resistance in Mtb strains at the time. When para-aminosalycilic acid (PAS) was discovered that same year, similar results were observed[29]. As scientists noticed that combining streptomycin and PAS was efficient in slowing the occurrence of antibioresistance, one of the main principles of modern anti-tuberculous regimens emerged: multi-therapy. In 1951, the discovery of isoniazid (INH) was an additional breakthrough in the field of anti-TB therapy as it was the most potent drug available at the time while being inexpensive and having moderate side effects. The combination of streptomycin, PAS, and INH for over 18 months soon became the go-to triple therapy for TB and remained a therapeutical standard for almost 20 years. Rifampicin, discovered in 1957 and added to the triple-therapy in 1966, enabled to shorten the treatment course to 9 months. This duration was further reduced to 6 months after pyrazinamide (PZA) at low doses was included. Finally, ethambutol (ETH) replaced streptomycin for safety and efficacy reasons, forming the modern quadri-therapy still used nowadays to treat drug-susceptible TB (DS-TB).

1.2.3 The limits of antibiotic therapy

However, the limits of the antibiotic multi-therapy became apparent shortly after its early implementation. The first nation-wide TB drug-resistance investigation took place in untreated patients from the United Kingdom between 1955 and 1956 and showed that barely ten years after their discovery, the levels of resistance to streptomycin, PAS, and INH had reached 2.5%, 2.6%, and 1.3% respectively[30]. This led to the recognition of newly characterized strains of multi-drug resistant MDR-TB (MDR-TB), defined as resistant to INH and rifampicin. Such numbers remained on the rise throughout the XXth century, with numerous outbreaks of drug-resistant TB (DR-TB) occurring consistently between the 1970s and the 1990s[31]. By the mid-1990s, no TB-endemic country was spared from MDR-TB. This spurred research incentives for more potent anti-TB drugs, novel or re-purposed: at the time, these included other rifamycins, and fluoroquinolones such as moxifloxacin[29], which became the first second line drugs.

1.2.4 Urbanization, migration, poverty: how neglecting to control TB shaped its modern epidemiology

However, simultaneously, as healthcare quality and living conditions globally improved in Europe and North America, many of the socio-economic risk factors associated with TB – such as precarity, overpopulation, and malnutrition – became characteristic of marginalized populations rather than the general public. As a consequence, in the late 1980s and early 1990s, public health policies started granting less and less attention to TB control, and media coverage of TB decreased. The antibiotic quadri-therapy still seemed efficient as a majority rule, and despite rising antibioresistance, TB was increasingly showcased as a fixable issue, while worldwide TB elimination was viewed as an achievable short-term goal[31]. However, as the fractures in our world's vastly differential economies widened along with globalization, the structure of the TB epidemic started following the ever-growing disconnect between Europe and North America versus the so-called Third World. Despite available antibiotic therapies, TB persisted in the poorest settings: at the worldwide scale, it became overwhelmingly more prevalent in low- and middle income countries, while awareness of TB in the general public dwindled to nonexistence elsewhere. And within developed countries, at the nationwide scale, TB became a synonym of extreme poverty, a threat only to the most marginalized populations, living in precarious conditions and with little access to quality

healthcare: homeless people, inmates, migrants, and travelers. For public health policy makers, it had become a disease deemed too long and complex to treat to warrant investment in lower-income settings[31]. This is still reflected by modern maps of worldwide active TB incidence (Figure 5..A.) and latent TB prevalence (Figure 5.B.). In 2020, one-fourth of the world's population was estimated to be latently infected by TB, and over 10 million new active TB infections as well as 1 million TB deaths were recorded[32,33]. Historically, the Southern tip of the African continent, Eastern Europe, and South Asia have concentrated the highest prevalence of TB, which is still reflected by the World Health Organization (WHO)-established list of the 30 highest-TB burden countries, in which the only country that is not located in Asia or Africa is Brazil. More specifically, as of 2019, the two thirds of all TB cases were localized in eight countries: India, Indonesia, China, the Philippines, Pakistan, Bangladesh, South Africa and Nigeria.

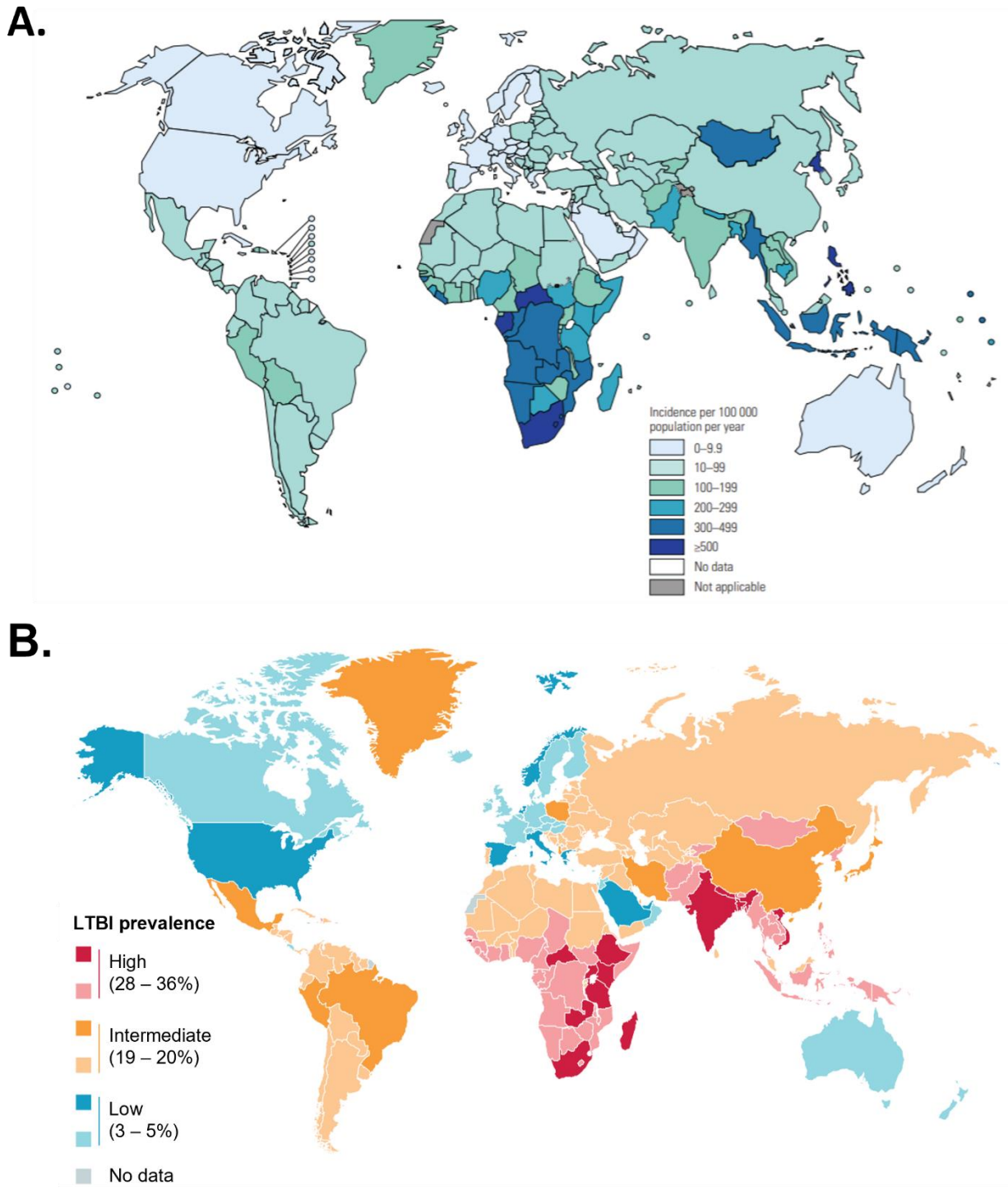

Figure 5. Worldwide TB epidemiology.
A. Incidence of active TB per 100,000 inhabitants in 2019. Source: WHO Global TB report 2020[33]. **B.** Prevalence of latent TB infection (LTBI) in 2019. Prevalence values were obtained by meta-analysis of 88 quantitative studies and correlation with WHO incidence data was verified. Adapted from Cohen et al., 2019[32].

1.2.5 From the shock of the HIV/AIDS epidemic to the rebirth of immunology

In the early 1980s, another epidemic had begun to spread from marginalized populations on to the general public. Between the first recorded cases of acquired immunodeficiency syndrome (AIDS) in 1981, to the discovery and establishment as causative agent of the Human Immunodeficiency Virus (HIV) in 1984, renewed public awareness had been brought to another player in the game of infection: the immune system. As the United States of America were hit hard by the HIV epidemic, what remained of TB research funding was sucked into the HIV vacuum, never to be seen again. But as patients, physicians, and scientists alike were confronted at a worldwide scale to the spectacular medical consequences of collapsing $CD4^+$ T-cell counts, two trends began to arise. The first one was a resurgence in TB infections, which soon enough became inseparable from HIV because of the two diseases' striking epidemiological synergy (Figure 6), shared risk factors for transmission, and physiological interplay at the tissular, cellular, and molecular levels. While HIV is a significant risk factor for progression from latent to active TB, TB is the leading cause of death among people living with HIV worldwide. The second trend was an renewed interest in immunology research, signing the beginning of a paradigm shift which would be crucial for TB control strategies: the key to reach beyond microbiological diagnosis and antibacterial chemotherapy, which the TB epidemic was starting to outgrow, may be in the host immune response to TB.

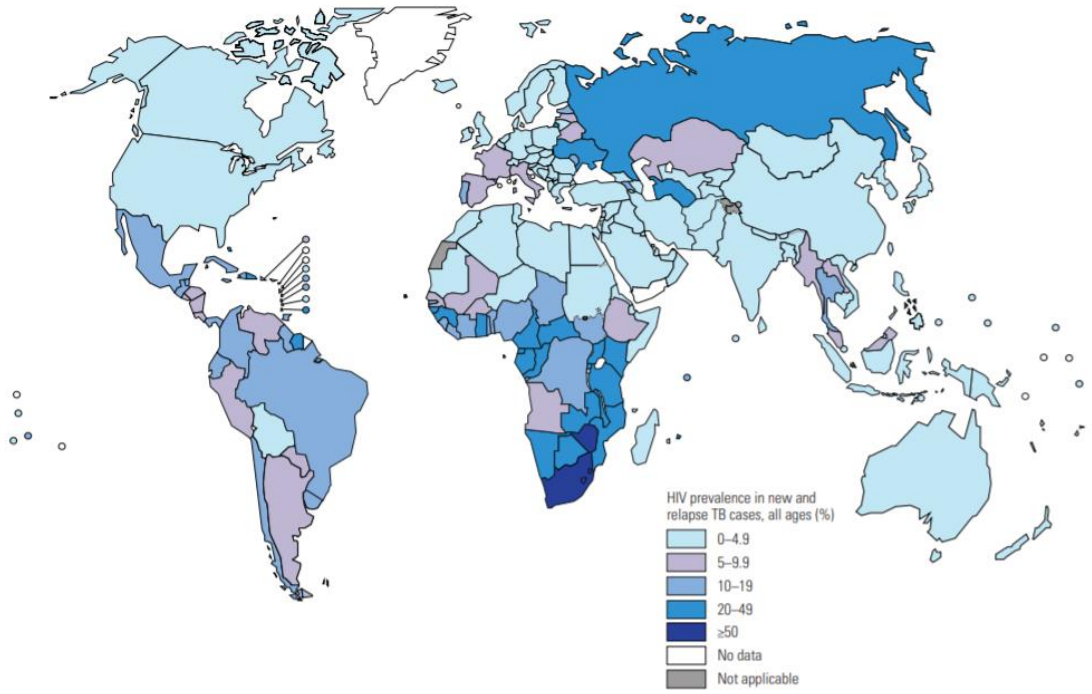

Figure 6. HIV prevalence in new and relapse TB cases.
Source: WHO Global Tuberculosis Report 2020[33].

Chapter 2. Physiopathology of the immune response to *M. tuberculosis* infection

2.1 A naturally resistant bacterium: structural and genomic characteristics of *M. tuberculosis*

Historically, physicians and scientists have found *M. tuberculosis* to be difficult to grow, difficult to stain, and hence difficult to diagnose and treat. As it doubles every 24h at most depending on the phenotype, it is a particularly slow growing bacterium, which is a major diagnostic challenge as *M. tuberculosis* colonies are detectable at the earliest three weeks after inoculation on solid media and one week on liquid media[34]. Upon diagnosis and during treatment monitoring, solid *M. tuberculosis* cultures are kept under surveillance for up to 12 weeks before declaring absence of growth. As for staining, species from the *Mycobacteria* genus are not included in the Gram classification as they poorly retain dyes under this protocol because of the characteristic layer of mycolic acids that surrounds their cell membrane (Figure 7). As a consequence, staining of *M. tuberculosis* bacilli was first performed using Ziehl-Neelsen staining, which requires heating and utilizes acid-alcohol washes to enable fuchsin staining of the mycolipidic wall.

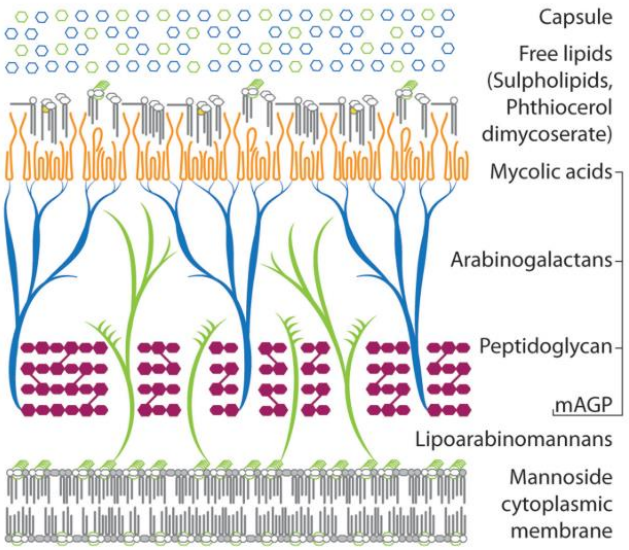

Figure 7. Chemical components of the mycobacterial cell wall.
The long-chained structure of mycolic acids is represented. mAGP: peptidoglycan-arabinogalactan-mycolic acid complex. Source: Gordon & Parish[34].

This thick, waxy wall is one of the intrinsic factors conferring phagocytosis resistance to *M. tuberculosis*[35]. Survival inside phagocytes is further facilitated by metabolic modifications exhibited by *M. tuberculosis* which enable the use of fatty acids as a primary carbon source when in microaerophilic environments[35]. Consistently, over 9% of the coding sequences found within the *M. tuberculosis* genome (which spans 4.4 Mb encoding 4,000 genes) are associated with lipid metabolism[34], which reflects the evolutive importance of the metabolic functions required for both mycolipidic cell wall synthesis and survival within host cells[35]. The mycolic acid wall was later shown to be involved in the natural tolerance of *M. tuberculosis* to antimicrobials[36], as it is a very efficient barrier stopping active molecules from reaching the cell: for example, the diffusion of β-lactams through this cell wall is over a hundred times slower than through that of *Escherichia coli*[37]. These intrinsic factors distinctive of the *Mycobacteria* genus and of *M. tuberculosis* in particular are associated with the complex course of TB disease and contribute to making it challenging to treat, hence the clinical need for consistent TB treatment monitoring.

2.2 Diagnosis and treatment of *M. tuberculosis* infection

2.2.1 Clinical presentation of *M. tuberculosis* infection

TB is transmitted *via* inhalation of aerosolized droplets with live bacteria. Thus, the lungs are the portal of entry and the primary site of latency, diffusion, and dissemination. Usually, upon transmission, latent TB infection (LTBI) develops as the infection is initially contained. Individuals with LTBI represent 90% of Mtb carriers and are asymptomatic and non-contagious; however, the bacteria persist in a dormant state. Progression from LTBI to active TB disease (ATB) occurs in 5 to 10% of the cases over the patient's lifetime. Risk factors for progression to active TB include older age, malnutrition, HIV infection, and immunosuppressive therapy. ATB is symptomatic and is characterized either by detectable Mtb bacilli or by detectable lesions. In 85% of cases, active Mtb infection is localized in the lungs; characteristic symptoms in non-immunosuppressed adult pulmonary TB (PTB) patients include prolonged cough (> 3 weeks), chronic fever, anorexia, night sweats, and alteration of the general status. Hemoptysis generally occurs late in the course of the disease. In the other 15% of cases, extrapulmonary Mtb infections (EPTB) can occur and may affect a large variety of organs. The most described occurrences include pleural infections, lymph nodes, bone infections (especially Pott's disease), central nervous system infection (meningitis), and genital TB. PTB

and EPTB may coexist in a single patient, as Mtb spreads from the lungs to extrapulmonary locations. Finally, in children, the clinical manifestations of ATB are vastly different from adult patients. Pediatric PTB is characterized by paucibacillary infections, with rare cavitation and mostly miliary forms generating little to no sputum expectoration and moderate symptoms, whereas pediatric EPTB includes mostly TB meningitis with very high lethality rates in children under 5 years of age.

2.2.2 Diagnosis of active TB

2.2.2.i Clinical diagnosis

In the early XXth century, diagnostic of active TB was commonly performed using chest X-rays, which was a quick and accessible methods to screen large number of people for TB, in military settings for example[26]. Nowadays, clinicians still use chest X-rays as well as CT-scans when available. When a tissular biopsy is performed, histo-pathology study is useful to diagnose TB. On chest radiographs or CT-scan imagery, PTB can manifest as lung infiltrates, confluent micronodular infiltrates, lung cavities predominantly in the upper lobes (Figure 8.A.). Military disease is a specific entity, characterized by a diffuse micronodular infiltrate of hematogenous origin (Figure 8.B.). These abnormalities can be associated with mediastinal lymphadenopathy(ies). For EPTB detection, imaging is a key diagnostic method, in particular for locations where biopsy is challenging (Figure 8.C.).

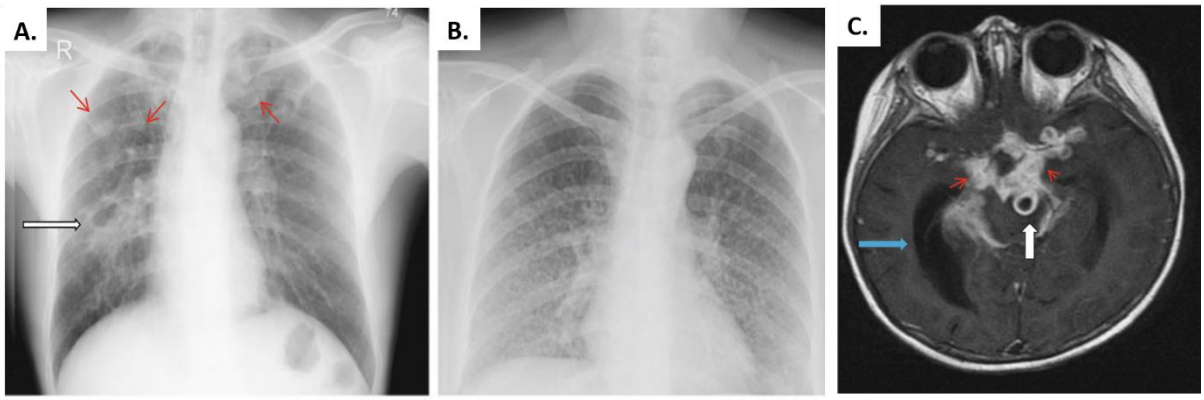

Figure 8. Radiological images of TB infection.
A. Characteristic presentation of PTB infection with cavities (white arrow) and upper lobe opacities (red arrows) evocative of lymphocyte recruitment. **B.** Miliary TB is characterized by the absence of cavities, with disseminated micronodular lesions in both lungs instead. **C.** TB meningitis in a nine-year-old child with hydrocephaly (blue arrow), "tubercle"-like TB lesion (white arrow), and meningeal inflammation (red arrows). Source: Heemskerk *et al.*, 2015[38].

2.2.2.ii Bacteriological diagnosis

To this day, the gold standard for PTB diagnosis is *M. tuberculosis* culture. Liquid medium Mtb culture is the fastest culture method available, as positive results may be yielded within a week. Bacteria are inoculated from a sputum sample into a liquid medium loaded with a fluorescent component which increases with bacterial growth. A solid medium tube is inoculated in parallel with liquid media to reduce contamination risks. Tubes are checked daily until either characteristic growth of Mtb is detected, contaminations are detected, or until 8 weeks have passed – after which the culture is deemed negative. Usually, sputum smear microscopy is also performed as soon as the sputum sample is received to establish a first intention diagnostic. After decontamination and heat-inactivation of *M. tuberculosis*, bacilli are visualized in sputum samples using Ziehl-Neelsen (Figure 9.A.) or fluorescent staining (Figure 9.B.).

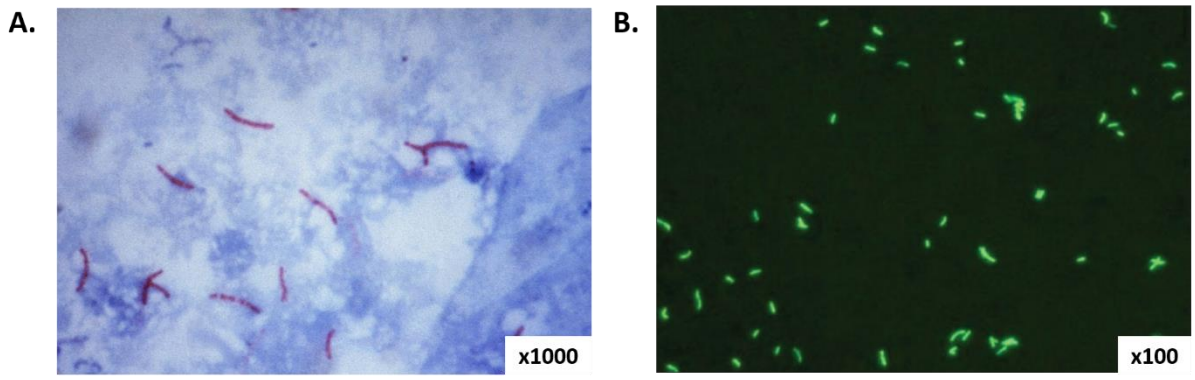

Figure 9. *M. tuberculosis* sputum smear microscopy.
Visualized with Ziehl-Neelsen (A.) or auramine O fluorescent staining (B.). Source: CDC (public domain) and Padmaja *et al.,* 2019[39].

Nowadays, gene amplification methods are also used for this purpose are they are quick and both more sensitive and specific than smear microscopy. This includes the cartridge-based, automated assay GeneXpert MTB/RIF, and now the more sensitive GeneXpert MTB/RIF Ultra, which rely on real time PCR to identify MTBC DNA as well as mutations associated with rifampicin resistance directly from unprocessed sputum samples. However, as such assays may detect DNA fragments from dead bacteria, microbiological confirmation remains required to ascertain diagnosis. Diagnosis of active TB is then followed by genotypic and/or phenotypic drug susceptibility testing whenever possible.

2.3 The challenges of pulmonary *M. tuberculosis* treatment

2.3.1 Mechanisms and evolution of drug resistance in *M. tuberculosis* in relation with clinical management

As presented in Chapter 1, several decades of struggling with TB management have helped identify two principles for TB therapy. First, a combination of multiple drugs is mandatory; and second, it must stretch long enough to ensure sterilization of the different mycobacterial phenotypes within the same disease entity. These principles stem directly from the capacity of *M. tuberculosis* to resist treatment, as it displays a variety of intrinsic and acquired mechanisms of drug resistance, which include structural modifications of drug target interaction sites[36], direct chemical modification or enzymatic degradation of drugs[37], and overexpression of drug targets by molecular mimicry. As horizontal gene transfer is rare in *M. tuberculosis*, the main drivers of acquired antimicrobial resistance are rather associated with chromosomal mutations than with mobile genetic elements in this species[36]. This explains that under- or misdiagnosis of drug-resistance, as well as poor treatment adherence or limited access to the appropriately potent drugs – particularly in primary care settings[3,4] – are thought to be important drivers of acquired drug resistance as they contribute to the selection of resistant strains among the diversity of bacterial subspecies present within the host[5–7] (Figure 10). Unequal access to quality healthcare has hence led to a disproportionate repartition of drug-resistant strains worldwide[36]. However, this is only a part of the problem because an increasing body of literature indicates that *M. tuberculosis* drug resistance may also arise despite strict treatment adherence[40], likely due to sublethal concentrations of some drugs after penetrating the various TB lesion compartments in the lung[41]. These two facts highlight the clinical need for consistently monitored treatment regardless of the healthcare setting level.

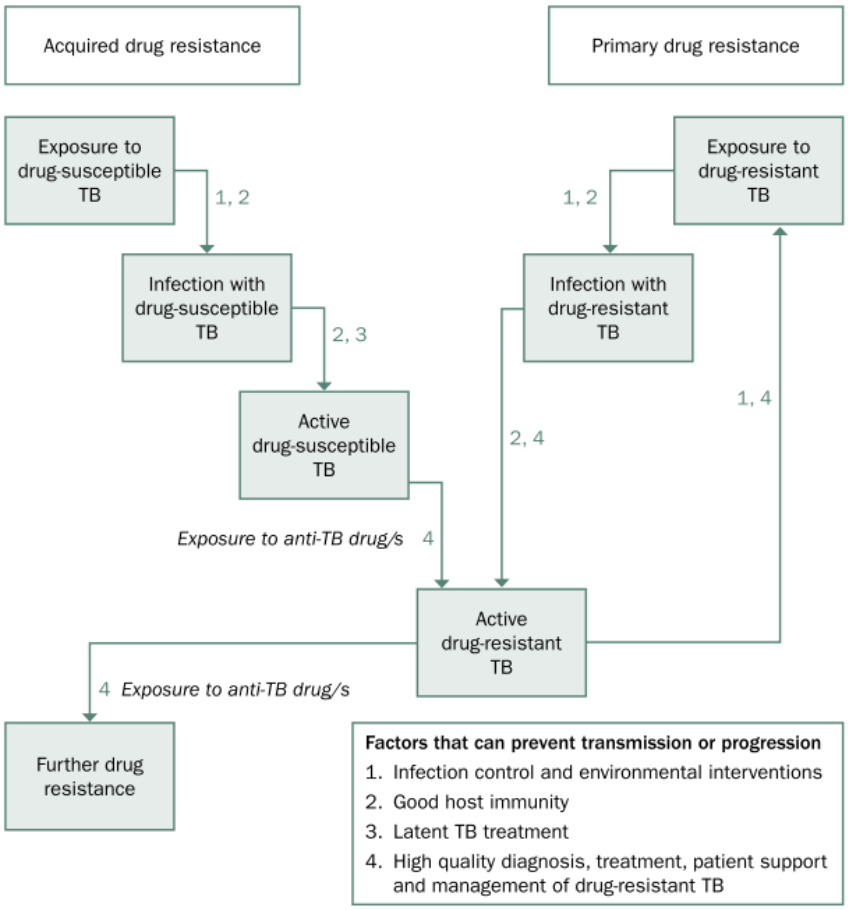

Figure 10. Pathways leading to increases in drug-resistant TB infections.
Source: WHO 2014[42].

2.3.2 Recommended treatment regimens: composition, length, and side effects

Anti-TB treatment regimens are built around an intensive phase followed by a continuation phase mobilizing fewer drugs and required to clear the remaining bacterial subpopulations within the host[43]. The WHO-recommended treatment regimen for drug-susceptible TB (DS-TB) utilizes first-line oral antibiotics (Figure 11) and consists in a six-month Directly Observed Treatment (DOT) with a 2-month intensive phase (H-R-E-Z) followed by a four-month continuation phase (H-R)[44]. However, research is ongoing to shorten this regimen to 4 months by replacing ethambutol or isoniazid with moxifloxacin, but non-inferiority has not yet been shown[45]. Strains that display resistance to one or more drugs are treated with second-line drugs (including injectable agents and fluoroquinolones) according to their resistance patterns, which are classified into several non-mutually exclusive categories (Table 1).

DESCRIPTION	DRUG	ABBREVIATION
First-line oral anti-TB drugs	Isoniazid	H
	Rifampicin	R
	Ethambutol	E
	Pyrazinamide	Z
	Rifabutin	Rfb
	Rifapentine	Rpt
Injectable anti-TB drugs (injectable agents or parenteral agents)	Streptomycin	S
	Kanamycin	Km
	Amikacin	Am
	Capreomycin	Cm
Fluoroquinolones (FQs)	Levofloxacin	Lfx
	Moxifloxacin	Mfx
	Gatifloxacin	Gfx
	Ofloxacin	Ofx
Oral bacteriostatic second-line anti-TB drugs	Ethionamide	Eto
	Prothionamide	Pto
	Cycloserine	Cs
	Terizidone	Trd
	p-aminosalicylic acid	PAS
	p-aminosalicylate sodium	PAS-Na
Anti-TB drugs with limited data on efficacy and/or long-term safety in the treatment of drug-resistant TB (This group includes new anti-TB agents).	Bedaquiline	Bdq
	Delamanid	Dlm
	Linezolid	Lzd
	Clofazimine	Cfz
	Amoxicillin/Clavulanate	Amx/Clv
	Imipenem/Cilastatin	Ipm/Cln
	Meropenem	Mpm
	High-dose isoniazid	High dose H
	Thioacetazone	T
	Clarithromycin	Clr

Figure 11. Second-line drugs used for the treatment of drug-resistant TB.
Source: WHO 2016[46].

Table 1. WHO-defined drug resistance categorization.
Source: WHO 2014[42].

Name	Resistance pattern
Single-resistance	One first-line anti-TB drug only (RIF, INH, ETH, or PZA).
Poly-resistance	More than one first-line anti-TB drug, other than INH and RIF.
Multi-drug resistance (MDR)	At least INH and RIF.
Extensive drug resistance (XDR)	Any fluoroquinolone, and at least one of three second-line injectable drugs (capreomycin, kanamycin, and amikacin), in addition to MDR.
Total drug resistance (TDR)	All anti-TB drugs.
Rifampicin resistance (RR)	Includes any of the above resistance patterns as long as rifampicin resistance is detected.

Drug-resistant TB regimens are often individualized within the frame of WHO recommendations to find the combinations which are the most potent, the best tolerated by each patient, and the most accessible, especially when a precise drug resistance pattern is identified along with levels of resistance. However, when phenotypic DST is not readily available, empiric treatment is initiated and standardized courses are adopted. In 2014, the WHO recommended a standardized version of the shortest available course for MDR-TB treatment, named the "Bangladesh regimen"[47] and built around an intensive phase of four to six months (if there is no sputum smear conversion) and a five-month continuation phase. This regimen uses gatifloxacin as the fluoroquinolone and kanamycin as the injectable agent, as well as prothionamide, clofazimine, high-dose isoniazid, pyrazinamide and ethambutol. However, individualized approaches remain the optimal treatment strategies whenever possible because both first- and second-line drugs are associated with heavy adverse effects. They may include gastro-intestinal disturbances, peripheral neuropathies which may cause irreversible cecity and hearing loss, hemato-, hepato-, and nephrotoxicity, risks of QT prolongation, and neuropsychiatric adverse effects (Figure 12.)[46].

MEDICINE	COHORTS USING THE DRUG AND REPORTING SAEs (N)	PATIENTS RECEIVING MEDICINE (N)	SAEs ATTRIBUTED TO INDIVIDUAL MEDICINE	
			N PATIENTS	% (95%CL)[a]
Pyrazinamide	19	2023	56	2.8% (2.1%–3.7%)
Ethambutol	16	1325	6	0.5% (0.2%–1.1%)
Second-line injectable agent	19	2538	184	7.3% (6.2%–8.4%)
Ofloxacin or ciprofloxacin	9	1408	40	2.8% (1.9%–4.1%)
Other fluoroquinolones	13	827	10	1.2% (0.6%–2.4%)
Ethionamide/ prothionamide	17	2106	173	8.2% (7.0%–9.6%)
Cycloserine	16	2140	96	4.5% (3.6%–5.5%)
p-aminosalicylic acid	16	1706	208	12.2% (10.6%–13.9%)
Linezolid	8	190	28	14.7% (10.0%–20.6%)

Figure 12. Occurrence of serious adverse events (SAE) in patients under treatment for MDR-TB.
Importantly, only studies within which SAEs had been recorded were included in this meta-analysis. Source: WHO 2016[46].

These adverse events – as well as the pain associated with the injection of some agents – contribute to low treatment adherence and poor treatment outcomes. And as the risk of adverse effects increases with the total cumulative antibiotic dose, in particular second-line injectables, the aim is thus to find both the shortest treatment duration and the least adverse effects[36]. This explains why there is a clinical need for both consistent monitoring, and research on early signatures of treatment response.

2.3.3 Current monitoring methods for PTB treatment: stakes and unmet needs

Currently, the monitoring of anti-TB treatment is based on the absence of clinical relapse rather than on the detection of signatures of cure. Physicians monitor weight gain and fever throughout treatment as they are quick robust clinical markers of health improvement and response to treatment. Simultaneously, microbiological follow-up using sputum culture and microscopy is recommended throughout treatment because clinical markers may keep improving even though bacterial sterilization has not been achieved, which is a risk factor for relapse. Sputum culture is the most sensitive method for live *M. tuberculosis* detection, in particular on liquid media, and hence is the reference standard recommended whenever possible by the WHO to define the outcomes of treatment[8,48] (Table 2).

Table 2. Definition of treatment outcomes in DS-TB and DR-TB patients.
Source: WHO 2020[48].

Outcome	**DS-TB patients**	**DR-TB patients**
Cured	Patient with microbiologically confirmed TB at the beginning of treatment who was smear- or culture-negative[1] in **the last month of treatment and on at least one previous occasion.**	Treatment completed as recommended by the national TB program without evidence of failure AND **three or more consecutive cultures taken at least 30 days** apart are negative after the intensive phase.
Treatment completed	PTB patient who completed treatment without evidence of failure BUT with no record to show that sputum smear or culture results **in the last month of treatment and on at least one previous occasion** were negative.	Treatment completed as recommended by the national policy without evidence of failure BUT no record of **three or more consecutive negative mycobacterial cultures at least 30 days** apart after the intensive phase
Treatment success	Combination of *cured* and *completed*.	
Treatment failed	PTB patient whose sputum smear or culture is positive **at month 5 or later during treatment.**	Need for treatment interruption or for permanent regimen change of at least two anti-TB drugs due to either of the following: - Lack of culture conversion[2] by the end of the intensive phase - Culture reversion[2] in the continuation phase - Additional acquired resistance to fluoroquinolones or second-line injectables - Adverse drug reactions.
Lost to follow-up	Treatment interrupted for two consecutive months at least.	
Death	Death during the course of treatment, for any reason.	
Not evaluated	Outcome unknown for any reason including transfer to another unit.	

Footnotes: "DR-TB" refers to RR-TB, MDR-TB, or XDR-TB patients. **1**. Sputum culture is the gold standard for outcome evaluation even if sputum smear microscopy is realized in parallel, as it is both less sensitive and less specific, and may generate falsely positive results[49]. Globally, sputum smear results during treatment should be used for definition of treatment outcome only in settings where culture is not readily available. **2**. Culture conversion is defined as two consecutively negative mycobacterial cultures taken 30 days apart. Culture reversion is defined as two consecutively positive mycobacterial cultures taken 30 days apart and occurring after an initial conversion.

As exposed in Chapter 1, these methods are over a hundred years old and have consequent technical and practical limitations, which takes a toll on the management of an epidemic that has outgrown them. *M. tuberculosis* sputum culture is very slow and requires BSL-3 environments which are not readily available in lower-income areas where TB is most prevalent[11]. In most settings across low- and middle-income countries, treatment monitoring relies uniquely on clinical symptom assessment and sputum smear microscopy, which is quicker, inexpensive, more commonly available, and relatively simple and specific for *M. tuberculosis.* However, it is highly operator- and sample dependent, and hence displays poor sensitivity and specificity for monitoring, especially in paucibacillary patients[9,10]; a 2010 meta-analysis of data from over 20,000 PTB patients indicated that 2-month smear microscopy was a poor predictor of treatment failure (57% sensitivity and 81% specificity)[11]. GeneXpert MTB/RIF testing is more sensitive (97% compared to the combination of sputum smear and culture[50]) but is not currently recommended for treatment monitoring, as it has been proven to detect dead bacteria (specificity estimated at 49% throughout treatment[50]) (Figure 13). Moreover, all of the above methods are sputum-dependent, but sputum composition is highly variable and may not always reflect the overall bacterial load. In addition, sputum samples may be difficult to collect during the later stages of treatment or in paucibacillary patients. This further complicates monitoring as sputum smear microscopy requires two or three sputum samples to be collected on consecutive mornings to increase sensitivity.

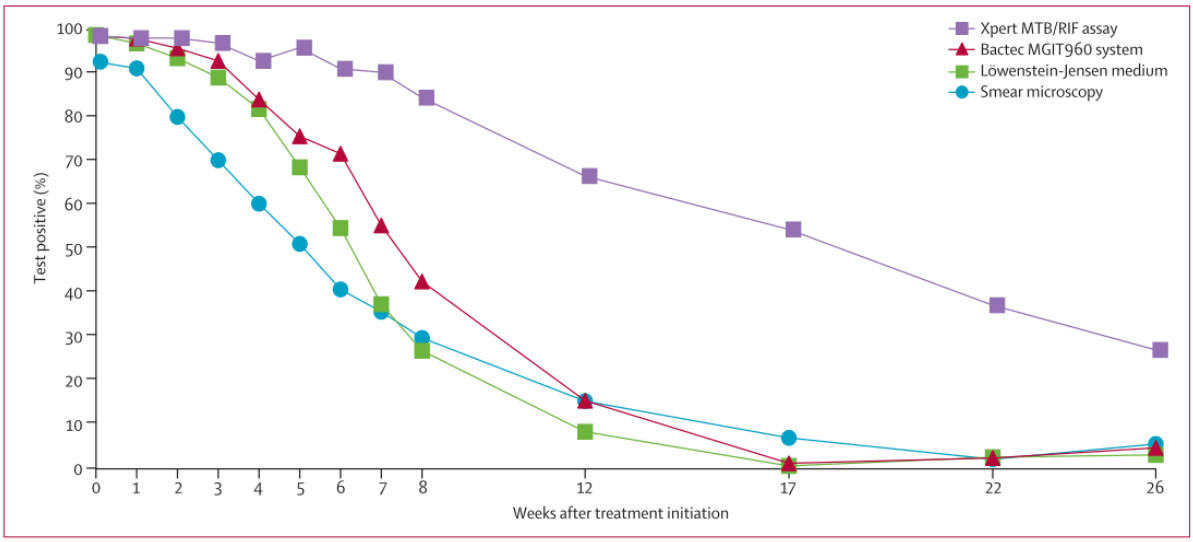

Figure 13. Qualitative results of the four most frequently used sputum-based treatment monitoring methods during PTB treatment.
Results from a 2013 study on 2741 sputum specimens collected from 221 PTB patients in South Africa and Tanzania[50].

To improve treatment monitoring in high-TB burden settings – but not only – there is a short-term clinical need for novel methods which are quick, affordable, with moderate expertise or scientific equipment requirement, and based on samples accessible more consistently that sputum[12,51]. Novel diagnostic tests are being investigated on samples other than sputum, such as tests detecting volatile organic compounds in breath[52], urine lipoarabinomannan tests[53], or stool-based methods[54]. These tests may be investigated for treatment monitoring as well, but they are still in early development stages, and are still part of a bacteria-centered approach. Hence, the monitoring of host biomarkers that are more specific to the response to TB than conventional clinical markers during treatment appears as a promising alternative.

As novel biomarker detection tests should ideally be able to detect the earliest signatures of cure possible to shorten treatment durations[52], the monitoring of immune responses – thought to be detectable prior to bacterial sterilization – shows potential. Even though monitoring of metabolic byproducts has also been investigated[55], the technical and scientific advances in the field of immunology throughout the past 20 years have yielded an abundance of encouraging results for the immuno-monitoring of TB treatment[13]. However, as the immune response to TB is a vastly complex, multifaceted, and only partially understood process, further work is needed to identify the most clinically relevant immune biomarkers and the associated antigenic determinants.

2.4 Immune response to pulmonary TB infection

Despite the fact that billions of people have historically been infected with PTB, our knowledge of the immune mechanisms which occur upon exposure and throughout acute infection, latency, or recovery is restricted by our limited ability to study immune responses directly at the site of infection. Hence, most of the following physiological processes were identified via autopsy, histology, animal models, *in vitro* infection of lineages or cells isolated from broncho-alveolar lavage (BAL), and *ex vivo* analyses of peripheral blood[56], which means that they are understood separately from their vastly more complex *in vivo* immunological dynamics.

2.4.1 Primary response to *M. tuberculosis* and formation of granuloma

Upon exposure with aerosolized droplets containing Mtb, alveolar macrophages (AM) are the first cells to internalize the bacteria. This leads to increased secretion of pro-inflammatory cytokines by the AMs, including TNF, IL-6, IL-1β, and IFN-γ, which are then detectable in serum[56]. This primary response induces the recruitment of uninfected macrophages, neutrophils, NK, and γδ T-cells at the site of infection, generating a highly inflammatory milieu. However, Mtb is able to resist phagocytosis, mainly by hindering phagosome acidification and by preventing the fusion of phagosomes and lysosomes[57]; as such, it persists and divides within the macrophages. As a consequence, a coalescent structure of epithelial cell-like, uninfected macrophages forms around Mtb-infected macrophages, which is then surrounded by a T and B lymphocyte cuff: the granuloma (Figure 14). Lymphocytes control the granuloma by maintaining a cytokine-rich microenvironment (TNF in early stages, then IFN-γ). Fibroblast recruitment and calcification may further contribute to this initially protective structure. The granuloma forms a physical barrier that helps contain Mtb spread and limits lung tissue damage. However, it acts a double-edged sword since it also hinders antibiotic diffusion, represents a safe harbor for dormant mycobacteria, and lowers the efficacy of adaptive immune responses at the site of infection.

2.4.2 Cavitation and lung colonization

Usually, a homeostatic balance is reached in the granuloma because Mtb eventually enter a nonreplicative dormancy state, and T-cells from the lymphocyte cuff exhibit downregulated pro-inflammatory cytokine secretion[58] and suppressed cytotoxic activity[59] that are partially independent from exhaustion[60]. This contributes to the asymptomatic, non-contagious state of TB infection which characterizes latency. However, granuloma are heterogeneous, dynamic structures which are shaped by immune changes and undergo structural and functional changes over time. A growing body of literature supports the hypothesis that active, Mtb-induced mechanisms turn the granuloma into a proliferation and dissemination hotspot[61]. Because infected macrophages undergo metabolism reprogramming towards lipid anabolism, their endosomes fill up with lipids, resulting in "foamy macrophages"[62]. They are poorly microbicidal compared to conventional macrophages, hence forming an Mtb survival niche[63]. Eventually, foamy macrophage necrosis occurring at the center of the granuloma causes their cytoplasmic contents to be released, along with free Mtb that multiply exponentially in this sheltered, lipid-rich extracellular environment called *caseum*. They in turn undergo phagocytosis by uninfected granuloma macrophages, which increases the number of infected cells[64].

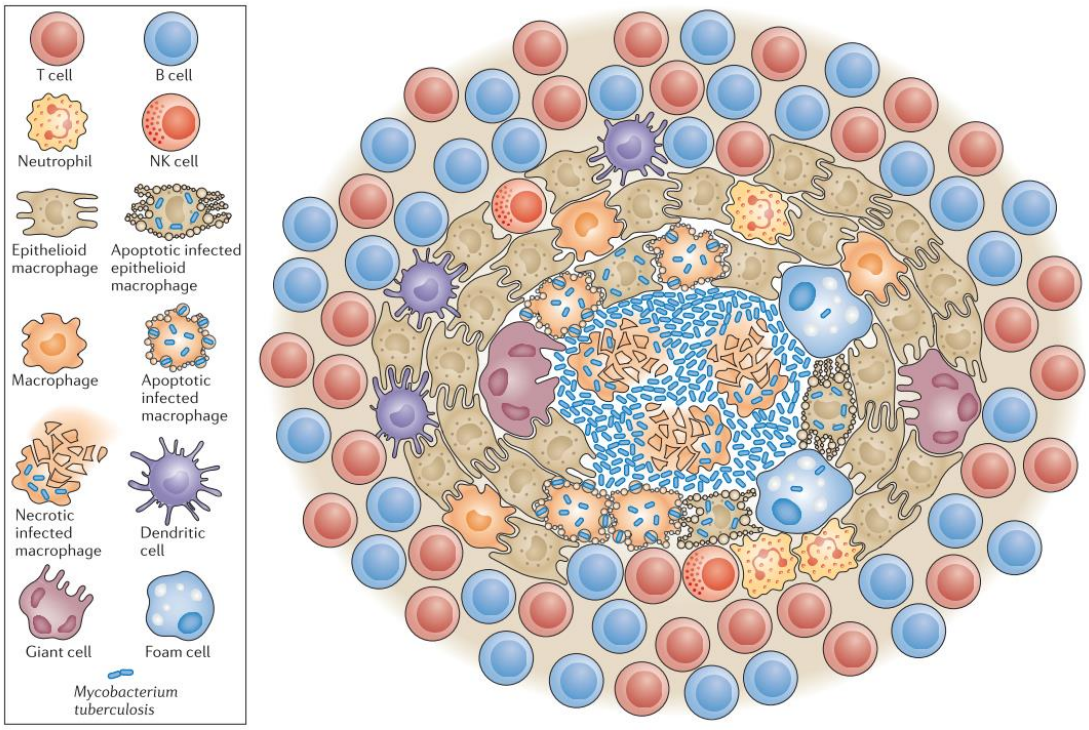

Figure 14. Spatial structure and cellular actors of the TB granuloma.
Source: Ramakrishnan, 2012[64].

This generates necrotic caseous lesions leading to the granuloma rupturing, causing cavities that facilitate Mtb dissemination through bronchial connection and are associated with high mycobacterial burden and poor treatment outcomes[65]. Cavity formation is known to be driven by long-lasting T-cell immune responses showing a Th1 polarity and enhanced IFN-γ secretion at the granuloma site[61], leading to site clearance of granuloma structure by effector and cytotoxic cells. This is supported by the fact that clinical presentation of PTB in HIV-positive patients canonically consists in an infection with few symptoms and infrequent granuloma formation. Regarding TB in the non-immunosuppressed individual, It is also enhanced by local inflammation, as increased TNF concentrations stimulate macrophage necrosis by producing reactive oxygen species (ROS)[63]. But the role of pro-inflammatory immunity in TB disease is far from straightforward. For example, T-cell IFN-γ secretion at the periphery of the granuloma activates macrophages, which enhances Mtb phagocytosis, but also induces mycobacterial spread and granuloma rupture. In contrast, initiation of immunosuppressive treatment can result in latent TB reactivation, and treatment with anti-TNF biologics has been shown to facilitate granuloma disorganization and mycobacterial spread[66]. Taken together, these observations are representative of the finely tuned immune balance of granulomas, and of the evolutionary success with which Mtb escapes, resists, and diverts host immune responses, eventually leading to the failure of granuloma-mediated containment. Fascinatingly, they suggest that Mtb seems to benefit from both suppressed immune responses and enhanced immune responses.

2.5 Peripheral immune biomarkers of pulmonary *M. tuberculosis* infection

This complex involvement of actors from the innate and adaptive immune system at the site of infection suggests that studying immune parameters during the course of TB infection could be equally as relevant as measuring mycobacterial markers. However, the highly localized character of PTB infection in inaccessible tissue forces us to evaluate peripheral markers as a proxy of the local response. In this context, the general working hypothesis tested when investigating immune biomarkers of TB treatment is that peripheral immune changes occur earlier than microbiological reversion and clinical improvement.

2.5.1 Immune biomarkers across the *M. tuberculosis* infection spectrum

In relation with our understanding of the granuloma pathophysiology, the current conception of TB disease is a spectrum of microbiological, clinical, and immunological manifestations which range from controlled infection to active disease[67] (Figure 15). This has generated a number of strategies to identify immune biomarkers associated with the different stages of TB, and efforts have been made to investigate markers that can either discriminate latent from active TB, change in response to treatment, predict microbiological outcomes, and predict vaccine efficacy[68]. In particular, markers of latency are being thoroughly investigated for treatment monitoring purposes, because latent infection and cured infection display similar manifestations on the TB spectrum. Despite the fact that other immune cells have been associated with TB disease outcome (*e.g.* peripheral neutrophilia, which is associated to disease severity and poor treatment outcomes[69]), T-cells remain considered as the key actors of the anti-TB response. Hence, most investigated biomarkers correspond to T-cell associated responses, either by measuring secreted cytokines, assessing T-cell functionality or abundance, and characterizing T-cell phenotypes. As a consequence, to ensure reliable monitoring assays and to detect Mtb-specific immune responses, stimulation with mycobacterial antigens is often necessary, and finding the most efficient stage-specific antigens is as hot a topic as identifying stage-specific biomarkers themselves.

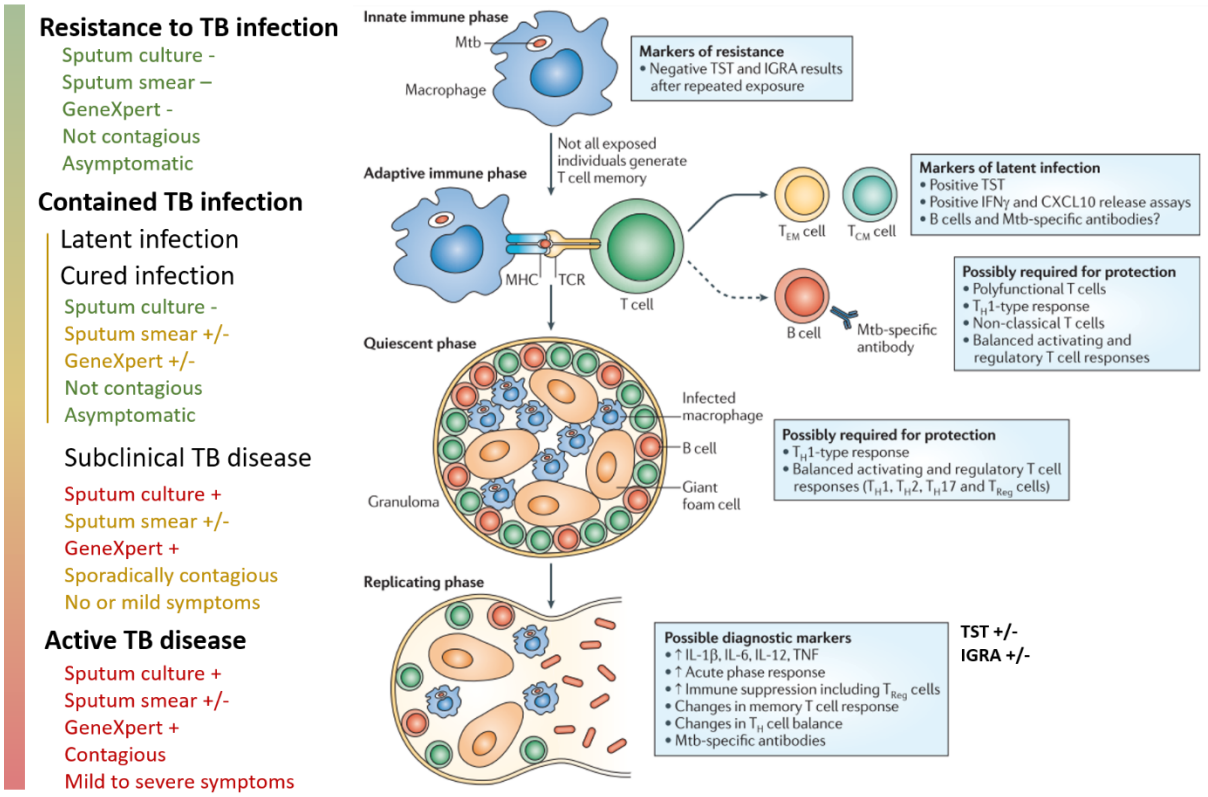

Figure 15. Immune host biomarkers across the TB spectrum, in relation with granuloma pathophysiology. In latent TB infection, sputum smear and GeneXpert are negative, whereas they may be persistently positive in cured infection due to dead bacilli detection. Adapted from Walzl *et al.,* 2011[68] and Pai, 2016[70].

2.5.2 Importance of the TB recall antigen choice

A large majority of the currently described T-cell epitopes (nearly 500) are highly conserved within the MTBC, hinting that they are selected as essential genes and that despite the partial protection that T-cell recognition offers, Mtb evolutionarily benefits from it[71]. However, the immune response to Mtb is characterized by the immunodominance of a select few of these antigens, which induce the majority of the anti-Mtb T-cell response. Although it is unclear whether T-cells specific of these dominant antigens actually efficiently recognize Mtb-infected cells or if they act as decoys[72,73], the associated T-cell responses are frequently detectable in people with Mtb infection, which justifies the use of these antigens for immune biomarker measurement. However, the accuracy of such antigens for TB diagnostic, prognostic, and treatment monitoring is decreased by a number of factors. Many Mtb T-cell epitopes are conserved across other *Mycobacteria* species, and some among other bacteria from the MTBC. This lowers the specificity of tests relying on these antigens because of BCG vaccination and exposure to environmental nontuberculous mycobacteria (NTM) or animal-adapted mycobacterial ecotypes[74]. This is further confounded by the heterogeneity of individual Mtb immune responses, in relation with microbiota composition, ethnic diversity, and inter-patient clinical background. In particular, for treatment monitoring biomarkers, it is suspected that TB therapy may selectively impact targeted immune responses to some antigens and not others; hence, there is a clinical need for novel efficient antigens for this purpose (Table 3). Many of the studies focusing on the topic are currently investigating latency-associated antigens.

Table 3. Common TB antigens used in or investigated for immunodiagnostics and/or vaccination.
Adapted from Meier *et al.,* 2018[75].

Antigen	Full name	Specificity	Uses in immunodiagnostics	
Validated Mtb infection-associated antigens				
PPD	Purified Protein Derivative	Mtb, BCG, NTM	TST	Standardized protein cocktail
ESAT-6	Early Secreted Antigenic Target 6kDa	Mtb	IGRA T-cell stimulation	>15aa peptide
CFP-10	Culture Filtrate Protein 10kDa	Mtb	IGRA T-cell stimulation	8-13aa peptide
Investigated latency-associated antigens				
HBHA (Rv0475)	Heparin-binding hemagglutinin	Mtb, NTM	IGRA T-cell stimulation	Recombinant full protein Differential methylation
DosR-encoded antigens (*e.g.* Rv0081, Rv1733c)		Mtb	Vaccine targets LTBI/aTB discrimination	Full proteins
RD-1-encoded antigens (*e.g.* Rv2659c)		Mtb	Additional antigens for ELISPOT	Full proteins
Ag85 antigens (Ag85A, Ag85B, Ag85C)		Mtb	Vaccine targets LTBI/aTB discrimination	Full proteins

Footnotes: BCG: Bacille Calmette-Guérin. DosR : dormancy of survival region. IGRA: interferon-gamma release assay. NTM: non-tuberculous mycobacteria. RD-1: region of difference 1. Rv: rough morphology virulent. TST: tuberculin skin test.

2.5.3 State of the art of peripheral immune biomarkers for TB treatment monitoring

The main trends in TB treatment immunomonitoring research were summarized in Table 4. Additional information on their performance and limits is given thereafter.

Table 4. Current trends in TB treatment immunomonitoring research.
Adapted from Goletti *et al.*, 2018[13].

Test	Antigen(s)	Measured markers
Immune cell abundance	None	Monocyte/lymphocyte ratio[76], neutrophilia[77] NK cells[78], $CD4^+$ T-cells[79] or $CD8^+$ T-cells[80,81]
Commercial IGRAs (QFT-P, T-SPOT.TB)	ESAT-6/CFP-10 $CD8^+$ peptide pool	Mtb-specific plasma or T-cell IFN-γ levels[82,83]
Custom IGRAs (non-validated antigens)	HBHA	Mtb-specific plasma or T-cell IFN-γ levels, custom antigens[84]
T-cell functionality	ESAT-6/CFP-10 QFT-P antigens PPD HBHA	IFN-γ, IL-17, IL-2, and TNF production by T-cells; polyfunctionality[85,86]
T-cell phenotypes		Differentiation/memory markers (CD27, CD45RA)[87,88] Chemokine receptors (CXCR3, CCR6, CCR4)[89] Activation markers (CD38, HLA-DR)[90,91] Exhaustion markers (PD-1)[92,93]
Plasma or serum inflammation markers	None	IFN-γ, IL-10, IP-10, CRP, TNF, IL-6, IL-12, IL-4[94,95]
Gene expression tests	None	T-cell, cytolytic and IFN genes[96] Signatures of inflammation (RISK6[97,98])

Footnotes: QuantiFERON Gold In Tube (QFT-GIT) is an older version of QFT-P and as such is not discussed within the scope of this work.

2.5.3.i Historical approaches to TB treatment immunomonitoring: from TST to blood counts

The earliest applications of immunodiagnostic to TB were LTBI diagnosis tools which measure the immune response upon re-challenge with Mtb antigens. The oldest of these methods is the Tuberculin Skin Test (TST), first introduced in the early XX^{th} century and still widely used nowadays. During TST, Purified Protein Derivative (PPD, a standardized cocktail of mycobacterial proteins) is injected under the skin. A local hypersensitivity reaction ensues, which reflects PPD-specific cell-mediated immunity. The resulting induration is measured and compared to reference values to assess likelihood of TB infection. However, this test is lowly specific because of BCG vaccination and NTM exposure[99], lowly sensitive in immunocompromised patients, does not discriminate between ATB and LTBI, and is not clinically relevant for treatment monitoring. A few decades later, early descriptions of immune changes at the cellular level during TB were provided by animal models. In 1930, an important concept was established by studies on rabbit models: a higher circulating proportion of peripheral monocytes compared to lymphocytes (monocyte/lymphocyte (M/L) ratio) was associated with active TB[100]. Hematological abnormalities such as leukocytosis, neutrophilia,

or lymphopenia during pulmonary TB disease in humans were then described in the literature since the eighties[101]. Since, low monocyte proportions have been associated with higher rates of progression towards active TB[76], and neutrophilia and lymphopenia have been associated with higher mortality risks during TB treatment[77]. The relevance of the M/L ratio was confirmed in humans and it was shown to decrease after successful treatment[102]. These simple and robust markers are still used routinely by clinicians to assess TB treatment efficacy, along with fever and weight gain. However, to date, absolute numbers of peripheral lymphocytes and monocytes have not been consistently associated with microbiological TB clearance, and may reflect overall inflammation levels.

2.5.3.ii IGRAs for treatment monitoring: the limits of repurposing LTBI screening tests

Besides TST and complete blood counts, the most widely used and readily accessible TB immunodiagnostic tests are the Interferon Gamma Release Assays (IGRA). IGRAs measure T-cell IFN-γ production after whole blood antigen stimulation and are hence used as tests for LTBI. Validated IGRA antigens include peptides from ESAT-6 and CFP-10, which are encoded by the RD-1 locus of the Mtb genome, and are absent from NTM and BCG[99]: they are hence recommended instead of TST because of their improved specificity. The first type of IGRA is T-SPOT.TB (Oxford Immunotec), an enzyme-linked immunosorbent spot test (ELISPOT) that quantifies IFN-γ-producing cells after ESAT-6/CFP-10 stimulation. As this test requires PBMC isolation, the other commercially available IGRA is more frequently used, especially in settings were the required equipment or scientific expertise are not readily available. The QuantiFERON-TB Gold Plus test (QFT-P, Qiagen) measures plasma IFN-γ levels by enzyme-linked immunosorbent assay (ELISA) after whole blood stimulation by two stimulation conditions: TB1 (ESAT-6/CFP-10, $CD4^+$ T-cell stimulation) and TB2 (same stimulation, enriched with an undisclosed peptide pool designed to induce $CD8^+$ T-cell stimulation). Because PPD and QFT-P antigens are well-described, validated, and commercially available, they are a good standardized antigenic stimulation possibly available in laboratories from middle- and lower-income settings, and applicable to a variety of different studies on TB immune biomarkers, including treatment immunomonitoring. However, neither TST nor IGRA can differentiate between active and latent infection, and accordingly, attempts to use for them for treatment response monitoring in relation with mycobacterial clearance have met limited success[13], although a decrease in TB2 IFN-γ has been observed after cure in a minority of studies[82,83].

2.5.3.iii Heparin-binding hemagglutinin (HBHA) IFN-γ in the TB spectrum

HBHA is an adherence protein that contributes to TB dissemination by inducing its binding to lung epithelial cells[103], a pivotal process for latency. Despite the fact that HBHA is produced by all members of the MTBC as well as other mycobacteria, plasma IFN-γ responses to recombinant methylated *Mycobacterium smegmatis* HBHA (rmsHBHA) as an additional stimulation antigen in combination with QFT-P have been shown to stratify Mtb infection stages and progression to disease since the early 2000's[104–108]. Low levels of IFN-γ production in response to rmsHBHA stimulation have been associated with active TB disease as opposed to latent infection. Other studies have then contributed to further characterizing these trends by showing that both $CD4^+$ and $CD8^+$ T-cells secreted IFN-γ upon HBHA stimulation[109], that the cytokine profile of HBHA-primed $CD4^+$ T-cells beyond just IFN-γ also stratified LTBI and ATB[110], and that HBHA-induced polycytotoxic $CD4^+$ T-cells were associated with Mtb infection control[111]. More recently, in two studies from 2017 and 2018, plasma rmsHBHA IFN-γ has also shown promise to monitor TB treatment outcomes in children[84] and adults, including BCG-vaccinated populations[112] (Figure 16). However, this has been explored only in small cohorts from non-TB endemic settings, or with no drug-resistant TB patients.

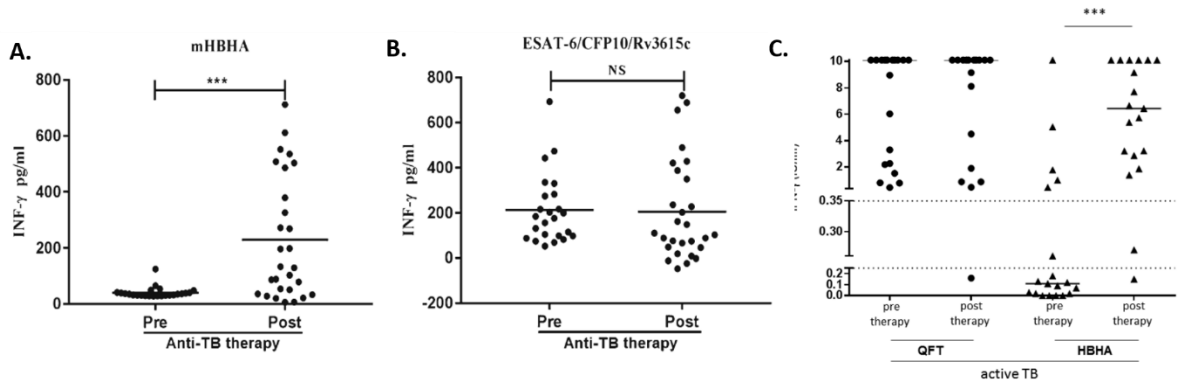

Figure 16. IFN-γ response to HBHA or QFT-GIT antigens in active TB patients before and after treatment.
A. and **B.** Data from 24 untreated drug-susceptible TB patients and 28 cured patients. Source: Wen *et al.*, 2017[112].
C. Data from 19 children with drug- susceptible TB before and after treatment. Source: Sali *et al.*, 2018[84]. Here, "HBHA" or "mHBHA" both refer to purified recombinant methylated HBHA.

2.5.3.iv T-cell phenotype and functionality characterization during TB treatment

As a plasma-based assays measuring secreted inflammation markers and cytokines showed promise for treatment monitoring, efforts were made to better understand the characteristics of T-cell response during TB treatment. Because of their central role in TB immunobiology, most studies on the topic investigate IFN-γ, IL-2, and/or TNF functionality in antigen-stimulated $CD4^+$ or $CD8^+$ T-cells. Upon Mtb antigen stimulation, IFN-γ-producing T-cells are generally believed to correspond to Mtb-specific cells, but the presence of basal IFN-γ secretion and the unclear role of IFN-γ-secreting $CD4^+$ T-cells in TB clearance challenge this assumption. An increasing number of studies hence rely on T-cell selection with antigen-loaded multimers to improve specificity. T-cell surface phenotypes are often investigated in parallel, in an attempt to understand the relation between cytokine profiles, differentiation, activation, and chemotaxis during treatment. The main trends were summarized in Table 5.

Table 5. Main markers investigated for TB immunomonitoring in relation with canonical T-cell differentiation stages.

Marker	Function	T_N	T_{CM}	T_{EM}	T_{EMRA}	Association with TB control
CD45RA	Differentiation	+	-	-	+	CM associates with LTBI EM associates with ATB Impaired CM and EM associate with disease severity
CD45RO		-	+	+	-	
CCR7	Chemokine receptor Differentiation	+	+	-	-	
CD27	Co-stimulation Maturation	+	+	+/-	-	Stratifies LTBI and ATB During treatment, decrease of $CD27^+$ $CD38^+$ Mtb-specific $CD4^+$, increase of other $CD27^+$ $CD38^+$ Mtb-specific $CD4^+$
CCR4	Chemokine receptor Th2 response	+/-	+	+	+/-	With CD27, stratifies LTBI and ATB
CCR6	Chemokine receptor Th17 response	-	+	+	+/-	Define main lymphocyte compartments involved in anti-TB response Differential expression between lungs and blood CXCR3+ CCR6+ in the lungs associate with TB control*
CXCR3	T-cell homing Th1 response Receptor for IP-10	-	+	+	+	
Perforin	Cytotoxicity Pore formation	-	+/-	+	+	Increased in ATB patients after 2 months of treatment
CD38	Activation	+	-	-	-	Decrease during treatment Correlation with culture conversion time
HLA-DR	Activation Antigen presentation	-	+/-	+	-	
PD-1	Exhaustion Inhibition of effectors	-	+	+	+	Decrease during treatment Reverse correlation with CD27 expression

Footnotes: T_N: naïve T-cells. T_{CM}: central memory T-cells. T_{EM}: effector memory T-cells. T_{EMRA}: effector T-cells re-expressing CD45RA. T_{SCM} (stem cell memory) and T_{TM} (transitional memory) T-cells were not represented. The definition of the different memory phenotypes was adapted from Mahnke *et al.*, 2013[113].
*data from non-human primate experiments[114].

The differential involvement of T-cell memory subsets has been studied across the spectrum of TB infection[115,116] and the during treatment[117–119]. In Mtb-specific total and $CD4^+$ T-cells, effector memory (EM) phenotypes have been associated with active TB disease, whereas central memory (CM) T-cells have been associated to latency, and increased upon anti-TB treatment in ATB patients. Impaired $CD4^+$ CM and EM responses to Region of Difference 1 (RD1) proteins before treatment have also been correlated with TB disease severity. After treatment, a decrease in total peripheral Mtb-specific $CD8^+$ T-cells[120] and in CM cells more specifically[81] has been observed, coupled with an increase in perforin production by effector cells[121].

In addition, the IFN-γ/IL-2/TNF functional profile of Mtb-specific $CD4^+$ T-cells has been shown to correlate with their degree of differentiation, prompting investigations of T-cell functionality during treatment[122]. The role of polyfunctionality (production of more than 1 cytokine simultaneously) in TB remains conflicting as it has been alternatively associated with TB disease and shown to decrease following TB treatment[123], or associated to latency and TB protective immunity as opposed to the production of a single cytokine type[124]. Other studies have further characterized the polarization of helper T-cells during TB by measuring the expression of chemokine receptors in parallel with cytokine production (IFN-γ or IL-17). Th1 lymphocytes are known to predominate compared to other T helper categories during TB infection[125], appearing as low-differentiated $CXCR3^+$ $CCR6^+$ cells in the blood and highly differentiated $CXCR3^{+/-}$ $CCR6^-$ cells in the lungs[89]. A recent study on non-human primates highlighted that recruitment of $CXCR3^+$ $CCR6^+$ cells at the site of infection was associated with TB control[114]. However, the abundance variations during treatment of T-cells expressing canonical and non-canonical combinations of these markers remain unclear.

Finally, these observations have been supplemented by studies on the surface expression of differentiation, maturation, and activation markers. CD27 expression on IFN-γ^+ and/or TNF^+ Mtb-specific $CD4^+$ T-cells has been studied extensively and shown to stratify LTBI and ATB, in particular when coupled with CCR4 expression[87]. CD27 associates with lung pathology[126] and disease severity[127]. A decrease in PPD-stimulated IFN-γ^+ $CD27^+$ $CD38^+$ $CD4^+$ T-cells was documented in treated TB patients, and a correlation between CD38 and HLA-DR expression on Mtb-specific $CD4^+$ T-cells and time to stable sputum culture conversion during treatment was established[91]. More recently, a comprehensive study demonstrated that decreased expression of HLA-DR and increased CD27 and CD153 expression on Mtb-specific $CD4^+$ T-cells

was associated with TB treatment[127], accompanying a decrease in PD-1 expression[93]. Finally, still on Mtb-specific IFN-γ$^+$ memory CD4$^+$ T-cells, loss of CD27 expression was correlated with increased PD-1 expression, and discriminated between LTBI and treated TB[88], suggesting that assimilating treated TB to a "latency-like" state has limits, and further reflecting the complexity of TB memory responses during and after treatment. Overall, the extensive body of literature on this topic shows that measurable T-cell responses to Mtb depend on the antigen nature, amount, and availability[128]. This further reinforces the concept that finding the right antigen to detect the right biomarker is pivotal to monitor TB treatment.

2.5.3.v Plasma inflammation markers and transcriptomic signatures for treatment monitoring

Finally, this section briefly summarizes topics that are relevant in the landscape of modern TB research, but are not the main focus of this thesis. Historically, plasma levels of the chemokine IP-10 (IFN-γ inducible protein 10) have been extensively studied across the different TB stages. Elevated IP-10 is associated with active TB and decreases after therapy[129]. This trend is conserved in HIV-positive patients, and is also verified when using dried blood spot assays (in EPTB)[130], which is relevant for implementation in lower-income settings. C-reactive protein (CRP) has also been shown to correlate with plasma IP-10 during TB, is associated with microbiological and radiological signs of TB and also decreases during treatment[131]. More recently, studies screening high numbers of other potential plasma immune biomarkers for treatment monitoring have helped narrow down options. Procalcitonin (PCT), IL-1β, and IL-6 emerged as molecular markers that are strongly modulated by treatment[132]; but in contrast, most pro-inflammatory cytokines were shown to display no significant changes (*e.g.* IL-2) or to undergo important unrelated fluctuations (*e.g.* TNF) in plasma during treatment[95]. However, for any of the above molecules, specificity to Mtb infection and association with mycobacterial clearance assessed by sputum culture remain to be established consistently. As a consequence, most investigated blood transcriptomic signatures of TB cure have also examined genes associated with inflammation. A 2012 transcriptional profiling study demonstrated that an initial downregulation of inflammatory mediators was linked with rapid killing of dividing Mtb, whereas longer-term changes in other targets were associated with lung damage improvement[96]. This led to several princeps studies identifying robust signatures of TB disease risk (16-gene signature by Zak *et al.,* 2016[97]), TB diagnostic (3-gene signature by Sweeney *et al.*, 2016[133]), treatment outcome prediction (5-gene signature by Thompson *et al.,* 2017[134]), or all of the above (6-gene signature "RISK6" by Penn-Nicholson *et al.,* 2020[98]; Figure 17).

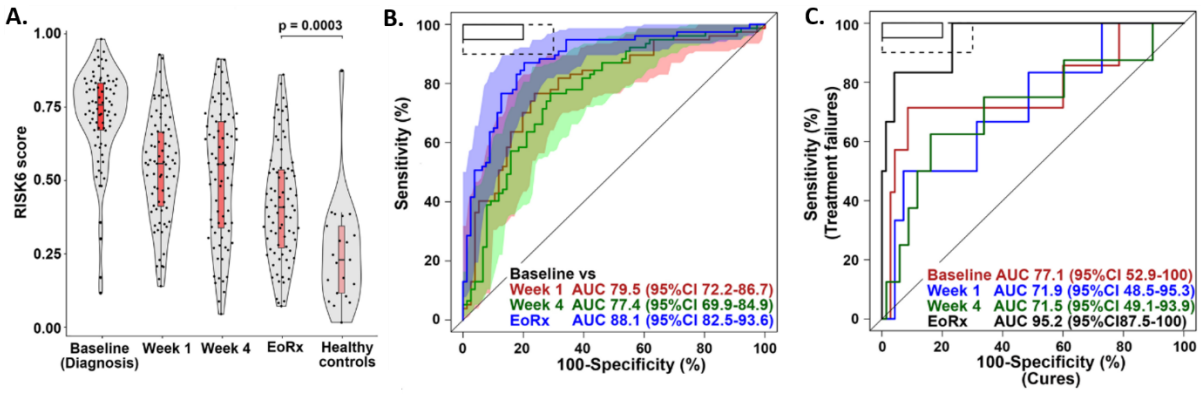

Figure 17. Performance of the RISK6 signature for PTB treatment monitoring.
A. RISK6 scores during treatment (formula based on the expression levels of each gene in the signature). EoRx: end of treatment. Cases: n=87. Controls: n=21. **B.** Receiver Operating Characteristic (ROC) curve illustrating the performance of RISK6 to discriminate each timepoint during treatment from the baseline gene expression at treatment initiation (n=87) C. ROC curve showing the performance of RISK6 for treatment failure prediction. Cured: n=70. Failure: n=7. Source: Penn-Nicholson et al., 2020[98].

Chapter 3. High-dimensional cytometry for new insights on TB treatment immunomonitoring.

3.1 The limits of flow cytometry

The cellular immune response to Mtb during treatment has been extensively studied over the past decades. Flow cytometry, which enables single cell analysis of the expression of surface, cytoplasmic, and nucleic markers, has been an indispensable tool for understanding the role of T-cell subpopulations across the spectrum of TB disease. This technique, invented in the late 1960s, was a revolution at the time and has generated countless key discoveries in fundamental and translational immunology. It has contributed so greatly to our modern understanding of cellular immunology, that the technique has become almost indissociable from the field of study. However, as we enter a numeric era, high-powered computers and analysis pipelines are becoming more and more accessible, both in terms of cost-effectiveness and expertise. High-dimensional proteomic, genomic, and transcriptomic analyses have become approachable and have brought new research frameworks and perspectives. In this context, the technical restrictions of modern conventional flow cytometers are limiting. In conventional flow cytometry, cell samples are stained with monoclonal antibodies specific of cellular markers of interest and tagged with fluorophores. Cells flow one by one through laser beams, and the photons emitted upon fluorophore excitation are detected, converted into electric signals, and processed by a computer (Figure 18.A.). However, the number of parameters that can be stained simultaneously is restricted, because the emission spectra emitted by different fluorophores overlap, and the spillover of signal from a given fluorophore into the detection channel of another fluorophore hinders the precise measurement of marker expression. Hence, despite advances in hardware and fluorochromes, most routinely used conventional flow cytometers enable the detection of about 18 parameters simultaneously. More recently, the detection of up to 28 to 30 colors has been reported with conventional flow cytometry[135], but only on certain machines, and provided that extensive panel design gymnastics are performed, followed by a variety of spillover compensation headaches. In the last decade, novel high-dimensional technologies have been developed to overcome the limits of spectral overlap, and are being increasingly used in translational cancer or infectious disease immunology studies: mass cytometry and spectral flow cytometry.

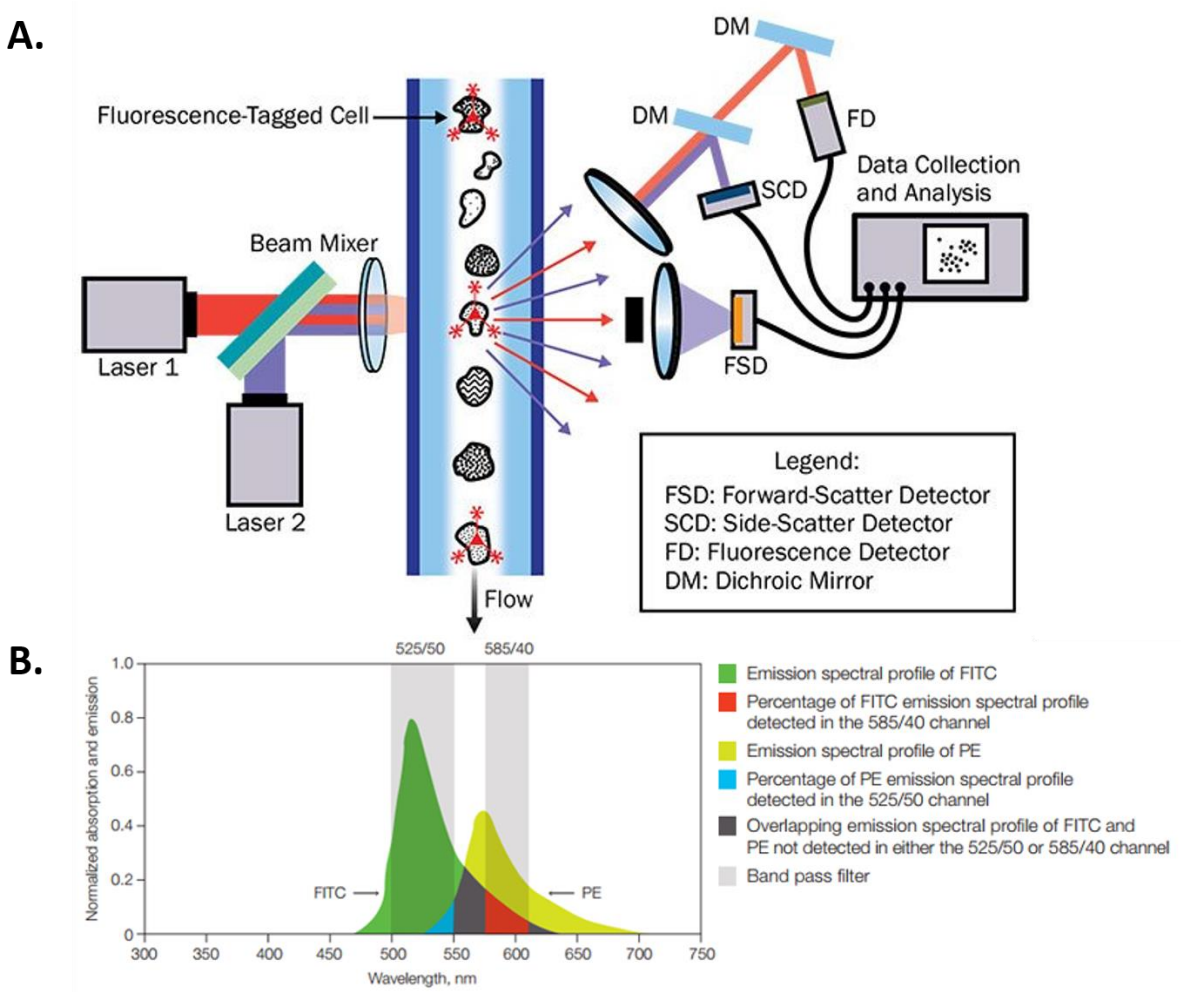

Figure 18. Conventional flow cytometry and technical limitations.
A. Principle of conventional flow cytometry. During conventional flow cytometry data acquisition, cells are stained with fluorescent-tagged antibodies. The liquid cell suspension is injected into the cytometer and a sheath fluid flow enables the cells to pass one-by-one in front of the laser beam(s). The resulting scattered light and emitted fluorescence are detected and converted into electric signals which are then digitalized. Source of image: Hamamatsu Photonics. **B. Spectral overlap.** The emission spectra of two commonly used flow cytometry dyes: fluorescein isothiocyanate (FITC, emission peak at 516nm) and phycoerythrin (PE, emission peak at 574nm) are represented. The red and blue colors represent the spillover of FITC signal detected in the PE-dedicated channel, and the spillover of PE detected in the FITC-dedicated channel, respectively. Source of image: Bio-Rad.

3.2 Principle of mass cytometry

Mass cytometry (or cytometry by time of flight, CyTOF) was invented in 2009 and combines a cytometry single cell injection procedure with a measurement system based on inductively coupled plasma time-of-flight mass spectrometry (ICP-TOF-MS)[136]. Instead of being tagged with fluorophores, mass cytometry antibodies are coupled to stable isotope lanthanide metal nanobeads. After staining with metal antibodies, single cells are nebulized into a chamber using a heated argon gas flow, and ionized through a beam of argon plasma (5,000°C). The resulting ion cloud is accelerated into a quadrupole whose electromagnetic field ejects low mass ions (atomic mass (m)/charge (z) < 80). This eliminates plasma ions (*e.g.* Ar^+, O_2^+) and lighter ions that come from the biological sample (*e.g.* C^+, Cl^-), which enables to measure uniquely the atomic mass of the lanthanides from the cell staining. This is performed by recording the time of flight of the ion cloud between the moment when it is accelerated into a vacuum chamber, and the moment each ion hits the detector. After digitization and conversion of the output signal, the metal composition of the sample is obtained and samples are analyzable with analysis methods similar to those used in conventional flow cytometry.

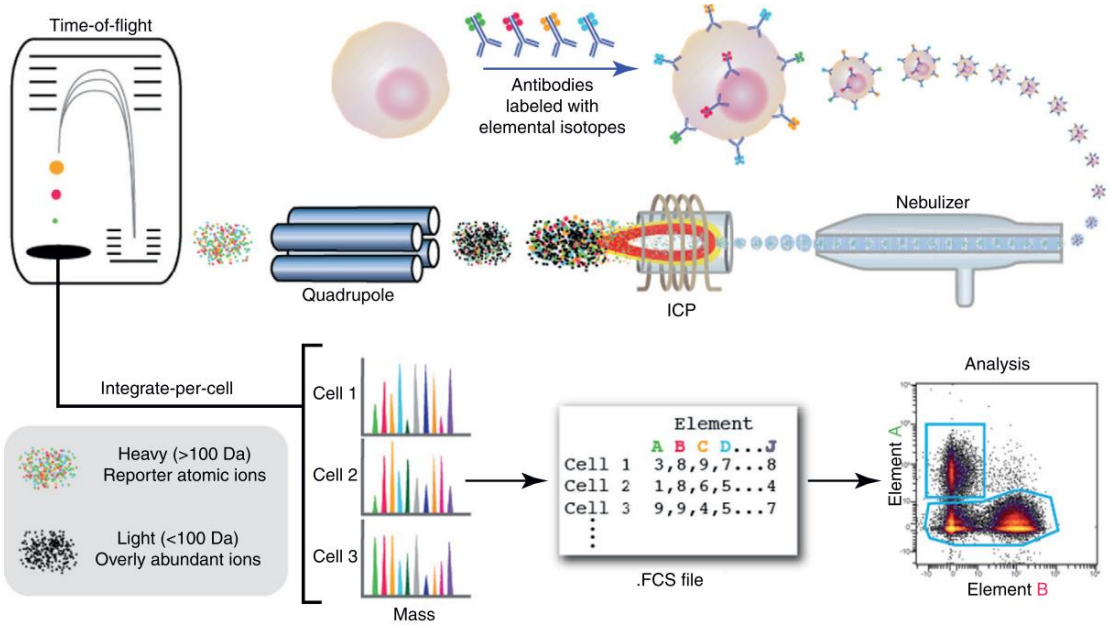

Figure 19. Principle of mass cytometry.
"Reporter atomic ions" refers to ions derived from the multiatom metal structures used for cell staining. The colored histograms refer to the mass signals detected for each cell (x axis: stable isotope mass in Da; y axis: signal intensity). Overlap between mass signals is extremely limited. ICP: inductively coupled plasma. Source: Bendall *et al.*, 2012[137].

Since it uses elemental isotope staining instead of fluorescence, mass cytometry is free from spectral overlap, which greatly improves signal resolution. It is estimated that a thousandfold abundance difference is required between two adjacent metal isotopes before spectral overlap caused by insufficient mass resolution needs to be compensated (*i.e.* > 0.1% spillover). As most lanthanide metal tags generate signal intensities that range within twofold of one another[137], mass cytometry enables rigorous and standardized measurement of up to 45 parameters simultaneously[138,139]. A major advantage of mass cytometry is the possibility to easily stain different samples with individual intracytoplasmic Palladium isotope combination barcodes and pool them together prior to staining and acquisition, which greatly reduces inter-sample experimental variability. There are still sources of overlap or signal interference in mass cytometry, which arise either from isotopic impurities in the metal nanobeads (usually +/- 1 Da) or oxidation during ionization (+16Da generated by the two extra oxygen atoms). However, they are minor compared to fluorescence spillover, and can be avoided with rigorous panel design (*e.g.* making sure that markers which are often co-expressed are not stained with metal tags that only differ from 1 Da), instrument tuning and calibration (*e.g.* verifying that oxidation interference is <3% of signal measured from ^{139}La isotopes, which are easily oxidized), and experiment controlling (*e.g.* Mass Minus One experiments for panel isotopes that are easily oxidized)[140]. However, different limitations arose with the high resolution and the technical prowess that came with mass cytometry. The low sample throughput and labor intensity (the whole staining to data acquisition protocol takes at least 2 days), poor cell transmission efficiency (only 60-75% of the original sample actually generates data), and operating costs decrease the practicality and accessibility of this technology.

3.3 Principle of full spectrum flow cytometry

The other commercially available high-dimensional cytometry is full spectrum flow cytometry (also known as "spectral flow cytometry"), invented in the 2000s and first commercialized in 2012[141]. In contrast to conventional flow cytometry, it records the entirety of the emission spectra for each fluorochrome, from ultraviolet to infrared, across up to five lasers (Figure 20.A.). Each fluorochrome is thus associated to a unique spectral signature, which enables to mathematically discriminate between fluorophores that have identical emission peaks as other differences can be detected elsewhere on the spectrum (Figure 20.B.). Panels of up to 40 markers have been published as recently as last year using this technology[142].

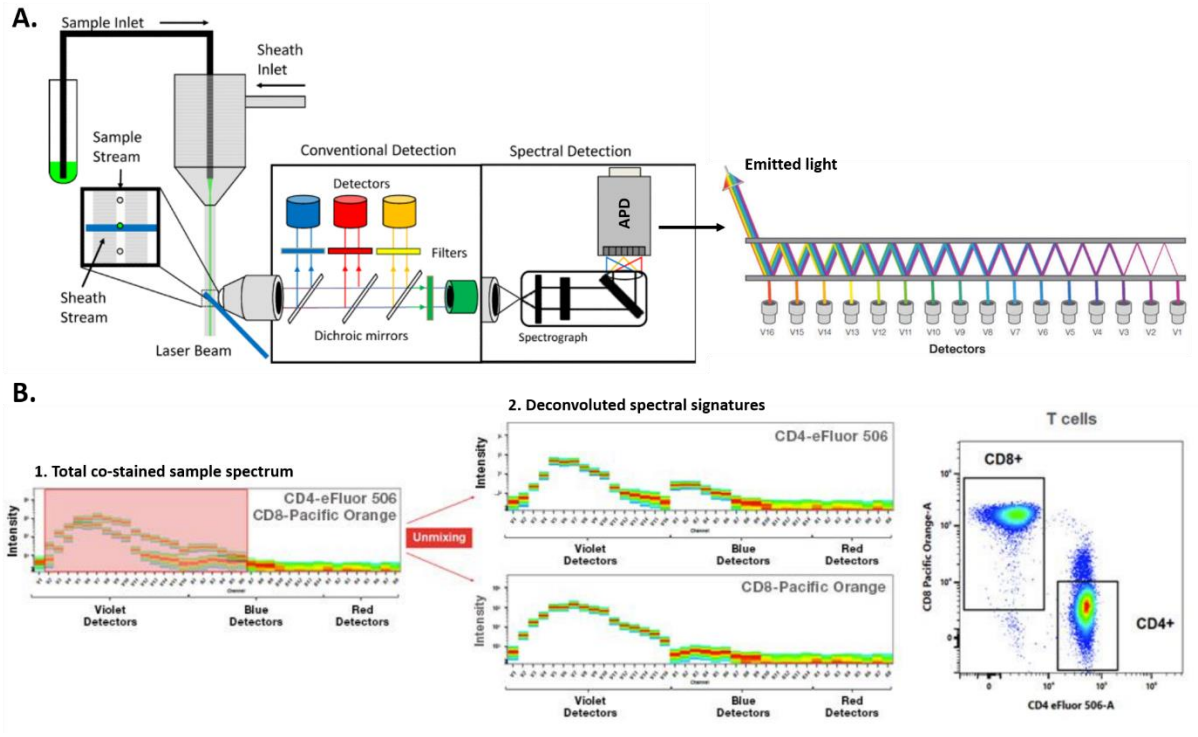

Figure 20. Principle of full spectrum flow cytometry.
A. While conventional flow cytometers use mirrors and filters to split emitted light towards individual detectors, full spectrum flow cytometers rely on a spectrograph to separate light. The individual beams are cast into a focusing lens prior to detection, then parallelized and directed linearly before reaching a detector. On the right, a violet laser avalanche photodiode (APD) detection system is represented, with its 16 individual channels. In total, on a 5-laser CYTEK Aurora spectral flow cytometer, the principle repeats itself for blue, yellow/green, red, and UV lasers, reaching a total of 64 channels. Source: adapted from Nolan, 2013[141] and ThermoFisher Scientific information sheets.
B. After data acquisition, the total recorded spectrum is mathematically separated into the autofluorescence signature of the sample, and the separate spectral signature of each fluorochrome used for staining. Source: ThermoFisher Scientific information sheets.

3.4 The case for high-dimensional analyses of TB immunity

The cellular immune response to Mtb is intrinsically multifaceted, and further complexified by mycobacterial mechanisms of immune evasion, individual immune heterogeneity, and poorly understood response to treatment. As shown in Chapter 2, the number of molecular markers and of cell phenotypes involved in TB control and of interest for monitoring keeps expanding as our knowledge of the disease progresses. To understand how all these separated insights relate to each other and are connected at the cellular and molecular levels during TB, a comprehensive, deeper profiling of the immune system in relation with TB stages is needed. With high dimensional single cell phenotyping technologies, insights that go beyond conventional binary immune cell classifications and relate to non-canonical populations are possible, while simultaneously assessing cellular function and overcoming the limitations of RNA analysis[143]. Mass cytometry approaches have been successfully applied to translational immunology topics ranging from immune alterations during sepsis[144] to mostly onco-immunology[145–147]. Although more recent, full spectrum flow cytometry is quickly garnering even more scientific attention and is more popular in the field of infectious disease immunology, as shown by recent high-impact contributions to influenza[148] and COVID-19 research[149]. There is evidence that these techniques have potentially huge implications on the identification of biomarker targets and the development of new therapeutic options. Yet, they are still niche techniques that mostly contributed to studying tumor microenvironments and are rarely used in infectious disease research, even more so for TB research given its complexity, long treatment durations, and skewed prevalence in lower-income settings.

RESEARCH OBJECTIVES

This research project was part of a larger multicentered study conducted within an international network of laboratory and health centers coordinated by the Mérieux Foundation ("*Global Approach to Biological Research, Infectious diseases and Epidemics in Low-income countries*"; GABRIEL). In relation with the scientific questions to address exposed previously, two main objectives were identified in this context.

First, by mobilizing local scientific capacity in areas heavily affected by TB, our work aimed to evaluate the relevance and monitoring performance of inexpensive, rapid, and easy-to-use tests for concrete short-term application in the communities concerned.

Then, by using state-of-the-art high-dimensional single-cell techniques available in France, we implemented an exploratory approach from bench to bioinformatics to discover targets for new tests that might improve diagnostic capabilities on the longer term.

The overarching aim of both aspects was to include the results in a framework which would help advance TB management research in accordance with clinical needs in high-burden countries, while remaining sustainable for local scientific partners.

PART B: RESULTS AND ORIGINAL PUBLICATIONS

1. The HINTT study: genesis of the project

The HINTT study (***H**BHA **In**terferon-γ Release Assay **T**est for **T**uberculosis*) was a multicentered study organized with partner institutions from the Fondation Mérieux GABRIEL network (***G**lobal **A**pproach to **B**iology **R**esearch, **I**nfectious diseases and **E**pidemics in **L**ow-income countries*)[150], which was created to build and enhance local research capacity in the field of infectious diseases in lower-income countries. The objective of HINTT was to evaluate the relevance of several immune tests and biomarkers for PTB treatment monitoring in TB-endemic countries. Partner institutions selected for participation in HINTT were located in countries with either high- or moderate nationwide TB incidence, had access to BSL-3 laboratory facilities, and had qualified staff available for TB patient follow-up and laboratory analyses (sputum culture and smear and whole blood sample processing). Hence, we conducted this study in five countries with the approval of national TB programs (Table 6).

Table 6. HINTT study clinical and laboratory partners.

Country	TB incidence[1]	City	Laboratory
Bangladesh	221	Dhaka	International center for diarrhoeal disease research, Bangladesh
Georgia	74	Tbilisi	National Center for Tuberculosis and Lung Diseases NTCLD
Lebanon	13	Tripoli	Laboratoire Microbiologie, Santé et Environnement, Université Libanaise
Madagascar	233	Antananarivo	Unité des Mycobactéries, Institut Pasteur de Madagascar
Paraguay	46	Asunción	Instituto de Investigationes en Ciencias de la Salud, Universidad Nacional de Asunción

Footnotes: 1. Nationwide TB incidence per 100,000 inhabitants, in 2019 (WHO Global TB Report).

The objective was to include 200 participants and to follow them at treatment initiation (T0), after the intensive phase of treatment (T1), at the end of therapy (T2; 6 months for drug-susceptible (DS-TB) patients, 9–24 months for drug-resistant (DR-TB) patients), and two months after the end of therapy (T3), which was not always possible as it was outside national TB program guidelines. Catchment areas were defined in each study sites in an attempt to minimize loss to follow-up. Patients from these areas presenting with suspected active PTB (symptoms, positive sputum smear and/or positive GeneXpert) were recommended by partner clinicians for laboratory diagnostic and drug susceptibility testing. Exclusion criteria were age < 15 years old, HIV co-infection, immunocompromising treatment, pregnancy, and diabetes mellitus. In the following analyses, patients with negative sputum culture at inclusion and patients lost to follow-up were excluded.

All the studies presented thereafter were nested within HINTT and involved subsets of patients from the same cohort, meeting the same inclusion and exclusion criteria, and followed according to the same timepoints. Technical details on microbiological diagnosis and drug susceptibility testing are detailed for all study sites in the Supplementary Data of Publication 1 (see Annexes). Conducting this multi-tool study with patients living in geographically distanced, lower-income settings was made possible by parsimonious biological sample use: all analyses were performed on samples derived from the same 10mL of whole blood collected at each timepoint (Figure 21).

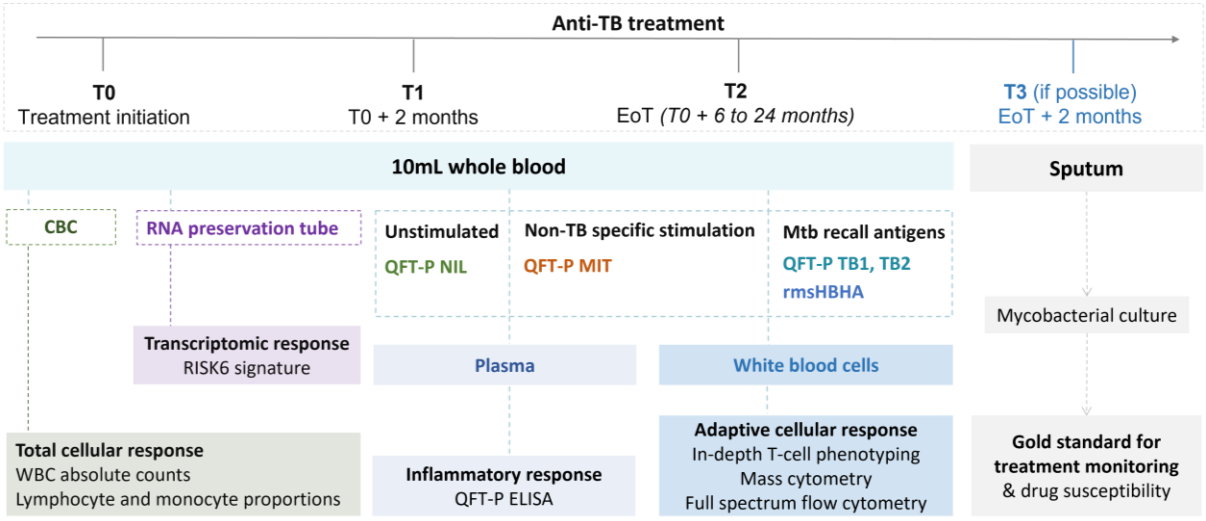

Figure 21. Sample collection and analysis workflow for the HINTT study.
Patient were followed at least until the end of treatment. Participants who were lost to follow-up before T2 were excluded from downstream analyses. As the T3 timepoint fell outside of national TB program-backed guidelines and most patients had achieved cured at T2, the rate of loss to follow up was much higher at T3. The transcriptomic response section (validation of the RISK6 signature[98]) is not within the scope of this thesis, and the associated original publication was added to the Annexes. CBC: complete blood count. EoT: end of treatment. QFT-P: QuantiFERON-TB Gold Plus. WBC: white blood cells. MIT refers to the Mitogen stimulation condition of QFT-P that contains phytohemagglutinin, a non-specific stimulator of T-cells.

2. Publication 1

Association of baseline white blood cell counts with tuberculosis treatment outcome: a prospective multicentered cohort study

Carole Chedid, Eka Kokhreidze, Nestani Tukvadze, Sayera Banu, Mohammad Khaja Mafij Uddin, Samanta Biswas, Graciela Russomando, Chyntia Carolina Díaz Acosta, Rossana Arenas, Paulo PR. Ranaivomanana, Crisca Razafimahatratra, Perlinot Herindrainy, Niaina Rakotosamimanana, Monzer Hamze, Mohamad Bachar Ismail, Rim Bayaa, Jean-Luc Berland, Giovanni Delogu, Hubert Endtz, Florence Ader, Delia Goletti, Jonathan Hoffmann.

International Journal of Infectious Diseases **2020; 100 (1); 199-206.**

Article summary

Mtb sputum culture is the gold standard for TB treatment monitoring. However, it is time-consuming and necessitates high-level biosafety laboratories. Quick alternatives that require less scientific expertise and laboratory equipment than most currently studied immunodiagnostic tests are needed to improve TB management in primary care settings. Here, we conducted a prospective international cohort study in five low-and middle-income countries with high- and moderate TB prevalence: Bangladesh, Georgia, Madagascar, Paraguay (>20 TB cases per 100,000 inhabitants per year) and Lebanon (11 cases per 100,000). We monitored the evolution of hematological parameters during pulmonary TB treatment, and characterized their association with microbiologically confirmed treatment failure.

Between December 2017 and February 2020, we enrolled 198 adult, non-immunocompromised, drug-susceptible (DS-TB) and drug- resistant (DR-TB) culture positive pulmonary TB patients. We followed 152 of them during treatment: at initiation (T0), at the end of intensive phase (T1), and at the end of treatment (T2) (23% lost to follow-up overall). At the end of treatment, 90.8% (138/152) of patients achieved cure. During treatment, white blood cell (WBC) absolute counts decreased, and lymphocyte proportions increased significantly. An increasing trend was observed in monocytes, but was inconsistent between study sites; hence, no conclusive result was obtained when monitoring the monocyte/lymphocyte ratio, a historical immune marker of TB resolution. In multivariate analyses (adjusted for age, sex, country of origin, drug resistance strain, and smoking habit), baseline high WBC counts and low lymphocyte proportions were associated with positive sputum culture results at the end of treatment (WBC > 11,450 cells/mm^3: p = 0.048; lymphocytes <16.0%: p = 0.039; WBC > 11,450 cells/mm^3 and lymphocytes <16.0%: p = 0.024; all thresholds were obtained using Receiver Operating Characteristic (ROC) curve cutoffs).

These trends are likely to reflect general clinical improvement in response to treatment, and are consistent with the characteristics of successful therapy. However, the association of these baseline parameters with treatment outcome may yield precious insights on treatment failure prediction, and warrants further investigation. A hypothesis is that patients with high baseline WBC counts and low lymphocyte proportions had highly inflammatory clinical

patterns, as a high WBC count is likely to reflect peripheral neutrophilia. This immune profile would be associated with more severe TB disease forms and could be more challenging to cure. Overall, as complete blood counts are performed routinely in health care centers worldwide and are usually evaluated in TB patients along the therapy course, our study suggests that they may be a helpful point-of-care tool to help clinicians identify which patients might be less responsive to treatment. They are cheap, quick tests that require a small volume of blood, their output is easy to interpret, and they can be performed without automated equipment. However, this warrants further investigation on larger cohorts.

International Journal of Infectious Diseases 100 (2020) 199–206

Contents lists available at ScienceDirect

International Journal of Infectious Diseases

journal homepage: www.elsevier.com/locate/ijid

Association of baseline white blood cell counts with tuberculosis treatment outcome: a prospective multicentered cohort study

Carole Chedid[a,b,*], Eka Kokhreidze[c], Nestani Tukvadze[c], Sayera Banu[d], Mohammad Khaja Mafij Uddin[d], Samanta Biswas[d], Graciela Russomando[e], Chyntia Carolina Díaz Acosta[e], Rossana Arenas[f], Paulo PR. Ranaivomanana[g], Crisca Razafimahatratra[g], Perlinot Herindrainy[g], Niaina Rakotosamimanana[g], Monzer Hamze[h], Mohamad Bachar Ismail[h], Rim Bayaa[h], Jean-Luc Berland[a], Giovanni Delogu[i], Hubert Endtz[j], Florence Ader[k], Delia Goletti[l,1], Jonathan Hoffmann[a,1], on behalf of the HINTT working group within the GABRIEL network

[a] Laboratoire des Pathogènes Emergents, Fondation Mérieux, Centre International de Recherche en Infectiologie, INSERM U1111, Lyon, France
[b] Département de Biologie, Ecole Normale Supérieure de Lyon, Lyon, France
[c] National Center for Tuberculosis and Lung Diseases (NCTBLD), Tbilisi, Georgia
[d] International Centre for Diarrhoeal Disease Research, Bangladesh (icddr,b), Dhaka, Bangladesh
[e] Instituto de Investigaciones en Ciencias de la Salud, National University of Asunción, Paraguay
[f] Hospital General de San Lorenzo, MSPyBS, Asunción, Paraguay
[g] Institut Pasteur de Madagascar, Antananarivo, Madagascar
[h] Laboratoire Microbiologie, Santé et Environnement (LMSE), Doctoral School of Sciences and Technology, Faculty of Public Health, Lebanese University, Tripoli, Lebanon
[i] Università Cattolica del Sacro Cuore, Milan, Italy
[j] Fondation Mérieux, Lyon, France
[k] Service des Maladies Infectieuses et Tropicales, Hospices Civils de Lyon, France
[l] Translational Research Unit, Department of Epidemiology and Preclinical Research, "L. Spallanzani" National Institute for Infectious Diseases (INMI), IRCCS, Rome, Italy

ARTICLE INFO

Article history:
Received 24 June 2020
Received in revised form 3 September 2020
Accepted 7 September 2020

Keywords:
Tuberculosis
Multi-drug resistance
Treatment monitoring
White blood cells
Lymphopenia
Immunomonitoring

ABSTRACT

Objectives: Tuberculosis (TB) is the leading infectious cause of death in the world. Cheaper and more accessible TB treatment monitoring methods are needed. Here, we evaluated white blood cell (WBC) absolute counts, lymphocyte, and monocyte proportions during TB treatment, and characterized their association with treatment failure.

Methods: This multicentered prospective cohort study was based in Bangladesh, Georgia, Lebanon, Madagascar, and Paraguay. Adult, non-immunocompromised patients with culture-confirmed pulmonary TB were included and followed up after two months of treatment and at the end of therapy. Blood counts were compared to treatment outcome using descriptive statistics, logistic regression, and Receiver Operating Characteristic (ROC) analyses.

Results: Between December 2017 and August 2020, 198 participants were enrolled, and 152 completed treatment, including 28 (18.5%) drug-resistant patients. The rate of cure at the end of treatment was 90.8% (138/152). WBC absolute counts decreased, and lymphocyte proportions increased throughout treatment. In multivariate analyses, baseline high WBC counts and low lymphocyte proportions were associated with positive sputum culture results at the end of treatment (WBC > 11,450 cells/mm^3: p = 0.048; lymphocytes <16.0%: p = 0.039; WBC > 11,450 cells/mm^3 and lymphocytes <16.0%: p = 0.024).

Conclusion: High WBC counts and low lymphocyte proportions at baseline are significantly associated with the risk of TB treatment failure.

* Corresponding author at: Laboratoire des Pathogènes Emergents, Centre International de Recherche en Infectiologie, 21 avenue Tony Garnier, 69365 Lyon Cedex 07, France.
E-mail address: carole.chedid@fondation-merieux.org (C. Chedid).
[1] These authors share the senior authorship.

https://doi.org/10.1016/j.ijid.2020.09.017
1201-9712/

Introduction

Tuberculosis (TB) is the leading cause of death by an infectious disease globally, responsible for 1.5 million deaths in 2018 (World Health Organization Geneva, 2019a). The treatment of active pulmonary TB lasts at least 6-months and can cause major side effects (World Health Organization Geneva, 2017, 2019a). Consequently, treatment adherence is poor, particularly in primary care settings (Woimo et al., 2017).

Mycobacterium tuberculosis culture from sputum samples is the gold standard for TB treatment monitoring (Wallis et al., 2016). However, it is time-consuming and requires high-level biosafety laboratories (Horne et al., 2010). Sputum smear microscopy is quicker for treatment monitoring, but it has limited accuracy (Ngabonziza et al., 2016). Hence, blood-based tests are a promising alternative. A variety of blood-based immunoassays, from interferon (IFN)-γ release assays to T cell activation tests, are being evaluated for treatment monitoring (Cingolani et al., 2012; Sali et al., 2018). However, in low-resource countries, these tests need to be adapted to limited laboratory equipment (MacLean et al., 2017) and a simple output (Goletti et al., 2018).

Hematological abnormalities-such as leukocytosis, neutrophilia, or lymphopenia-during pulmonary TB disease have been described in the literature since the eighties (Morris et al., 1989). Low monocyte proportions have been associated with higher rates of progression towards active TB (Rakotosamimanana et al., 2015). Neutrophilia and lymphopenia have been associated with higher mortality risks during TB treatment (Lowe et al., 2013). However, many these studies were either small case-control studies (Abay et al., 2018), focused on the risk of developing active TB disease (Kurup et al., 2016), or assessed kinetics during treatment and not association with treatment failure (Morris et al., 1989; Rakotosamimanana et al., 2015). Most available comprehensive studies were in low-burden, high-healthcare standards areas (Ritchie et al., 2016).

Here, we describe a prospective multicentered cohort study conducted in five low- and middle-income countries across four continents: Bangladesh, Georgia, Lebanon, Madagascar, and Paraguay. Four of these countries are on the 2019 WHO high incidence TB country list (≥20 cases per 100,000 population), with the exception of Lebanon (eleven cases per 100,000 population) (World Health Organization Geneva, 2019a). The target population was adult, HIV-uninfected, drug-susceptible (DS-TB), and drug-resistant (DR-TB) pulmonary TB patients.

This study's primary objective was to monitor the evolution of simple hematological parameters during pulmonary TB treatment in higher TB incidence settings: absolute WBC counts, lymphocyte, and monocyte proportions. These markers of inflammation were chosen because they are routinely monitored in primary care settings. The focus was kept on cellular parameters.

A secondary objective was to characterize their association with treatment failure, defined by sputum culture positivity (the gold standard) at the end of treatment, in relation to clinical and sociodemographic factors.

Materials and methods

Study design and sample population

Study design

This descriptive study was nested within a multicentered prospective cohort study evaluating the prognostic value of blood-based immunological markers for TB treatment monitoring, based in five partner institutions from the Mérieux Foundation GABRIEL network (Komurian-Pradel et al., 2013) with the approval of national TB programs: the international center for diarrheal diseases and research, Bangladesh (icddr,b) in Dhaka, Bangladesh; the National Center for Tuberculosis and Lung Diseases (NTCLD) in Tbilisi, Georgia; the *Laboratoire Microbiologie, Santé et Environnement (LMSE, Université Libanaise)*, in Tripoli, Lebanon; the *Institut Pasteur de Madagascar* in Antananarivo, Madagascar; and the *Instituto de Investigationes en Ciencias de la Salud (Universidad Nacional de Asunción; IICS-UNA)* in Asunción, Paraguay.

Ethical considerations

This study was conducted with the approval of the ethical boards in Bangladesh, the Research Review Committee and the Ethical Review Committee of icddr,b; in Georgia, the Institutional Review Board of the NTCLD (IORG0009467); in Lebanon, the institutional review board of NINI hospital (IRB-F-01); in Madagascar, the Ministry of Public Health and the Ethical Committee for Biomedical Research (reference number: n°099–MSANP/CERBM); in Paraguay, the Research Ethics Committee and the Scientific Committee of the IICS-UNA (IRB number: IRB00011984; Federal Wide Assurance number: FWA00029097). All recruited patients provided written informed consent.

Cohort recruitment, TB diagnosis, and patient follow-up

We calculated that a sample size of 156 was required to reach a level of significance of 95% and a power of 80%, assuming an average rate of treatment failure of 10% (World Health Organization Geneva, 2019a), a baseline prevalence of lymphopenia (<15% of total WBC) of 30%, and that treatment failure was three times more likely in patients with lymphopenia (Lowe et al., 2013). We aimed to include 200 participants to account for lower prevalence values, failure rates, or missing data.

Patients were recruited if diagnosed with microbiologically confirmed pulmonary TB (positive culture and/or sputum smear and/or GeneXpert; see "Microbiological diagnosis" section for further detail). Patients with HIV or diabetes mellitus (defined by HBA1C levels >6.5%; Cobas (Roche) automated analyzer) and children under 15 years were excluded. In downstream analyses, patients under immunocompromising treatment (corticosteroids, calcineurin inhibitors, biologics, or other chemotherapeutic agents), patients with negative cultures at inclusion, and patients who were lost-to-follow-up were excluded.

Patients were followed up: at inclusion (T0), after two months of treatment (T1), at the end of therapy (T2; 6 months for drug-susceptible (DS-TB) patients, 9–24 months for drug-resistant (DR-TB) patients), and two months after the end of therapy when possible (T3). All patients were on Directly Observed Treatment, Short Course (DOTS), and received treatment according to standard protocols (Aung et al., 2014; World Health Organization Geneva, 2017, 2019a). Detail of therapeutic regimens can be found in Supplementary Table 1.

Microbiological diagnosis and definition of treatment outcome

At each visit, at least one sputum sample per patient was collected for culture (solid and/or liquid media) and smear microscopy (Ziehl-Neelsen and/or Auramine O staining). Molecular amplification of *M. tuberculosis* DNA was conducted at inclusion (GeneXpert MTB/RIF, Cepheid, Sunnyvale, CA). Drug susceptibility testing (DST) and multi-drug resistance diagnosis were performed according to standard protocols (World Health Organization Geneva, 2019b). Microbiological methods and DST protocols are detailed in Supplementary Table 2.

Treatment outcomes were defined as follows: failed (positive sputum culture at T2); cured (negative sputum culture at T2 and no evidence of positive culture at T3); relapse or reinfection (culture conversion at T2 but positive culture recorded at T3); completed (patient not lost to follow up, but no available culture data at T2 or T3) (World Health Organization (WHO), 2013).

On-site whole blood collection and cell count

At each visit, 10 mL of whole blood were drawn, 1 mL of which was collected in EDTA tubes used for the present study. Complete blood counts were performed on automated analyzers (details of manufacturing references per study site are in Supplementary Table 2).

Clinical data collection and standardization

Data collection forms were created with clinicians from partner sites and standardized to ensure dataset homogeneity. Follow-up sheets were used to track sample handling and time flow from the collection in health centers to receipt in laboratories. All forms were translated into the local official language upon request from staff. Data were entered into the cloud-based database system CASTOR (CASTOR Electronic Data Capture, Version 1.4, Netherlands).

Descriptive statistical analysis

Data were cleaned and analyzed in R (version 3.6.2). As the sample size was small, discrete variables were analyzed using Fisher's Exact test with Bonferroni's post-hoc test (Kim, 2017). Normality was assessed using the Shapiro–Wilk Normality Test (test statistics available in Supplementary Table 3). Normal, continuous variables were analyzed with Student's *t*-test. Non-normal, continuous variables were analyzed with the Mann–Whitney test or the Kruskal–Wallis rank-sum test with Dunn's Kruskal–Wallis Multiple Comparisons post-hoc test (Dunn, 1964). Repeated measures of non-independent continuous variables were analyzed using the Friedman rank-sum test, with Wilcoxon-Nemenyi-McDonald-Thompson's post-hoc test (Paro Pedro et al., 2015).

Logistic regression and receiver operating characteristic (ROC) analyses

For these analyses, the assessed outcome was a recorded positive *M. tuberculosis* culture result at T2. Patients with unavailable culture data at T2 and patients with relapse were excluded from the analyses. The evaluated variables were leukocyte counts, lymphocyte proportions, and monocyte proportions at T0 or T1. If missing data exceeded 10% of the sample size, the variable was not considered. Otherwise, missing data were replaced by the most frequent group (categorical variables) or the mean (continuous variables). Highly skewed, non-normal continuous variables were log-transformed prior to analyses. Variables were first evaluated in univariate logistic regression analyses, then multivariate analyses were performed. Adjustment variables were selected as follows: sociodemographic variables of known clinical importance (*e.g.*, sex, country of origin), TB risk factors (*e.g.*, smoking), and additional sociodemographic variables that were at least moderately associated ($p < 0.10$) with the outcome in univariate analyses (*e.g.*, prison). Irrelevant adjustment variables were then removed by backward model selection. The combination of variables that minimized the Akaike Information Criterion (AIC) for most tested predictors, while including important adjustment variables, was selected (age, sex, smoking habit, drug sensitivity, country of origin). For lymphocyte proportions, odds ratios (OR) were calculated for each increase of 5.0% because the total range of measured values was 5.0–70.0%. Similarly, for absolute WBC counts, OR were calculated for each increase of 1000 cells per mm^3.

For both ROC analyses and logistic regression, since the sample size was small, model performance metrics (respectively, the Area Under the Curve (AUC) and the C-statistic) were corrected for optimism using bootstrap to assess model validity as described elsewhere (Smith et al., 2014).

Results

Demographic and clinical characteristics of the cohort

Between December 2017 and February 2020, 198 eligible patients with culture-confirmed active pulmonary TB were recruited in Dhaka (Bangladesh), Tbilisi (Georgia), Tripoli and Akkar (Lebanon), Antananarivo (Madagascar), and Asunción (Paraguay). As of July 2020, 152 of them were followed at least until the end of treatment and had available blood count data (Figure 1). As the T3 time point was later than the local TB program visits, the dropout rate was highest between T2 and T3 (26%).

Among patients followed until T2 at least, 18.4% (28/152) were diagnosed with DR-TB. The sociodemographic and clinical characteristics of DS-TB and DR-TB patients were comparable at inclusion (Table 1). The characteristics of patients at inclusion were compared between study sites (Supplementary Table 4). There was no significant difference in baseline absolute WBC counts and

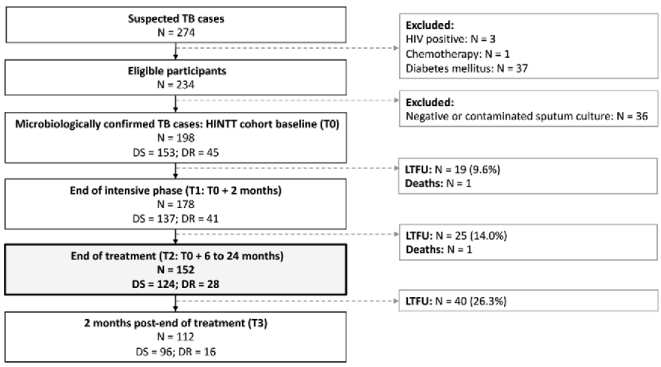

Figure 1. Inclusion and data collection process between December 2017 and July 2020.
DR: drug-resistant. DS: drug-susceptible. LTFU: lost to follow-up. TB: tuberculosis. HIV: human immunodeficiency virus. Treatment for DS-TB patients lasted 6 months. Treatment for DR-TB patients lasted 9–24 months.

Table 1
Sociodemographic and clinical characteristics of drug-susceptible and drug-resistant patients at inclusion.

N	ALL 152	DS-TB 124	DR-TB 28	*p DS-TB vs DR-TB*
Patient demographics				
Age (years)	28 (22–37.25)	28 (22–39)	27.5 (19.75–33.25)	*0.22*
Sex (male)	63.2% (96/152)	64.5% (80/124)	57.1% (16/28)	*0.52*
Country of origin				
Bangladesh	25% (38/152)	16.9% (21/124)	60.7% (17/28)	*>0.001*
Georgia	21.7% (33/152)	18.5% (23/124)	35.7% (10/28)	*0.072*
Lebanon	11.8% (18/152)	14.5% (18/124)	0	*0.045*
Madagascar	23.7% (36/152)	29% (36/124)	0	*>0.001*
Paraguay	17.8% (27/152)	21% (26/124)	3.6% (1/28)	*0.028*
BMI at inclusion	18.8 (17.1–21.4)	18.9 (16.9–21.4)	18.8 (17.5–21.0)	*0.87*
Sputum smear microscopy at inclusion				
High grade (2+ or 3+)	51.1% (76/149)	50.4% (61/121)	53.6% (15/28)	*0.83*
Low grade (1+ or scanty)	18.8% (43/149)	29.8% (36/121)	25% (7/28)	*0.81*
Negative	20.1% (30/149)	19.8% (24/121)	21.4% (6/28)	*0.79*
WBC absolute count at inclusion (/mm^3)	9590 (7468–11770)	9500 (7365–11640)	10,150 (7725–11850)	*0.54*
Lymphocytes at inclusion (% of WBC)	18 (14–24)	18 (14–23.2)	17 (13.8–24.5)	*0.65*
Monocytes at inclusion (% of WBC)	5 (2–7.48)	5 (2–8.23)	4 (3–5.25)	*0.35*
Number of household contacts	4 (3–6)	4 (3–6)	4 (3.75–6.25)	*0.91*
BCG vaccination	81.1% (99/122)	80.2% (81/101)	85.7% (18/21)	*0.64*
Risk factors and comorbidities				
Smoking	47.7% (72/151)	48% (59/123)	46.4% (13/28)	*1*
Alcohol abuse	21.9% (33/151)	23.6% (29/123)	14.3% (4/28)	*0.55*
Injectable drug use	3.3% (5/150)	2.4% (3/123)	7.4% (2/27)	*0.36*
Jail detention history	10.1% (15/149)	11.6% (14/121)	3.6% (1/28)	*0.44*
Chronic HCV infection	2.1% (3/146)	2.5% (3/118)	0	*1*
Other disease[a]	5.5% (7/128)	6.7% (7/105)	0	*0.35*
History of TB				
Previous TB	18.9% (28/148)	16.4% (20/122)	30.8% (8/26)	*0.1*
Of which are documented	78.5% (22/28)	70.0% (14/20)	88.9% (8/9)	*0.05*
Prior exposure to active TB patients	30.9% (46/149)	31.4% (38/121)	28.6% (8/28)	*0.22*
Previous TB treatment outcome				
Cured and completed	57.1% (12/21)	56.2% (9/16)	60% (3/5)	*1*
Completed	14.3% (3/21)	12.5% (2/16)	20% (1/5)	*1*
Treatment failure	14.3% (3/21)	18.8% (3/16)	0	–
Outcome not evaluated or unknown	14.3% (3/21)	12.5% (2/16)	20% (1/5)	*1*

DS-TB: drug-susceptible tuberculosis. DR-TB: drug-resistant tuberculosis. BMI: body mass index. IQR: interquartile range. WBC: white blood cells.
[a] Asthma, hypertension, inflammation. No patients presented with either pregnancy, renal disease, solid tumors or other cancers, HIV infection, chronic pulmonary disease, or chronic HBV infection. Data were given as % (N) or median (IQR).

lymphocyte proportions between cohorts, but several other parameters differed. Monocyte counts were significantly higher in the Lebanon and Madagascar cohorts than in the other sites. Patients in Bangladesh were younger than those recruited in Georgia and Paraguay. The body mass index (BMI) at inclusion of patients from Bangladesh and Madagascar was significantly lower than in the other study sites. Finally, BCG vaccination rates were significantly lower in the Georgia and Lebanon cohorts.

Microbiological characterization of treatment response over time and assessment of treatment outcome

All enrolled patients were positive for sputum culture at inclusion. Most patients were also positive for sputum smear microscopy (78.2%, 119/152) and/or GeneXpert (98.6%, 150/152). Culture positivity rates decreased significantly upon treatment (Table 2). No significant difference was detected between DR-TB and DS-TB patients (data not shown). At the end of treatment, 90.8% (138/152) of patients were cured, and eight had unavailable culture data and were classified as having completed treatment with no evidence of cure (5.3%, 8/152). One patient

Table 2
Microbiological characterization of treatment response and outcome definition.

Sputum culture results	Positive	Negative	Unavailable
Timepoint			
T0	100% (152/152)	0	0
T1	13.8% (21/152)	70.4% (107/152)	15.8% (24/152)
T2	3.3% (5/152)	94.8% (144/152)	1.9% (3/152)
T3	0.9% (1/112)	43.8% (49/112)	55.4% (62/112)

	All patients	DS-TB	DR-TB
Treatment outcome			
Cured and completed[a]	90.8% (138/152)	88.7% (110/124)	100% (28/28)
Completed[b]	5.3% (8/152)	6.5% (8/124)	0
Failed[c]	3.3% (5/152)	4% (5/124)	0
Relapse or reinfection[d]	0.7% (1/152)	0.8% (1/124)	0

T0: baseline. T1: baseline + 2 months. T2: end of treatment. T3: end of treatment + 2 months. DS-TB: drug-susceptible tuberculosis. DR-TB: drug-resistant tuberculosis.
[a] Positive culture at T2.
[b] Negative culture at T2 but positive culture at T3.
[c] Negative culture at T2 and no evidence of positive culture at T3.
[d] Patients not lost to follow-up, but with no available culture data at T2 or T3. Unavailable culture data were caused by contaminations or failure to expectorate sputum. Unavailable sputum smear microscopy results were caused either by technical issues or failure to expectorate enough sputum for both culture and smear.

(0.7%, 1/152) was culture-negative at T2 but had a positive culture result at T3, which was classified as relapse or reinfection. Treatment failure was observed in five DS-TB patients (3.3%, 5/152; Supplementary Table 5 for demographic and microbiological characteristics). Notably, 80% (4/5) of treatment failure patients had high sputum smear microscopy grades at baseline (2+ or 3+). At T1, two of them were culture positive, and one was microscopy positive.

Absolute WBC counts and lymphocyte proportions vary significantly throughout therapy

In all cohorts (n = 152), we observed a significant decrease in median absolute WBC counts during treatment (Figure 2A), and a significant increase in median lymphocyte proportions (Figure 2B). Monocyte proportions were heterogeneous between study sites and increased significantly only in the Bangladesh and Georgia cohorts (Figure 2C). At all time points, they were significantly higher in the Lebanon and Madagascar cohorts. Neutrophil responses were assessed in a subset of the cohort (n = 129) and decreased significantly during treatment (Supplementary Figure 1).

Early absolute WBC counts and lymphocyte proportions were significantly different between successfully and unsuccessfully treated TB patients

Absolute WBC counts, lymphocyte, and monocyte proportions were then compared between successfully and unsuccessfully treated patients with available culture data at T2 (n = 143; Figure 3). At baseline and after two months, unsuccessfully treated patients had significantly higher absolute WBC counts (Figure 3A) and significantly lower lymphocyte proportions than successfully treated patients (Figure 3B). No significant difference was observed for monocyte proportions (Figure 3C).

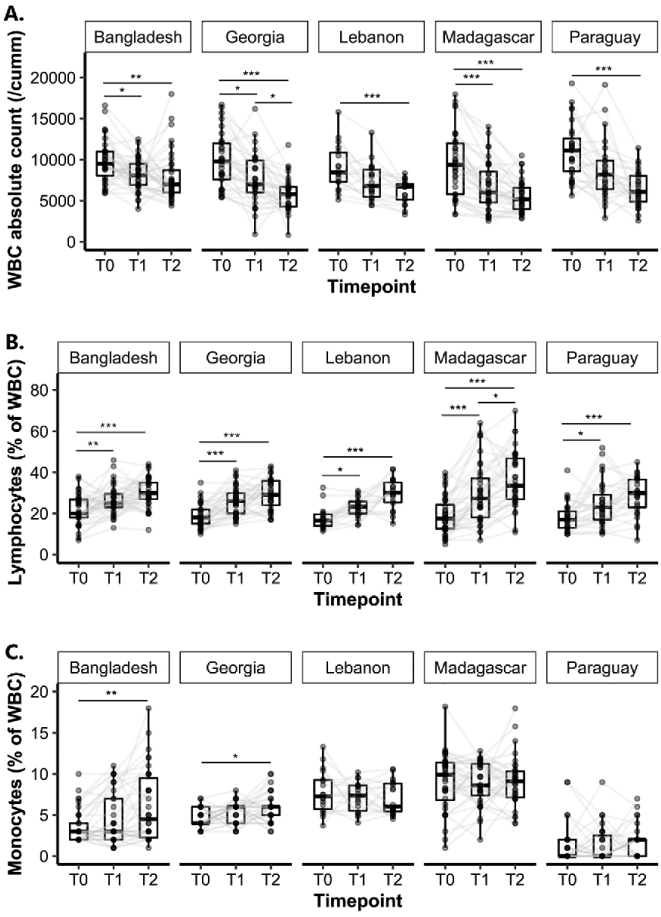

Figure 2. Dynamics of main white blood cell types throughout TB treatment.
(A) White blood cell (WBC) absolute count. cumm: cubic millimeter of whole blood. (B) Lymphocyte percentage of WBC. (C) Monocyte percent of WBC. Data are given as median + interquartile range. Each dot represents one patient at one timepoint. Grey lines connect data points from the same patient. T0: baseline. T1: baseline + 2 months. T2: end of treatment. Data were analyzed using Friedman's test, with the Wilcoxon-Nemenyi-McDonald-Thompson test as a post-hoc correction for multiple pairwise comparisons. *: $p < 0.05$. **: $p < 0.01$. ***: $p < 0.001$.

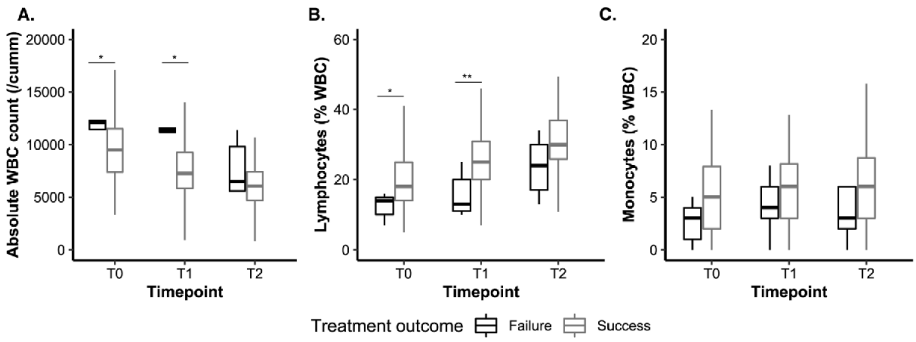

Figure 3. Main white blood cell types over time stratified by sputum smear microscopy and treatment outcome.
White blood cell (WBC) absolute counts (A), lymphocyte percent of WBC (B), and monocyte percent of WBC (C) were assessed over time in cured (n = 138) and treatment failure patients (n = 5). Data are given as median + interquartile range. T0: baseline. T1: baseline + 2 months. T2: end of treatment. T3: end of treatment + 2 months. cumm: cubic millimeter of whole blood. Treatment failure was defined as a positive sputum culture result at T2. Treatment success was defined as a negative sputum culture result at T2, and no evidence of positive culture at T3. Data were analyzed using the Mann–Whitney *U* test at each time point. *: $p < 0.05$. **: $p < 0.01$.

As most treatment failure patients had high AFB at baseline (2+ or 3+), we compared WBC absolute counts and lymphocyte proportions according to AFB results, in a subset of all patients presenting with high AFB at baseline (51.7%, 74/143). In this subset, median WBC and lymphocyte counts were similar at baseline, but at T1, WBC counts were higher, and lymphocyte proportions were lower in unsuccessfully than in successfully treated patients (Supplementary Figure 2).

Table 3
Association of selected baseline sociodemographic and clinical factors with treatment outcome.

Sociodemographic factors and clinical parameters at baseline and at 2 months	Descriptive analysis (n = 143)			Logistic regression - association with treatment failure					
	Cured (n = 138)	Failed (n = 5)	*p*	Univariate analysis		Multivariate analysis[a]			
				OR (95% CI)	*p*	aOR	*p*	AIC	Corrected C-statistic
Age (years)	27.5 (21–37)	31 (29–45)	*0.22*	1.02 (0.96–1.08)	*0.38*	–	–	–	–
Sex (male)	62.3% (86/138)	100% (5/5)	*0.15*	–	–	–	–	–	–
Drug resistance	20.3% (28/138)	0	*0.58*	–	–	–	–	–	–
Smoking habit	45.3% (62/137)	100% (5/5)	*0.021*	–	–	–	–	–	–
BMI at inclusion	18.8 (17.1–21.4)	16.0 (15.8–20.9)	*0.31*	0.87 (0.61–1.15)	*0.39*	0.74 (0.46–1.05)	*0.14*	44.68	0.862
Alcohol consumption	21.9% (30/137)	40% (2/5)	*0.32*	2.38 (0.3–14.9)	*0.35*	0.52 (0.02–8.55)	*0.66*	47.23	0.861
History of prison	8.9% (12/135)	40% (2/5)	*0.075*	6.94 (0.85–46.1)	*0.047*	1.96 (0.14–25.81)	*0.59*	47.16	0.856
Previous TB episode	19.4% (26/134)	20% (1/5)	*1*	1.07 (0.05–7.59)	*0.95*	1.72 (0.06–29.24)	*0.71*	47.30	0.860
Absolute WBC count at T0 (cells/mm^3)[b]	9500 (7403–11575)	12,100 (11470–12300)	*0.032*	1.26 (0.97–1.64)	*0.080*	1.40 (0.99–2.23)	*0.092*	43.87	0.862
Lymphocytes at T0 (% of WBC)[c]	18 (14–25)	14 (10–15)	*0.019*	0.32 (0.10–0.80)	*0.032*	0.09 (0.0040–0.52)	*0.042*	37.85	0.866
Monocytes at T0 (% of WBC)	4.9 (2–7.8)	3 (1–4)	*0.12*	0.75 (0.49–1.03)	*0.13*	0.21 (0.01–0.78)	*0.12*	40.57	0.861
Absolute WBC count at T1 (cells/mm^3)[b]	7385 (5907–9382.5)	11,440 (11200–11600)	*0.014*	1.04 (0.94–1.11)	*0.23*	4.75 (1.45–55.6)	*0.081*	35.03	0.860
Lymphocytes at T1 (% of WBC)[c]	25 (20.25–31)	13 (11–20)	*0.0079*	0.32 (0.11–0.68)	*0.0091*	0.18 (0.02–0.68)	*0.063*	39.25	0.864
Monocytes at T1 (% of WBC)	4 (3–8.4)	4 (3–6)	*0.41*	0.89 (0.66–1.16)	*0.40*	0.9 (0.4–1.95)	*0.79*	47.36	0.866
Baseline WBC > 11,450/mm^3	26.8% (37/138)	80% (4/5)	*0.024*	11.2 (1.60–223.5)	*0.031*	16.4 (1.52–592)	*0.048*	41.94	0.867
Baseline lymphocytes <16%	31.9% (44/138)	80% (4/5)	*0.044*	8.45 (1.21–168.0)	*0.061*	12.1 (1.44–264)	*0.039*	42.06	0.858
Baseline WBC > 11,450/mm^3 and lymphocytes <16%	14.5% (20/138)	60% (3/5)	*0.029*	8.77 (1.37–69.9)	*0.019*	29.9 (2.19–1088)	*0.024*	40.73	0.864

Data are given as % (n) or median (interquartile range). Treatment failure was defined as a positive sputum culture result at T2 or T3. BMI: body mass index. OR: odds ratio. aOR: adjusted odds ratio. AIC: Akaike Information Criterion. C-statistic: concordance statistic (corrected for optimism). WBC: white blood cells. T0: baseline. T1: baseline + 2 months. T2: end of treatment. T3: end of treatment + 2 months.
[a] Adjusted for age, sex, country of origin, drug resistance strain, and smoking habit.
[b] OR or aOR given for each increase in 1000 units.
[c] OR or aOR given for each increase in 5 units.

Low baseline lymphocyte proportions are significantly associated with a positive sputum culture at the end of treatment

Sociodemographic characteristics and blood counts at T0 and T1 were compared between cured (n = 138) and failed (n = 5) patients, and logistic regression was performed (Table 3). In univariate analyses, significant associations with treatment failure were detected for lymphocyte proportions at baseline (OR 0.32, 95% CI 0.10–0.80, p = 0.032) and at two months (OR 0.32, 95% CI 0.11–0.68, p = 0.0091). No significant association was detected for absolute WBC counts or monocytes proportions at T0 and T1. In multivariate analyses, low lymphocyte proportions at T0 remained moderately associated with treatment failure (adjusted OR 0.090, 95% CI 0.0040–0.52, p = 0.042).

ROC analyses were then performed to identify a threshold discriminating successfully and unsuccessfully treated patients based on baseline WBC counts and lymphocyte proportions (Supplementary Table 6). Baseline WBC counts predicted treatment outcome performed with an AUC of 0.788 (95% CI: 0.664–0.912; optimal cutoff >11,435 cells/mm^3). Baseline lymphocyte proportions performed with an AUC of 0.807 (95% CI: 0.671–0.943; optimal cutoff <16% of total WBC). The AUC of both variables combined into a new parameter performed better (AUC 0.841 95% CI 0.722–0.959).

Data was then stratified according to the ROC obtained cutoffs. Significant associations were observed in univariate analyses for patients absolute WBC > 11,450 cells/mm^3 (OR 8.45, 95% CI 1.21–168, p = 0.031), and for patients with both WBC > 11,450 cells/mm^3 and lymphocytes <16.0% at baseline (OR 8.77, 95% CI 1.37–69.8, p = 0.019), but not for lymphocytes <16.0% alone (p = 0.061). These variables remained moderately associated in multivariate analyses (WBC > 11,450 cells/mm^3: p = 0.048; lymphocytes <16.0%: p = 0.039; WBC > 11,450 cells/mm^3 and lymphocytes <16.0%: p = 0.024).

Discussion

In this multicentered prospective study, we monitored the evolution of absolute WBC counts, lymphocyte and monocyte proportions during pulmonary TB treatment, and described their association with treatment failure in five cohorts (Bangladesh, Georgia, Lebanon, Madagascar, and Paraguay), four of which were in high-incidence TB countries. We included 152 HIV-negative, culture-confirmed pulmonary TB patients, including 28 drug-resistant TB cases.

We showed that the lymphocyte proportions increased significantly during treatment, whereas the absolute WBC counts decreased significantly. These trends are indicative of general clinical improvement in response to treatment and are consistent with the characteristics of successful therapy. WBC counts are usually higher in TB patients than in healthy individuals, with distinct lymphocyte rates before and after TB treatment (Morris et al., 1989; Rakotosamimanana et al., 2015). No significant evolution of monocyte proportions during treatment was detected in our cohort, consistently with previous work (Rakotosamimanana et al., 2015).

Five patients had positive culture results at the end of treatment and were classified as treatment failure. Two of them had negative smears or cultures at T1, likely due to poor sputum quality. The main finding is that at baseline and after two months of treatment, unsuccessfully treated patients had significantly higher WBC counts and lower lymphocyte proportions than those successfully treated. In adjusted logistic regression analyses, treatment failure was significantly associated with high WBC counts and low lymphocyte proportions at baseline. This result is significant because WBC counts are usually evaluated in TB patients at baseline and along the therapy course. They are cheap, quick tests that are used routinely in health care centers worldwide. They require a small volume of blood, their output is easy to interpret, and they can be performed without automated equipment. Therefore, they may be a helpful point-of-care tool to help clinicians identify which patients might be less responsive to treatment. Larger studies on this topic are needed to assess whether early WBC or lymphocyte counts should be taken into account when considering changes to treatment composition or duration.

We hypothesize that patients with high baseline WBC counts and low lymphocyte proportions had highly inflammatory clinical patterns. In the context of mycobacterial infection, WBC counts are mostly reflective of neutrophil counts as markers of persisting inflammation or failure to clear the bacteria (Srivastava et al., 2014). Sustained inflammation in chronic TB infection has been described as an impairment of the TB-specific immune response and a marker of active disease (Sia and Rengarajan, 2019). Previous studies have highlighted a correlation between elevated neutrophils, lymphopenia, and TB disease severity, based on chest X-rays (Naghavi et al., 2017; Panteleev et al., 2017). Therefore, a hypothesis is that in this cohort, patients with high baseline WBC and low lymphocytes also had more severe TB manifestations and were less likely to achieve a cure.

We observed that in the subset of our cohort with high smear microscopy grades (n = 74), WBC counts and lymphocyte proportions at baseline were not associated with the treatment outcome; however, significant associations were detected at T1. This suggests that in patients who possibly had a higher bacterial burden, cellular inflammatory markers did not stratify risks of failure at baseline, but persistent cellular differences between failed and cured patients were noticeable after the intensive phase of treatment. A limitation is that TB disease severity at baseline could not be assessed in our cohort other than with microscopy (through chest X-rays, Erythrocyte Sedimentation Rate (ESR), or hemoglobin measurements). Further work is needed to assess the relevance of WBC and lymphocytes' association with treatment failure in cohorts with better-defined disease severity.

Moreover, a feature of TB infection is a delayed initiation of an adaptive response after infection, and lymphocyte anergy during chronic infection (Urdahl et al., 2011). This could indicate that *M. tuberculosis*-specific adaptive immunity might be hindered during treatment in patients with high WBC or low lymphocyte proportions. Alternatively, as blood counts are measured in the periphery, this may suggest that *M. tuberculosis*-specific lymphocytes are localized in the lungs for infection clearance: their decreased frequency in peripheral blood would indicate a persisting infection. We observed that the majority of unsuccessfully treated patients (80%, 4/5) presented either high WBC counts or low lymphocyte proportions at baseline, and 60% (3/5) with both, suggesting that the mechanisms behind a persistently activated innate immune response and an anergic adaptive immune response during anti-TB therapy might be linked. Consequently, whether systemic inflammation hinders TB treatment needs to be further investigated.

Our cohort included patients from developing countries, in diverse geographical areas, with varying sociodemographic backgrounds and living standards. We have also enrolled both DS-TB and DR-TB patients, which implies different clinical presentations of the disease. This design suggests similar trends might be occurring in heterogeneous settings and clinical contexts. However, it creates significant limitations and analytical challenges as it hinders the control of some patient- and pathogen-dependent factors such as antibiotic regimens, malnutrition levels, untested infections (*e.g.*, parasites), mycobacterial strains, and genetic background. Moreover, the sample size was small. To account

for these limitations, adjustment with the available patient-dependent factors and optimism corrections with a method adapted to small sample sizes (Smith et al., 2014) was performed. However, the clinical interpretation of these results should remain cautious, given the cohort's heterogeneity and size. Another limitation was the significant dropout rate, particularly between T2 and T3 (26%, 40/152), as T3 was not a timepoint that fell within the time frame of national TB programs. As a consequence, it is likely that some occurrences of TB relapse could not be recorded in our study.

In conclusion, this study confirms that WBC counts and lymphocyte proportions are simple biomarkers for TB treatment monitoring. In this cohort, early measurements of these parameters were associated with treatment failure; these results are encouraging but need to be confirmed on larger cohorts.

Author contributions

JH is the principal investigator and initiated the project together with DG, NT, SBa, GR, NR, and MH. Data was collected by EK, MU, SBi, CA, PR, CR, PH, and RB. CC performed all statistical analyses and wrote the manuscript. All authors have contributed to the content and have given their final approval.

Funding

This work was supported by Fondation Mérieux; Fondation Christophe et Rodolphe Mérieux; and Fondation AnBer. A minor part of the study was supported by the Italian Ministry of Health "Ricerca Corrente, Linea 3".

Conflicts of interest

MH, BMI, and RB had logistic support from the National TB program in Lebanon. DG reports personal fees from Quidel, Qiagen, Janssen, BioMérieux, and Celgene, outside the submitted work. All authors have submitted the ICMJE Form for Disclosure of Potential Conflicts of Interest.

Acknowledgments

We are grateful to the patients participating in our study and to the healthcare staff at our study sites.

Appendix A. Supplementary data

Supplementary material related to this article can be found, in the online version, at doi:https://doi.org/10.1016/j.ijid.2020.09.017.

References

Abay F, Yalew A, Shibabaw A, Enawgaw B. Hematological abnormalities of pulmonary tuberculosis patients with and without HIV at the University of Gondar Hospital, Northwest Ethiopia: a comparative cross-sectional study. Tuberc Res Treat 2018;2018:1–6.

Aung KJM, Van Deun A, Declercq E, Sarker MR, Das PK, Hossain MA, et al. Successful "9-month Bangladesh regimen" for multidrugresistant tuberculosis among over 500 consecutive patients. Int J Tuberc Lung Dis [Internet] 2014;18(10)1180–7. . Available from: http://www.embase.com/search/results?subaction=viewrecord&from=export&id=L600054258.

Cingolani A, Lepri AC, Castagna A, Goletti D, De Luca A, Scarpellini P, et al. Impaired CD4 T-Cell count response to combined antiretroviral therapy in antiretroviral-naive HIV-infected patients presenting with tuberculosis as AIDS-defining condition. Clin Infect Dis 2012;54(6):853–61.

Dunn OJ. Multiple comparisons using rank sums. Technometrics 1964;6(3):241–52.

Goletti D, Lindestam Arlehamn CS, Scriba TJ, Anthony R, Maria Cirillo D, Alonzi T, et al. Can we predict tuberculosis cure? Current tools available. Eur Respir J [Internet] 2018;1801089. doi:http://dx.doi.org/10.1183/13993003.01089-2018 Available from:.

Horne DJ, Royce SE, Gooze L, Narita M, Hopewell PC, Nahid P, et al. Sputum monitoring during tuberculosis treatment for predicting outcome: systematic review and meta-analysis. Lancet Infect Dis [Internet] 2010;10(6)387–94. doi:http://dx.doi.org/10.1016/S1473-3099(10)70071-2 Available from:.

Kim H-Y. Statistical notes for clinical researchers: Chi-squared test and Fisher's exact test. Restor Dent Endod 2017;42(2):152.

Komurian-Pradel F, Grundmann N, Siqueira MM, Chou M, Diallo S, Mbacham W, et al. Enhancing research capacities in infectious diseases: the GABRIEL network, a joint approach to major local health issues in developing countries. Clin Epidemiol Glob Heal 2013;1(1):40–3.

Kurup R, Flemming K, Daniram S, Marks-James S, Roberts Martin R. Hematological and biochemistry profile and risk factors associated with pulmonary tuberculosis patients in guyana. Tuberc Res Treat 2016;2016:1–6.

Lowe DM, Bandara AK, Packe GE, Barker RD, Wilkinson RJ, Griffiths CJ, et al. Neutrophilia independently predicts death in tuberculosis. Eur Respir J 2013;42(6):1752–6.

MacLean E, Broger T, Yerliyaka S, Fernandez-carballo BL, Pai M, Denkinger CM. A systematic review of biomarkers to detect active tuberculosis. Nat Microbiol [Internet] 2017;. doi:http://dx.doi.org/10.1038/s41564-019-0380-2 Available from:.

Morris CDW, Bird AR, Nell H. The haematological and biochemical changes in severe pulmonary tuberculosis. QJM [Internet] 1989;73(December (3))1151–9, doi:http://dx.doi.org/10.1093/oxfordjournals.qjmed.a068405 Available from:.

Naghavi M, Abajobir AA, Abbafati C, Abbas KM, Abd-Allah F, Abera SF, et al. Global, regional, and national age-sex specific mortality for 264 causes of death, 1980–2016: a systematic analysis for the Global Burden of Disease Study 2016. Lancet (North Am Ed) 2017;390(10100):1151–210.

Ngabonziza JCS, Ssengooba W, Mutua F, Torrea G, Dushime A, Gasana M, et al. Diagnostic performance of smear microscopy and incremental yield of Xpert in detection of pulmonary tuberculosis in Rwanda. BMC Infect Dis [Internet] 2016;16(1)1–7, doi:http://dx.doi.org/10.1186/s12879-016-2009-x Available from:.

Panteleev AV, Nikitina IY, Burmistrova IA, Kosmiadi GA, Radaeva TV, Amansahedov RB, et al. Severe Tuberculosis in humans correlates best with neutrophil abundance and lymphocyte deficiency and does not correlate with antigen-C specific CD4 T-Cell response. Front Immunol 2017;8(August):1–16.

Paro Pedro Hda S, Tonelli Nardi SM, Ferreira Pereira MI, Oliveira RS, Suffys PN, Gomes HM, et al. Clinical and epidemiological profiles of individuals with drug-resistant tuberculosis. Mem Inst Oswaldo Cruz 2015;110(2):235–41.

Rakotosamimanana N, Richard V, Raharimanga V, Gicquel B, Doherty TM, Zumla A, et al. Biomarkers for risk of developing active tuberculosis in contacts of TB patients: a prospective cohort study. Eur Respir J 2015;46(4)1095–103 2015/08/08.

Ritchie A, Singanayagam A, Manalan K, Connell D, Chalmers J, Sridhar S, et al. Serum inflammatory biomarkers as predictors of treatment outcome in pulmonary tuberculosis. Thorax [Internet] 2016;71(Supplement 3)A143. . Available from: http://ovidsp.ovid.com/ovidweb.cgi?T=JS&PAGE=reference&D=emed17&NEWS=N&AN=615030521.

Sali M, Buonsenso D, D'Alfonso P, De Maio F, Ceccarelli M, Battah B, et al. Combined use of Quantiferon and HBHA-based IGRA supports tuberculosis diagnosis and therapy management in children. J Infect [Internet] 2018;. doi:http://dx.doi.org/10.1016/j.jinf.2018.09.011 Available from:.

Sia JK, Rengarajan J. Immunology of Mycobacterium tuberculosis Infections. Microbiol Spectr 2019;7(4):3–22.

Smith GCS, Seaman SR, Wood AM, Royston P, White IR. Correcting for optimistic prediction in small data sets. Am J Epidemiol 2014;180(3):318–24.

Srivastava S, Ernst JD, Desvignes L. Beyond macrophages: the diversity of mononuclear cells in tuberculosis. Immunol Rev 2014;262(1):179–92.

Urdahl KB, Shafiani S, Ernst JD. Initiation and regulation of T-cell responses in tuberculosis. Mucosal Immunol [Internet] 2011;4(3)288–93, doi:http://dx.doi.org/10.1038/mi.2011.10 Available from:.

Wallis RS, Maeurer M, Mwaba P, Chakaya J, Rustomjee R, Migliori GB, et al. Tuberculosis-advances in development of new drugs, treatment regimens, host-directed therapies, and biomarkers. Lancet Infect Dis [Internet] 2016;16(4)e34–46. . Available from: http://www.journals.elsevier.com/the-lancet-infectious-diseases.

Woimo TT, Yimer WK, Bati T, Gesesew HA. The prevalence and factors associated for anti-tuberculosis treatment non-adherence among pulmonary tuberculosis patients in public health care facilities in South Ethiopia: a cross-sectional study. BMC Public Health 2017;17(269):1–10.

World Health Organization (WHO). Definitions and Reporting Framework for Tuberculosis–2013 Revision (updated December 2014) [Internet], vol. 18. Euro surveillance: bulletin Européen sur les maladies transmissibles = European communicable disease bulletin; 2013. . Available from: http://www.ncbi.nlm.nih.gov/pubmed/23611033.

World Health Organization Geneva. Guidelines for Treatment of Drug-Susceptible Tuberculosis and Patient Care [Internet], vol. 1. WHO press; 2017, doi:http://dx.doi.org/10.1586/17476348.1.1.85 Available from:.

World Health Organization Geneva. Global Tuberculosis Report 2019. 2019.

World Health Organization Geneva. WHO Consolidated Guidelines on Drug-Resistant Tuberculosis Treatment. 2019.

3. Publication 2

Relevance of QuantiFERON-TB Gold Plus and Heparin-Binding Hemagglutinin Interferon-γ Release Assays for Monitoring of Pulmonary Tuberculosis Clearance: A Multicentered Study.

Carole Chedid, Eka Kokhreidze, Nestani Tukvadze, Sayera Banu, Mohammad Khaja Mafij Uddin, Samanta Biswas, Graciela Russomando, Chyntia Carolina Díaz Acosta, Rossana Arenas, Paulo PR. Ranaivomanana, Crisca Razafimahatratra, Perlinot Herindrainy, Julio Rakotonirina, Antso Hasina Raherinandrasana, Niaina Rakotosamimanana, Monzer Hamze, Mohamad Bachar Ismail, Rim Bayaa, Jean-Luc Berland, Flavio De Maio, Giovanni Delogu, Hubert Endtz, Florence Ader, Delia Goletti, Jonathan Hoffmann.

***Frontiers in Immunology* 2020; 11 (1); 1-11.**

Article summary

QFT-P is an IGRA that is routinely used to test for exposure to Mtb, by measuring the T-cell-driven IFN-γ production upon *in vitro* antigen stimulation of whole blood. It is essential for the triage of suspected TB patients, or as a precautionary test in patients starting immunosuppressive therapy. However, previous attempts to use it for TB treatment monitoring have met limited success. Novel IGRAs based on other recall antigens are being investigated, in particular rmsHBHA, which stratifies TB cases by stages of infection. However, the rmsHBHA IGRA has been evaluated only in studies in non-TB endemic settings, or with no DR-TB patients. Here, we monitored the plasma IFN-γ response to rmsHBHA and QFT-P antigens during anti-TB treatment in DS-TB and DR-TB patients. Then, we analyzed these results according to sociodemographic characteristics, immune cell counts, and culture conversion during treatment. This study was nested in the HINTT prospective international cohort study conducted in Bangladesh, Georgia, Lebanon, Madagascar, and Paraguay.

Between December 2017 and September 2020, we enrolled 199 adult, non-immunocompromised, culture positive PTB patients. As of September 2020, 132 of them had been followed at T0, T1, and T2 at least and had available IGRA data, including 21.2% (28/132) DR-TB patients. The median IFN-γ response to QFT-P antigen pools TB1 and TB2 remained constant over time, while the median response to rmsHBHA increased significantly (0.086 IU/ml at T0 vs. 1.03 IU/ml at T2, $p < 0.001$). Individual IFN-γ levels were heterogeneous, but an increased IFN-γ response to TB1, TB2, and rmsHBHA was observed in 55.3% (73/132), 56.8% (75/132), and 77.3% (102/132) of patients respectively. Patients with low lymphocyte percentages (<14%) or high neutrophil percentages (>79%) at baseline had significantly lower IFN-γ responses to QFT-P and rmsHBHA at T0 and T1. Among patients with available sputum culture results at T0, T1, and T2 at least (84.8%, 112/132), we stratified IFN-γ levels in cured patients according to culture conversion at T1, defining a subset of fast converters (definitive culture conversion between T0 and T1; 82.1%, 92/112) or slow converters (definitive culture conversion between T1 and T2; 14.2%, 16/112). Slow converters had lower QFT-P positivity rates and TB1 and TB2 IFN-γ levels at T0 and T1, and lower rmsHBHA IGRA positivity rates and IFN-γ levels at T1 and T compared to fast converters. However, the separate performances of the QFT-P and rmsHBHA IGRAs for TB treatment monitoring at T1 and T2 were poor (accuracy

between 44 and 55%, using culture as a reference standard). When evaluating a combined QFT-p/rmsHBHA IGRA score the sensitivity improved (86% at T1 and 82% at T2) as well as the accuracy (77% at T1 and 81% at T2) but the specificity remained inferior to 30%. Finally, in multivariate logistic regression analyses, significant associations were found between slow culture conversion and MIT IFN-γ at T0 (adjusted odds ratio 0.65, p = 0.009), QFT-P IGRA positivity at T0 (aOR 0.045, p = 0.013), and rmsHBHA IGRA positivity at T1 (aOR 0.076, p = 0.045). Overall, we observed a slow converter profile including consistent clinical patterns at baseline (low BMI, high neutrophil percentages, low lymphocyte percentages, low TB1 and TB2 IFN-γ responses), as well as a downregulated rmsHBHA response at the end of treatment.

This study adds to a growing body of literature showing that rmsHBHA IFN-γ stratifies TB infection stages, including during treatment, which for this purpose is an improvement compared to QFT-P alone; however, the specificity of this test compared to culture remained insufficient to efficiently monitor treatment. While this may be partially attributed to immune cross-reactivity with HBHA homologs present in NTM, it highlights that further research is needed to clarify how the rmsHBHA response is regulated at the cellular level during treatment and whether it is specifically associated with Mtb clearance. These results also complete the previous article presented in this thesis (publication 1) and generate further evidence for an association between general inflammation and poor TB control before and during treatment, as total peripheral neutrophil and lymphocyte percentages directly impacted IFN-γ responsiveness to the evaluated TB-specific antigens, and as a low IFN-γ response to non-TB specific stimulation at T0 was associated with slow culture conversion. This must be taken into account when evaluating novel immune tests for treatment monitoring.

frontiers in Immunology

ORIGINAL RESEARCH
published: 02 February 2021
doi: 10.3389/fimmu.2020.616450

Relevance of QuantiFERON-TB Gold Plus and Heparin-Binding Hemagglutinin Interferon-γ Release Assays for Monitoring of Pulmonary Tuberculosis Clearance: A Multicentered Study

Carole Chedid[1,2], Eka Kokhreidze[3], Nestani Tukvadze[3], Sayera Banu[4], Mohammad Khaja Mafij Uddin[4], Samanta Biswas[4], Graciela Russomando[5], Chyntia Carolina Diaz Acosta[5], Rossana Arenas[6], Paulo PR. Ranaivomanana[7], Crisca Razafimahatratra[7], Perlinot Herindrainy[7], Julio Rakotonirina[8], Antso Hasina Raherinandrasana[8], Niaina Rakotosamimanana[7], Monzer Hamze[9], Mohamad Bachar Ismail[9], Rim Bayaa[9], Jean-Luc Berland[1], Flavio De Maio[10,11], Giovanni Delogu[10], Hubert Endtz[12], Florence Ader[13], Delia Goletti[14†] and Jonathan Hoffmann[1†] on behalf of the HINTT working group within the GABRIEL network*

[1] Laboratoire des Pathogènes Emergents, Fondation Mérieux, Centre International de Recherche en Infectiologie, INSERM U1111, Lyon, France, [2] Département de Biologie, Ecole Normale Supérieure de Lyon, Lyon, France, [3] National Center for Tuberculosis and Lung Diseases (NCTBLD), Tbilisi, Georgia, [4] International Centre for Diarrhoeal Disease Research, Bangladesh (icddr,b), Dhaka, Bangladesh, [5] Instituto de Investigaciones en Ciencias de la Salud, National University of Asunción, Asunción, Paraguay, [6] Hospital General de San Lorenzo, MSPyBS, Asunción, Paraguay, [7] Institut Pasteur de Madagascar, Antananarivo, Madagascar, [8] Centre Hospitalier Universitaire de Soins et Santé Publique Analakely (CHUSSPA), Antananarivo, Madagascar, [9] Laboratoire Microbiologie, Santé et Environnement (LMSE), Doctoral School of Sciences and Technology, Faculty of Public Health, Lebanese University, Tripoli, Lebanon, [10] Dipartimento di Scienze di Laboratorio e Infettivologiche, Fondazione Policlinico Universitario "A. Gemelli", IRCCS, Rome, Italy, [11] Dipartimento di Scienze biotecnologiche di base, cliniche intensivologiche e perioperatorie – Sezione di Microbiologia, Università Cattolica del Sacro Cuore, Rome, Italy, [12] Fondation Mérieux, Lyon, France, [13] Service des Maladies Infectieuses et Tropicales, Hospices Civils de Lyon, Lyon, France, [14] Translational Research Unit, Department of Epidemiology and Preclinical Research, "L. Spallanzani" National Institute for Infectious Diseases (INMI), IRCCS, Rome, Italy

Background: Tuberculosis (TB) is a leading infectious cause of death. To improve treatment efficacy, quicker monitoring methods are needed. The objective of this study was to monitor the response to a heparin-binding hemagglutinin (HBHA) interferon-γ (IFN-γ) release assay (IGRA) and QuantiFERON-TB Gold Plus (QFT-P) and to analyze plasma IFN-γ levels according to sputum culture conversion and immune cell counts during treatment.

Methods: This multicentered cohort study was based in Bangladesh, Georgia, Lebanon, Madagascar, and Paraguay. Adult, non-immunocompromised patients with culture-confirmed pulmonary TB were included. Patients were followed up at baseline (T0), after two months of treatment (T1), and at the end of therapy (T2). Clinical data and blood samples were collected at each timepoint. Whole blood samples were stimulated with QFT-P antigens or recombinant methylated *Mycobacterium tuberculosis* HBHA

OPEN ACCESS

Edited by:
Adam Penn-Nicholson, Foundation for Innovative New Diagnostics, Switzerland

Reviewed by:
Edward A. Graviss, Houston Methodist Research Institute, United States
Björn Corleis, Friedrich-Loeffler-Institute, Germany

***Correspondence:**
Carole Chedid
carole.chedid@fondation-merieux.org

[†]These authors share senior authorship

Specialty section:
This article was submitted to Microbial Immunology, a section of the journal Frontiers in Immunology

Received: 12 October 2020
Accepted: 03 December 2020
Published: 02 February 2021

Citation:
Chedid C, Kokhreidze E, Tukvadze N, Banu S, Uddin MKM, Biswas S, Russomando G, Acosta CCD, Arenas R, Ranaivomanana PPR, Razafimahatratra C, Herindrainy P, Rakotonirina J, Raherinandrasana AH, Rakotosamimanana N, Hamze M, Ismail MB, Bayaa R, Berland J-L, De Maio F, Delogu G, Endtz H, Ader F, Goletti D and Hoffmann J (2021) Relevance of QuantiFERON-TB Gold Plus and Heparin-Binding Hemagglutinin Interferon-γ Release Assays for Monitoring of Pulmonary Tuberculosis Clearance: A Multicentered Study. Front. Immunol. 11:616450. doi: 10.3389/fimmu.2020.616450

(produced in *Mycobacterium smegmatis;* rmsHBHA). Plasma IFN-γ levels were then assessed by ELISA.

Findings: Between December 2017 and September 2020, 132 participants completed treatment, including 28 (21.2%) drug-resistant patients. rmsHBHA IFN-γ increased significantly throughout treatment (0.086 IU/ml at T0 *vs*. 1.03 IU/ml at T2, $p < 0.001$) while QFT-P IFN-γ remained constant (TB1: 0.53 IU/ml at T0 *vs*. 0.63 IU/ml at T2, $p = 0.13$). Patients with low lymphocyte percentages (<14%) or high neutrophil percentages (>79%) at baseline had significantly lower IFN-γ responses to QFT-P and rmsHBHA at T0 and T1. In a small group of slow converters (patients with positive cultures at T1; n = 16), we observed a consistent clinical pattern at baseline (high neutrophil percentages, low lymphocyte percentages and BMI, low TB1, TB2, and MIT IFN-γ responses) and low rmsHBHA IFN-γ at T1 and T2. However, the accuracy of the QFT-P and rmsHBHA IGRAs compared to culture throughout treatment was low (40 and 65% respectively). Combining both tests improved their sensitivity and accuracy (70–80%) but not their specificity (<30%).

Conclusion: We showed that QFT-P and rmsHBHA IFN-γ responses were associated with rates of sputum culture conversion. Our results support a growing body of evidence suggesting that rmsHBHA IFN-γ discriminates between the different stages of TB, from active disease to controlled infection. However, further work is needed to confirm the specificity of QFT-P and rmsHBHA IGRAs for treatment monitoring.

Keywords: tuberculosis, immunomonitoring, interferon-gamma release assays, heparin-binding haemagglutinin adhesin, QuantiFERON, treatment monitoring, inflammatory markers

INTRODUCTION

Tuberculosis (TB) is one of the leading causes of death by infectious disease in the world, causing 1.5 million deaths in 2019 (1). The treatment of pulmonary TB requires antibiotic multitherapies that last at least six months (2, 3) and can have toxic side effects. Consequently, treatment adherence is not optimal, especially in primary care settings (4, 5). Currently, anti-TB treatment monitoring relies on *Mycobacterium tuberculosis* (*M. tuberculosis*) detection by sputum smear microscopy and culture when possible (6). Sputum culture is the gold standard, but it is slow and requires high biosafety laboratory environments (7), while smear microscopy is highly sample- and operator-dependent and has poor sensitivity (8, 9). There is a clinical need for quicker anti-TB treatment monitoring tests adapted to primary care settings (10), that require accessible samples (blood, urine, feces) and limited laboratory equipment (11).

QuantiFERON-TB Plus (QFT-P; Qiagen) is an ELISA-based IFN-γ release assay (IGRA) that tests for exposure to *M. tuberculosis*. While it is useful for the triage of suspected TB patients, it cannot discriminate between active and latent TB (12) and has shown little clinical relevance for TB treatment monitoring so far (10). Previous works highlighted a general decrease in IFN-γ levels across TB treatment (13–18), and a study on QuantiFERON Gold In-Tube highlighted the presence of downregulated non-TB specific IFN-γ responses (Mitogen tube) were associated with poor treatment outcomes (19). However, persistently high quantitative results as well as heterogeneous QFT-P conversion rates make the test unlikely to be adapted for individual treatment monitoring (20–22).

Recently, the use of QFT-P in combination with the detection of IFN-γ responses to recombinant *Mycobacterium smegmatis* heparin-binding hemagglutinin (hereafter called "rmsHBHA IGRA") as an additional stimulation antigen has shown promise to stratify TB cases by stage of infection and progression to disease (23–27), and to monitor TB treatment outcomes (28). In particular, negative or low levels of IFN-γ production in response to rmsHBHA stimulation have been associated with active TB disease as opposed to latent infection. However, this assay has been explored only in studies in non-TB endemic settings, or with no drug-resistant TB patients.

The primary objective of this prospective multicentered cohort study was to monitor the plasma IFN-γ response to rmsHBHA and QFT-P antigens during anti-TB treatment. Moreover, recent data collected in the same cohort highlighted an association between baseline circulating white blood cells (WBC) and TB treatment outcome (29); hence, a secondary objective was to describe rmsHBHA and QFT-P IFN-γ values in subsets of patients stratified according to demographics, immune cell counts, and culture conversion during treatment. For that purpose, we conducted a cohort study in five countries with low- or middle income status and high- or middle TB incidence rates (30) (Bangladesh, Georgia, Lebanon, Madagascar, and Paraguay), focusing on adult, HIV-uninfected, culture confirmed drug-susceptible or drug-resistant pulmonary TB patients.

MATERIALS AND METHODS

Study Design and Sample Population

This descriptive study was nested within a multicenter prospective cohort study assessing the prognostic value of blood-based immunological markers for TB treatment monitoring. The study was based in five institutions from the Mérieux Foundation GABRIEL network (31), with the approval of national TB programs and the following ethical committees: the international center for diarrheal diseases and research, Bangladesh (icddr,b) in Dhaka, Bangladesh; the National Center for Tuberculosis and Lung Diseases (NTCLD) in Tbilisi, Georgia; the *Laboratoire Microbiologie, Santé et Environnement (LMSE, Université Libanaise)*, in Tripoli, Lebanon; the *Institut Pasteur de Madagascar* in Antananarivo, Madagascar; and the *Instituto de Investigationes en Ciencias de la Salud (Universidad Nacional de Asunción; IICS-UNA)* in Asunción, Paraguay. All recruited patients provided written informed consent and standard biosecurity and institutional safety procedures were followed in all study sites.

Cohort Recruitment, TB Diagnosis, and Patient Follow-Up

The sample size was evaluated to detect a difference in rmsHBHA IFN-γ between baseline and end of treatment, with the following assumptions: we aimed for a level of significance of 95% and a power of 80%, assuming a minimum average expected difference of 1.6 IU/ml in rmsHBHA IFN-γ levels throughout treatment based on reported estimates (32), with an expected standard deviation of 3 IU/ml at each repeated measurement. We calculated (33) that a sample size of 117 was required to reach significance. As this study was nested in a cohort study with a sample size of 200, we aimed to enroll more patients to account for missing data. Patients were recruited if diagnosed with microbiologically confirmed pulmonary TB (positive culture and/or sputum smear and/or GeneXpert). Patients with HIV or diabetes mellitus and children under 15 years were excluded. In downstream analyses, patients under immunocompromising treatment, patients with negative cultures at inclusion, and patients who were lost-to-follow-up were excluded. Detailed procedures for microbiological diagnosis, drug sensitivity testing, and therapeutic regimen composition were described previously (29).

Patients were followed up: at inclusion (T0), after two months of treatment (T1), at the end of therapy [T2; 6 months for drug-susceptible (DS-TB) patients, nine to 24 months for drug-resistant (DR-TB) patients]. Data were presented for all patients followed up until T2 at least. Patients were on Directly Observed Treatment (DOT) and received treatment according to standard protocols (2, 3, 34). In this study, culture conversion at T1 was used to define three patient subsets: fast converters (definitive culture conversion between T0 and T1), slow converters (definitive culture conversion between T1 and T2), and patients with poor treatment outcome (positive culture results at T2: treatment failure; or positive culture at T3: relapse).

On-Site Whole Blood Collection and Cell Count

At every follow-up visit, 10 ml of whole blood were drawn: 4 ml was used for other downstream analyses, 1 ml was collected in EDTA tubes and used to measure whole blood cell counts by standardized automated systems available in the study sites as listed previously (29), and 5 ml was used for *in vitro* blood stimulation. For the QFT-P assay, 1 ml of whole blood was seeded directly into each of four QuantiFERON-TB Gold Plus (QFT-P, Qiagen) tubes as per the manufacturer's instructions. The NIL tube contained no antigens and was used as a negative control. The TB1 and TB2 QFT-P tubes are coated with commercial *M. tuberculosis*-specific antigenic peptide pools. TB1 tubes contain two mycobacterial peptides, ESAT-6 (>15aa) and CFP-10 (8–13aa), which elicit specific immune responses from CD4+ T lymphocytes (35). TB2 tubes contain an additional commercial peptide pool designed to induce CD8+ T lymphocyte stimulation. MIT tubes are coated with commercial phytohemagglutinin-like bacterial antigens and were used as a positive control (35). For the rmsHBHA assay, 1 ml of blood was seeded into a NIL tube which was complemented with rmsHBHA (provided by the Delogu laboratory, UNICATT, Rome, Italy (23)), at a final concentration of 5 μg/ml. Within 2 h of blood collection, samples were placed at 37°C in a 5% CO_2 atmosphere and incubated for 24 h. After incubation, plasmas were separated from the cell fraction by decantation, and stored at −80°C until further use.

Interferon-γ Release Assay

IFN-γ secretion was quantified using the QFT-P ELISA kit (Qiagen) according to the manufacturer's instructions. Briefly, plasma samples were thawed at room temperature, and 50 μl of plasma was tested. Optical density results were compared to log-normalized values from freshly reconstituted IFN-γ kit standards. To account for potential immunomodulation phenomena unrelated with TB treatment, baseline IFN-γ level values (NIL tubes) were subtracted from antigen-stimulated IFN-γ values (MIT, TB1, TB2, rmsHBHA). According to the kit's sensitivity range, the maximum for IFN-γ level values was set at 10 IU/ml and negative values were rescaled to 0.

Assay Comparability Between Study Sites

To optimize comparability, a sample handling and processing protocol common to all study sites was developed, and on-site trainings were performed to standardize experimental processes such as instrument settings and timings. A tracking sheet was developed and used to follow sample shipment and standardize storage conditions in all sites. As the models of measurement instruments used in the different sites could not be homogenized, instrument readings were tested with QuantiFERON Control Panel (Qiagen) prior to launching the project. Finally, internal controls were added to each ELISA run to control for experimental variation and verify storage quality. Briefly, whole blood from a healthy donor was collected and stimulated with QFT-P antigens following the same protocol as described previously. Plasma was then separated and aliquoted and added to each ELISA run.

Clinical Data Collection and Statistical Analysis

Standardized clinical report and data collection forms were implemented to ensure dataset homogeneity as described previously (29). Data were entered into the CASTOR database

system (Version 1.4, Netherlands) (36), and cleaned and analyzed in R (version 3.6.2). Discrete variables were analyzed using Fisher's Exact test with Bonferroni's *post-hoc* test (37). Normal, continuous variables were analyzed with Student's t-test. Non-normal, continuous variables were analyzed with the Mann–Whitney test, or the Kruskal–Wallis rank sum test with Dunn's Kruskal–Wallis Multiple Comparisons *post-hoc* test (38). Repeated measures of non-independent continuous variables were analyzed using the Friedman rank sum test, with the Wilcoxon–Nemenyi–McDonald-Thompson *post-hoc* test (39). As the HBHA IGRA was not commercialized and QFT-P was designed to screen latent rather than active TB patients, we used Receiver Operating Curve (ROC) analyses to identify optimal IFN-γ thresholds adapted for this cohort, discriminating culture positive from culture negative patients. The overall QFT-P test was considered positive if either TB1 or TB2 was above their respective thresholds. ROC analyses and logistic regression were performed as described previously (29). In particular, multivariate logistic regression analyses were adjusted with the combination of variables that minimized the Akaike Information Criterion (AIC) for most tested predictors, while including important adjustment variables (age, sex, drug sensitivity, country).

RESULTS

Sociodemographic, Clinical, and Microbiological Characteristics of the Cohorts

Between December 2017 and September 2020, 199 eligible patients with culture confirmed active pulmonary TB were recruited in Dhaka (Bangladesh), Tbilisi (Georgia), Tripoli and Akkar (Lebanon), Antananarivo (Madagascar), and Asunción (Paraguay). As of September 2020, 132 of them were followed at least until the end of treatment and had available IGRA data (**Figure 1**). Among these patients, 21.2% (28/132) were diagnosed with DR-TB. The sociodemographic characteristics of DS-TB and DR-TB patients were similar at inclusion (**Table 1**). Sociodemographic characteristics were compared between study sites, and significant differences were observed concerning age, BMI at inclusion, and BCG vaccination rates (**Supplementary Table 1**). All enrolled patients were sputum culture positive at inclusion. Most patients were also positive for sputum smear microscopy (sensitivity: 78.0%, 103/132) and/or GeneXpert (98.4%, 125/132). Three (3.9%) cases of treatment failure and one (0.7%) case of relapse were recorded (**Table 1**).

Dynamics of Interferon-γ Levels During Treatment and Influence of Sociodemographic Factors

Plasma IFN-γ levels in response to TB1, TB2, or HBHA stimulations were measured during anti-TB treatment (**Figure 2**). The median IFN-γ response to TB1 and TB2 remained constant over time, while the median response to rmsHBHA increased significantly (**Figure 2A**). Individual IFN-γ levels were heterogeneous in all three stimulation conditions (**Figure 2B**). To account for individual variations, rmsHBHA/TB1 and rmsHBHA/TB2 IFN-γ ratios were evaluated, and a significant increase in both ratios was still observed overall (**Supplementary Figures 1A–C**). We also measured the TB2-TB1 IFN-γ response, as a proxy for the QFT-P $CD8^+$ T-cell response (**Supplementary Figure 1D**). No significant difference was detected over time.

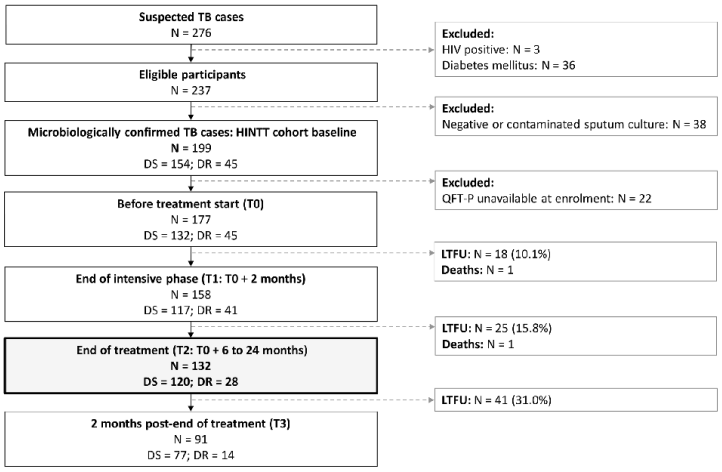

FIGURE 1 | Patient inclusions between December 2017 and September 2020. DR, drug-resistant; DS, drug-susceptible; LTFU, lost to follow-up. TB, tuberculosis. HIV, human immunodeficiency virus. Treatment for DS-TB patients lasted 6 months. Treatment for DR-TB patients lasted 9 to 24 months.

TABLE 1 | Sociodemographic and clinical characteristics of drug-susceptible and drug-resistant patients at inclusion.

N	ALL 132	DS-TB 104	DR-TB 28	*p*
Patient demographics				
Age (years)	27 (21–36.2)	27 (21–37.2)	27.5 (19.7–33.2)	*0.41*
Sex (male)	62.9% (83/132)	64.4% (67/104)	57.1% (16/28)	*0.51*
Treatment outcome				
Cured and completed	95.5% (126/132)	94.2% (98/104)	100% (28/28)	*0.34*
Completed	1.5% (2/132)	1.9% (2/104)	0	-
Failure	2.3% (3/132)	2.9% (3/104)	0	-
Relapse	0.8% (1/132)	1% (1/104)	0	-
Country of origin				
Bangladesh	28.8% (38/132)	20.2% (21/104)	60.7% (17/28)	***>0.001***
Georgia	23.5% (31/132)	20.2% (21/104)	35.7% (10/28)	*0.13*
Lebanon	5.3% (7/132)	6.7% (7/104)	0	*0.34*
Madagascar	27.3% (36/132)	34.6% (36/104)	0	***>0.001***
Paraguay	15.2% (20/132)	18.3% (19/104)	3.6% (1/28)	*0.073*
BMI at inclusion	18.7 (16.9–21.3)	18.83 (16.9–21.4)	18.7 (17.5–21.0)	*0.79*
WBC absolute count at inclusion (cells/mm^3)	9745 (7365–12032)	9695 (7350–12055)	10150 (7725–11850)	*0.65*
Neutrophils at inclusion (% of WBC)	75 (68–79.1)	75 (68.3–79)	78 (66.7–80.2)	*0.34*
Lymphocytes at inclusion (% of WBC)	18 (14–25)	18 (14–25)	17 (13.7–24.5)	*0.52*
Monocytes at inclusion (% of WBC)	4.4 (2–7)	5 (2–8.0)	4 (3–5.2)	*0.42*
Number of household contacts	4 (3–6)	4 (3–6)	4 (3.75–6.2)	*0.86*
BCG vaccination	86.2% (94/109)	86.4% (76/88)	85.7% (18/21)	*1*
Risk factors and comorbidities				
Smoking	46.2% (61/132)	46.2% (48/104)	46.4% (13/28)	*1*
Alcohol abuse	22% (29/132)	24% (25/104)	14.3% (4/28)	*0.57*
Injectable drug use	3.8% (5/131)	2.9% (3/104)	7.4% (2/27)	*0.27*
Jail detention history	8.5% (11/130)	9.8% (10/102)	3.6% (1/28)	*0.57*
Chronic HCV infection	1.6% (2/129)	2% (2/101)	0	*0.75*
Other disease[1]	6.2% (7/113)	7.8% (7/90)	0	*0.34*
History of TB				
Prior exposure to active TB patients	29% (38/131)	29.1% (30/103)	28.6% (8/28)	*0.23*
Documented previous TB episode	15.1% (20/132)	11.5% (12/104)	28.5% (8/28)	***0.048***
Previous TB outcome				
Cured and completed	61.1% (11/18)	61.5% (8/13)	60% (3/5)	*1*
Treatment completed	11.1% (2/18)	7.7% (1/13)	20% (1/5)	*0.49*
Outcome not evaluated or unknown	16.7% (3/18)	15.4% (2/13)	20% (1/5)	*1*
Treatment failure	11.1% (2/18)	15.4% (2/13)	0	-

Data are given as % (N) or median (interquartile range). DS-TB, drug-susceptible tuberculosis; DR-TB, drug-resistant tuberculosis; BMI, body mass index; WBC, white blood cells; 1: asthma, hypertension, inflammation. P-values are given for DS-TB vs. DR-TB.

No patients had HIV, non-TB chronic pulmonary diseases, renal diseases, solid tumors, chronic HBV infection, were pregnant, or under immunosuppressive therapies (corticosteroids, calcineurin inhibitors, biologics).

The impact of sociodemographic parameters on IFN-γ levels was assessed but no significant association was detected (data not shown).

Overall, QFT-P positivity rates remained constant during treatment (T0 *vs.* T2: 52 vs. 55%, p = 0.71), whereas rmsHBHA positivity rates increased significantly (T0 *vs.* T2: 31 *vs.* 67%, p < 0.001 (**Table 2**). We also calculated the slopes of rmsHBHA and QFT-P IFN-γ variations during treatment (**Table 2**). An increased INF-γ response to TB1, TB2, and rmsHBHA was observed in 55.3% (73/132), 56.8% (75/132), and 77.3% (102/132) of patients respectively.

IFN-γ levels over time were then stratified per study site (**Figures 2C–E**). Similar trends were observed in all cohorts for TB1 and TB2 IFN-γ levels, except in the Madagascar site in which an increase in TB1 IFN-γ was recorded between T0 and T2. Variation in IFN-γ levels produced by rmsHBHA-stimulated samples was different between study sites: similar in increase and order of magnitude in the Bangladesh and Georgia cohorts on the one hand, as well as in Paraguay and Lebanon on the other hand; however, no increase was observed in the Madagascar cohort, as well as lower IFN-γ values (**Supplementary Table 2**). Mitogen IFN-γ levels were also significantly lower in the Madagascar cohort than in the Georgia cohort at all timepoints (**Supplementary Table 2**).

Effect of Neutrophil and Lymphocyte Percentages on Interferon-γ Release Assay Interferon-γ Response During Treatment

We analyzed the distribution of neutrophil percentages, and stratified IFN-γ results according to three groups: low neutrophils (less than the first quartile), intermediate neutrophils (between first and third quartiles), and high neutrophils (**Figure 3A**; threshold values are available in **Supplementary Table 3**). Similar analyses were performed with lymphocyte percentages (**Figure 3C**). We also evaluated the proportion of QFT-P and rmsHBHA positivity at each timepoint, stratified by neutrophil (**Figure 3B**) and

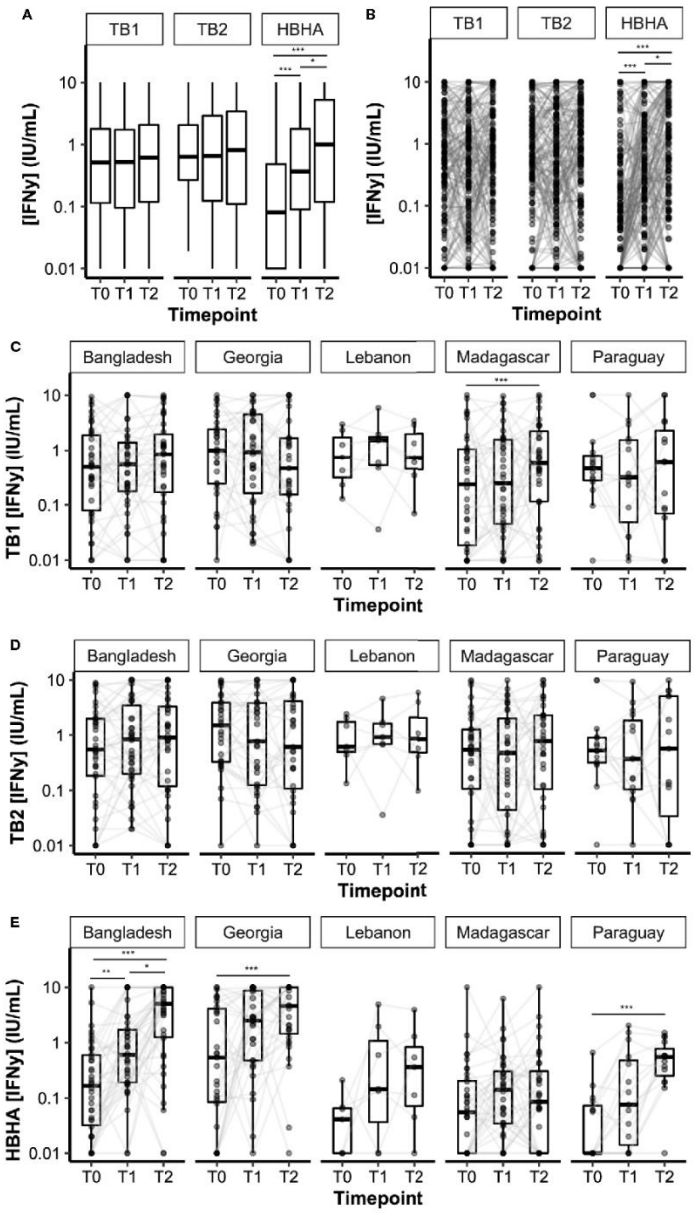

FIGURE 2 | Dynamics of plasma IFN-γ response to QFT-P and HBHA stimulations over the course of TB therapy. Data are given as median + interquartile range. Each black dot represents one patient at one timepoint. Grey lines connect data points from the same patient. **(A)** Median IFN-γ responses in the complete cohort (n = 132 per timepoint). **(B)** Individual IFN-γ responses in the complete cohort. **(C–E)** Stratification per study site. Bangladesh (n = 38), Georgia (n = 31), Lebanon (n = 7), Madagascar (n = 36), Paraguay (n = 20). T0: baseline. T1: baseline + 2 months. T2: end of treatment. Data were compared using Friedman's Exact Test with the Wilcoxon–Nemenyi–McDonald-Thompson *post-hoc*, or the Mann–Whitney U test **(B)**. *$p < 0.05$; **$p < 0.01$; ***$p < 0.001$.

TABLE 2 | Qualitative evolution of QFT-P and HBHA IFN-γ levels during treatment.

Positivity rate at each timepoint	HBHA	TB1 only	TB2 only	QFT-P (TB1 and/or TB2)
T0	31.1% (41/132)	4.5% (6/132)	34.8% (46/132)	52.3% (69/132)
T1	56.1% (74/132)	2.3% (3/132)	42.4% (56/132)	50.8% (67/132)
T2	67.4% (89/132)	2.3% (3/132)	43.9% (58/132)	55.3% (73/132)
Trend between T0 and T1				
Increase	66.7% (88/132)	56.1% (74/132)	47.7% (63/132)	–
Decrease	24.2% (32/132)	41.7% (55/132)	47.7% (63/132)	
Constant	9.1% (12/132)	2.3% (3/132)	4.5% (6/132)	
Trend between T0 and T2				
Increase	77.3% (102/132)	55.3% (73/132)	56.8% (75/132)	-
Decrease	15.2% (20/132)	40.9% (54/132)	41.7% (55/132)	
Constant	7.6% (10/132)	3.8% (5/132)	1.5% (2/132)	

Data are given as % (N). T0, baseline; T2, end of treatment; QFT-P, QuantiFERON-TB Gold Plus; Constant, no difference in IFN-γ levels between T0 and T2, regardless of variations during treatment. Positivity was set at 0.75 IU/ml for QFT-P and at 0.22 IU/ml for HBHA based on ROC analyses.

lymphocyte percentages (**Figure 3D**). As HBHA stimulation was not performed using a commercial kit, Receiver Operating Curve (ROC) analyses were performed to identify the optimal rmsHBHA IFN-*γ* threshold value differentiating culture-positive patients from culture-negative patients at any timepoint. The resulting Area Under the Curve (AUC) was maximized for an IFN-*γ* cutoff value of 0.24 IU/ml (AUC 0.725, 95% CI 0.674–0.777). Overall, neutrophil and lymphocyte percentages directly impacted IFN-*γ* responsiveness to TB-specific antigens: QFT-P and rmsHBHA IFN-*γ* levels and positivity rates were significantly higher in patients with low neutrophil (**Figures 3A, B**) or with high lymphocyte proportions (**Figures 3C, D**). This statistically significant trend was also observed when comparing the subgroup of patients with both low neutrophil and high lymphocyte percentages to the rest of the cohort (data not shown).

Effect of the Culture Conversion Status at 2 Months on the Interferon-γ Release Assay Interferon-γ Response Throughout Treatment

Overall, 112 patients had available culture data at T0, T1, and T2. Most patients were fast converters (definitive culture conversion between T0 and T1; 82.1%, 92/112) or slow converters (definitive culture conversion between T1 and T2; 14.2%, 16/112). Poor treatment outcomes were recorded in four patients (treatment failure, 2.7%, 3/112; relapse, 0.9%, 1/112; data not shown).

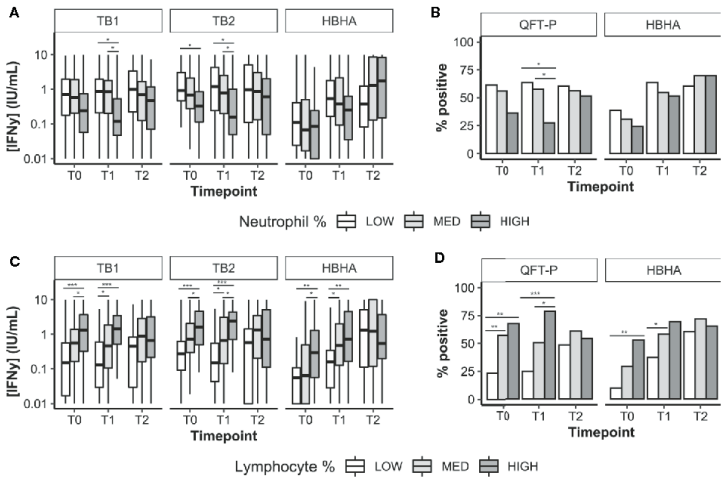

FIGURE 3 | Plasma IFN-γ response to TB-specific QFT-P antigens or HBHA stimulation in patients stratified by WBC counts over the course of TB therapy. **(A, C)** Quantitative IFN-γ response. Data are given as median + interquartile range and were compared using Kruskal–Wallis' test with Dunn's *post-hoc* when necessary. **(B, D)** Data were given as a percentage of each group and were compared using Fisher's Exact Test with Bonferroni's correction when necessary. Positivity was set at 0.75 IU/ml for QFT-P TB1, 0.71 IU/ml for QFT-P TB2 (the overall QFT-P result was positive if TB1 and/or TB2 were positive) and at 0.22 IU/ml for HBHA, based on ROC analyses. Low, medium, and high WBC or lymphocyte groups were defined as follows: low: <1st quartile; medium: 1st–3rd quartiles; high: >3rd quartile. WBC, white blood cells; T0, baseline; T1, baseline + 2 months; T2, end of treatment; *p < 0.05; **p < 0.01; ***p < 0.001.

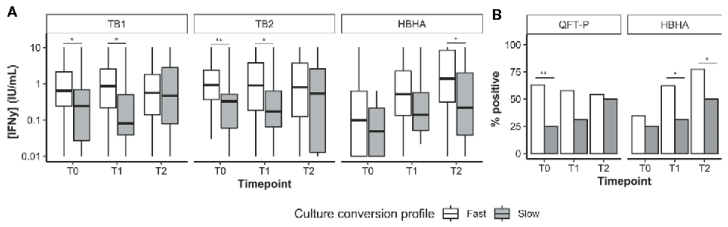

FIGURE 4 | Culture conversion profiles and plasma IFN-γ dynamics. Plasma IFN-γ levels (**A**, represented as medians + interquartile range) and IGRA positivity rates (**B**). T0, enrolment; T1, T0 + 2months; T2, end of treatment; Fast, conversion between T0 and T1 (n = 92). Slow, conversion between T1 and T2 (n = 16). *p < 0.05; **p < 0.01 (Mann–Whitney U Test or Fisher's Exact Test).

Among successfully cured patients (n = 108), median IFN-γ levels (**Figure 4A**) as well as QFT-P and rmsHBHA IGRA positivity rates (**Figure 4B**) were stratified according to the culture conversion profiles. In slow converters, TB1 and TB2 IFN-γlevels at T0 and T1 and rmsHBHA IFN-γlevels at T2 were significantly lower than in fast converters. Similarly, QFT-P positivity rates at T1 and rmsHBHA positivity rates at T1 and T2 were significantly lower in slow converters.

Then, we calculated the sensitivity, specificity, and accuracy of the QFT-P and rmsHBHA IGRAs for TB treatment monitoring at T1 and T2, using culture as a reference standard (**Supplementary Table 4**). At T1 and T2 respectively, the accuracy of the QFT-P IGRA was of 44 and 46%, and the accuracy of TB2-TB1 was of 52 and 55%. For the rmsHBHA IGRA, we evaluated the test performances of negative rmsHBHA results (*i.e.* rmsHBHA IFN-γ ≤ 0.22 IU/ml), since lower rmsHBHA IFN-γ values were observed before treatment. The accuracy of the rmsHBHA IGRA was of 64 and 65% at T1 and T2, respectively. Finally, we generated a score which was positive when the QFT-P result was positive and the rmsHBHA result was negative. The sensitivity of this combined score was of 86% at T1 and 82% at T2, and its accuracy reached 77% at T1 and 81% at T2, but its specificity remained inferior to 30% at both timepoints. Similar results were observed with a score combining rmsHBHA and TB2-TB1.

Association Between White Blood Cell Counts, Culture Conversion, and Interferon-γ Release Assay Interferon-γ Response During Treatment

We compared the immune cell counts (**Supplementary Table 5**) and the baseline sociodemographic characteristics (**Supplementary Table 6**) of patients according to their culture conversion profiles. No difference was detected between slow and fast converters for immune cell counts, but at T0 and T1, patients with treatment failure or relapse had significantly higher neutrophil percentages (at T0, median 84%, interquartile range (IQR) 81.5–86.5; at T1, 79%, IQR 75–81.75), and lower lymphocyte percentages (at T0, 12.5%, IQR 9.2–15.2; at T1, 15.5%, IQR 11–21.2) than successfully treated patients. The BMI at inclusion was significantly lower in slow than in fast converters, and slower conversion rates were observed in the Madagascar cohort.

Then, logistic regression analyses were performed to identify associations between slow culture conversion and immune cell counts or IGRA results (**Table 3**). In univariate analyses, significant associations were detected between slow conversion and MIT IFN-γ at T0 (odds ratio (OR) 0.78, p = 0.001) and T1 (OR 0.84, p = 0.021), with QFT-P IGRA positivity at T0 (OR 0.19, p = 0.008), and with rmsHBHA IGRA positivity at T1 (OR 0.24, p = 0.015) and T2 (OR 0.29, p = 0.029). The BMI at inclusion was also associated (OR 0.791, p = 0.025).

In multivariate analyses, significant associations were maintained for MIT IFN-γ at T0 (adjusted OR 0.65, p = 0.009), QFT-P IGRA positivity at T0 (aOR 0.045, p = 0.013), and HBHA IGRA positivity at T1 (aOR 0.076, p = 0.045). No significant association was found otherwise (**Supplementary Table 7**). Adjusting the models with neutrophil and monocyte proportions at baseline yielded similar results, but with higher AIC values (**Supplementary Table 8**).

Overall, we observed a slow converter profile including consistent clinical patterns at baseline (low BMI, high neutrophil percentages, low lymphocyte percentages, low TB1 and TB2 IFN-γresponses), as well as a downregulated rmsHBHA response at the end of treatment.

DISCUSSION

In this multicentered prospective study, we assessed the value of QFT-P or rmsHBHA-based IGRAs for pulmonary TB sputum culture conversion monitoring in five cohorts (Bangladesh, Georgia, Lebanon, Madagascar, and Paraguay). We recruited 132 HIV-uninfected culture confirmed pulmonary TB patients, including 28 DR-TB cases. To our knowledge, this is the first time that QFT-P and HBHA IGRAs are prospectively evaluated for treatment monitoring in DS-TB and DR-TB cohorts from high-TB incidence countries.

Consistently with previous works (20, 21), we found that individual monitoring of TB1 and TB2 IFN-γ levels during treatment showed little relevancy; we observed important inter-patient heterogeneity, and no significant changes in median values over time. On the contrary, median rmsHBHA

TABLE 3 | Associations between time to culture conversion, IFN-γ response, and selected clinical parameters.

Parameter	Timepoint	Descriptive analysis (n = 108)			Univariate analysis		Multivariate analysis[1]			
		Slow responders (n = 16; reference)	Fast responders (n = 92)	*P*	OR (95%CI)	*p*	aOR (95%CI)	*p*	C	AIC
MIT IFN-γ (IU/ml)	*T0*	4.9 (1.8–10)	10 (9.82–10)	*0.0028*	0.78 (0.67–0.91)	*0.001*	0.65 (0.44–0.86)	*0.009*	0.75	57.5
	T1	8.3 (3.9–10)	10 (9.93–10)	*0.0039*	0.84 (0.72–0.98)	*0.021*	0.77 (0.56–1.01)	*0.076*	0.68	63.9
	T2	9.4 (4.8–10)	10 (9.94–10)	*0.023*	0.88 (0.76–1.04)	*0.11*	0.78 (0.57–1.05)	*0.10*	0.66	64.7
Positive QFT-P IGRA	*T0*	25% (4/16)	63% (58/92)	*0.006*	0.19 (0.051–0.61)	*0.008*	0.045 (0.002–0.35)	*0.013*	0.77	57.6
	T1	31.2% (5/16)	56.5% (52/92)	*0.10*	0.33 (0.099–0.99)	*0.059*	0.39 (0.064–1.97)	*0.27*	0.64	66.2
	T2	50% (8/16)	53.3% (49/92)	*0.98*	0.88 (0.29–2.57)	*0.81*	3.27 (0.59–24.1)	*0.20*	0.65	65.7
Positive HBHA IGRA	*T0*	25% (4/16)	35.9% (33/92)	*0.57*	0.62 (0.16–1.96)	*0.44*	0.39 (0.075–1.71)	*0.24*	0.64	66.7
	T1	31.2% (5/16)	65.2% (60/92)	*0.013*	0.24 (0.071–0.73)	*0.015*	0.076 (0.003–0.67)	*0.045*	0.74	61.9
	T2	50% (8/16)	77.2% (71/92)	*0.033*	0.29 (0.097–0.89)	*0.029*	0.79 (0.17–4.13)	*0.77*	0.61	67.1
Lymphocyte % of WBC	*T0*	17.5 (12.8–19.5)	19.0 (15–26)	*0.099*	0.93 (0.84–1.00)	*0.086*	0.94 (0.83–1.05)	*0.33*	0.64	66.4
	T1	23.0 (16.2–28.0)	25.0 (20.7–31)	*0.099*	0.93 (0.86–0.99)	*0.052*	0.92 (0.83–0.99)	*0.078*	0.68	63.3
	T2	29.5 (23.5–36.2)	30.0 (25.9–36)	*0.93*	1.01 (0.95–1.06)	*0.76*	1.01 (0.94–1.08)	*0.89*	0.62	67.5
Body mass index	*T0*	17.0 (16.3–18.6)	19.7 (17.4–21.5)	*0.0088*	0.79 (0.63–0.93)	*0.025*	0.78 (0.56–1.02)	*0.098*	0.65	65.5

T0, inclusion. T1, T0 + 2 months. T2, end of treatment. OR, odds ratio; aOR, adjusted odds ratio; CI, confidence interval; WBC, white blood cells; C, model C statistic; AIC, Akaike Information Criterion. Only parameters with significant association to the outcome were shown; other tested parameters are available in ***Supplementary Table 7****. Slow culture conversion was defined as a persistently positive culture result at T1 followed by a culture conversion at T2. For MIT IFN-γ associations were calculated for each unit increase. For lymphocyte proportions, associations were calculated for each increase of 5%. [1]models were adjusted for age, sex, country of origin, drug resistance strain, body mass index at inclusion, and BCG vaccination rate.*

IFN-γ levels increased significantly throughout treatment, and an increase was observed in most patients. This is consistent with studies associating high rmsHBHA IFN-γ levels to latency and controlled infection (23, 25–27), as well as in children (28) and in adults (32) receiving anti-TB treatment. The differences observed between the QFT-P and rmsHBHA IFN-γ responses during treatment can be explained by distinct antigen compositions. TB1 and TB2 are peptide pools obtained from secreted antigens, whereas rmsHBHA is a native protein found in mycobacterial cell walls *in vivo*; hence, antigen processing and presentation may differ. Bacterial pathogenesis mechanisms (40) as well as the bactericidal effect of anti-TB treatment could also affect the release of QFT-P and HBHA antigens. In addition, mycobacterial immune escape mechanisms involving HBHA (41, 42) could explain the downregulated *in vitro* IFN-γ responses to rmsHBHA during active disease.

Characterization of the association between QFT-P, rmsHBHA IFN-γ, and mycobacterial clearance has led us to identify two subsets of conversion rates. In particular, slower culture conversion was associated with QFT-P negativity at T0, consistently with a prior study linking negative or indeterminate QFT-P results with poor treatment outcomes (43), and with HBHA IGRA negativity at T1. More generally, both a general immunosuppression with low non-specific IFN-γ (44), and low *M. tuberculosis*-specific IFN-γ (45) have been demonstrated during active TB. Thus, an anergic early T-cell-driven response might be involved in slower mycobacterial clearance (43). At the other end of the spectrum, lower levels of IFN-γ in slow converters at T2 suggest a link between magnitude of the rmsHBHA-mediated response and mycobacterial clearance.

Our data indicate that rmsHBHA and/or QFT-P IFN-γ had low specificity and accuracy compared to the gold standard culture conversion. Because of the small cohort size, this result must be interpreted with caution; but if confirmed, it could suggest that the increase in rmsHBHA IFN-γ might be representative of general immune recovery during treatment rather than a specific response to *M. tuberculosis*. Here, this hypothesis is supported by the fact that a low IFN-γ response to non-TB specific stimulation (Mitogen tubes) at T0 was also significantly associated with slow culture conversion in multivariate analysis. In addition, immune cross-reactions with HBHA homologs present in environmental mycobacteria have been previously reported (23).

Finally, our study had several limitations. The sample size was relatively small, and patients were included in diverse geographical areas and had different antibiotic regimens. As a consequence, malnutrition levels, untested co-infections (besides HIV and virus B and C hepatitis), different genetic and epigenetic backgrounds, or potential differences in bacterial loads during sputum collection could not be controlled. We were intrigued by differences in IFN-γ response to HBHA in the different study sites, which could be linked to ethnic-specific influences over *M. tuberculosis* responses (46). Although adjustment with sociodemographic factors and optimism corrections with a method adapted to small sample sizes (47) were performed, our results need to be confirmed in larger cohorts.

In conclusion, this study described the associations between mycobacterial clearance and immune responses to QFT-P and rmsHBHA IGRAs throughout anti-TB treatment. Lower QFT-P and rmsHBHA IFN-γ levels were associated with slower mycobacterial clearance. Our results support a growing body of evidence suggesting that rmsHBHA IFN-γ discriminates between the different stages of TB. However, the specificity of both IGRAs was insufficient for treatment monitoring. Further research is needed to clarify how the rmsHBHA response is regulated at the cellular level during treatment, and whether there is any specific interaction with mycobacterial clearance. In particular, evaluating how long rmsHBHA IFN-γ values remain stable after treatment would help assess whether it could be a relevant biomarker for relapse prediction.

DATA AVAILABILITY STATEMENT

The raw data supporting the conclusions of this article will be made available by the authors, without undue reservation.

ETHICS STATEMENT

The studies involving human participants were reviewed and approved by: in Bangladesh, the Research Review Committee and the Ethical Review Committee of icddr, b; in Georgia, the Institutional Review Board of the NTCLD (IORG0009467); in Lebanon, the Institutional Review Board of NINI hospital (IRB-F-01); In Madagascar, the Ministry of Public Health and the Ethical Committee for Biomedical Research (reference number: n°099–MSANP/CERBM); in Paraguay, the Research Ethics Committee and the Scientific Committee of the IICS-UNA (IRB number: IRB00011984; Federalwide Assurance number: FWA00029097). The patients/participants provided their written informed consent to participate in this study.

AUTHOR CONTRIBUTIONS

JH is the principal investigator and initiated the project together with DG, NT, SBa, GR, NR, and MH. Data were collected by EK, MU, SBi, CA, PR, CR, PH, JR, AR, and RB. CC performed all the analyses and wrote the manuscript. All authors contributed to the article and approved the submitted version.

FUNDING

This work was supported by Fondation Mérieux, Fondation Christophe et Rodolphe Mérieux, and Fondation AnBer, and the grant ANR-18-CE17-0020. A minor part of the study was supported by the Italian Ministry of Health "Ricerca Corrente, Linea 4."

ACKNOWLEDGMENTS

We would like to thank all the patients participating in our study, as well as the local healthcare staff in each clinical site. In particular, we are very grateful to Leticia Rojas and Laura Franco, from the Molecular Biology Department at the Instituto de Investigaciones en Ciencias de la Salud (Asunción, Paraguay) for their valuable help with patient data collection. Finally, we would like to dedicate this work to the memory of María Maldonado, from the Hospital General de San Lorenzo (Asunción, Paraguay). We are beyond grateful to her for her dedication during the recruitment and follow-up process of the patients in this study, as well as for her unfailing involvement in the fight against tuberculosis in Paraguay.

SUPPLEMENTARY MATERIAL

The Supplementary Material for this article can be found online at: https://www.frontiersin.org/articles/10.3389/fimmu.2020.616450/full#supplementary-material

REFERENCES

1. World Health Organization Geneva. *Global tuberculosis report 2020*. Geneva: World Health Organization (2020).
2. World Health Organization Geneva. *Guidelines for treatment of drug-susceptible tuberculosis and patient care* Vol. vol. 1. Geneva: World Health Organization (2017).
3. World Health Organization Geneva. *WHO consolidated guidelines on drug-resistant tuberculosis treatment*. Geneva: World Health Organization (2019).
4. Woimo TT, Yimer WK, Bati T, Gesesew HA. The prevalence and factors associated for anti-tuberculosis treatment non-adherence among pulmonary tuberculosis patients in public health care facilities in South Ethiopia: a cross-sectional study. *BMC Public Health* (2017) 17:1–10. doi: 10.1186/s12889-017-4188-9
5. Munro SA, Lewin SA, Smith HJ, Engel ME, Fretheim A, Volmink J. Patient Adherence to Tuberculosis Treatment: A Systematic Review of Qualitative Research. *PLoS Med* (2007) 4(7):e238. doi: 10.1371/journal.pmed.0040238
6. World Health Organization Geneva. *Global Tuberculosis Report 2018*. Geneva: World Health Organization (2018).
7. Horne DJ, Royce SE, Gooze L, Narita M, Hopewell PC, Nahid P, et al. Sputum monitoring during tuberculosis treatment for predicting outcome : systematic review and meta-analysis. *Lancet Infect Dis* (2010) 10:387–94. doi: 10.1016/S1473-3099(10)70071-2
8. Parrish NM, Carroll KC. Role of the clinical mycobacteriology laboratory in diagnosis and management of tuberculosis in low-prevalence settings. *J Clin Microbiol* (2011) 49:772–6. doi: 10.1128/JCM.02451-10
9. World Health Organization. *Early detection of Tuberculosis : an overview of approaches, guidelines and tool*. World Health Organization (2011).
10. Goletti D, Arlehamn CSL, Scriba TJ, Anthony R, Cirillo DM, Alonzi T, et al. Can we predict tuberculosis cure? Current tools available. *Eur Respir J* (2018) 52:1801089. doi: 10.1183/13993003.01089-2018
11. MacLean E, Broger T, Yerlikaya S, Fernandez-Carballo BL, Pai M, Denkinger CMA. A sytematic review of biomarkers to detect active tuberculosis. *Nat Microbiol* (2019) 4(5):748–58. doi: 10.1038/s41564-019-0380-2
12. Goletti D, Lee MR, Wang JY, Walter N, Ottenhoff THM. Update on tuberculosis biomarkers: From correlates of risk, to correlates of active disease and of cure from disease. *Respirology* (2018) 23:455–66. doi: 10.1111/resp.13272
13. Liang L, Shi R, Liu X, Yuan X, Zheng S, Zhang G, et al. Interferon-gamma response to the treatment of active pulmonary and extra-pulmonary tuberculosis. *Int J Tuberc Lung Dis* (2017) 21:1145–9. doi: 10.5588/ijtld.16.0880
14. Chang P, Wang PH, Chen KT. Use of the QuantiFERON-TB Gold In-Tube Test in the Diagnosis and Monitoring of Treatment Efficacy in Active Pulmonary Tuberculosis. *Int J Environ Res Public Health* (2017) 14(3):236. doi: 10.20944/preprints201701.0035.v1
15. Petruccioli E, Chiacchio T, Vanini V, Cuzzi G, Codecasa LR, Ferrarese M, et al. Effect of therapy on Quantiferon-Plus response in patients with active and latent tuberculosis infection. *Sci Rep* (2018) 8(1):1–11. doi: 10.1038/s41598-018-33825-w
16. Kamada A, Amishima M. QuantiFERON-TB Gold Plus as a potential tuberculosis treatment monitoring tool. *Eur Respir J* (2017) 49:10–2. doi: 10.1183/13993003.01976-2016
17. Goletti D, Carrara S, Mayanja-Kizza H, Baseke J, Mugerwa MA, Girardi E, et al. Response to M. tuberculosis selected RD1 peptides in Ugandan HIV-infected patients with smear positive pulmonary tuberculosis: A pilot study. *BMC Infect Dis* (2008) 8(1):1–13. doi: 10.1186/1471-2334-8-11
18. Kabeer BSA, Raja A, Raman B, Thangaraj S, Leportier M, Ippolito G, et al. IP-10 response to RD1 antigens might be a useful biomarker for monitoring tuberculosis therapy. *BMC Infect Dis* (2011) 11(1):135. doi: 10.1186/1471-2334-11-135
19. Feng JY, Pan SW, Huang SF, Chen YY, Lin YY, Su WJ. Depressed Gamma Interferon Responses and Treatment Outcomes in Tuberculosis Patients:

a Prospective Cohort Study. *J Clin Microbiol* (2018) 56(10):e00664–18. doi: 10.1128/JCM.00664-18
20. Denkinger CM, Pai M, Patel M, Menzies D. Gamma Interferon Release Assay for Monitoring of Treatment Response for Active Tuberculosis : an Explosion in the Spaghetti Factory. *J Clin Microbiol* (2013) 51:607–10. doi: 10.1128/JCM.02278-12
21. Bartalesi F, Spinicci M, Mencarini J, Veloci S, Mantella A, Bartoloni A. The role of Quantiferon-TB Gold in-Tube in the diagnosis and treatment monitoring of active tuberculosis The role of Quantiferon-TB Gold in-Tube in the diagnosis and treatment monitoring of active tuberculosis. *Infect Dis (Auckl)* (2017) 49 (6):474–7. doi: 10.1080/23744235.2017.1279747
22. Clifford V, He Y, Zufferey C, Connell T, Curtis N. Interferon gamma release assays for monitoring the response to treatment for tuberculosis : A systematic review. *Tuberculosis* (2015) 95:639–50. doi: 10.1016/j.tube.2015.07.002
23. Delogu G, Chiacchio T, Vanini V, Butera O, Cuzzi G, Bua A, et al. Methylated HBHA produced in M. smegmatis discriminates between active and non-active tuberculosis disease among RD1-responders. *PLoS One* (2011) 6(3): e18315. doi: 10.1371/journal.pone.0018315
24. Locht C, Hougardy JM, Rouanet C, Place S, Mascart F. Heparin-binding hemagglutinin, from an extrapulmonary dissemination factor to a powerful diagnostic and protective antigen against tuberculosis. *Tuberculosis* (2006) 86:303–9. doi: 10.1016/j.tube.2006.01.016
25. Hougardy JM, Schepers K, Place S, Drowart A, Lechevin V, Verscheure V, et al. Heparin-binding-hemagglutinin-induced IFN-γ release as a diagnostic tool for latent tuberculosis. *PLoS One* (2007) 2(10):e926. doi: 10.1371/journal.pone.0000926
26. Corbière V, et al. Risk stratification of latent tuberculosis defined by combined interferon gamma release assays. *PLoS One* (2012) 7. doi: 10.1371/journal.pone.0043285
27. Tang J, Huang Y, Jiang S, Huang F, Ma T, Qi Y, et al. QuantiFERON-TB Gold Plus combined with HBHA-Induced IFN-γ release assay improves the accuracy of identifying tuberculosis disease status. *Tuberculosis* (2020) 124:101966. doi: 10.1016/j.tube.2020.101966
28. Sali M, Buonsenso D, D'Alfonso P, De Maio F, Ceccarelli M, Battah B, et al. Combined use of Quantiferon and HBHA-based IGRA supports tuberculosis diagnosis and therapy management in children. *J Infect* (2018) 77(6):526–33. doi: 10.1016/j.jinf.2018.09.011
29. Chedid C, Kokhreidze E, Tukvadze N, Banu S, Uddin MKM, Biswas S, et al. Association of baseline white blood cell counts with tuberculosis treatment outcome: a prospective multicentered cohort study. *Int J Infect Dis* (2020) 100:199–206. doi: 10.1016/j.ijid.2020.09.017
30. World Health Organization Geneva. *Global Tuberculosis Report 2019*. Geneva: World Health Organization (2019).
31. Komurian-Pradel F, Grundmann N, Siqueira MM, Chou M, Diallo S, Mbacham W, et al. Enhancing research capacities in infectious diseases: The GABRIEL network, a joint approach to major local health issues in developing countries. *Clin Epidemiol Glob Heal* (2013) 1(1):40–3. doi: 10.1016/j.cegh.2012.11.002
32. Wen HL, Li CL, Li G, Lu YH, Li HC, Li T, et al. Involvement of methylated HBHA expressed from Mycobacterium smegmatis in an IFN-γ release assay to aid discrimination between latent infection and active tuberculosis in BCG-vaccinated populations. *Eur J Clin Microbiol Infect Dis* (2017) 36(8):1415–23. doi: 10.1007/s10096-017-2948-1
33. Guo Y, Logan HL, Glueck DH, Muller KE. Selecting a sample size for studies with repeated measures. *BMC Med Res Methodol* (2013) 13(1):100. doi: 10.1186/1471-2288-13-100
34. Aung KJM, Van Deun A, Declercq E, Sarker MR, Das PK, Hossain MA, et al. Successful '9-month Bangladesh regimen' for multidrugresistant tuberculosis among over 500 consecutive patients. *Int J Tuberc Lung Dis* (2014) 18 (10):1180–7. doi: 10.5588/ijtld.14.0100
35. Qiagen. QuantiFERON®-TB Gold Plus (QFT®-Plus) Package Insert. (2013) 96:1101062.
36. Castor EDC. Castor Electronic Data Capture [online]. (2019). Available at: https://castoredc.com.
37. Kim H-Y. Statistical notes for clinical researchers: Chi-squared test and Fisher's exact test. *Restor Dent Endod* (2017) 42:152. doi: 10.5395/rde.2017.42.2.152
38. Dunn OJ. Multiple Comparisons Using Rank Sums. *Technometrics* (1964) 6:241–52. doi: 10.1080/00401706.1964.10490181
39. Pedro HDSP, Nardi SMT, Pereira MIF, Oliveira RS, Suffys PN, Gomes HM, et al. Clinical and epidemiological profiles of individuals with drug-resistant tuberculosis. *Mem Inst Oswaldo Cruz* (2015) 110(2):235–48. doi: 10.1590/0074-02760140316
40. Delogu G, et al. The hbhA gene of Mycobacterium tuberculosis is specifically upregulated in the lungs but not in the spleens of aerogenically infected mice. *Infect Immun* (2006) 74:3006–11. doi: 10.1128/IAI.74.5.3006-3011.2006
41. Zheng Q, et al. Heparin-binding hemagglutinin of Mycobacterium tuberculosis is an inhibitor of autophagy. *Front Cell Infect Microbiol* (2017) 7:1–11. doi: 10.3389/fcimb.2017.00033
42. Hougardy JM, et al. Regulatory T cells depress immune responses to protective antigens in active tuberculosis. *Am J Respir Crit Care Med* (2007) 176:409–16. doi: 10.1164/rccm.200701-084OC
43. Auld SC, Lee SH, Click ES, Miramontes R, Day CL, Gandhi NR, et al. IFN-γ release assay result is associated with disease site and death in active tuberculosis. *Ann Am Thorac Soc* (2016) 13(12):2151–8. doi: 10.1513/AnnalsATS.201606-482OC
44. Roberts T, Beyers N, Aguirre A, Walzl G. Immunosuppression during Active Tuberculosis Is Characterized by Decreased Interferon-γ Production and CD25 Expression with Elevated Forkhead Box P3 , Transforming Growth Factor – b , and Interleukin-4 mRNA Levels. *J Infect Dis* (2007) 195(6):870–8. doi: 10.1086/511277
45. Goletti D, Butera O, Bizzoni F, Casetti R, Girardi E, Poccia F. Region of Difference 1 Antigen–Specific CD4 + Memory T Cells Correlate with a Favorable Outcome of Tuberculosis. *J Infect Dis* (2006) 194(7):984–92. doi: 10.1086/507427
46. Jasenosky LD, Scriba TJ, Hanekom WA, Goldfeld AE. T cells and adaptive immunity to Mycobacterium tuberculosis in humans. *Immunol Rev* (2015) 264:74–87. doi: 10.1111/imr.12274
47. Smith GCS, Seaman SR, Wood AM, Royston P, White IR. Correcting for optimistic prediction in small data sets. *Am J Epidemiol* (2014) 180:318–24. doi: 10.1093/aje/kwu140

Conflict of Interest: MH, MI, and RB had logistic support from the National TB program in Lebanon. DG reports personal fees from Quidel, Qiagen, Janssen, BioMérieux, and Celgene, outside the submitted work. All authors have submitted the ICMJE Form for Disclosure of Potential.

4. Beyond secreted biomarkers: a high-dimensional cytometric analysis of the T-cell response over the course of TB treatment.

4.1 Publication 3

In-depth immunophenotyping with mass cytometry reveals antigen-driven, non-canonical T-cell subset abundance changes during anti-TB treatment.

Carole CHEDID, Thibault ANDRIEU, Eka KOKHREIDZE, Nestani TUKVADZE, Md. Fahim ATHER, Samanta BISWAS, Mohammad Khaja Mafij UDDIN, Sayera BANU, Flavio DE MAIO, Giovanni DELOGU, Hubert ENDTZ, Delia GOLETTI, Marc VOCANSON, Oana DUMITRESCU, Jonathan HOFFMANN, Florence ADER.

(Submitted to Science Translational Medicine on September 24, 2021)

Article summary

Novel non-sputum-based tests are needed to improve TB treatment monitoring and shorten treatment. Blood-based host immune biomarkers are promising targets because immune cells undergo phenotypic changes over the course of the disease, in particular T-cells. However, they have been mostly investigated in low-TB prevalence settings, with conventional flow cytometry that measures a limited number of cell markers, or with high-dimensional cytometry across diverse PBMC subpopulations but at the expense of deep profiling. In particular, detailed phenotypic data on Mtb-stimulated $CD8^+$ T-cells during treatment are scarce. Here, in a prospective cohort study of adult patients treated for TB in Bangladesh and Georgia, we characterized peripheral blood T-cell immune-profiles with a 29-marker mass cytometry panel. Deep T-cell profiling was performed using unsupervised analysis. Results were examined throughout treatment at first, and then according to culture conversion at the end of the intensive phase to study the association between T-cell profiles and Mtb clearance.

Between May 2019 and July 2020, we analyzed 144 samples collected from 22 adult, culture confirmed, non-immunosuppressed PTB patients (4 in Bangladesh and 18 in Georgia; 11 DS-TB and 11 DR-TB patients). Samples were either unstimulated or Mtb antigen-stimulated (QFT-P TB2 or rmsHBHA). All patients achieved microbiological cure at the end of treatment. At T1, definitive culture conversion occurred in 18 patients (fast converters) and cultures remained positive in 4 patients (slow converters). Unsupervised cell subpopulation clustering based on lineage markers revealed 196 distinct clusters grouped into 12 meta-clusters consistent with canonical T-cell subpopulations. The abundance of each cluster was assessed during treatment and clusters within which significant abundance changes were detected were examined. Hierarchical clustering based on functional markers uncovered four subgroups of phenotypically similar T-cell clusters with comparable abundance changes during treatment. Four of these subgroups were associated with cure and remained relevant at the individual level (central memory $CD4^+$ $CCR6^+$ $IL7Ra^+$ $CD27^+$ $CD40L^+$ $CD38^+$ $HLA\text{-}DR^+$; effector memory $CD8^+$ $CD7^+$ $perforin^+$; central memory $CD4^+$ $CCR6^+$ $CD26^+$ $IL7Ra^+$ $CD27^+$ $CD40L^+$ $CD38^+$ $HLA\text{-}DR^-$; effector memory $CD4^+$ $CD26^+$ $IL7Ra^+$ $CD7^+$ $CD27^+$), which was verified with manual gating analyses. T-cell immune-profile comparison at each timepoint according to culture status at T1 revealed that cytotoxic and terminally differentiated $CD8^+$ T-cells were under-represented

and naïve $CD4^+$ T-cells were over-represented in slow compared to fast converters during treatment. Then, PCA on non-lineage markers highlighted that most of the immune variance observed between slow and fast converters was explained by CCR4, CD26, CD7, and CD27 expression, and to a lesser extent by cytotoxicity and activation markers.

These results show that T-cell phenotype changes during TB treatment are detectable in Mtb-stimulated samples without restriction to Mtb-specific cells. They indicate an antigen-driven immune shift towards differentiated subpopulations, including cytotoxic $CD8^+$ T-cells, which is associated with TB cure. Importantly, this shift appears to be delayed in patients with slower microbiological cure. We were able to discover these new insights on TB immunobiology during treatment precisely because $CD8^+$ T-cell-stimulating antigens were used, differently from previous works mobilizing canonical Mtb antigens without HLA-DR-I loading. These results suggest that T-cell immune profile combinations may be possible surrogate non-sputum biomarkers of TB treatment efficacy. External validation in cohorts with higher rates of treatment failure is necessary to confirm the observed trends. Ideally, a comparison with broncho-alveolar lavage fluid lymphocytes and an assessment of T-cell subset abundance changes in latently TB infected participants would help further characterize identify T-cell phenotypes associating with TB control in the periphery and at the site of infection.

In-depth immunophenotyping with mass cytometry reveals antigen-driven, non-canonical T-cell subset abundance changes during TB treatment.

One-sentence summary: High-dimensional immune profiling during active TB treatment reveals non-canonical $CD8^+$ T-cell phenotypes associated with *Mycobacterium tuberculosis* culture sterilization.

Authors: Carole CHEDID[1,2,3#], Thibault ANDRIEU[4], Eka KOKHREIDZE[5#], Nestani TUKVADZE[5#], Samanta BISWAS[6#], Md. Fahim ATHER[6#], Mohammad Khaja Mafij UDDIN[6#], Sayera BANU[6#], Flavio DE MAIO[7], Giovanni DELOGU[7], Hubert ENDTZ[8#], Delia GOLETTI[9], Marc VOCANSON[1], Oana DUMITRESCU[1,10,11], Jonathan HOFFMANN[1,2*#], Florence ADER[1,12*].

Affiliations:

1. Centre International de Recherche en Infectiologie, Legionella Pathogenesis Group, INSERM U1111, Université Claude Bernard Lyon 1, CNRS UMR5308, École Normale Supérieure de Lyon, Lyon, France
2. Medical and Scientific Department, Fondation Mérieux, Lyon, France
3. Département de Biologie, Ecole Normale Supérieure de Lyon, Lyon, France
4. Cytometry Core Facility, Centre de Recherche en Cancérologie de Lyon, Université Claude Bernard Lyon 1, Inserm 1052, CNRS 5286, Centre Léon Bérard, 69373, Lyon, France
5. National Center for Tuberculosis and Lung Diseases (NCTBLD), Tbilisi, Georgia
6. Infectious Diseases Division, International Centre for Diarrhoeal Disease Research, Bangladesh (icddr,b), Dhaka, Bangladesh
7. Dipartimento di Scienze biotecnologiche di base, cliniche intensivologiche e perioperatorie – Sezione di Microbiologia, Università Cattolica del Sacro Cuore, Rome, Italy
8. Fondation Mérieux, Lyon, France
9. Translational Research Unit, Department of Epidemiology and Preclinical Research, "L. Spallanzani" National Institute for Infectious Diseases (INMI), IRCCS, Rome, Italy
10. Hospices Civils de Lyon, Institut des Agents Infectieux, Laboratoire de Bactériologie, Lyon, France
11. Université Lyon 1, Facultés de Médecine et de Pharmacie de Lyon, Lyon, France

12. Hospices Civils de Lyon, Hôpital de la Croix-Rousse, Département des Maladies Infectieuses et Tropicales, F-69004, Lyon, France.

* These authors share the senior authorship. #: On behalf of the HINTT working group within the GABRIEL network.

Keywords: tuberculosis; treatment monitoring; immunophenotyping; $CD8^+$ T-cells; heparin-binding hemagglutinin; inflammatory markers; mass cytometry; unsupervised data analysis.

Corresponding author:

Carole CHEDID

Centre International de Recherche en Infectiologie INSERM U1111 – CNRS UMR5308

Département des Maladies Infectieuses et Tropicales

Hôpital de la Croix-Rousse, Hospices Civils de Lyon,

104, Grande Rue de la Croix-Rousse

69004 Lyon, FRANCE

carole.chedid@fondation-merieux.org;

+33 6 72 68 69 35

Abstract

Tuberculosis (TB) is a difficult-to-treat infection because of multidrug regimen requirements based on drug susceptibility profiles and treatment observance issues. TB cure is defined by mycobacterial sterilization, technically complex to systematically assess. We hypothesized that microbiological outcome was associated with stage-specific immune changes in peripheral whole blood during TB treatment. The T-cell phenotypes of treated TB patients were prospectively characterized in a blinded fashion using mass cytometry after *Mycobacterium tuberculosis* (*Mtb*) antigen stimulation, and then correlated to sputum culture status. At two months of treatment, cytotoxic and terminally differentiated $CD8^+$ T-cells were under-represented and naïve $CD4^+$ T-cells were over-represented in positive- *versus* negative-sputum culture patients, regardless of *Mtb* drug susceptibility. At treatment completion, an antigen-driven T-cell immune shift towards differentiated subpopulations was associated with TB cure. Overall, we identified specific T-cell profiles associated with slow sputum converters, which brings new insights in TB prognostic biomarker research designed for clinical application.

Introduction

Tuberculosis (TB) is a leading cause of death of infectious origin, responsible for 1.5 million deaths worldwide in 2020 *(1)*. TB treatment regimens have toxic side effects *(2)* requiring monitoring throughout treatment to adapt it and assess effectiveness. Pulmonary TB treatment monitoring relies on *Mycobacterium tuberculosis* (*Mtb*) detection in sputum samples *(3)*, which can be difficult to collect in later stages of treatment *(4)*. Smear microscopy yields highly sample- and operator-dependent results and has poor sensitivity *(5)*. Sputum culture is the gold standard, although slow and requiring biosafety laboratory environments *(6)*. Simultaneously, one of the main stakes in improving TB management is shortening TB treatment *(7)*. Overall, there is a need for novel non-sputum-based tools to monitor disease resolution and assess cure while remaining feasible in primary care settings *(8)*. Blood-based host immune biomarkers have recently gained interest in TB research as immune cells undergo phenotypic changes throughout the disease. Numerous past investigations have pointed to variations in the abundance and marker expression of several targeted subpopulations *(9–12)*, in particular T-cells, which are pivotal effectors for *Mtb* clearance *(13)*. However, this has been explored mostly in low-TB prevalence settings or with conventional flow cytometry, targeting a limited number of cell markers *(14, 15)*.

High-dimensional single-cell technologies such as mass cytometry enable the detection and quantification of a high number of cell markers *(16)*. This technique bypasses the limitations of spectral overlap by using monoclonal antibodies coupled to metal polymers, and has allowed high-dimensional exploration of the immune landscape in several domains *(17, 18)*. It has been applied to immune profiling during TB treatment in a 2018 study by Roy Chowdhury and colleagues *(19)*, in which the authors have provided a general overview of changes in the main immune blood cells during treatment.

Here, in a prospective, international cohort study of adult patients treated for pulmonary TB in high prevalence countries, peripheral blood T-cell immune-profiles were characterized using a 29-marker mass cytometry panel. In-depth T-cell phenotypical analysis was performed upon TB treatment initiation, after two months and at completion of treatment. To examine the relation between mycobacterial clearance in hosts and changes in T-cell immune-profiles, the results of these analysis were compared in negative and positive sputum culture conversion patients after two months of treatment.

Results

Study design and analysis strategy

Between May 2019 and July 2020, 144 cell samples collected from 22 adult TB patients were analyzed (Bangladesh, n=4 and Georgia, n=18; DS- and DR-TB, n=11 each) (Supp. Figure 1). Patient demographic, microbiological and clinical characteristics are available in Supp. Table 1. All patients achieved microbiological cure at the end of treatment, but were retrospectively classified into two response groups according to their *M. tuberculosis* culture status at T1 (after two months of treatment): fast converters (n=18; negative culture at T1 and T2) and slow converters (n=4; positive culture at T1 and negative culture at T2). Among the latter, three patients were treated for DS-TB and one for DR-TB.

An overview of the data collection and analysis process is shown in Figure 1. Briefly, data from all samples were clustered automatically into subsets of homogeneous phenotypes to provide a framework for analysis. Clusters were then color-coded and plotted onto a two-dimension map to create a visual reference used throughout the paper (Figure 2). On this basis, automatically detected clusters were first quantified and analyzed dynamically throughout treatment to identify median clusters abundance variations associated with treatment completion (Figure 3). Cluster phenotypes were deduced from marker expression heatmaps, and hierarchical clustering was applied based on marker expression (Figure 4). In a supervised manner, clusters of similar abundance changes and immunophenotypes were then re-grouped into larger subsets, in order to assess relevance of the detected abundance variations at the individual level, and consistency with manual gating (Figure 5). Finally, a cross sectional analysis was performed at T1 to identify which automatically detected clusters differentiated patients based on the microbiological response to the intensive phase of treatment (*Mtb* culture positivity at T1; Figures 6 and 7).

Overall analysis of peripheral T lymphocyte subset abundance changes throughout TB treatment.

First, a phenotype analysis was performed to identify the main expected T-cell subpopulations. As no apparent difference was seen in UMAP structures within samples from the different timepoints and stimulation conditions despite some marker expression differences between stimulation conditions (Supp. Figure 2; exact p-values and test statistics in Supp. Table 2), we performed the phenotype analysis on all single $CD3^+$ events. The purpose

of this study was not to compare the stimulations, but rather to use them to uncover clusters that might be associated with treatment response and that would not be visible in unstimulated samples. FlowSOM automated clustering was performed on $CD3^+$ events, revealing a total of 196 automatically detected clusters (Figure 2.A to 2.C). They were automatically grouped into 18 meta-clusters, which were assembled into 12 canonical T-cell subpopulations in a supervised manner (Figure 2.D and 2.E). FlowSOM clusters and meta-clusters were then visualized on the initial UMAP to create a reference map of all automatically detected T-cell subsets (Figure 2.F and 2.G).

To initiate the abundance analysis, variations of the main T-cell subpopulations throughout treatment were then studied using a stratification according to each stimulation condition. No significant change in the proportion of total $CD4^+$, $CD8^+$, γδ, double negative (DN, $CD4^-$ CD8) or double positive (DP, $CD4^+$ $CD8^+$) T-cells was observed throughout treatment in any stimulation condition (Supp. Figure 3). For all main studied subpopulations, no significant difference was observed between DS- and DR-TB patients (data not shown).

Differential abundance of non-canonical T-cell subsets throughout TB treatment.

To identify non-canonical T-cell subsets whose abundance changed throughout treatment, we calculated the percentage of each automatically determined FlowSOM cluster at each timepoint and in each stimulation condition. These clusters were then categorized into two groups: enriched or decreased after treatment completion. Abundance changes were studied between T0 and T1 and T0 and T2 to characterize the main clusters associated with response to treatment intensive phase and with treatment completion respectively. As these clusters represent non-canonical cell subpopulations, their frequencies among total $CD3^+$ events were low (< 5% in most samples). Hence, the differences analyzed thereafter describe rare populations and warrant cautious analysis.

When comparing the reference UMAP (Figure 2.G) to the UMAP of clusters which were increased between T0 and T1 (Supp. Figure 4.A), we observed that they were either DN T-cells, or effector memory (EM) or terminally differentiated effectors re-expressing CD45RA (TEMRA) cells from both $CD4^+$ and $CD8^+$ subpopulations. In unstimulated samples, significant increases were detected within three clusters corresponding to $CD8^+$ and DN T-cell subsets (Supp. Figure 4.B), whereas increases were detected in one $CD4^+$ and one $CD8^+$ cluster in TB2-stimulated samples (Supp. Figure 4.C) and only in $CD4^+$ clusters in rmsHBHA samples (Supp. Figure 4.D).

Clusters that decreased between T0 and T1 (Supp. Figure 4.E)were detected only within $CD8^+$ EM and TEMRA cells in all stimulation conditions (Supp. Figure 4.F to 4.H).

Between T0 and T2, 11 increased clusters were detected (Figure 3.A). They corresponded mostly (8/11 clusters, 73%) to $CD4^+$ EM and CM subpopulations rather than naïve subsets, regardless of the stimulation condition (Figure 3.B. to 3.D.). One DN cluster was increased in unstimulated samples (Figure 3.B. as well as one $CD8^+$ TEMRA cluster and one γδ T-cell cluster in rmsHBHA stimulated samples (Figure 3.D.). One $CD4^+$ CM cluster (number 38) increased significantly in samples from all three stimulation conditions. Clusters which decreased between T0 and T2 were detected in one $CD8^+$ EM and two $CD8^+$ TEMRA subsets, and in seven clusters within $CD4^+$ subpopulations in all three stimulation conditions (Figure 3.E to 3.H). Regarding the latter clusters, no clear trend was observed regarding memory subset compartmentalization, which suggests that the abundance decrease spared memory functions and rather affected $CD4^+$ T-cells in general. One γδ and one DN T-cell cluster also decreased significantly within *Mtb*-stimulated samples (Figure 3.G. and 3.H.).

Antigen-driven cluster abundance changes during TB treatment show involvement of effector and memory T-cells.

To further refine patterns in functional marker expressions within increased or decreased clusters, we then performed a detailed phenotype analysis using marker expression heatmaps and hierarchical clustering (Figure 4). Four subgroups of cellular subsets of similar abundance changes and similar immunophenotypes were identified (labeled from A to D). Subgroup A included four $CD4^+$ T-cell clusters with naive (n=2) and CM (n=2) phenotypes, which decreased from T0 to T2 in rmsHBHA-stimulated samples. Subgroup B included five $CD8^+$ T-cell clusters that decreased throughout treatment, two of them between T0 and T1 and three of them between T0 and T2. Consistently with the above results (Figure 3.E.), the latter were either EM or TEMRA cells, with low CD45RA levels and intermediate levels of perforin. The other two clusters were naïve clusters with low CCR7, CD45RA, and CD27 expression levels.

In contrast, subgroup C and D included only $CD4^+$ T-cell clusters, most of which (70%, 7/10) increased between T0 and T2. Subgroup C consisted in five clusters exhibiting a CM phenotype and expressing activation markers, detected in unstimulated and TB2-stimulated samples. Subgroup D clusters were detected in *Mtb*-stimulated samples (3 in rmsHBHA and 2 in TB2) and had an EM phenotype, except for cluster 69 that had a CM phenotype with low levels of

CCR7. These clusters co-expressed CD26, IL7Ra, CD7 and CD27. They were characterized by an absence of activation marker expression and an enhanced expression of exhaustion markers, in particular CTLA-4 and PD-1. Overall, we observed antigen-driven T-cell subset abundance changes between T0 and T2. In TB2 and rmsHBHA samples, $CD4^+$ EM clusters mostly increased, while $CD8^+$ EM clusters mostly decreased.

Individual profiling confirms abundance changes in phenotypically homogeneous, correlated subsets after treatment in cured patients.

As the differentially abundant clusters identified above accounted for a small fraction of $CD3^+$ T-cells (<1%), we intended to identify the largest possible subsets of phenotypically homogeneous cells within which a significant abundance change was detectable (Figure 5). Within the subgroups of similar immunophenotypes and abundance change identified in Figures 3 and 4, we performed correlation analyses at baseline and pooled the best correlated clusters together within the subgroups identified in Figure 4 (Figure 5.A and 5.D). We then visualized the individual abundance change of these pooled subsets before and after treatment completion in cured patients (Figure 5.B-C and 5.D-E). Within rmsHBHA samples, a decrease in subgroup A and an increase in subgroup D were both detected in 93% (13/14) of cured participants (Table 1). Within unstimulated samples, a decrease in subgroup B and an increase in subgroup C were recorded in 81% (13/16) and 88% (14/16) of patients respectively. This confirmed that the median trends observed previously were maintained individually in most patients. Finally, we visualized the immunophenotypes of these four subgroups of interest in comparison to cells from similar subpopulations which were not associated to cure (Figure 5.F). Subgroup A and subgroup C corresponded to $CD4^+$ CM cells expressing CCR6, IL7Ra, CD27, and activation markers (CD40L, CD38). However, cells within subgroup A expressed HLA-DR while subgroup C did not; in addition, cells from subgroup C expressed high levels of CD26, as well as CCR4, CXCR3, and CD7. Subgroup B corresponded to $CD8^+$ $CD7^+$ $Perforin^+$ EM cells. Subgroup D corresponded $CD4^+$ EM cells expressing high levels of CD26, as well as CCR4, CCR6, CXCR3, IL7Ra, CD7, and CD27. We then confirmed these findings by manually gating the identified subpopulations and comparing the percentages at T0 and T2 (Figure 5.G-K, representative dot plots).

Patients with persistent positive cultures at T1 show decreased peripheral CD8$^+$ cytotoxic subsets and enriched peripheral CD4$^+$ naïve subsets throughout treatment compared to patients with negative cultures at T1.

Then, we aimed to detect a cellular signature associated with mycobacterial conversion. To do so, we analyzed individual cluster abundance in slow *vs*. fast converters throughout treatment. At T0, T1, and T2, respectively 21, 24, and 21 clusters with significantly different abundance in slow converters compared to fast converters were detected (quantification in Supp. Fig. 5). After phenotyping, the proportions of the main T-cell subpopulation phenotypes in each group of enriched or decreased clusters at T0, T1, and T2 were calculated and summarized in Table 2.

Before treatment initiation, of 21 clusters with different abundance, 18 (86%) were decreased (Supp. Figure 5.A) and three (14%) were enriched (Supp. Figure 5.B) in slow compared to fast converters. Clusters which were under-represented in slow converters corresponded mostly to DN, γδ, and CD8$^+$ T-cells (77%, 13/18 clusters), specifically γδ and CD8$^+$ EM T-cell subpopulations (38%, 5/13 each); in addition, a majority of these clusters was perforin$^+$ (67%, 12/18) (Supp. Figure 6.A). In contrast, the three enriched clusters were naive CD4$^+$ and CD8$^+$ T-cells, as well as one CD8$^+$ TEMRA subset.

At T1, of 24 clusters with significantly different abundance between slow and fast converters, 15 (62%) were decreased (Figure 6.A and 6.C) and 9 (38%) were enriched in slow converters (Figure 6.B and 6.D). These clusters were mostly detected in TB2-stimulated samples (63%; 15/24 clusters). Comparison to the reference UMAP (Figure 6.E) and hierarchical clustering (Figure 6.F) indicated that enriched and decreased subsets respectively had similar immunophenotypes. Clusters which were under-represented at T1 in slow converters were mostly perforin$^+$ cells (67%, 10/15 clusters); mostly CD8$^+$ TEMRA and DN T-cell phenotypes were represented (40%, 6/15 clusters respectively). In contrast, enriched clusters comprised a majority of CD4$^+$ T-cells (78%, 7/9 clusters), with predominantly naïve phenotypes (45%, 3/7). One CD8$^+$ naive and one CD8$^+$ EM cluster were also enriched in slow converters at T1, with the latter expressing ICOS.

After treatment completion, of 21 clusters with significantly different abundance between slow and fast converters, 11 (52%) were decreased (Supp. Figure 5.C) and 10 (48%) were enriched in slow converters (Supp. Figure 5.D). The immunophenotype profile at T2 was similar to that of T1 for the enriched subsets: a majority of ICOS$^+$ CD4$^+$ naïve T-cell subsets

(50%, 5/10) were detected, as well as two $CD8^+$ naïve clusters (Supp. Figure 6.B). Regarding the decreased subsets, no specific phenotype polarization was observed, and clusters were detected within diverse subsets (four $CD8^+$ EM clusters, four $CD4^+$ EM clusters, and three DN T-cells clusters). Similarly to the T1 immune profile, all of the above clusters were mostly detected in TB2-stimulated samples (67%, 14/21 clusters).

Maturation markers and chemokine receptors, rather than activation or cytotoxic markers, discriminate slow from fast converters during treatment.

Finally, we sought to assess more precisely which combinations of cellular markers were the most involved in the discrimination between fast and slow converters within the clusters identified in the prior section. A principal component analysis (PCA) was performed on marker expression data within these clusters. As a higher number of differentially abundant clusters had been detected in *Mtb*-stimulated samples than in unstimulated samples during treatment (T1 and T2), and because a complete overlap between the PCA profiles of fast and slow converters was observed in unstimulated samples, we focused on *Mtb*-stimulated samples (TB2 and rmsHBHA). PCA profiles were mostly separated when split by culture conversion group (Figure 7.a). Dimension 1 (Dim1) explained 37.3% of the total observed variance, versus 12.5% for Dim2. The main markers accounting for variance described by Dim1 were markers of memory subset definition (CCR7 and CD45RA), lineage (CD4 and TCRγδ), maturation (CD27 and CD7), chemokine receptors (CCR4 and to a lesser extent CXCR3) or other receptors or costimulatory molecules (*e.g.*, CD26, CD161) (Figure 7.B. and 7.C). In contrast, variance described by Dim2 was mostly explained by cytotoxicity (Perforin, CD56, CD8), activation (CD38, CD40L, CD69), or exhaustion markers (CD152, PD-1) (Figure 7.B and 7.D). The PCA scores were significantly higher in slow converters than in fast converters at all timepoints for Dim1 (Figure 7.E), indicating that the immune profile of slow converters was more correlated to Dim1 than that of fast converters regardless of the timepoint. In contrast, no significant differences were detected at the end of treatment (T2) for Dim2 (Figure 7.F). When comparing these results with PCA analyses performed on total $CD3^+$ T-cells, fast and slow converter profiles were less separated, but similar marker involvement was observed in Dim1 and Dim2 respectively (Supp. Figure 7).

Discussion

In a population of adults treated for TB, we observed a shift towards more differentiated profiles among peripheral $CD8^+$ and $CD4^+$ T-cell subsets driven by the timing of *Mtb* culture conversion, using a high-dimensional single cell approach after stimulation with standardized, IVD-level TB2 antigens. In particular, differentiated $CD8^+$ cytotoxic effector subsets were under-represented in positive- versus negative-sputum culture patients after two months of treatment.

Over the course of TB treatment, we observed as a general trend that non-canonical subsets within CM $CD4^+$ and TEMRA $CD8^+$ populations increased, whereas naïve $CD4^+$ and naïve/EM $CD8^+$ subsets decreased. This is consistent with prior works addressing T-cell differentiation and T-cell memory subsets during TB treatment *(20–22)*. *Mtb*-specific $CD4^+$ EM T-cells have been associated with active TB disease, whereas CM T-cells have been associated to latency and increased upon treatment *(23, 24)*. In *Mtb*-specific $CD8^+$ T-cells, an overall decrease in peripheral blood *(25)* and a decrease in CM cells *(26)* have been documented after treatment. In contrast, the central result of this study was to distinguish negative- from positive-sputum culture patients at two months, whether infected with a DS- or DR-*Mtb* strain, through differential peripheral T-cell populations. When retrospectively analyzing the T-cell profiles of fast and slow converters at diagnosis, a pre-existing difference in percentages of cytotoxic EM $CD8^+$ T-cell subpopulations was already observed. After two months of treatment, this trend shifted into an under-representation of $CD8^+$ TEMRA, which persisted after cure. These changes were revealed upon stimulation with QFT-P TB2 antigenic peptide pools. Although many studies characterizing T-cell subsets during treatment have clearly underlined the importance of *Mtb*-specific $CD4^+$ T-cells *(9, 13, 27)*, less is known about the role of $CD8^+$ T-cells in TB resolution and the most appropriate epitopes to study them in this context *(28, 29)*. Yet, effector $CD8^+$ T-cells are known to secrete cytolytic and antimicrobial factors that kill *Mtb*-infected macrophages *in vitro (30)*, inhibit *Mtb* growth *(28)*, and are required for long-term infection control in mice *(31)* and humans *(32)*; perforin production by $CD8^+$ T-cells is also higher in treated than in untreated TB patients *(33)*. In addition, a 2012 study by Rozot and colleagues had associated *Mtb*-specific TEMRA $CD8^+$ T cells to LTBI and EM cells to active TB *(34)*. Here, although we cannot establish causality, a lower peripheral $CD8^+$ TEMRA subset abundance may be associated with slower mycobacterial culture conversion. In relation with abundance changes during treatment, our study hints that the $CD8^+$ T-cell phenotype shift

occurring during TB treatment would be delayed in patients with slower microbiological conversion. Consistently, it has been shown that $CD8^+$ response importantly contributed to the control of other granulomatous infections such as *Brucella (35)*. Regarding $CD4^+$ T-cells, naïve subsets were over-represented in slow converters, which suggests a delayed differentiation within the $CD4^+$ compartment as well. Previous work has shown that the IFN-γ/IL-2/TNF-α functional profile of *Mtb*-specific $CD4^+$ T-cells, which is key in anti-TB immunity *(14)*, was correlated with their degree of differentiation *(36)*. Taken together, these results support the hypothesis that $CD4^+$ and $CD8^+$ T-cell responses should be monitored together during TB treatment, as successful mycobacterial clearance involves $CD8^+$ T-cell effectors, which in turn require $CD4^+$ T-cell involvement *(37)*.

Although the aim of this study was not to compare stimulation conditions, but to use them to uncover cell clusters, our results suggest that the abundance changes observed throughout treatment are antigen-driven. This adds to previous work highlighting differential *Mtb*-specific $CD8^+$ T-cells marker profiles according to the nature of the antigen stimulation *(38)*. We used QFT-P TB2, which elicits cytotoxic $CD8^+$ responses in addition to ESAT-6/CFP-10-induced $CD4^+$ responses *(39)*, as well as rmsHBHA, a recombinant *Mtb* protein exposing many different epitopes. The latter was included because the IFN-γ response to HBHA, to which both $CD4^+$ and $CD8^+$ cells participate *(40)*, is impaired in active TB patients and restored during treatment *(41–43)*. Here, changes during treatment in $CD8^+$, $CD4^+$, DN, and γδ T-cell subsets were detectable within unstimulated and TB2 samples, consistently with previous works *(39)*. In contrast, in rmsHBHA-stimulated samples, significant abundance changes were mostly detected within $CD4^+$ T-cells, suggesting a preferential $CD4^+$ T-cell response to HBHA epitopes during treatment. This indicates that antigen-driven changes during the response to *Mtb* are part of a complex process involving a variety of different epitopes *(26)* that induce responses from phenotypically diverse T-cell subsets *(38)*, despite well-described immunodominance features. Our results confirm that a major stake in discovering blood-based immune signatures of mycobacterial sterilization lies in finding the appropriate epitopes.

Finally, our study enabled profiling of non-lineage markers. A $CXCR3^+$ $CCR6^+$ $CD27^+$ $CD4^+$ EM subset was increased in cured patients compared to pre-treatment, corresponding to a subset enriched in Th1/Th17 cells *(44, 45)*. Consistently with previous work on LTBI *(46)*, this suggests that an increase in these cells upon cure might be associated with infection control. Compared to the other $CD4^+$ EM cells, this subset displayed higher CD26 and IL7Ra expression. CD26

participates in T-cell activation and proliferation *(47)*, and correlates with Th1-like responses *(48)*. In parallel, a significant decrease was also observed in a highly activated CCR6$^+$ IL7Ra$^+$ CD4$^+$ CM subset, which expressed higher levels of CD40L, CD38, and HLA-DR than other CD4$^+$ CM cells. Interestingly, an increase in another CD4$^+$ CM subset – which differed from the latter because it expressed CD26 and CD27, but not HLA-DR – was observed simultaneously. This adds to previous works with previous works highlighting a decrease in CD38$^+$ and HLA-DR$^+$ *Mtb*-specific CD4$^+$ T-cells in successfully treated TB patients *(13, 49, 50)*. This suggests that upon TB treatment, differentiated Th1/Th17-like CD4$^+$ subsets expressing high levels of CD26 and IL7Ra are enriched in peripheral blood, likely at the expense of less differentiated subsets expressing high levels of CD27 and CD38. Finally, principal components analysis showed that within the subpopulations that differentiated slow from fast converters during treatment, differentiation markers and chemokine receptors contributed to most of the variance, followed by activation and cytotoxicity markers. CD27, CD26, and CCR4 were among the markers which best discriminated fast and slow responders, consistently with prior studies associating CD27 and CCR4 expression in *Mtb*-specific CD4$^+$ T-cells with active TB compared to latent infection *(51)*. HLA-DR and CD38 also contributed to a lesser extent, which adds to a recent study in which co-expression of CD27, HLA-DR, and CD38 on PPD-stimulated CD4$^+$ T-cells stratified fast and slow responders without restriction to IFN-γ-producing cells *(52)*.

This descriptive study has limitations. The number of patients included was low, resulting in few slow converters, consistently with treated TB course (15 to 20% of slow culture converters). In addition, the presence of within-host *Mtb* isolate micro-diversity has been recently proven in patients treated for DS-TB without culture conversion after two months of well-conducted TB treatment *(53)*, suggesting that it could modulate the host response. We are currently conducting a larger validation study including DS-TB patients only, from whom *Mtb* isolates collected upon treatment initiation and at two months will be screened by whole genome sequencing. In addition, the analyses were not conducted on live cells, but on fixed, cryopreserved peripheral blood cells due to the design of the study using samples collected in lower-income, high TB prevalence settings. For the same reason, the study was conducted on peripheral blood, while the main infectious focus of TB is in the lungs. In addition, since the study required to IGRAs to be performed on the same blood samples prior to cell cryopreservation *(41)*, we did not perform intracellular cytokine staining. Hence, the integrality of the observed cell phenotype changes may not be associated with *Mtb*-specific

responses. However, whether the bulk of anti-TB response relies purely on *Mtb*-specific cells is debated. Given the complexity of the immune response to TB, cellular and molecular interactions are likely to occur between *Mtb*-specific and non-specific subpopulations during mycobacterial clearance, and hence influence the overall T-cell profiles. In addition, the hypothesis that T-cells specific for immunodominant epitopes actually recognize *Mtb*-infected cells has been challenged by studies on mouse models *(54)*, protective immunity post-BCG vaccination*(55)*, and failures of vaccine candidates based on immunodominant antigens *(56)*. These limitations are linked to the "bench to bedside" approach adopted in our study. They reflect the reality of the needs for novel TB management tools: accessible samples, simple experimental process, straightforward output. Here, we captured the complexity of T-cell profiles during treatment and narrowed it down to subpopulations of interest associated with cure at the individual level. Although mass cytometry requires complex equipment, experiments, and analyses, we have shown that relevant T-cell profiles could be identified in cryopreserved samples, obtained from small blood volumes, using manual gating analyses and a smaller number of core markers. Future validation studies might confirm the relevancy of simpler phenotypic signatures translatable in primary care settings. Importantly, our study revealed T-cell populations discriminating patient status based on culture conversion, which has a dual impact: on TB management, to better characterize the phenotypes of T-cells involved in TB clearance; and on biomarker research, further supporting that a diversity of epitopes is needed to fully disclose the spectrum of these cells. This work may help identify simpler prognostic biomarkers associated with mycobacterial clearance and the antigens appropriate for their discovery.

Materials and methods

Experimental design

Study design and research objectives

This prospective cohort study was nested in a multicentered study coordinated by the Mérieux Foundation GABRIEL network *(57)*. The primary objective was to investigate the association between sputum culture sterilization during active TB treatment and characteristic T-cell profiles obtained by high-dimensional phenotyping. The sample size was maximized based on availability of clinical samples. No prospective sample size calculations were performed.

Recruitment centers and ethical considerations

Recruitment centers were the National Center for Tuberculosis and Lung Disease (NTCLD) in Tbilisi, Georgia (approval of the Institutional Review Board of the NTCLD; IORG0009467); and the International Centre for Diarrhoeal Disease Research, Bangladesh (icddr,b) in Dhaka, Bangladesh (approval of the Research Review Committee and the Ethical Review Committee of icddr,b; PR-17076; Version No. 1.3; Version date: 04-01-2018). All participants provided written informed consent.

Cohort recruitment, patient follow-up, and clinical data collection

Patients were recruited if diagnosed with sputum culture confirmed pulmonary TB and older than 15 years old. Patients with HIV, immune deficiency, diabetes mellitus, and lost-to-follow-up were excluded. Detailed procedures for microbiological diagnosis, drug susceptibility testing, and treatment regimens are described elsewhere *(57)*. As antimicrobial resistance is a major challenge for TB management and treatment, both drug-susceptible (DS-TB) and drug-resistant (DR-TB) patients were recruited to examine immune profiles in these settings. Patients were followed up: at inclusion (T0), after two months of treatment (T1), and at the end of TB treatment (T2; 6 months for DS-TB patients, 9 to 24 months for DR-TB patients). The T1 timepoint was chosen because it marks the moment after which antibiotic treatment is reduced during clinical DS-TB management. For DR-TB monitoring, the same timepoint was used for consistency. Patients were on Directly Observed Treatment (DOT) and received treatment according to standard protocols *(2)*. Treatment regimens are detailed in Supp. Table 1.

Whole blood stimulation and processing

Detailed whole blood collection and stimulation processes were described elsewhere *(41)*. Briefly, at every follow-up visit, 1mL of whole blood was seeded directly into each QuantiFERON-TB Gold Plus (QFT-P, Qiagen) tube and incubated for 24 hours. Three stimulation conditions were used: NIL as unstimulated control; TB2 which tubes contain the *M. tuberculosis* antigenic peptides ESAT-6 (>15aa) and CFP-10 (8-13aa), which induce responses from $CD4^+$ T lymphocytes *(39)*, and an undisclosed peptide pool inducing $CD8^+$ T lymphocyte stimulation *(58)*; rmsHBHA which tubes contain recombinant *M. tuberculosis* heparin-binding hemagglutinin generated in *M. smegmatis* at a final concentration of 5µg/mL and graciously provided by the Delogu laboratory, UNICATT, Rome, Italy *(59)*.

After incubation, plasma separation, and red blood cell lysis, the resulting fixed white blood cells pellets were stored at -80°C. Cryopreserved samples were air-shipped in dry ice with freezing controls to the Mérieux Foundation Emerging Pathogens Laboratory in Lyon, France (International Center for Infectiology Research, INSERM U1111).

Experimental procedure

Sample preparation

Cryopreserved cells were thawed and resuspended in phosphate buffer saline (PBS) to a concentration of $3.5x10^6$cells/mL. Between 1 and $1.5x10^6$ cells from each sample were aliquoted for staining. Cells were incubated 10 minutes with FcR Blocking Reagent (6µL/10^6 cells; Miltenyi Biotec) and heparin sodium salt reconstituted in Millipore water (36µg/10^6 cells; Sigma-Aldrich) to reduce nonspecific staining *(60)*.

Panel design

A 29-marker panel of metal-labeled antibodies was used. All antibodies were obtained from Fluidigm (Supp. Table 8). Briefly, the panel contained 28 T-cell oriented surface markers (lineage markers, chemokine receptors, activation markers, and exhaustion markers) and one intracellular target (perforin).

Experimental design and barcoding

As the study followed a longitudinal design, samples from a same patient were acquired in the same barcoded batch of 3 timepoints and 3 stimulation conditions to reduce experimental variation. Palladium barcoding *(61)* (Cell-ID 20-Plex, Fluidigm) was performed according to the manufacturer's instructions for simultaneous staining and data acquisition. For each barcoding run, 18 patient T-cell samples were stained with unique combinations of

intracellular palladium isotopes (Figure 1). Patient batches were processed in a random order and investigators were blinded to patient sputum culture results during data collection.

Staining procedure

Extracellular staining was performed on pooled barcoded cells in Maxpar cell staining buffer (Fluidigm) for 30 minutes at room temperature. Intracellular staining (perforin) was performed in Maxpar Perm-S Buffer (Fluidigm) for 30 minutes at room temperature. Stained cells were then incubated for 10 minutes in 1.6% formaldehyde (FA) freshly prepared from 16% stock FA (Sigma-Aldrich). DNA staining was performed by overnight incubation at 4°C in 2mL of 125nM Cell-ID Iridium intercalator solution (Fluidigm). Cells were then washed, pelleted, and kept at 4°C until acquisition.

Data acquisition

Samples were analyzed on a CyTOF2 mass cytometer upgraded to Helios (Fluidigm) hosted by the AniRA cytometry facility (Structure Fédérative de Recherche Lyon Gerland, INSERM U1111, Lyon, France). Samples were filtered twice through a 50µm nylon mesh and resuspended in EQ™ Four Element Calibration Beads (Fluidigm) diluted to 0.5X in Maxpar ultra-pure water (Fluidigm), to reach an acquisition rate of 150-200 events per second (0.5 x 10^6 cells/mL). Data were collected using the on-board Fluidigm software.

Data analysis

All data analyses were performed in RStudio (version 1.3.1073 with R version 4.0.3) and FlowJo (version 10.7.1).

Data cleaning and preliminary manual gating

Signal normalization, concatenation, debarcoding, and conversion into Flow Cytometry Standard (FCS) 3.0 format were performed using the Helios Software (Fluidigm). Debarcoded files were imported into FlowJo and arcsinh-transformed (cofactor = 5). Gaussian parameters of the Helios system were used for doublet exclusion *(62)*, then $^{191}Ir^+$ $^{193}Ir^+$ single events were manually isolated, and debris ($CD45^-$ events) and calibration beads ($^{140}Ce^+$ events) were excluded). A preliminary manual gating analysis was then performed on $CD45^+$ single events (Supp. Figure 8) to verify that the proportions of the main white blood cell subpopulations in biobanked samples were consistent with the expected proportions, and sufficient for downstream analysis. Samples with less than 1,000 $CD3^+$ events, and batches with missing samples from a given timepoint were removed from the analysis to preserve a matched

sample design. The exact number of available files per patient and per stimulation condition is provided in Supp. Table 1.

Workflow for unsupervised analyses

$CD3^+$ single events were down-sampled to ensure equal contribution of each sample, exported into separate Comma Separated Value (.csv) files, and uploaded into R software (version 4.0.3). Panel markers were defined as either lineage or functional markers for use as clustering channels in downstream analyses (Supp. Table 9). Lineage-defining markers included canonical surface markers such as CD4 which display a theoretically stable expression. Functional markers included markers of activation (*e.g.* CD69), proliferation (CD38), maturation (CD27), or migration (CCR7).

Dimension reduction, automated clustering, and phenotyping

After file concatenation, dimension reduction was performed with UMAP (Uniform Manifold Approximation and Projection; version 3.1) *(63)*. UMAPs were created in R using the package Spectre *(64)*. Unsupervised clustering was performed using FlowSOM *(65)* (version 2.7). FlowSOM meta-cluster phenotyping was assessed by visualizing the surface expression of lineage markers in each FlowSOM cluster (CD4, CD8, TCRgd, TCRVa7.2, CD56, CD25, IL7Ra, CD26, and CD161) on a heatmap and performing hierarchical clustering. Marker expression heatmaps were obtained in R using Spectre by plotting normalized, median arcsinh-transformed mass signals. Biological consistency of FlowSOM meta-clusters with the main expected T-cell subpopulations (Supp. Table 3) was controlled, and manual reassignment of clusters which were in inconsistent meta-clusters was then performed when necessary (Supp. Figure 9). Meta-clusters with an abundance <1% of all events were pooled with the most phenotypically similar meta-cluster. Then, the proportion of corrected FlowSOM meta-clusters in each node on the initial FlowSOM minimum spanning tree was visualized to control reassignment consistency *(66)*.

Statistical analysis

The proportion (percent of $CD3^+$) of each FlowSOM cluster was calculated. For all statistical analyses, exact p-values, test statistics and/or estimates of effect size are provided either in the figure legend or in indicated Supplementary Tables. Normality was assessed using the Shapiro-Wilk test. The evolution of cluster proportions over time corresponded to repeated measures of non-normal, non-independent continuous variables, and was analyzed in matched samples using the two-sided Friedman rank sum test with the Wilcoxon–Nemenyi–

McDonald-Thompson post-hoc test *(67)*. Independent, non-normal continuous variables were analyzed with the two-sided Mann–Whitney U test or the Kruskal–Wallis test with Dunn's Kruskal–Wallis Multiple Comparisons *post-hoc* test *(68)* when more than two categories were compared. For discovery of clusters with significantly different abundance between slow and fast converters, conservative corrections for multiple comparisons (*e.g.* Benjamini-Hochberg *(69)*) were not used in order to minimize type II errors. Instead, all p-values were computed for each timepoint, and the p-value corresponding to the null hypothesis being rejected in 5% of all comparisons was used as the significance threshold instead of 0.05 *(70)*. This novel significance threshold enabled to control type I error while maintaining an exploratory approach; its value was always inferior to 0.05 and is reported in the corresponding figure captions.

List of Supplementary Materials

Supp. Figure 1. Flowchart of patient inclusions.

Supp. Figure. 2. Impact of in vitro whole blood stimulation with Mtb antigens on surface marker expression in the main T-cell subpopulations.

Supp. Figure. 3. Frequencies of the main peripheral T-cell subpopulations throughout anti-TB treatment.

Supp Figure 4. Significant abundance changes in non-canonical T-cell subsets after the intensive phase of treatment.

Supp. Figure. 5. Patients with slow microbiological culture conversion show decreased $CD8^+$ and γδ and enriched $CD4^+$ naïve peripheral T-cell subsets during treatment.

Supp. Figure 6. Patients with slow microbiological culture conversion show decreased cytotoxic CD8+ and γδ and enriched CD4+ naïve T-cell subsets before treatment initiation and after treatment completion compared to fast converters.

Supp. Figure 7. Variance between fast and slow responders within all Mtb-stimulated $CD3^+$ T-cells.

Supp. Figure 8. Main $CD45^+$ non-granulocyte whole blood subpopulations and T-cell oriented gating strategy.

Supp. Figure 9. Control of automated FlowSOM metaclustering.

Supp. Table 1. Sociodemographic and clinical characteristics of the cohort.

Supp. Table 2. Exact p-values and test statistics for marker expression comparisons between stimulation conditions, presented in Supp. Figure 2.

Supp. Table 3. Exact p-values and test statistics for cluster abundance comparisons during treatment, presented in Figure 3 and Supp. Figure 4.

Supp. Table 4. Pearson's correlation effect sizes (*r*) presented in Figure 5 for increased clusters.

Supp. Table 5. Pearson's correlation effect sizes (*r*) presented in Figure 5 for decreased clusters.

Supp. Table 6. Exact p-values and test statistics for cluster abundance comparisons between fast and slow converters, presented in Figure 6 and Supp. Figure 5.

Supp. Table 7. Exact p-values and test statistics for comparison of PCA scores between fast and slow converters, presented in Figure 7 and Supp. Figure 7.

Supp. Table 8. Mass cytometry panel components.

Supp. Table 9. Definition of clustering channels and expected cell subpopulations for dimension reduction and automated clustering of $CD3^+$ T-cells.

References

1. World Health Organization Geneva, *Global Tuberculosis Report 2020* (2020).
2. World Health Organization Geneva, *WHO consolidated guidelines on drug-resistant tuberculosis treatment* (2019).
3. World Health Organization Geneva, *Global Tuberculosis Report 2018* (2018).
4. A. Singhania, R. Verma, C. M. Graham, J. Lee, T. Tran, M. Richardson, P. Lecine, P. Leissner, M. P. R. Berry, R. J. Wilkinson, K. Kaiser, M. Rodrigue, G. Woltmann, P. Haldar, A. O'Garra, A modular transcriptional signature identifies phenotypic heterogeneity of human tuberculosis infection, *Nat. Commun.* **9** (2018), doi:10.1038/s41467-018-04579-w.
5. N. M. Parrish, K. C. Carroll, Role of the clinical mycobacteriology laboratory in diagnosis and management of tuberculosis in low-prevalence settings, *J. Clin. Microbiol.* **49**, 772–776 (2011).
6. D. J. Horne, S. E. Royce, L. Gooze, M. Narita, P. C. Hopewell, P. Nahid, K. R. Steingart, Sputum monitoring during tuberculosis treatment for predicting outcome : systematic review and meta-analysis, *Lancet Infect. Dis.* **10**, 387–394 (2010).
7. C. Lienhardt, K. Lönnroth, D. Menzies, M. Balasegaram, J. Chakaya, F. Cobelens, J. Cohn, C. M. Denkinger, T. G. Evans, G. Källenius, G. Kaplan, A. M. V. Kumar, L. Matthiessen, C. S. Mgone, V. Mizrahi, Y. diul Mukadi, V. N. Nguyen, A. Nordström, C. F. Sizemore, M. Spigelman, S. B. Squire, S. Swaminathan, P. D. Van Helden, A. Zumla, K. Weyer, D. Weil, M. Raviglione, Translational Research for Tuberculosis Elimination: Priorities, Challenges, and Actions, *PLoS Med.* **13**, 1–11 (2016).
8. D. Goletti, C. S. Lindestam Arlehamn, T. J. Scriba, R. Anthony, D. Maria Cirillo, T. Alonzi, C. M. Denkinger, F. Cobelens, Can we predict tuberculosis cure? Current tools available, *Eur. Respir. J.* , 1801089 (2018).
9. M. I. M. Ahmed, N. E. Ntinginya, G. Kibiki, B. A. Mtafya, H. Semvua, S. Mpagama, C. Mtabho, E. Saathoff, K. Held, R. Loose, I. Kroidl, M. Chachage, U. von Both, A. Haule, A. M. Mekota, M. J. Boeree, S. H. Gillespie, M. Hoelscher, N. Heinrich, C. Geldmacher, E. Pan African Consortium, Phenotypic Changes on Mycobacterium Tuberculosis-Specific CD4 T Cells as Surrogate Markers for Tuberculosis Treatment Efficacy, *Front. Immunol.* **9**, 13 (2018).

10. T. Adekambi, C. C. Ibegbu, S. Cagle, A. S. Kalokhe, Y. F. Wang, Y. Hu, C. L. Day, S. M. Ray, J. Rengarajan, Biomarkers on patient T cells diagnose active tuberculosis and monitor treatment response (vol 125, pg 1827, 2015), *J. Clin. Invest.* **125**, 3723 (2015).
11. D. Goletti, O. Butera, F. Bizzoni, R. Casetti, E. Girardi, F. Poccia, Region of Difference 1 Antigen–Specific CD4 + Memory T Cells Correlate with a Favorable Outcome of Tuberculosis, *J. Infect. Dis.* **194**, 984–992 (2006).
12. S. Agrawal, O. Parkash, A. N. Palaniappan, A. K. Bhatia, S. Kumar, D. S. Chauhan, M. Madhan Kumar, Efficacy of T regulatory cells, Th17 cells and the associated markers in monitoring tuberculosis treatment response, *Front. Immunol.* **9**, 1–16 (2018).
13. C. Riou, E. Du Bruyn, S. Ruzive, R. T. Goliath, C. S. Lindestam Arlehamn, A. Sette, A. Sher, D. L. Barber, R. J. Wilkinson, Disease extent and anti-tubercular treatment response correlates with *Mycobacterium tuberculosis*-specific CD4 T-cell phenotype regardless of HIV-1 status, *Clin. Transl. Immunol.* **9**, e1176 (2020).
14. T. Chiacchio, G. Delogu, V. Vanini, G. Cuzzi, F. De Maio, C. Pinnetti, A. Sampaolesi, A. Antinori, D. Goletti, Immune characterization of the HBHA-specific response in mycobacterium tuberculosis-infected patients with or without HIV infection, *PLoS One* **12**, 1–18 (2017).
15. M. Musvosvi, D. Duffy, E. Filander, H. Africa, S. Mabwe, L. Jaxa, N. Bilek, A. Llibre, V. Rouilly, M. Hatherill, M. Albert, T. J. Scriba, E. Nemes, T-cell biomarkers for diagnosis of tuberculosis: candidate evaluation by a simple whole blood assay for clinical, *Eur Respir J* **51** (2018), doi:10.1183/13993003.00153-2018.
16. M. Gossez, T. Rimmelé, T. Andrieu, S. Debord, F. Bayle, C. Malcus, F. Poitevin-Later, G. Monneret, Proof of concept study of mass cytometry in septic shock patients reveals novel immune alterations, *Sci. Rep.* **8**, 1–12 (2018).
17. T. V Kourelis, J. C. Villasboas, E. Jessen, S. Dasari, A. Dispenzieri, D. Jevremovic, Mass cytometry dissects T cell heterogeneity in the immune tumor microenvironment of common dysproteinemias at diagnosis and after fi rst line therapies, *Blood Cancer J.* **9** (2019), doi:10.1038/s41408-019-0234-4.
18. S. J. S. Rubin, L. Bai, Y. Haileselassie, G. Garay, C. Yun, L. Becker, S. E. Streett, S. R. Sinha, A. Habtezion, Mass cytometry reveals systemic and local immune signatures that distinguish inflammatory bowel diseases, *Nat. Commun.* **10** (2019), doi:10.1038/s41467-019-10387-7.

19. R. Roy Chowdhury, F. Vallania, Q. Yang, C. J. Lopez Angel, F. Darboe, A. Penn-Nicholson, V. Rozot, E. Nemes, S. T. Malherbe, K. Ronacher, G. Walzl, W. Hanekom, M. M. Davis, J. Winter, X. Chen, T. J. Scriba, P. Khatri, Y. Chien, A multi-cohort study of the immune factors associated with M. tuberculosis infection outcomes, *Nature* (2018), doi:10.1038/s41586-018-0439-x.

20. I. Marriott, R. Stephens, C. J. Serrano, M. L. Gennaro, R. Arrigucci, K. Lakehal, P. Vir, D. Handler, A. L. Davidow, R. Herrera, J. Dolores Estrada-Guzmán, Y. Bushkin, S. Tyagi, A. A. Lardizabal, Active Tuberculosis Is Characterized by Highly Differentiated Effector Memory Th1 Cells, *Front. Immunol.* **9**, 2127 (2018).

21. T. Chiacchio, E. Petruccioli, V. Vanini, G. Cuzzi, C. Pinnetti, A. Sampaolesi, A. Antinori, E. Girardi, D. Goletti, Polyfunctional T-cells and effector memory phenotype are associated with active TB in HIV-infected patients, *J. Infect.* **69**, 533–545 (2014).

22. X. Wang, Z. Cao, J. Jiang, H. Niu, M. Dong, A. Tong, X. Cheng, Association of mycobacterial antigen-specific CD4+ memory T cell subsets with outcome of pulmonary tuberculosis, *J. Infect.* **60**, 133–139 (2010).

23. E. Petruccioli, L. Petrone, V. Vanini, A. Sampaolesi, G. Gualano, E. Girardi, F. Palmieri, D. Goletti, IFNγ/TNFα specific-cells and effector memory phenotype associate with active tuberculosis, *J. Infect.* **66**, 475–486 (2013).

24. D. Goletti, O. Butera, F. Bizzoni, R. Casetti, E. Giradi, F. Poccia, Region of difference 1 antigen-specific CD4+ memory T cells correlate with a favorable outcome of tuberculosis, *J. Infect. Dis.* **194**, 984–992 (2006).

25. M. R. Nyendak, B. Park, M. D. Null, J. Baseke, G. Swarbrick, H. Mayanja-Kizza, M. Nsereko, D. F. Johnson, P. Gitta, A. Okwera, S. Goldberg, L. Bozeman, J. L. Johnson, W. H. Boom, D. A. Lewinsohn, D. M. Lewinsohn, Mycobacterium tuberculosis specific CD8+ T cells rapidly decline with antituberculosis treatment, *PLoS One* **8** (2013), doi:10.1371/journal.pone.0081564.

26. R. Axelsson-Robertson, M. Rao, A. G. Loxton, G. Walzl, M. Bates, A. Zumla, M. Maeurer, Frequency of Mycobacterium tuberculosis-specific CD8+ T-cells in the course of anti-tuberculosis treatment, *Int. J. Infect. Dis.* **32**, 23–29 (2015).

27. C. Riou, C. M. Gray, M. Lugongolo, T. Gwala, A. Kiravu, P. Deniso, L. Stewart-Isherwood, S. V. Omar, M. P. Grobusch, G. Coetzee, F. Conradie, N. Ismail, G. Kaplan, D. Fallows, A subset of circulating blood mycobacteria-specific CD4 T cells can predict the time to Mycobacterium tuberculosis sputum culture conversion, *PLoS One* **9** (2014), doi:10.1371/journal.pone.0102178.

28. D. A. Lewinsohn, G. M. Swarbrick, B. Park, M. E. Cansler, M. D. Null, K. G. Toren, J. Baseke, S. Zalwango, H. Mayanja-Kizza, L. L. Malone, M. Nyendak, G. Wu, K. Guinn, S. McWeeney, T. Mori, K. A. Chervenak, D. R. Sherman, W. H. Boom, D. M. Lewinsohn, Comprehensive definition of human immunodominant CD8 antigens in tuberculosis, *npj Vaccines* **2**, 1–10 (2017).

29. T. Chiacchio, E. Petruccioli, V. Vanini, G. Cuzzi, M. P. La Manna, V. Orlando, C. Pinnetti, A. Sampaolesi, A. Antinori, N. Caccamo, D. Goletti, Impact of antiretroviral and tuberculosis therapies on CD4+ and CD8+ HIV/M. tuberculosis-specific T-cell in co-infected subjects, *Immunol. Lett.* **198**, 33–43 (2018).

30. N. V. Serbina, C.-C. Liu, C. A. Scanga, J. L. Flynn, CD8+ CTL from Lungs of Mycobacterium tuberculosis -Infected Mice Express Perforin In Vivo and Lyse Infected Macrophages, *J. Immunol.* **165**, 353–363 (2000).

31. P. L. Lin, J. L. Flynn, CD8 T cells and Mycobacterium tuberculosis infection, *Semin Immunopathol.* **37**, 239–249 (2015).

32. H. Bruns, C. Meinken, P. Schauenberg, G. Härter, P. Kern, R. L. Modlin, C. Antoni, S. Stenger, Anti-TNF immunotherapy reduces CD8+ T cell–mediated antimicrobial activity against Mycobacterium tuberculosis in humans, *JCI* **119**, 1167–1177 (2009).

33. H. B. Jiang, H. L. Gong, Q. Zhang, J. Gu, L. Liang, J. Zhang, Decreased expression of perforin in CD8(+) T lymphocytes in patients with Mycobacterium tuberculosis infection and its potential value as a marker for efficacy of treatment, *J. Thorac. Dis.* **9**, 1353-+ (2017).

34. V. Rozot, S. Vigano, J. Mazza-stalder, E. Idrizi, C. L. Day, M. Perreau, C. Lazor-blanchet, E. Petruccioli, W. Hanekom, P. Bart, L. Nicod, G. Pantaleo, A. Harari, Mycobacterium tuberculosis-specific CD8+ T cells are functionally and phenotypically different between latent infection and active disease, *Eur. J. Immunol.* **43**, 1568–1577 (2013).

35. M. Durward, G. Radhakrishnan, J. Harms, C. Bareiss, D. Magnani, G. A. Splitter, Active evasion of CTL mediated killing and low quality responding CD8+ T cells contribute to persistence of brucellosis., *PLoS One* **7** (2012), doi:10.1371/journal.pone.0034925.

36. C. Riou, N. Berkowitz, R. Goliath, W. A. Burgers, R. J. Wilkinson, Analysis of the phenotype of Mycobacterium tuberculosis-specific CD4+ T cells to discriminate latent from active tuberculosis in HIV-Uninfected and HIV-Infected individuals, *Front. Immunol.* **8** (2017), doi:10.3389/fimmu.2017.00968.

37. J. E. Grotzke, D. M. Lewinsohn, Role of CD8+ T lymphocytes in control of Mycobacterium tuberculosis infection, *Microbes Infect.* **7**, 776–788 (2005).

38. R. Axelsson-Robertson, J. H. Ju, H. Y. Kim, A. Zumla, M. Maeurer, Mycobacterium tuberculosis-specific and MHC class I-restricted CD8+ T-cells exhibit a stem cell precursor-like phenotype in patients with active pulmonary tuberculosis, *Int. J. Infect. Dis.* **32**, 13–22 (2015).

39. E. Petruccioli, T. Chiacchio, I. Pepponi, V. Vanini, R. Urso, G. Cuzzi, L. Barcellini, D. M. Cirillo, F. Palmieri, G. Ippolito, D. Goletti, First characterization of the CD4 and CD8 T-cell responses to QuantiFERON-TB Plus, *J. Infect.* **73**, 588–597 (2016).

40. C. Masungi, S. Temmerman, J. P. Van Vooren, A. Drowart, K. Pethe, F. D. Menozzi, C. Locht, F. Mascart, Differential T and B cell responses against Mycobacterium tuberculosis heparin-binding hemagglutinin adhesin in infected healthy individuals and patients with tuberculosis, *J. Infect. Dis.* **185**, 513–520 (2002).

41. C. Chedid, E. Kokhreidze, N. Tukvadze, S. Banu, M. K. M. Uddin, S. Biswas, G. Russomando, C. C. D. Acosta, R. Arenas, P. P. Ranaivomanana, C. Razafimahatratra, P. Herindrainy, J. Rakotonirina, A. H. Raherinandrasana, N. Rakotosamimanana, M. Hamze, M. B. Ismail, R. Bayaa, J.-L. Berland, F. De Maio, G. Delogu, H. Endtz, F. Ader, D. Goletti, J. Hoffmann, Relevance of QuantiFERON-TB Gold Plus and Heparin-Binding Hemagglutinin Interferon-γ Release Assays for Monitoring of Pulmonary Tuberculosis Clearance: A Multicentered Study, *Front. Immunol.* **11**, 1–11 (2021).

42. M. Sali, D. Buonsenso, P. D'Alfonso, F. De Maio, M. Ceccarelli, B. Battah, I. Palucci, T. Chiacchio, D. Goletti, M. Sanguinetti, P. Valentini, G. Delogu, Combined use of Quantiferon and HBHA-based IGRA supports tuberculosis diagnosis and therapy management in children, *J. Infect.* (2018), doi:10.1016/j.jinf.2018.09.011.

43. F. De Maio, F. Squeglia, D. Goletti, G. Delogu, The Mycobacterial HBHA Protein: A Promising Biomarker for Tuberculosis, *Curr. Med. Chem.* **26**, 2051–2060 (2018).

44. C. H. Kim, L. Rott, E. J. Kunkel, M. C. Genovese, D. P. Andrew, L. Wu, E. C. Butcher, Rules of chemokine receptor association with T cell polarization in vivo, *J. Clin. Invest.* **108**, 1331–1339 (2001).

45. E. V. Acosta-Rodriguez, L. Rivino, J. Geginat, D. Jarrossay, M. Gattorno, A. Lanzavecchia, F. Sallusto, G. Napolitani, Surface phenotype and antigenic specificity of human interleukin 17-producing T helper memory cells, *Nat. Immunol.* **8**, 639–646 (2007).

46. C. S. Lindestam Arlehamn, A. Gerasimova, F. Mele, R. Henderson, J. Swann, J. A. Greenbaum, Y. Kim, J. Sidney, E. A. James, R. Taplitz, D. M. McKinney, W. W. Kwok, H. Grey, F. Sallusto, B. Peters, A. Sette, Memory T Cells in Latent Mycobacterium tuberculosis Infection Are Directed against Three Antigenic Islands and Largely Contained in a CXCR3+CCR6+ Th1 Subset, *PLoS Pathog.* **9** (2013), doi:10.1371/journal.ppat.1003130.

47. C. Klemann, L. Wagner, M. Stephan, S. von Hörsten, Cut to the chase: a review of CD26/dipeptidyl peptidase-4's (DPP4) entanglement in the immune system, *Clin. Exp. Immunol.* **185**, 1–21 (2016).

48. K. Ohnuma, N. H. Dang, C. Morimoto, Revisiting an old acquaintance: CD26 and its molecular mechanisms in T cell function, *Trends Immunol.* **29**, 295–301 (2008).

49. M. I. M. Ahmed, N. E. Ntinginya, G. Kibiki, B. A. Mtafya, H. Semvua, S. Mpagama, C. Mtabho, E. Saathoff, K. Held, R. Loose, I. Kroidl, M. Chachage, U. von Both, A. Haule, A. M. Mekota, M. J. Boeree, S. H. Gillespie, M. Hoelscher, N. Heinrich, C. Geldmacher, Phenotypic Changes on Mycobacterium Tuberculosis-Specific CD4 T Cells as Surrogate Markers for Tuberculosis Treatment Efficacy, *Front. Immunol.* **9**, 2247 (2018).

50. T. Adekambi, C. C. Ibegbu, S. Cagle, A. S. Kalokhe, Y. F. Wang, Y. Hu, C. L. Day, S. M. Ray, J. Rengarajan, Biomarkers on patient T cells diagnose active tuberculosis and monitor treatment response, *J. Clin. Invest.* **125**, 1827–1838 (2015).

51. I. Latorre, M. A. Fernández-Sanmartín, B. Muriel-Moreno, R. Villar-Hernández, S. Vila, M. L. De Souza-Galvão, Z. Stojanovic, M. A. Jiménez-Fuentes, C. Centeno, J. Ruiz-Manzano, J.-P. Millet, I. Molina-Pinargote, Y. D. González-Díaz, A. Lacoma, L. Luque-Chacón, J. Sabriá, C. Prat, J. Domínguez, Study of CD27 and CCR4 Markers on Specific CD4+ T-Cells as Immune Tools for Active and Latent Tuberculosis Management, *Front. Immunol.* **9**, 1–11 (2019).

52. M. A. Vickers, F. Darboe, C. N. Muefong, G. Mbayo, A. Barry, A. Gindeh, S. Njie, A. J. Riley, B. Sarr, B. Sambou, H. M. Dockrell, S. Charalambous, A. Rachow, O. Owolabi, S. Jayasooriya, J. S. Sutherland, Monitoring Anti-tuberculosis Treatment Response Using Analysis of Whole Blood Mycobacterium tuberculosis Specific T Cell Activation and Functional Markers, *Front. Immunol.* **11**, 1–13 (2020).

53. C. Genestet, E. Hodille, A. Barbry, J.-L. Berland, J. Hoffmann, E. Westeel, F. Bastian, M. Guichardant, S. Venner, G. Lina, C. Ginevra, F. Ader, S. Goutelle, O. Dumitrescu, Rifampicin exposure reveals within-host Mycobacterium tuberculosis diversity in patients with delayed culture conversion, *PLOS Pathog.* **17**, e1009643 (2021).

54. Y. R. Patankar, R. Sutiwisesak, S. Boyce, R. Lai, C. S. Lindestam Arlehamn, A. Sette, S. M. Behar, Limited recognition of Mycobacterium tuberculosis-infected macrophages by polyclonal CD4 and CD8 T cells from the lungs of infected mice, *Mucosal Immunol.* **13**, 140–148 (2020).

55. B. M. N. Kagina, B. Abel, T. J. Scriba, E. J. Hughes, A. Keyser, A. Soares, H. Gamieldien, M. Sidibana, M. Hatherill, S. Gelderbloem, H. Mahomed, A. Hawkridge, G. Hussey, G. Kaplan, W. A. Hanekom, Specific T cell frequency and cytokine expression profile do not correlate with protection against tuberculosis after bacillus Calmette-Guérin vaccination of newborns, *Am. J. Respir. Crit. Care Med.* **182**, 1073–1079 (2010).

56. A. O. Moguche, M. Musvosvi, A. Penn-Nicholson, C. R. Plumlee, H. Mearns, H. Geldenhuys, E. Smit, D. Abrahams, V. Rozot, O. Dintwe, S. T. Hoff, I. Kromann, M. Ruhwald, P. Bang, R. P. Larson, S. Shafiani, S. Ma, D. R. Sherman, A. Sette, C. S. Lindestam Arlehamn, D. M. McKinney, H. Maecker, W. A. Hanekom, M. Hatherill, P. Andersen, T. J. Scriba, K. B. Urdahl, Antigen Availability Shapes T Cell Differentiation and Function during Tuberculosis, *Cell Host Microbe* **21**, 695-706.e5 (2017).

57. C. Chedid, E. Kokhreidze, N. Tukvadze, S. Banu, M. K. M. Uddin, S. Biswas, G. Russomando, C. C. D. Acosta, R. Arenas, P. P. Ranaivomanana, C. Razafimahatratra, P. Herindrainy, N. Rakotosamimanana, M. Hamze, M. B. Ismail, R. Bayaa, J.-L. Berland, G. Delogu, H. Endtz, F. Ader, D. Goletti, J. Hoffmann, Association of baseline white blood cell counts with tuberculosis treatment outcome: a prospective multicentered cohort study, *Int. J. Infect. Dis.* (2020), doi:10.1016/j.ijid.2020.09.017.

58. Qiagen, QuantiFERON®-TB Gold Plus (QFT®-Plus) Package Insert**96**, 1101062 (2017).

59. G. Delogu, T. Chiacchio, V. Vanini, O. Butera, G. Cuzzi, A. Bua, P. Molicotti, S. Zanetti, F. N. Lauria, S. Grisetti, N. Magnavita, G. Fadda, E. Girardi, D. Goletti, Methylated HBHA produced in M. smegmatis discriminates between active and non-active tuberculosis disease among RD1-responders, *PLoS One* **6** (2011), doi:10.1371/journal.pone.0018315.

60. A. H. Rahman, L. Tordesillas, M. C. Berin, Heparin Reduces Nonspecific Eosinophil Staining Artifacts in Mass Cytometry Experiments, *Cytometry* **89A**, 601–607 (2016).

61. H. E. Mei, M. D. Leipold, A. R. Schulz, C. Chester, H. T. Maecker, Barcoding of Live Human Peripheral Blood Mononuclear Cells for Multiplexed Mass Cytometry, *J. Immunol.* **194**, 2022–2031 (2015).

62. M. D. Leipold, E. W. Newell, H. T. Maecker, Multiparameter Phenotyping of Human PBMCs Using Mass Cytometry, *Methods Mol Biol.* **1343**, 1–14 (2015).

63. E. Becht, L. McInnes, J. Healy, C. A. Dutertre, I. W. H. Kwok, L. G. Ng, F. Ginhoux, E. W. Newell, Dimensionality reduction for visualizing single-cell data using UMAP, *Nat. Biotechnol.* **37**, 38–47 (2019).

64. T. M. Ashhurst, F. Marsh-Wakefield, G. H. Putri, A. G. Spiteri, D. Shinko, M. N. Read, A. L. Smith, N. J. C. King, Integration, exploration, and analysis of high-dimensional single-cell cytometry data using Spectre, *bioRxiv* (2020), doi:10.1101/2020.10.22.349563.

65. S. Van Gassen, B. Callebaut, M. J. Van Helden, B. N. Lambrecht, P. Demeester, T. Dhaene, Y. Saeys, FlowSOM: Using self-organizing maps for visualization and interpretation of cytometry data, *Cytom. Part A* **87**, 636–645 (2015).

66. K. Quintelier, A. Couckuyt, A. Emmaneel, J. Aerts, Y. Saeys, S. Van Gassen, Analyzing high-dimensional cytometry data using FlowSOM, *Nat. Protoc.* (2021), doi:10.1038/s41596-021-00550-0.

67. D. G. Pereira, A. Afonso, F. M. Medeiros, Overview of Friedmans Test and Post-hoc Analysis, *Commun. Stat. Simul. Comput.* **44**, 2636–2653 (2015).

68. O. J. Dunn, Multiple Comparisons Using Rank Sums, *Technometrics* **6**, 241–251 (1964).

69. Yoav Benjamini, Yosef Hochberg, Controlling the False Discovery Rate: A Practical and Powerful Approach to Multiple Testing, *J. R. Stat. Soc. Ser. B* **57**, 289–300 (1995).

70. A. D. Althouse, Adjust for Multiple Comparisons? It's Not That Simple, *Ann. Thorac. Surg.* **101**, 1644–1645 (2016).

Acknowledgements

We would like to thank the patients participating in our study, as well as the healthcare staff and laboratory collaborators in each study site.

Funding

This work was supported by Fondation Mérieux, Fondation Christophe et Rodolphe Mérieux, and Fondation AnBer, and the grant ANR-18-CE17-0020. A minor part of the study was supported by the Italian Ministry of Health "Ricerca Corrente, Linea 4."

Author contributions

FA and JH are the principal investigators and initiated the project together with DG, NT, and SBa. Samples were collected by EK, NT, MU, and SBi. CC and TA designed and optimized the mass cytometry protocol. CC performed all experiments and analyses. CC and FA wrote the manuscript. All authors contributed to the article and approved the submitted version.

Competing Interests

DG reports personal fees from Biomérieux (consulting), Qiagen (consulting, lectures), and Diasorin (lectures) outside the submitted work. The authors declare no other competing interests.

Data availability

The datasets generated and used in this study are available from the corresponding author upon reasonable request, excluding confidential patient information.

Figures

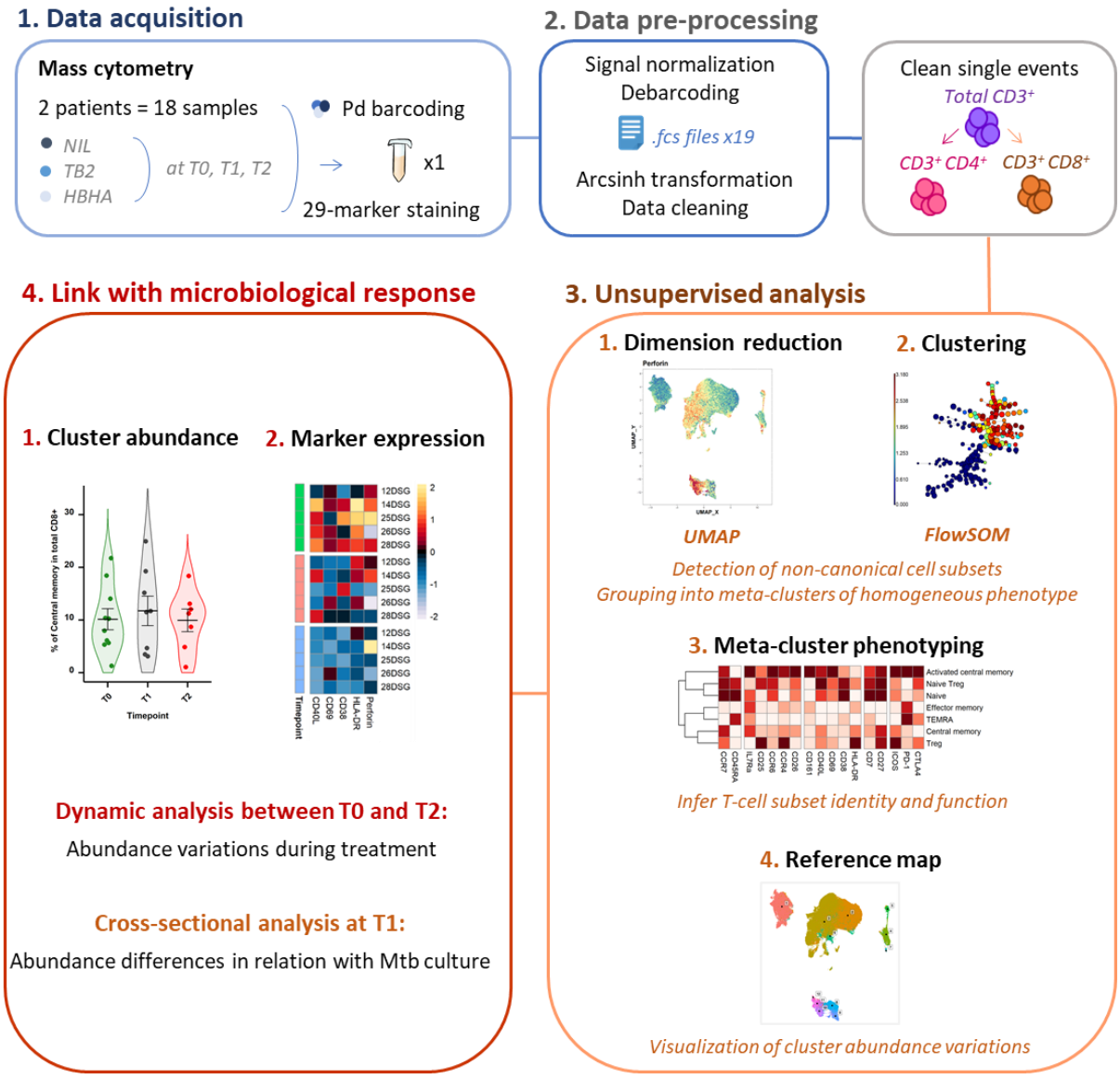

Figure 1. Experimental and analytical workflow.

NIL, TB2 and rmsHBHA refer to whole blood stimulation conditions. NIL: negative control. TB2: QuantiFERON TB2 tube (ESAT-6 + CFP-10 + undisclosed $CD8^+$ T-cell stimulating peptide pool). rmsHBHA: heparin-binding hemagglutinin. T0, T1 and T2 refer to patient follow-up timepoints (T0: baseline. T1: T0 + 2 months. T2: end of treatment). Pd barcoding: palladium barcoding for unique sample identification before multiplexing. UMAP: Uniform Manifold Approximation and Projection. FlowSOM: self-organizing map.

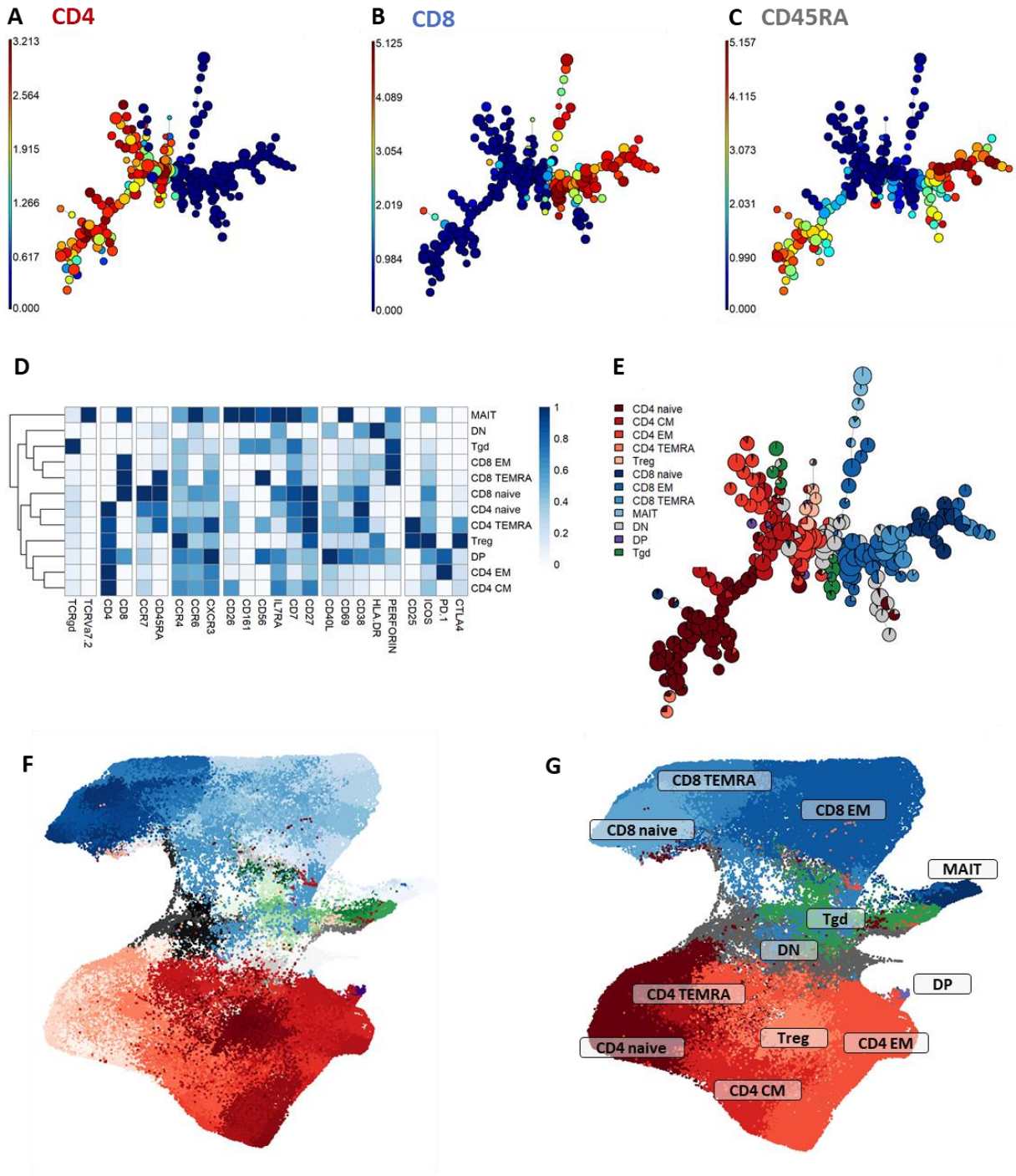

Figure 2. Peripheral CD3⁺ T-cell unsupervised clustering and phenotyping.

Peripheral whole blood samples were collected from active TB patients at three timepoints throughout treatment (n = 22). After whole blood stimulation with selected *Mtb* antigens or with a negative control, total white blood cells were extracted, and T-cells were analyzed with a 29-marker mass cytometry panel.

A to E. FlowSOM automated clustering. The surface expression of selected lineage markers used for FlowSOM calculations was visualized in all CD3⁺ events (200,000 events from equally

down-sampled files) regardless of timepoint or stimulation. FlowSOM enabled automated repartition of all $CD3^+$ events into 196 clusters according to the surface expression of selected lineage markers such as CD4 (**A**), CD8 (**B**), and CD45RA (**C**). Scales indicate arcsinh-transformed mass signal values. Clusters were automatically grouped into 18 meta-clusters of homogeneous phenotype, which were assembled into 12 canonical T-cell subpopulations in a supervised manner after meta-cluster phenotyping with heatmap visualization of normalized, arcsinh-transformed median mass signal values for each surface marker (**D**). Manual reassignment of clusters which were in biologically inconsistent meta-clusters was performed when necessary (Supp. Figure 2.H.). Then, the proportion of the identified T-cell subpopulations in each node on the initial FlowSOM minimum spanning tree was visualized to control phenotyping consistency (**E**).

F and G. Reference mapping. Data were mapped onto two dimensions with UMAP and overlayed with automatically determined FlowSOM clusters (**F**) and meta-clusters (**G**) to generate a phenotype reference map. Cluster labels were not displayed for legibility. Abbreviations: CM: central memory. DN: double-negative $CD4^-CD8^-$. DN: double-positive $CD4^+$ $CD8^+$. EM: effector memory. MAIT: mucosal associated invariant T-cells. Tgd: gamma delta T-cells. Treg: T-regulators. TEMRA: terminally differentiated effectors re-expressing CD45RA.

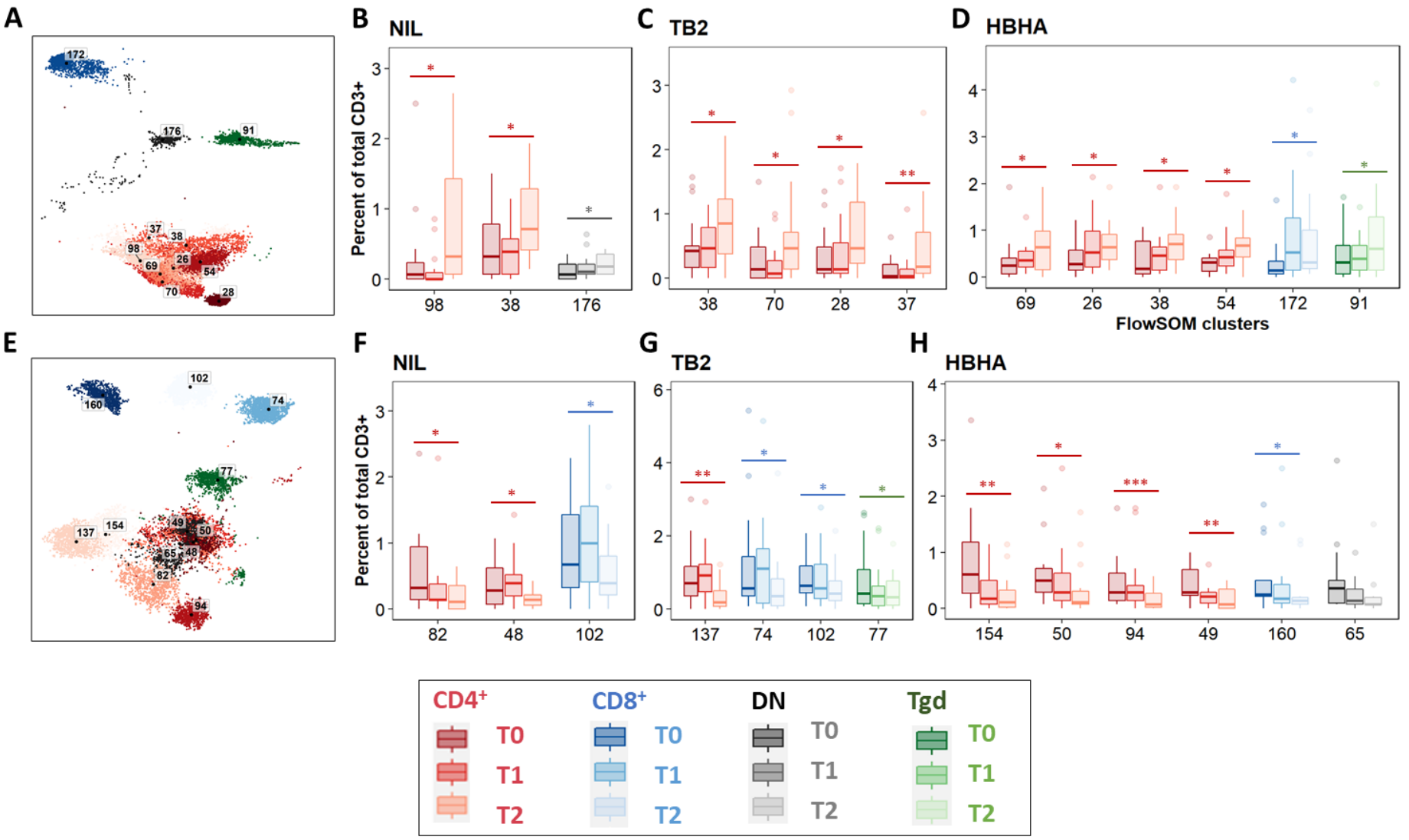
A
172
176
91
37
38
98
69
26
54
70
28
B
NIL
Percent of total CD3+
98
38
176
C
TB2
38
70
28
37
D
HBHA
69
26
38
54
172
91
FlowSOM clusters
E
102
160
74
77
137
154
49
50
65
48
82
94
F
NIL
Percent of total CD3+
82
48
102
G
TB2
137
74
102
77
H
HBHA
154
50
94
49
160
65
CD4+
T0
T1
T2
CD8+
T0
T1
T2
DN
T0
T1
T2
Tgd
T0
T1
T2

Figure 3. Significant abundance changes in non-canonical T-cell subsets throughout TB treatment.

The evolution of FlowSOM cluster abundance was analyzed over time in unstimulated or *Mtb*-stimulated samples (TB2 or rmsHBHA), and only the clusters within which significant abundance changes were detected were displayed. $CD4^+$ clusters were represented in red, $CD8^+$ clusters in blue, γδ T-cell clusters in green, and $CD4^-$ $CD8^-$ clusters in grey. Number of matched data points per timepoint for all panels: NIL: n = 16. TB2: n = 18. rmsHBHA: n = 14. Data are represented as medians + interquartile range.

A to D. Significantly increased clusters at treatment completion (T2) compared to treatment initiation (T0). Clusters within which a significant increase was detected between T0 and T2 were first visualized on the reference UMAP shown in Figure 3 (**A**). Cluster abundance quantification was then was performed in unstimulated (**B**), TB2-stimulated (C) or rmsHBHA-stimulated samples (**D**).

E to H. Significantly decreased clusters at treatment completion (T2) compared to treatment initiation (T0). Mapping (**E**) and abundance quantification of clusters which increased between T0 and T2 in unstimulated (**F**), TB2-stimulated (**G**) or rmsHBHA -stimulated samples (**H**). Abbreviations: DN: double negative $CD4^-$ $CD8^-$. Tgd: gamma delta T-cells. Statistical analysis: Friedman rank sum test and Wilcoxon-Nemenyi-Thompson post-hoc for pairwise comparisons between non-independent observations at T0, T1, and T2. *: $p<0.05$. **: $p<0.01$. ***: $p<0.001$. Exact p-values and test statistics are available in Supp. Table 3.

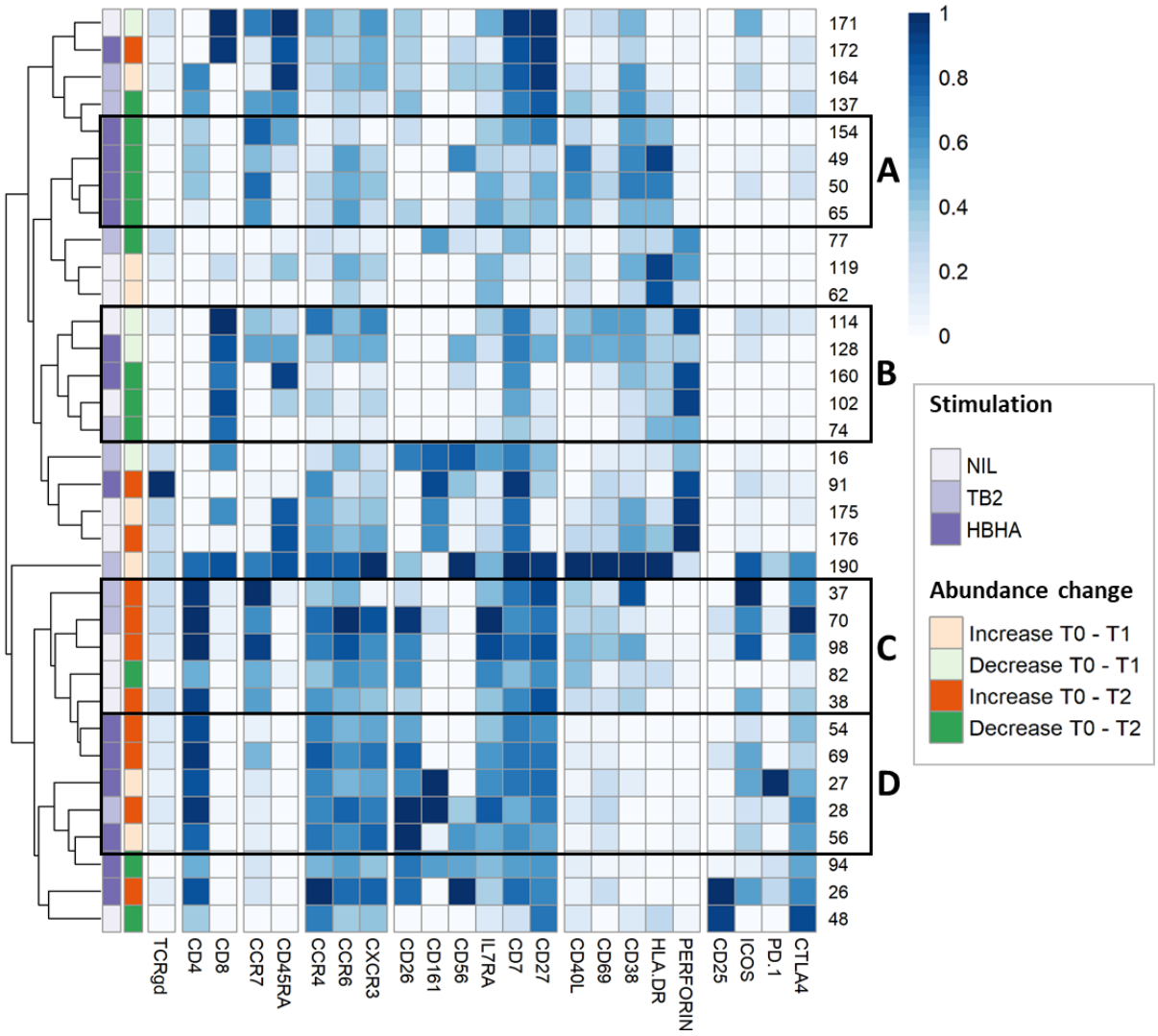

Figure 4. In-depth phenotyping shows differential involvement of effector and memory T-cells in antigen-driven cluster abundance changes during anti-TB treatment. Mean marker expression levels were visualized using heatmapping for clusters which increased (orange color code) or decreased (green color code) throughout treatment. Each line represents one cluster. Scales indicate normalized mass signal intensity. Black rectangles annotated from A to D indicate cluster subgroups with similar immunophenotypes and abundance changes.

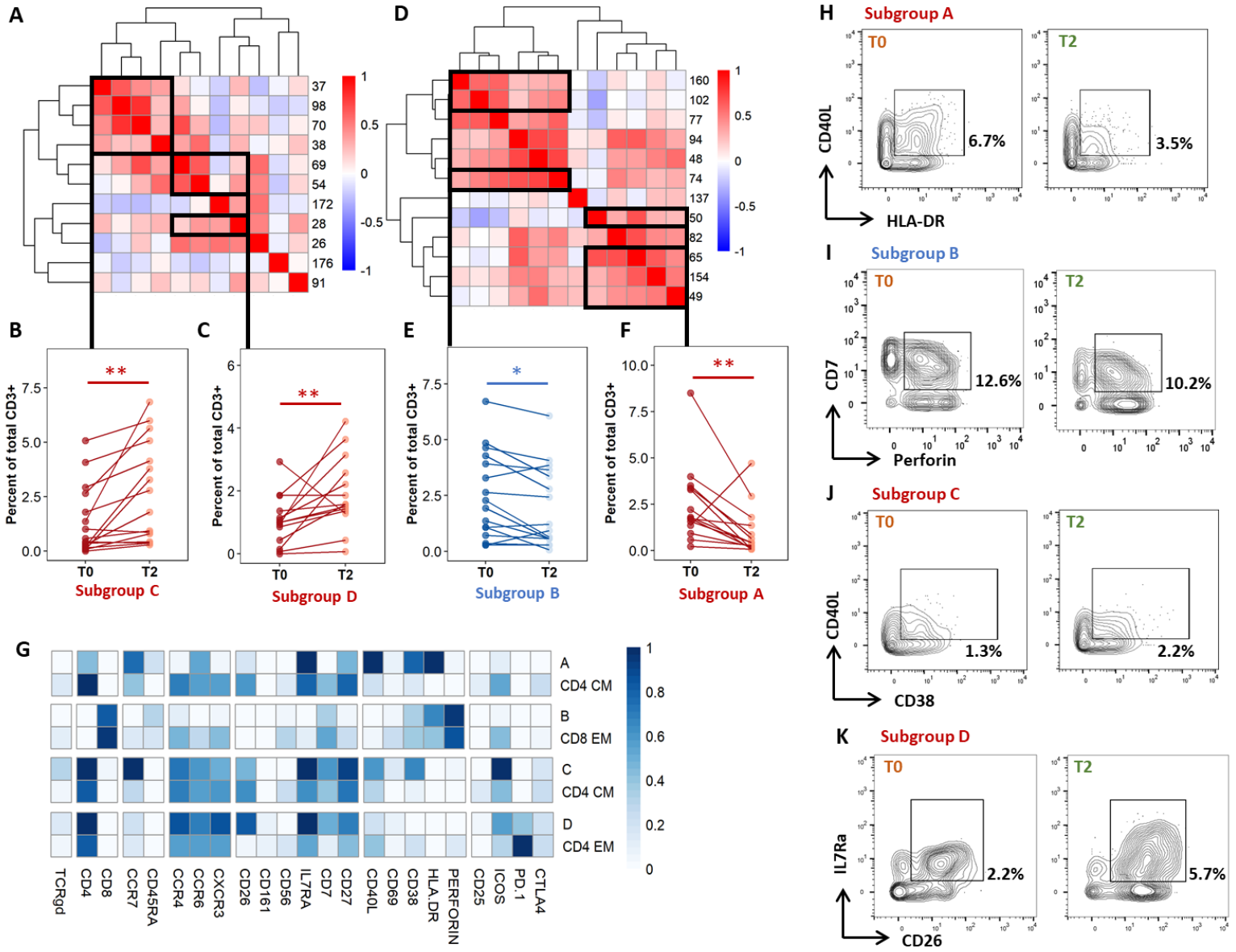
A
37
98
70
38
69
54
172
28
26
176
91
1
0.5
0
-0.5
-1
D
160
102
77
94
48
74
137
50
82
65
154
49
1
0.5
0
-0.5
-1
B
C
E
F
Percent of total CD3+
**
**
*
**
T0
T2
Subgroup C
Subgroup D
Subgroup B
Subgroup A
G
A
CD4 CM
B
CD8 EM
C
CD4 CM
D
CD4 EM
1
0.8
0.6
0.4
0.2
0
TCRgd
CD4
CD8
CCR7
CD45RA
CCR4
CCR6
CXCR3
CD26
CD161
CD56
IL7RA
CD7
CD27
CD40L
CD69
CD38
HLA.DR
PERFORIN
CD25
ICOS
PD.1
CTLA4
H
Subgroup A
T0
T2
CD40L
6.7%
3.5%
HLA-DR
I
Subgroup B
T0
T2
CD7
12.6%
10.2%
Perforin
J
Subgroup C
T0
T2
CD40L
1.3%
2.2%
CD38
K
Subgroup D
T0
T2
IL7Ra
2.2%
5.7%
CD26

Figure 5. Individual immunoprofiling confirms differential abundance of correlated subsets in cured patients after treatment.

Cluster were stratified by type of significant abundance change: enrichment (**A to C**) or depletion (**D to F**) after treatment completion.

A and D. Pearson's correlations were calculated on cluster abundance at T0 and displayed on a heatmap with hierarchical clustering. Clusters with similar immunophenotypes (Figures 3 and 4) and positive correlation coefficients were grouped. Estimates of effect sizes are in Supp. Tables 4 and 5.

B, C, E, F. The abundance of each subgroup was visualized. Each dot represents data for one patient. Statistical analysis: Friedman rank sum test. *: $p<0.05$. **: $p<0.01$. Subgroup A: data from rmsHBHA samples (n =14), clusters 49, 50, 65, 154; p = 0.0013, Friedman's Chi-Square (Fchisq) = 10.3. Subgroup B: data from unstimulated samples (n =16), clusters 74, 102, 160; p = 0.020, Fchisq = 5.4. Subgroup C: data from unstimulated samples, clusters 37, 38, 70, 98; p = 0.0027, Fchisq = 9. Subgroup D: data from rmsHBHA samples, clusters 28, 54, 69; p = 0.0023, Fchisq = 9.3.

F. For each subgroup, normalized mean marker expression levels were compared with similar T-cell subsets.

G to K. Manual gating analysis was performed to verify unsupervised results (representative plots, 500 to 1,000 events). Numbers indicate the percentage of gated cells among total $CD3^+$ cells. Subgroup A: $CD4^+CCR7^+CD45RA^-CCR6^+IL7Ra^+CD27^+CD40L^+CD38^+HLA\text{-}DR^+$. Subgroup B: $CD8^+CCR7^-CD45RA^-CD7^+$ $Perforin^+$. Subgroup C: $CD4^+CCR7$ $CD45RA^-CCR4^+CCR6^+CXCR3^+CD26^+IL7Ra^+CD7^+CD27^+$ $CD40L^+CD38^+$. Subgroup D: $CD4^+CCR7^-CD45RA^-CCR4^+CCR6^+$ $CXCR3^+CD26^+IL7Ra^+CD7$ $CD27^+CD40L^+CD38^+$ $HLA\text{-}DR^-$.

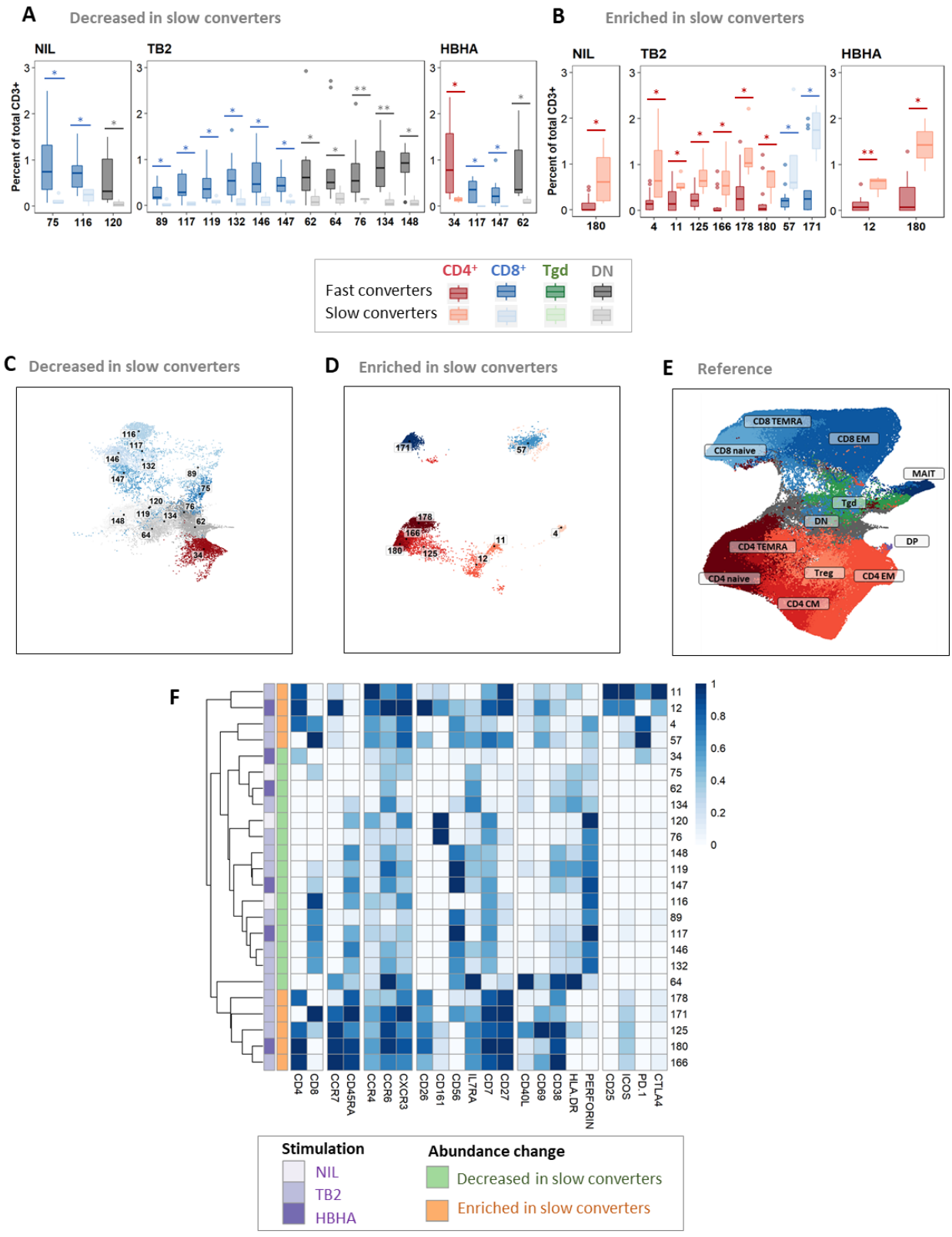

Figure 6. Patients with slow microbiological culture conversion show decreased cytotoxic CD8⁺ and γδ enriched CD4⁺ naïve T-cell subsets before treatment initiation and after two months of treatment compared to fast converters.

Fast converters (n = 18) were defined as patients with permanently negative *M. tuberculosis* culture after two months of treatment (T1), whereas slow converters (n = 4) were defined as patients with persistently positive cultures at T1. The abundance of all FlowSOM clusters at baseline was compared between fast and slow converters. $CD4^+$ clusters were represented in red, $CD8^+$ clusters in blue, and γδ T-cell clusters in green. Clusters which were significantly decreased (**A** and **C**) or enriched (**B** and **D**) at T1 in slow converters compared to fast converters were compared to the reference UMAP (**E**). Normalized, arcsinh-transformed mean marker expression levels were visualized (**F**). Each row represents one cluster. Scales indicate normalized mass signal intensity. Boxplot data represent medians + interquartile range.

Statistical analysis: Only clusters within which significant differences were detected were represented. Significance threshold: $p<0.031$ (Mann-Whitney U test). *: $p<0.031$. **: $p<0.001$. Exact p-values and test statistics are available in Supp. Table 6.

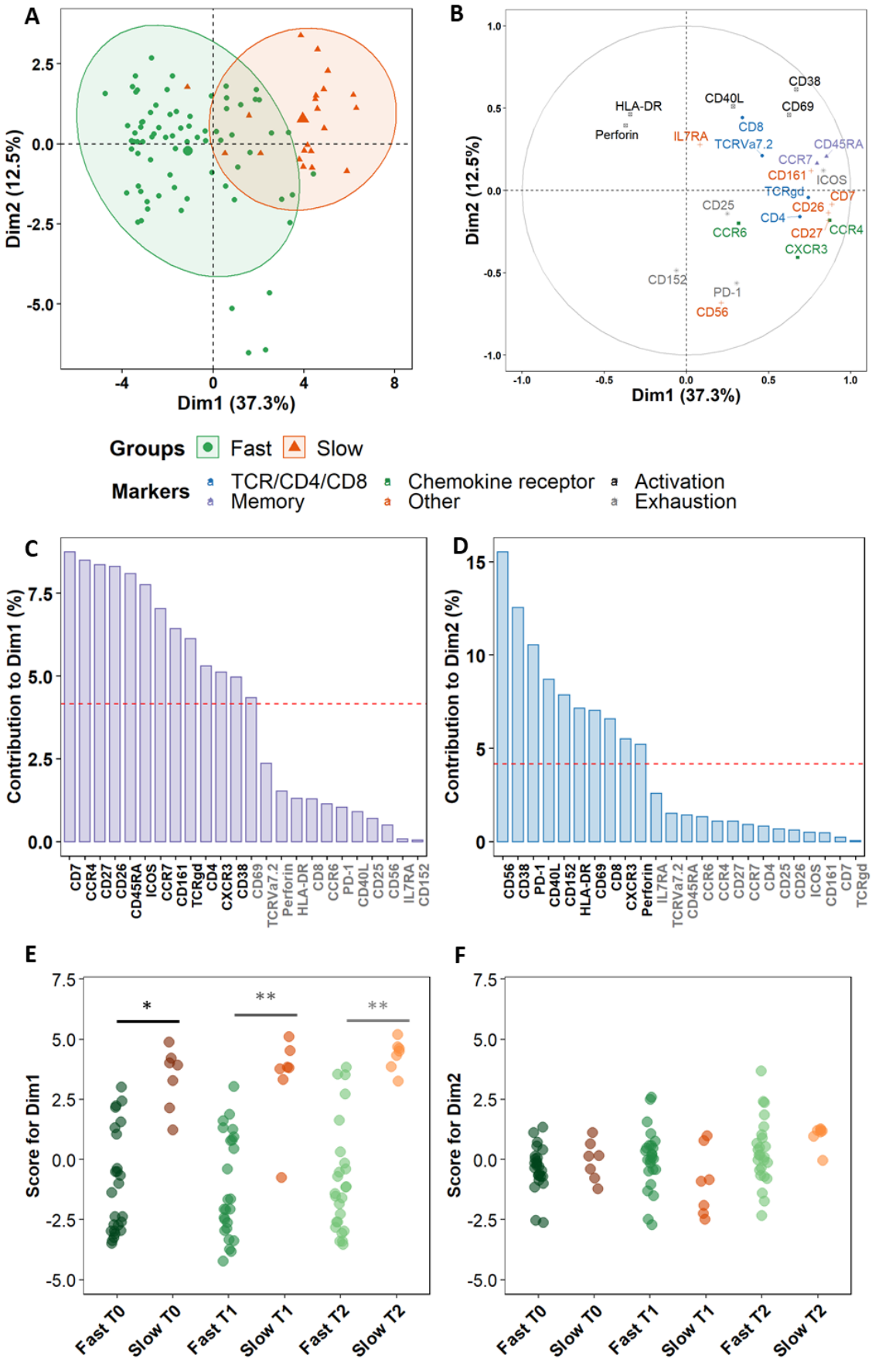
A
Dim2 (12.5%)
Dim1 (37.3%)
B
Dim2 (12.5%)
Dim1 (37.3%)
HLA-DR
Perforin
CD40L
CD38
CD69
CD8
IL7RA
TCRVa7.2
CD45RA
CCR7
CD161
ICOS
TCRgd
CD7
CD25
CD26
CD4
CCR6
CD27
CCR4
CXCR3
CD152
PD-1
CD56
Groups Fast Slow
Markers TCR/CD4/CD8 Chemokine receptor Activation
Memory Other Exhaustion
C
Contribution to Dim1 (%)
CD7 CCR4 CD27 CD26 CD45RA ICOS CCR7 CD161 TCRgd CD4 CXCR3 CD38 CD69 TCRVa7.2 Perforin HLA-DR CD8 CCR6 PD-1 CD40L CD25 CD56 IL7RA CD152
D
Contribution to Dim2 (%)
CD56 CD38 PD-1 CD40L CD152 HLA-DR CD69 CD8 CXCR3 Perforin IL7RA TCRVa7.2 CD45RA CCR6 CCR4 CD27 CCR7 CD4 CD25 CD26 ICOS CD161 CD7 TCRgd
E
Score for Dim1
*
**
**
Fast T0 Slow T0 Fast T1 Slow T1 Fast T2 Slow T2
F
Score for Dim2
Fast T0 Slow T0 Fast T1 Slow T1 Fast T2 Slow T2

Figure 7. Non-lineage markers discriminate slow and fast responders within differentially abundant subsets. Principal Component Analysis (PCA) was performed on marker expression data from the clusters identified in Figure 6 within 96 *Mtb*-stimulated samples matched at T0, T1, and T2 (TB2: 54 samples; rmsHBHA: 42 samples). **A.** Explanation of the variance between fast converters (25 samples at each timepoint) and slow converters (7 samples at each timepoint). Each dot represents one patient. The color code represents the culture conversion group. Axes represent the principal components 1 (Dimension 1, Dim1) and 2 (Dim2) and percentages indicate their contribution to the total observed variance. Axis values represent individual PCA scores. Concentration ellipses correspond to 90% data coverage. **B.** Contribution of cellular markers to the variance described by Dim1 and Dim2. Axis values represent marker PCA scores. The color code represents broad marker functions. **C. and D.** Quantification of panel B. for Dim1 (**C.**) and Dim2 (**D.**). Contributions of each marker are expressed as a percentage of the dimensions. The red dashed line corresponds to the expected reference value if each marker contributed uniformly to the variance. Markers indicated in gray are below this reference value. **E. and F.** Distribution of individual PCA score values according to the culture conversion group and to the timepoint, for Dim1 (**E.**) and Dim2 (**F.**). Data were compared with the Wilcoxon Rank Sum Test. ***: $p<0.001$.

Tables

Table 1. Selected subset abundance changes before and after treatment completion.

Sample	Abundance between T0 and T2 (%, N)
Subset A decreased	
NIL (n=16)	62% (10)
TB2 (n=18)	67% (12)
rmsHBHA (n=14)	**93% (13)**
Subset B decreased	
NIL	**81% (13)**
TB2	72% (13)
rmsHBHA	71% (10)
Subset C increased	
NIL	**88% (14)**
TB2	72% (13)
rmsHBHA	57% (8)
Subset D increased	
NIL	69% (11)
TB2	78% (14)
rmsHBHA	**93% (13)**

Footnotes: these data were obtained from Figure 5.

Table 2. Proportions of the main T-cell subpopulations within enriched or decreased subsets in slow converters compared to fast converters.

	T0 (21 clusters)		T1 (24 clusters)		T2 (21 clusters)	
Abundance in slow vs. fast converters	**Decreased**	**Enriched**	**Decreased**	**Enriched**	**Decreased**	**Enriched**
	86% (18)	**14% (3)**	**62% (15)**	**38% (9)**	**52% (11)**	**48% (10)**
Total $CD8^+$ and γδ	**72% (13)**	**67% (2)**	**53% (8)**	**22% (2)**	**36% (4)**	**20% (2)**
γδ T-cells	38 (5)	-	-	-	-	-
$CD8^+$ TEMRA	24 (3)	50 (1)	75 (6)	-	-	-
$CD8^+$ EM	38 (5)	-	25 (2)	50 (1)	100 (4)	-
$CD8^+$ naïve	-	50 (1)	-	50 (1)	-	100 (2)
Total $CD4^+$	**11% (2)**	**33% (1)**	**7% (1)**	**78% (7)**	**36% (4)**	**80% (8)**
$CD4^+$ TEMRA	-	-	-	14 (1)	-	-
$CD4^+$ EM	50 (1)	-	100 (1)	29 (2)	100 (4)	-
$CD4^+$ CM	50 (1)	-	-	14 (1)	-	38 (3)
$CD4^+$ naïve	-	100 (1)	-	43 (3)	-	62 (5)
Total DN	**17% (3)**	**0**	**40% (6)**	**0**	**27% (3)**	**0**

Footnotes: these data were obtained from Figure 6 and Supp. Figure 6. Data are given as percentage of clusters in each category (number of clusters in each category/total number of clusters).

4.2 From mass to full spectrum flow cytometry: technology transfer

4.2.1 Cost-effectiveness comparison

As exposed previously, our results confirmed that mass cytometry met two of the main experimental needs required for high-dimensional TB immunomonitoring and biomarker discovery: high resolution at a high numbers of parameters, reproduceable measurements appropriate for prospective study designs. However, we also fully experienced its low throughput, high cost, and low sample recovery. In September 2020, the latest implementation of full spectrum flow cytometry, the CYTEK Aurora spectral flow cytometer, which was first acquired in Lyon in its 5-laser version (violet, blue, yellow-green, red, and UV) along with three scatter detectors and 64 fluorescence detectors[151]. As one of the main background themes of this thesis was scientific sustainability and cost-effectiveness of high-dimensional technologies for efficient translational research, a cost analysis of mass vs. full spectrum flow cytometry was performed on an indicative basis (Table 7).

Table 7. From mass to spectral flow: a cost analysis.
Original work with T. Andrieu.

Technology	**Fluidigm Helios**	**CYTEK Aurora 5-laser**
Maximal number of parameters	47-50	45
Panel design	Complex: limited to 30-40 parameters in practice	
	Fast development	Time consuming Multiple panel iterations
Cells acquired per hour	1 million	30 million
Sample efficiency	60-70%	95%
Commercial range cost per tube[1]	€1,390 (with specimen multiplexing)	€70.5

Footnotes:
1. The price per test tube includes the reagent costs for a 30-parameter panel and the running costs of each machine in our local facilities in Lyon necessary to stain and acquire 10 million cells. It was calculated as follows: (€ per antibody) + (cost of number of hours to acquire 10.10^6 cells)*(correction for sample efficiency).

In this context, the overall cost of spectral flow cytometry data acquisition was nearly 20 times lower than that of mass cytometry. This was mainly because machine running costs were lower, but also because the maximal cell acquisition rate was much higher on Aurora. This reduced the sample acquisition duration from nine hours on average on Helios, to three hours on average Aurora for the same number of cells acquired, which is a major parameter to take into account when performing infectious disease immunomonitoring for clinical purposes.

4.2.2 Resolution comparison

As a preliminary experiment, we then performed a comparison of the resolution obtained on a Helios mass cytometer and an Aurora 5-laser spectral flow cytometer with a 30-marker panel (Table 8).

Table 8. From mass to spectral flow cytometry: a resolution analysis.
Source: T. Andrieu.

Parameters	**Fluidigm Helios**	**CYTEK Aurora 5-laser**
rSD[1] around 0	1.99	817
DNR[2]	32,768 (15bits)	4,194,304 (22bits)
Median of negative populations[3]	1.06	1,370
Maximal resolution[4]	23,240	146,678

Footnotes:
1. The robust standard deviation (rSD) measures the signal spread around the median for each metal or fluorophore.
2. The dynamic range (DNR) is defined as the ratio of the largest detectable signal to the smallest detectable signal. It depends on the cytometer's detector system. Here, the value is also given in bits to reflect signal digitization.
3. The median of negative populations is indicated because it plays a role in the overall resolution of the machine: the better the negative events are separated from the positive events, the higher the resolution.
4. Here, the maximum resolution of this specific panel was calculated as follows:
$(Maximal\ DNR - mean(median(negative\ populations)))/\sqrt{mean(rSD\ of\ negative\ populations)}$

Because mass cytometry does not rely on fluorescence spectra and measures discrete masses, the robust standard deviation (rSD) of events that are negative for a given marker is very low, which explains the high resolution that is reach even when measuring high parameter numbers. However, at an equal number of parameters, we found that the maximal resolution attained on the Aurora spectral flow cytometer was approximately six times higher than that of the Helios mass cytometer. This is because the detection and signal digitization systems on Aurora yield a much higher dynamic range (DNR) and hence allow for improved separation of negative and positive events for a given marker. Thus, we adapted the Helios mass cytometry antibody panel used in the previous publication for use on a 5-laser Aurora. Preliminary results are exposed and discussed thereafter.

4.2.3 Proof of concept and technology transfer

For the technology transfer, all antibody clones from the initial mass panel were conserved, except for one which was commercially unavailable, and an anti-CD19 antibody was added to improve T-cell gating (see Supp. Table 10 - Annex 3, p. 183). Antibody titration was graciously performed by CYTEK.

4.2.3.i Experimental procedures

Briefly, between 1 and 1.5x10^6 cells were aliquoted and incubated for 10 minutes in FcR Blocking Reagent (6µL/10^6 cells; Miltenyi Biotec) and heparin sodium salt (36µg/10^6 cells; Sigma-Aldrich). Cells were stained in 50µL of BD Brilliant Stain Buffer (30 minutes, RT, in the dark). A 10-minute fixation step was performed in 300µL of freshly reconstituted 4% formaldehyde (FA) prior to intracellular staining (30 minutes, RT, in the dark, in 1X BD PhosFlow Perm/Wash Buffer I). Samples were fixed for 20 minutes in 300µL of 1% FA and kept at 4°C until acquisition at a maximal rate of 10,000 events per second on a CYTEK Aurora 5-laser spectral analyzer, hosted by the CYLE flow cytometry core facility at the Cancer Research Center of Lyon (CRCL, UMR INSERM 1052 CNRS 5286, Centre Léon Bérard). Quality control and spectral unmixing were performed using SpectroFlo software (CYTEK). Autofluorescence was extracted individually from an unstained aliquot of each patient sample. Unmixed, compensated data were cleaned in FlowJo (version 10.7.1) and analyzed in R software (version 4.0.3) using analysis pipelines adapted from those presented in Manuscript 3.

4.2.3.ii Preliminary results

Between September and December 2020, optimization experiments and technical comparisons were performed. For canonical T-cell phenotyping purposes, similar results were obtained with Aurora and Helios, with a better spatial separation of phenotypically distinct subpopulations with Aurora (Figure 22), possibly because the dynamic range of full spectrum flow cytometry detectors is broader.

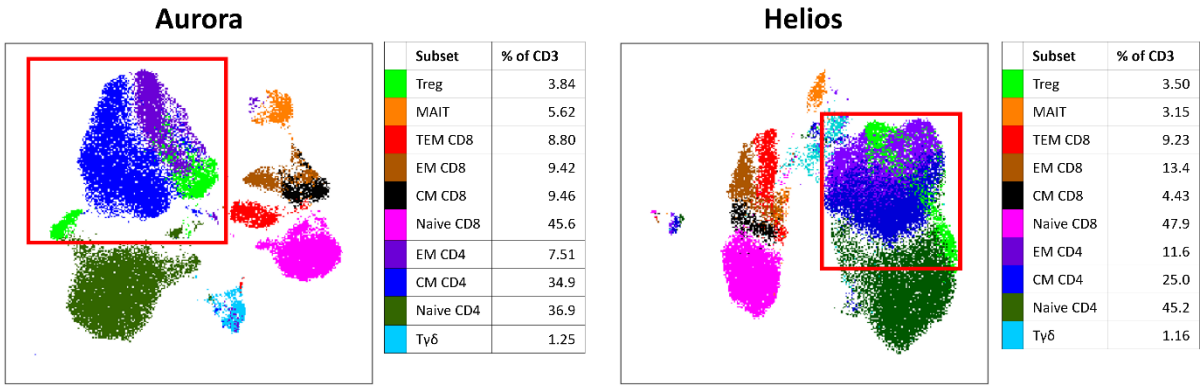

Figure 22. Preliminary comparison of basic T-cell phenotyping with spectral flow and mass cytometry. Aliquoted healthy donor cells from the same sample were acquired on Aurora (full spectrum flow cytometer) and Helios (mass cytometer). For each technique, a UMAP showing 80,000 $CD3^+$ events was plotted using the same graphing and clustering parameters. Red squares indicate areas of the UMAP were spatial separation differs between Helios and Aurora.

Then, between December 2020 and May 2021, 80 samples collected from 12 adult, culture-positive DS-TB patients from the Georgia and Lebanon HINTT cohorts were acquired (Georgia, n=8 and Lebanon, n=4) (Figure 23). All patients achieved microbiological cure at the end of treatment. Manual gating analysis was first performed to verify the proportions of the main expected $CD45^+$ immune cell subpopulations on biaxial plots (Figure 24, representative plots).Then, $CD3^+$ single events were analyzed using a workflow adapted from that of the mass cytometry project. The main subpopulations observed were similar to those found with mass cytometry, except for double negative $CD4^-$ $CD8^-$ T-cell subpopulations which were not detected with spectral flow (Figure 25). This might be sample- or staining-dependent and will be further investigated, as double negative T-cells usually represent 1 to 5% of peripheral lymphocytes[152].

Overall, we mainly aimed to validate the main result of manuscript 3 regarding T-cell subpopulations differentiating fast and slow converters. However, there were 3 slow converters (positive culture at T1 and negative culture at T2), two of which had cell samples insufficient event numbers for analysis. Overall, T-cell data remain to be fully examined in relation with patient clinical and microbiological characteristics and during treatment in general. In this study, B cell and NK cell phenotypes will be analyzed as well.

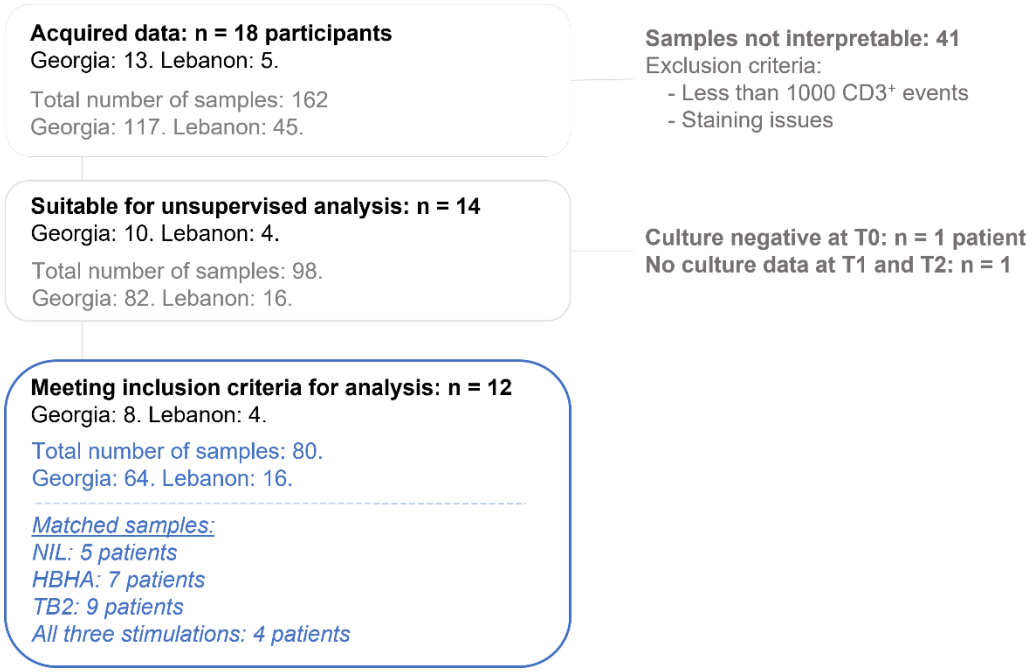

Figure 23. Flowchart of sample analysis.

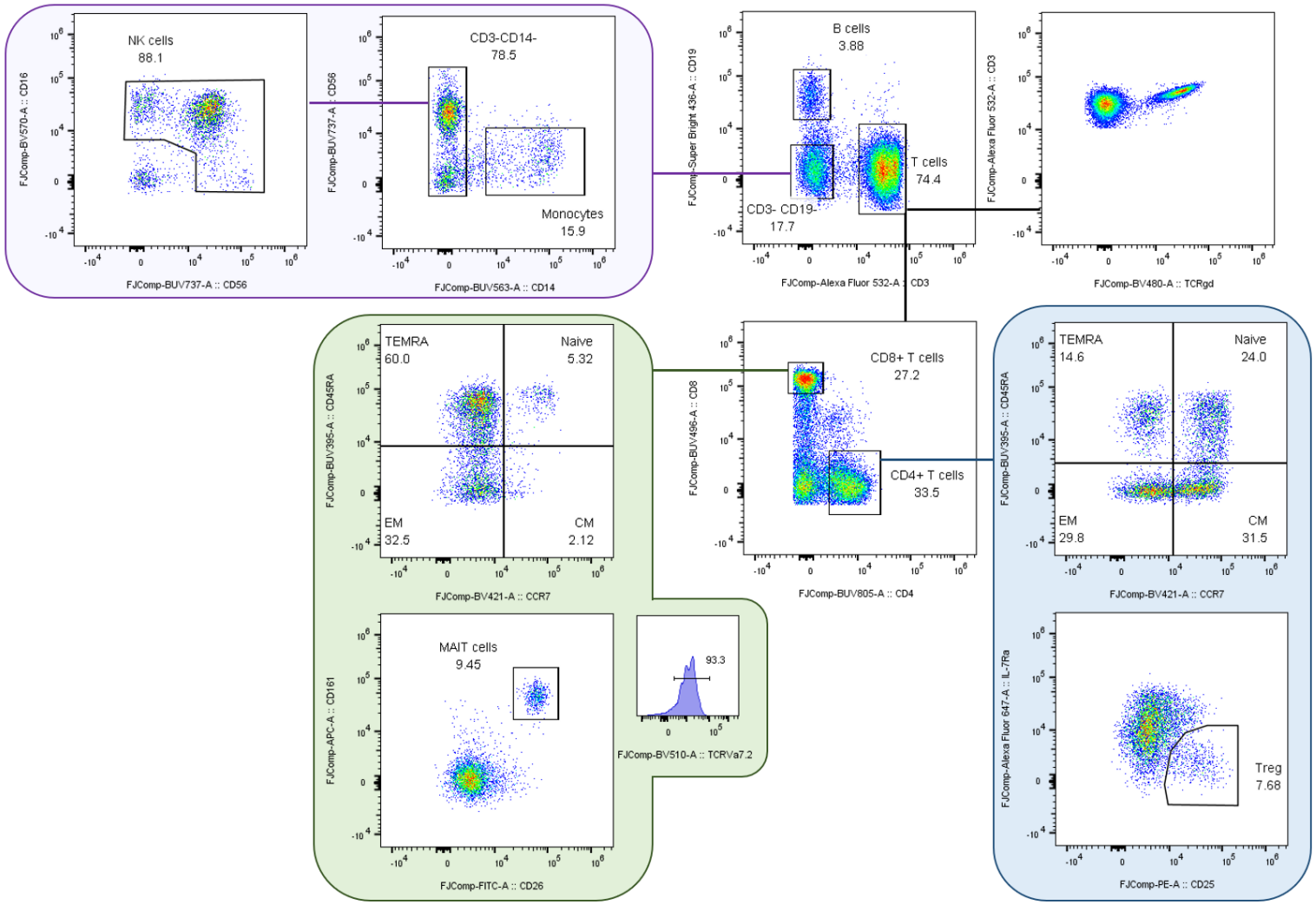

Figure 24. Representative morphology and gating strategy for the main CD45^{+} non-granulocyte whole blood subpopulations in Aurora-acquired data.
CM: central memory. EM: effector memory MAIT: mucosal-associated invariant T-cells. NK: natural killers. TEMRA: terminally differentiated effectors re-expressing CD45RA. Tgd: gamma delta T-cells. Treg: T regulators.

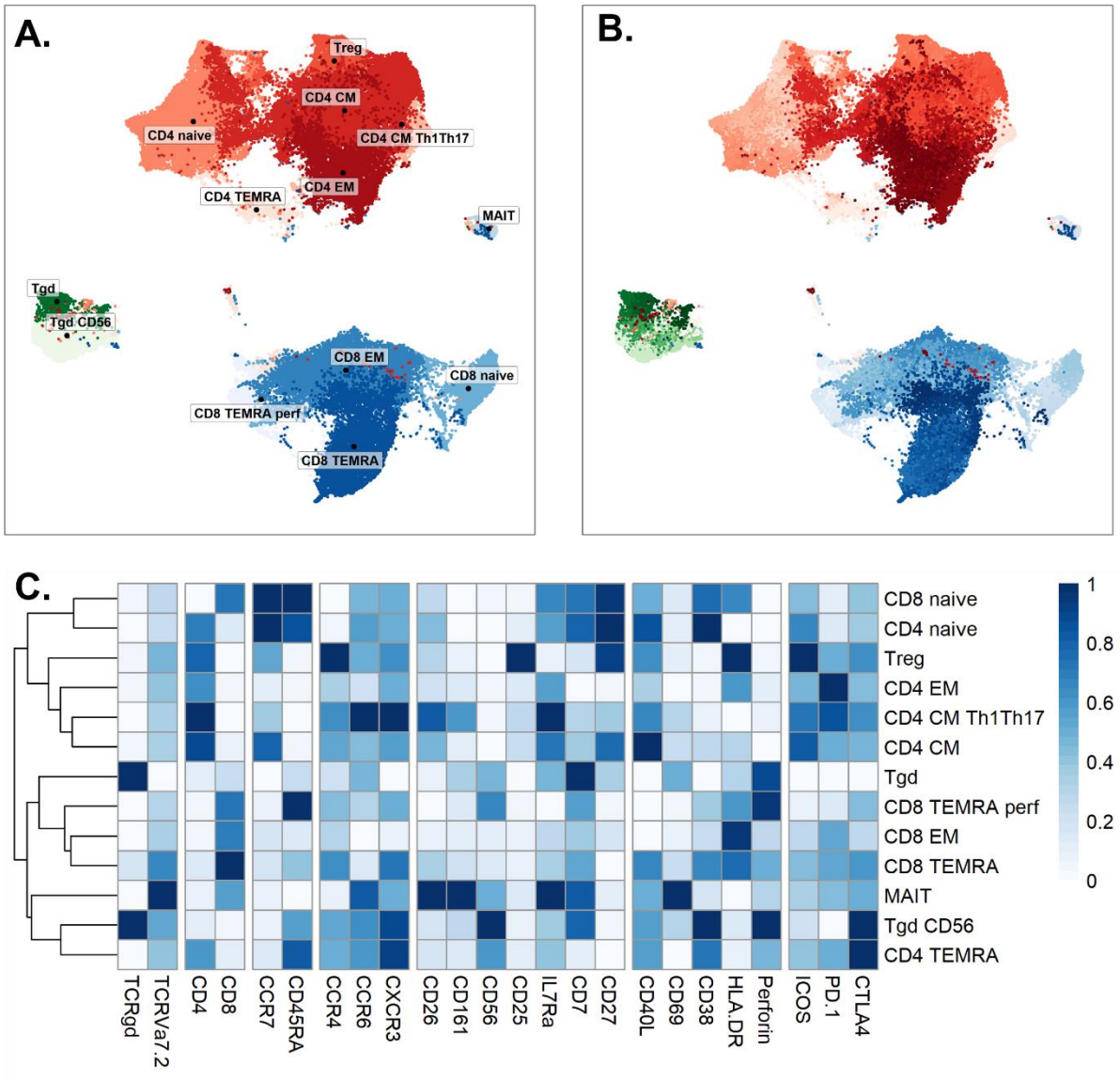

Figure 25. Unsupervised clustering and phenotyping of peripheral CD3⁺ T-cells using full spectrum flow cytometry.

Peripheral whole blood samples were collected from 12 active DS-TB patients at diagnosis, after 2 months of treatment, and at the end of treatment. After whole blood stimulation with either QFT-P NIL, TB2, or rmsHBHA, T-cells were stained with a 30-marker panel and analyzed on a CYTEK Aurora 5-laser full spectrum flow cytometer. A total of 80,000 CD3⁺ events were recorded. FlowSOM enabled automated repartition of all CD3⁺ events 13 phenotypically similar meta-clusters (**A.**) corresponding to 196 clusters (**B**.). Meta-cluster phenotyping was conducted with heatmap visualization of normalized, biexponential-transformed median fluorescence intensity values for each surface marker (**C.**). Hierarchical clustering was performed to identify phenotypically similar FlowSOM meta-clusters.

Abbreviations: CM: central memory. EM: effector memory. MAIT: mucosal associated invariant T-cells. Perf: perforin. Tgd: gamma delta T-cells. Treg: T-regulators. TEMRA: terminally differentiated effectors re-expressing CD45RA. Th1Th17: cells with a combined T helper 1/T helper 17 phenotype (co-expression of CXCR3 and CCR6).

PART C: DISCUSSION AND PERSPECTIVES

"The title of the paper by Dr. Irving Willner in this issue of *Diseases of the Chest* is in the form of a question: "*Can Tuberculosis Be Eradicated?*". This question is definitely answerable in the affirmative. If the title has been "*Will Tuberculosis Be Eradicated?*", the answer would be "*probably not for centuries, if ever*". This answer is because humans have never freed themselves from diseases for which much simpler and more specific methods of treatment and prevention have been available, including diphtheria, gonorrhoea, malaria, smallpox, and syphillis."[153].

If it had not been for the final mention of smallpox – eradicated in 1980 – this excerpt from a 1963 editorial would still fit perfectly in modern opinion takes on TB research. As exposed in Chapter 1, the causes for this are vastly multifactorial, but boil down to the following: because TB disproportionately affects people living in precarity, massive funding gaps cause active TB diagnostics, therapeutics, and monitoring tools to remain outdated despite scientific advances. This contributes to millions of missed cases and to low treatment adherence, which maintains disease transmission and worsens secondary drug resistance, which in turn requires harsher and more expensive treatment. Simultaneously, the estimated 25% of all humanity living with latent TB infection form a huge reservoir of potential progressors to active TB, generating a parallel need for widespread LTBI screening and possible prophylactic treatment. In addition to difficulties of public health and political nature, the slow growth of Mtb, the difficulty of accessing host samples at the site of infection, and our resulting incomplete knowledge of the immune response to TB have hindered innovation for these purposes.

The work presented in this thesis bears witness to the complexity of the anti-TB immune response, and to the magnitude of the translational research that remains to be done to meet clinical needs. Despite the fact that we are not on track to eradicate TB by 2035 – an objective set by the WHO in its 2015 implementation of the END-TB strategy[154] – improving TB management is concretely possible, and has succeeded in a decline of 14% in TB mortality rates since 2015[155]. Here, we focused on novel non-sputum-based, immune tools to monitor treatment. The stakes are many: advancing treatment monitoring methods helps improve treatment adherence and efficacy, but also brings new scientific insights translatable to

diagnostic tools, LTBI screening, discrimination between remote or recent infection, and TB "resister" phenotypes. Mainly, the current TB treatment immunomonitoring candidate tests lack specificity compared to sputum culture to be relevant during treatment, and require too much scientific instrumentation or expertise for rapid implementation in high-TB burden areas. Here, we adopted two types of approaches to advance TB immunomonitoring research. First, we evaluated simple, previously described host immune biomarkers with relatively inexpensive methods in high-TB burden settings. Then, we explored new cellular signatures of TB treatment using high-dimensional single-cell technologies. As our main results have already been discussed within the earlier publications, some selected additional aspects and final perspectives are reviewed thereafter.

1. A multi-centered study in lower-income settings: how practical constraints guided our research

The main characteristic of the HINTT study was its multicentered design, implemented in five lower-middle-income countries with high TB incidence: >20 TB cases per 100,000 inhabitants per year, with the exception of Lebanon (11 cases per 100,000 per year). This design was the greatest strength of the study, because it enabled evaluation of immunomonitoring tests in settings that were consistent with the current epidemiology of TB disease, in patients representative of those who bear most of the TB burden – excluding TB/HIV patients. Recent studies evaluating novel biomarkers of TB have often been conducted in middle- or high-income settings with low TB incidence (*e.g.* Italy[156], Canada[157], Japan[158]), because patient follow-up and access to research infrastructures are considerably easier. There are numerous high-quality studies based in high-TB incidence areas, but they are mostly conducted in China[129,159] or across the African continent, in particular in countries that have a history of TB research because large TB laboratories have long been implanted there (*e.g.* South Africa[124,160–162], Tanzania[163,164]). Here, we have brought new data collected across three continents, in countries that have traditionally hosted fewer TB research studies despite a high TB burden (*e.g.* Madagascar, Paraguay). This is important to better understand the immunobiology of TB in ethnically diverse populations exposed to different TB strains, and to test the robustness and applicability of candidate immunomonitoring tests in these diverse settings.

Moreover, the bulk of the patients enrolled in our study were recruited in Bangladesh and Georgia, across which the prevalence of DR-TB is particularly high. Bangladesh is among the WHO list of 20 high-MDR-TB burden countries ranked by absolute number[165]: in 2019, an estimated 11.7% of TB cases were registered as MDR/RR-TB, 0.7% of which were new cases. This corresponds to over 1,300 laboratory-confirmed MDR/RR-TB cases, although the actual burden is likely much higher. Dhaka – the capital city of Bangladesh, where our patients were recruited – is the most densely populated metropolitan area in the world, home to approximately 47,000 people per km^2. This translates into an overall population of 21 million people, many of whom live in slums, have limited access to healthcare, and are exposed to malnutrition. Georgia, although less populated, has an extensive history of TB/HIV and is also hit hard by drug-resistant TB: in 2019, an estimated 12% of new TB patients and 32% of re-

treated patients were infected with strains that were at least MDR-TB[165]. This corresponds to over 500 cases of MDR-TB enrolled by the Georgian national TB program yearly, over 10% of which are pre-XDR or XDR-TB. In our study, we have enrolled and followed 28 patients treated for either RR-TB, MDR-TB, pre-XDR-TB, and XDR-TB within the Bangladesh, Georgia, and Paraguay (1 patient) study sites. As drug resistance is on the rise worldwide, data for this part of the cohort are particularly valuable, since the follow-up of DR-TB patients – treated for longer periods, with harsher medication – is considerably more difficult than that of DS-TB patients.

Hence, despite being this study's greatest strength, this multicentered design in lower-income settings was also the reason for most its challenges, from patient recruitment to data analysis. In particular, we had expected important loss to follow-up (LTFU), which we experienced despite planning follow-up visits that coincided with national TB program planned visits, and especially despite all the extensive efforts deployed by healthcare staff and community health workers in partner study sites. Among the total HINTT cohort comprising 198 enrolled participants (see flowchart in Publication 1), 23% (46) were LTFU between enrolment (T0) and treatment completion (T2), and an additional 20% (40) between T2 and two months post-end of treatment (T3, which was outside of national TB program planned visits for all study sites). Between T0 and T2, LTFU was greatest in the Dhaka cohort, amounting for 20 patients (43% of all LTFU), 15 of whom were treated for DR-TB. This is due DR-TB treatment regimens being less well tolerated, coupled with the difficulty of keeping track of patients who live in the slums. For follow-up during treatment, we chose to implement a two-month follow-up visit (T1) over other clinically relevant, earlier timepoints often described in the literature (*e.g.* two weeks, one month) for several reasons. Firstly, the two-month timepoint was the only moment during treatment coinciding with a sputum collection visit planned by national TB-programs in all study sites, which helped reduce loss to follow-up to 9% (19) between enrolment and two months. In addition, during clinical DS-TB management, the two-month timepoint is a critical step because it marks the end of the intensive phase, after which antibiotic treatment is reduced. The same timepoint was kept for monitoring of DR-TB patients for consistency, and to compare immune profiles despite heterogeneous treatment regimens. Here, all DR-TB patients benefitted from last-generation antituberculous agents (bedaquiline, linezolid) except for RR-TB patients, and 89% (25/28) had achieved definitive culture conversion after two months.

Downstream of patient enrolment and follow-up processes, this study also presented a number of logistic and technical challenges. In particular, as blood collection is challenging depending on local cultures and settings, collecting large volumes of peripheral blood was not a realistic option. We aimed for this work to be sustainable for partners and adapted to local constraints, while evaluating a variety of blood-based immunological tests. Hence, we had to adopt a parsimonious sample processing protocol making the most of 10mL of whole blood maximum per visit, which were split into CBC monitoring, qRT-PCR experiments (see Annex 5), and five different *in vitro* stimulation conditions for IGRAs and cytometry analyses. While this admittedly generated a number of data analysis limitations, it reflected the reality of the logistic needs for novel TB management tools, and was an opportunity to document the relevance of cheaper tests such as CBC and IGRA as previously discussed.

2. Single-cell technology at the service of translational TB immunology

Despite the constraints associated with in multicentered settings, we have applied high-dimensional mass cytometry analyses in a subset of patients from the HINTT cohort to capture the complexity of T-cell profiles during TB treatment. As conventional flow cytometry is deeply engrained in the commercial supply and in users' habits, in particular in infectious disease immunology, high dimensional cytometry is currently igniting passions among cytometrists. While conventional flow cytometry users praise the technology's maturity, extensive use worldwide, and practicality of use, the other party criticizes the low parameter number or difficult panel design, with opinion pieces asking "is pain and anguish a necessary component of good flow cytometry?" or affirming that "current flow cytometers are the least advanced technologies in the field of spectroscopy, period."[166]. Here, we have chosen to benefit from the analytical power of high-dimensional cytometry data to generate new, detailed insights on T-cell differentiation during TB treatment. However, we have also narrowed the most important features of the observed T-cell profiles down to simpler marker combinations, applicable to validation studies using conventional flow cytometry and eventually translatable to simpler techniques for treatment monitoring. Although we had to attribute a cellular identity to subsets of interest to understand their biological role, our data hint that rather than distinct cellular categories, the phenotypes of T-cells during treatment appear as a complex spectrum whose detection is conditioned by the antigenic stimulation used.

2.1 Insights on treatment monitoring

Overall, we observed a shift towards more differentiated profiles among peripheral $CD8^+$ and $CD4^+$ T-cell subsets. We gained more insight on marker involvement within memory compartments during treatment by phenotyping in detail three peripheral T-cell subpopulations which were associated with cure at the individual level (despite heterogeneity) but were more frequent in peripheral blood than automatically detected clusters. We have shown that they could be identified in cryopreserved samples obtained from small blood volumes, using manual gating analyses. They require a smaller number of core markers to be isolated (13 surface markers), which would enable detection with cheaper, more accessible conventional cytometers, and without cytokine staining. Regarding in-depth phenotypic profiles, a $CXCR3^+$ $CCR6^+$ $CD27^+$ $CD4^+$ EM subset was increased in cured patients compared to pre-treatment. Although it is not possible to infer the full function of this subset without its cytokine expression profile, this phenotype possibly corresponds to a subset enriched in Th1/Th17 cells[167,168], which have been shown to be the main peripheral $CD4^+$ effectors involved in the TB response[89,125]. This is consistent with previous works that showed that peripheral Mtb-specific memory T-cells from latent TB patients were mostly $CXCR3^+$ $CCR6^+$ Th1[169], and supports the hypothesis that an increase in these cells upon cure might be associated with infection control. This subset of interest also expressed CCR4 in lower levels, which has been observed previously in Th1/Th17 cells[170]. Compared to the other $CD4^+$ EM cells, this subset of interest displayed higher CCR6, CD26, IL7Ra, and CD7 expression. CD26 is known to participate in T-cell activation, co-stimulation, and proliferation[171], and its expression levels on $CD4^+$ T-cells have been correlated with Th1-like immune responses[172,173]. However, its role in TB clearance is still unclear. Studies on PTB have mostly investigated CD26 levels on $CD8^+$ cells, showing that a $CD26^{hi}$ phenotype was restored on bacteria-reactive, peripheral MAIT cells during TB treatment[174]. In contrast, a recent nationwide cohort study highlighted an increased risk of active TB disease in diabetes patients treated with high-dose CD26 inhibitors[175]. Along with our results, this warrants further investigation on the role of CD26 expression on $CD4^+$ T-cells in mycobacterial clearance during treatment.

In parallel, a $CCR6^+$ $CD27^+$ $CD4^+$ naïve subset was decreased. It expressed high levels of CD27 and CD38. This is consistent with previous works documenting a decrease in purified protein derivative (PPD)-stimulated $CD27^+$ $CD38^+$ Mtb-specific $CD4^+$ T-cells in treated TB[176]. Our

results suggest that this decrease in $CD38^+$ cells may not be restricted to Mtb-primed T-cells, but could affect naïve cells, perhaps within the frame of general $CD4^+$ T-cell differentiation during treatment. This subset also expressed low levels of CD26 and IL7Ra compared to the $CD4^+$ EM subset analyzed previously. Taken together, these findings indicate that upon TB treatment, differentiated Th1/Th17-like $CD4^+$ subsets expressing high levels of CD26 and IL7Ra are enriched in peripheral blood at the expense of less differentiated subsets expressing high levels of CD27 and CD38.

Then, a main subset of interest we identified corresponded to $CD8^+$ EM cells expressing CD7 and perforin, but not CXCR3, that decreased upon cure. As CXCR3 is involved in effector cell recruitment to inflammatory sites[177], it is possible that this reflects a contraction in peripheral cytotoxic $CD8^+$ T-cells that were circulating as a consequence of the chronic inflammation generated by TB disease, but lacked the ability to migrate to the lung. However, as the role of CXCR3 in TB has mostly been investigated in $CD4^+$ T-cells so far, these results call for further work on $CXCR3^+$ $CD8^+$ T-cells during TB resolution. Overall, to fully understand the underlying processes behind the prior observations, future works including analyses on lymphocytes harvested from broncho-alveolar lavage are needed.

2.2 Differentiating slow from fast converters

Finally, our results suggested that T-cell differentiation during treatment was delayed in slow converters. Beyond the differentiation and memory functions discussed in the publication, our data showed that maturation markers and chemokine receptors discriminated slow from fast converters during treatment to a larger extent than activation and cytotoxicity markers. CD26 and CD27 were also the markers which were responsible for most of the variance observed between fast and slow responders during treatment, along with CCR4. CD27 and CCR4 in Mtb-specific $CD4^+$ T-cells have previously been associated with active TB compared to latent infection[87]. In mouse models, CCR4 has also been shown to inhibit the suppressor function of Tregs and to play a role in TB control[178]. In addition, we observed that HLA-DR and CD38 also contributed to the discrimination between fast and slow converters. These results add up to the observations made by Vickers and colleagues who observed that co-expression of CD27, HLA-DR, and CD38 on PPD-stimulated $CD4^+$ T-cells stratified fast and slow responders without restriction to IFN-γ-producing cells[179]. The fact that HLA-DR and CD38 accounted for a lesser fraction of the observed variance than CCR4, CD27, and CD26, is consistent with studies showing that there was no detectable relationship between bacterial loads and CD38 or HLA-DR expression on total CD4 T-cells[180]. Interestingly, the study by Vickers *et al.* also highlighted a retrospective association between higher pre-treatment frequency of $CD8^+$ $CD27^-$ IFN-γ^+ $CD8^+$ T-cells and $CD27^+$ $CD38^+$ HLA-DR^+ $CD4^+$ T-cells, and lack of culture conversion after two months of treatment[179]. A similar trend was also observed in more detail in our study, with a pre-existing under-representation of cytotoxic $CD8^+$ EM T-cells and an over-representation of $CD38^+$ $CD27^+$ $CD4^+$ naïve T-cells in slow converters at diagnosis (Supp. Figure 11 of Publication 3). In parallel, in successfully treated TB patients who experienced relapse, excessive *in vitro* cytolytic responses and upregulation of genes involved in cytotoxic cell-mediated killing have been observed at diagnosis and up to 4 weeks after treatment initiation[181]. Taken together, our results and prior works suggest that measuring these T-cell populations pre-treatment may possibly predict risks of treatment failure or relapse[182].

3. Limitations

The studies presented in this thesis share limitations, most of which are linked to the "bench to bedside" approach adopted in our study and to constraints specific to study sites in lower income settings. The number of slow converters and of treatment was low, which reflects the current epidemiology of TB in patients undergoing treatment. In addition, the DR-TB cohort was heterogeneous in terms of drug resistance patterns, treatment regimens, and duration. Some inter-patient variation factors could not be controlled, such as antibiotic regimens or malnutrition levels. The genetic background of patients in relation with ethnicity may also bias results, for example via polymorphisms in the *IFNG* gene[183]. In addition, although mycobacterial strain variation is known to impact the immune response[184,185], Mtb genotyping could not be performed. Moreover, immune parameters may be influenced by other untested infections that are highly prevalent in the our study sites, such as parasitic infections that may impact CBC through eosinophilia, or arboviral diseases that may bias IFN-γ levels. Regarding the cytometry study in particular, experiments were conducted on peripheral blood cells, which might induce an imbalance in T-cell proportions between blood and the lungs, the main infectious focus of TB. Due to the design of the study, cytometry analyses were not conducted on live cells, but on fixed, cryopreserved cells. Despite the fact that staining quality was controlled, fixation might induce bias, in particular regarding chemokine receptor expression as they are recycled between the endosomes and the cell membrane in live cells[186]. Cells were extracted from a small volume of blood and yielded a small number of analyzed events per sample, which may cause rare populations to have been undetected. In addition, only samples from the Bangladesh and Georgia cohorts were shipped to Lyon. Moreover, since IGRAs were conducted on the same blood samples prior to cell cryopreservation, intracellular cytokine staining was not performed. Hence, the integrality of the observed cell phenotype changes may not be associated with Mtb-specific responses. However, whether the bulk of anti-TB response relies purely on Mtb-specific cells is debated. Given the complexity of the immune response to TB, cellular and molecular interactions are likely to occur between Mtb-specific and non-specific subpopulations during treatment and mycobacterial clearance. Moreover, this study design enabled us to detect outcomes of interest in naïve compartments, and to gain insights on the involvement of T-cell differentiation in the global response during TB treatment.

4. Ongoing validation studies and associated perspectives

As the studies presented in this thesis warrant further investigation, their main results will be evaluated in a validation study for which recruitment and follow-up are currently ongoing at the Hospices Civils de Lyon: OPTI4TB (*Optimization of Tuberculosis Diagnosis and Management Using Four Immunological Biomarkers*). This study was designed to address some of the shortcomings discussed above, by targeting a population of 20 non-immunocompromised adult DS-TB patients. Standardized disease severity assessment and chest X-rays are performed, and biological samples are collected at two additional timepoints during treatment compared to HINTT (at two weeks and one month post-treatment initiation). Whole genome sequencing of *Mtb* strains is performed at treatment initiation and after two months. Full spectrum flow cytometry analyses will be conducted on live PBMC instead of fixed white blood cells.

In addition, the results obtained in the ensemble of this thesis may be translatable to other associated unmet needs in TB management. In particular, this applies to LTBI management, which is a major public health concern and represents one of the pillars of the WHO END-TB strategy[154,187]. In this context, our team within the Mérieux Foundation is currently conducting an associated study named APRECIT (***A**mélioration de la **PR**ise **E**n **C**harge de l'**I**nfection **T**uberculeuse latente en milieu communautaire*). Its objective is to improve screening and overall management LTBI in partner institutions in Yaoundé, Cameroon, and Antananarivo, Madagascar, where LTBI screening and treatment are not routinely performed. In each study site, the aim is to include 125 index TB cases and 1250 TB household contacts (Figure 26). In household contacts, QFT-P and T-SPOT.TB are performed, and PBMC are collected. rmsHBHA IGRAs will also be performed in a subset of the cohort. In this context, an analysis of plasma IFN-γ and T-cell subset abundance changes using workflows similar to those conducted in this thesis is performed in LTBI and uninfected household contacts, to further characterize immune determinants of TB control.

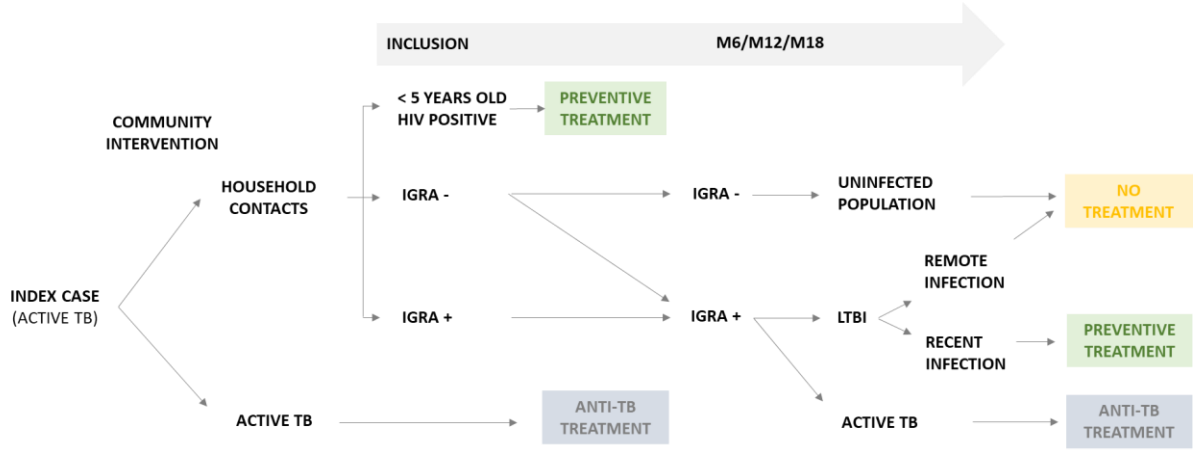

Figure 26. Flowchart of inclusions and follow-up in the APRECIT study.
Adapted from J. Hoffmann.

In addition, an extension of APRECIT called APRECIT-BIS is currently being designed and has been submitted in September 2021 to a call for proposals hosted by the *Agence Nationale de Recherches contre le SIDA et les hépatites virales | Maladies Infectieuses Emergentes*. Its objective is to assess the diagnostic performances of novel immune tools to distinguish participants with remote LTBI from those with recent LTBI (< 2 years after *Mtb* primo-infection), the latter being at higher risk of progressing to active TB[188,189]. For this purpose, the biobank collected in APRECT will be used retrospectively to (i) evaluate a flow cytometry tool measuring the surface expression of HLA-DR within *Mtb*-specific $CD3^+$ IFN-γ^+ T cells, recently validated in a large-scale clinical study conducted by the South African Tuberculosis Vaccine Initiative (SATVI)[161,190], and (ii) compare the diagnostic performances of this test to those of the RISK6 signature[191] and of a novel plasma cytokine signature adapted from previous works[192,193] and evaluated within the framework of HINTT. This work conducted in APRECIT-BIS could also help document the cellular and molecular immune characteristics of "TB resisters", defined as individuals who do not develop LTBI despite long-term exposure to *Mtb*[194,195].

ANNEXES

1. Supplementary data from original publications

1.1 Annex 1 – Supplementary data from publication 1

Drug resistant patients were recruited in Bangladesh (17/28, 60.7%), Georgia (10/28, 35.7%), and Paraguay (1/28, 3.6%). Among them, 2/28 (7.1%) were rifampicin-resistant (RR-TB), 4/28 (14.2%) were poly-resistant (PR-TB), 17/28 (60.7%) were MDR-TB, 4/28 (14.2%) were pre-extensively drug resistant (pre-XDR-TB), and 1/28 (3.7%) was XDR-TB. All pre-XDR-TB or XDR-TB patients were recruited in Georgia.

Supplementary Table 1. Therapeutic regimens used in each study site.

	Bangladesh (n = 38)	Georgia (n = 33)	Lebanon (n = 18)	Madagascar (n = 36)	Paraguay (n = 27)
DS-TB patients	New cases (n = 16) 2HRZE/4HR[1]	New cases (n = 15) Re-treated (n = 2) 2HRZE/4HR[1,4]	New cases (n = 16) Re-treated (n = 2) 2HRZE/4HR[1,4]	New cases (n = 31) Re-treated (n = 5) 2HRZE/4HR[1,4]	New cases (n = 20) Re-treated (n = 6) 2HRZE/4HR[1,4]
	Re-treated (n = 5) 2SHRZE/1HRZE/5RHE[2]	New cases (n = 5) 2HRZE/4HRE[5]			
		Poly-DR (isoniazid-resistant, n = 1) RZE[6]			
DR-TB patients	New cases (n = 11) Re-treated (n = 6) 4-6 Km-Mfx-Pto-Cfz-Z-HHigh dose-E/5-6 Mfx-Cfz-Z-E[3]	New cases (n = 9) and re-treated (n = 1) RR-TB: H+E+Z+Km+Mfx+Pto+Cfz / Mfx+E+Z+cfz; MDR-TB: H+Z+Km+Lfx+cfz+Bdq / Z+Lfx+cfz+Bdq; Cm+Lfx+Pto+Cs+Cfz+H / Cm+Lfx+Cs+Bdq+Lzd / Lfx+Cs+Bdq+Lzd; Z)+Cm+Mfx+Cs+Pto+Cfz / Lfx+Cfz+Bdq+Lzd Pre-XDR-TB: (Z)+Lfx+Pto+Cfz+Bdq+Lzd / Cs+Cfz+Bdq+Lzd; Bdq+Cfz+Lfx+H+Pto+E+Z / Bdq+Cfz+Lzd+H+E / Bdq+Cfz+Lfx+H+Z / Bdq+Cfz+Lfx+E+Z; H+Z+Km+Lfx+Cfz+Bdq / Z+Lfx+Cfz+Bdq; Cm+Lfx+Cs+Cfz+Bdq+Lzd / Lfx+Cs+Cfz+Bdq+Lzd XDR-TB: Bdq+Lzd+Cfz+Cs	*No cases*	*No cases*	Re-treated (n = 1) 4 Km-Hhigh dose-12E-Z-Mfx-Pto-Cfz

Footnotes: DS-TB: drug-susceptible. DR-TB: drug-resistant. RR-TB: rifampicin-resistant. MDR-TB: multi-drug resistant. XDR: extensively drug resistant. For treatment regimens, antibiotic abbreviations are summarized at the end of the manuscript. Numbers refer to the total duration in months for each drug. Drug regimens were prescribed according to each study site's National TB program and could not be altered.

Supplementary Table 2. Methods for microbiological diagnosis of tuberculosis, drug susceptibility testing, and cell count in each study site.

	Sputum culture			Smear microscopy		Drug susceptibility testing (DST)				Reference of cell counting machine
Country	**MGIT**	**LJ**	**OK**	**ZN**	**Auramine O**	**GeneXpert**	**LPA**	**LJ-DST**	**MGIT-DST**	
Bangladesh		X		X		X		X		Callatac ES Automated Hematology Analyzer, MEK-7300 (Nihon Kohden)
Georgia	X	X		X	X	X			X	XT-20001 (Sysmex)
Lebanon	X	X		X		X			X	CELL-DYN Ruby (Abbott)
Madagascar		X			X	X	X	X		XT2100i and XN1000 (Sysmex)
Paraguay			X	X		X				XT-20001 (Sysmex)

Footnotes: Crosses indicate the method(s) performed in each study site.MGIT: Mycobacteria Growth Indicator Tube (liquid medium). LJ: Löwenstein-Jensen (solid medium). OK: Ogawa Kudoh (solid medium). ZN: Ziehl-Neelsen staining. LPA: line probe assay. Smear microscopy was performed after NALC-NaOH decontamination.

Critical drug concentrations used for DST:

MGIT: Streptomycin 4.0 µg/mL, Rifampicin 40.0 µg/mL, Isoniazid 0.2 µg/mL, and Ethambutol 2.0 µg/mL.

L-J: Streptomycin 1.0 µg/mL, Rifampicin 1.0 µg/mL, Isoniazid 0.1 µg/mL, and Ethambutol 5.0 µg/mL.

Supplementary Table 3. Normality assessment of evaluated continuous variables.

Timepoint	T0		T1		T2	
	W value	p-value	W value	p-value	W value	p-value
Body mass index	0.947	>0.001	0.975	0.011	0.977	0.021
Leucocytes (/mm^3)	0.971	0.003	0.444	>0.001	0.575	>0.001
Monocytes (%)	0.945	>0.001	0.964	0.001	0.966	0.001
Lymphocytes (%)	0.957	>0.001	0.924	>0.001	0.976	0.009
Age	0.881	>0.001	-	-	-	-

Footnotes: normality was assessed using the Shapiro-Wilk test. The H0 hypothesis of normality was rejected for $p<0.05$.

Supplementary Table 4. Sociodemographic characteristics of the cohort, stratified by country.

	Bangladesh	Georgia	Lebanon	Madagascar	Paraguay	*p*
N	**38**	**33**	**18**	**36**	**27**	
Patient demographics						
Age (years), median	22 (18.2-28)^{G}	35 (28-44)^{B,M,P}	29.5 (22.2-36.5)	26 (19.7-36.7)	29 (23-39)	*>0.001*
Sex (male)	65.8% (25/38)	78.8% (26/33)	55.6% (10/18)	55.6% (20/36)	55.6% (15/27)	*0.22*
Drug-resistant strain	44.7% (17/38)^{L,M,P}	30.3% (10/33)^{M}	0^{B,G}	0^{B,G}	3.7% (1/27)^{B}	*>0.001*
BMI at inclusion, median	17.6 (16.3-20.7)^{G,L,P}	20.3 (18.8-23.6)^{B,M}	20.7 (19.4-21.4)^{B,M}	17.1 (16.3-18.2)^{G,L,P}	20.2 (17.8-22.4)^{B,M}	*>0.001*
White blood cell absolute count at inclusion (/mm^3)	9500 (8050-10975)	9800 (7600-12000)	8455 (7297.5-10875)	9370 (5802.5-12002.5)	11110 (8590-12585)	*0.29*
Lymphocyte proportion at inclusion (% of WBC)	20 (18-26.7)	18 (15-22)	16.5 (14.3-19.5)	17.6 (12.6-24.2)	17 (13-21)	*0.10*
Monocyte proportion at inclusion (% of WBC)	3 (2-4)^{G,L,M,P}	4 (4-6)^{B,L,M,P}	7.26 (5.7-9.2)^{B,G,P}	9.9 (6.8-11.3)^{B,G,P}	0 (0-2)^{B,G,L,M}	*>0.001*
Number of household contacts, median	4.5 (3-7)	4 (2.75-4.25)	5 (4-6)	5 (4-6)	5 (4-7)	*0.056*
BCG	84.2% (32/38)^{G,L}	36.6% (12/33)^{B,M,P}	26.7% (4/15)^{B,M,P}	94.3% (33/35)^{G,L}	85.7% (18/21)^{G,L}	*>0.001*
Risk factors and comorbidities						
Smoking	44.7% (17/38)	57.6% (19/33)	50% (9/18)	38.9% (14/36)	50% (13/26)	*0.62*
Alcohol abuse	13.2% (5/38)	6.1% (2/33)^{M,P}	5.6% (1/18)	41.7% (15/36)^{G}	38.5% (10/26)^{G}	*>0.001*
Injectable drug use	10.5% (4/38)	0	0	0	3.8% (1/26)	*0.052*
Jail detention history	5.3% (2/38)	6.1% (2/33)	16.7% (3/18)	2.9% (1/34)^{P}	26.9% (7/26)^{M}	*0.013*
Chronic HCV infection	0	6.1% (2/33)	0	2.8% (1/36)	0	-
Other disease[1]	0	0	5.6% (1/18)	8.3% (3/36)	14.3% (3/21)	-
History of TB						
Previous TB	29.7% (11/37)	9.7% (3/31)	11.1% (2/18)	13.9% (5/36)	26.9% (7/26)	*0.15*
Of which are documented	*100% (11/11)*	*66.7% (2/3)*	*50% (1/2)*	*40% (2/5)*	*85.7% (6/7)*	*0.12*
Prior exposure to active TB patients	28.9% (11/38)	6.2% (2/32)	44.4% (8/18)	36.1% (13/36)	48% (12/25)	*0.17*
Previous TB outcome						
Cured and completed	45.5% (5/11)	0	50% (1/2)	40% (2/5)	57.1% (4/7)	-
Treatment completed	18.1% (2/11)	0	0	0	14.3% (1/7)	-
Treatment failure	0	33.3% (1/3)	0	20% (1/5)	14.3% (1/7)	-
Outcome not evaluated or unknown	36.4% (4/11)	66.7% (2/3)	50% (1/2)	40% (2/5)	14.3% (1/7)	-
Current TB outcome						
Cured and completed	100% (38/38)	90.9% (30/33)	61.1% (11/18)	97.2% (35/36)	88.9% (24/27)	*0.39*
Completed	0	3% (1/33)	38.9% (7/18)	0	0	-
Treatment failure	0	6.1% (2/33)	0	2.8% (1/36)	7.4% (2/27)	-
Relapse or reinfection	0	0	0	0	3.7% (1/27)	-

Footnotes: BMI: body mass index. TB: tuberculosis. WBC: white blood cells. Data are given as % (N) or median (interquartile range).

1: asthma, hypertension, inflammation. $^{B, G, L, M, P}$: initial of study sites that are different from each other ($p<0.05$). *: different from all other sites.

Data were compared with Kruskal-Wallis' test with Dunn's post-hoc, or Fisher's test with Bonferroni's post-hoc when significant.

Supplementary Table 5. Characteristics of patients with treatment failure

Demographics			T0		T1		T2	
Drug susceptibility	**Country**	**Age (years)**	**Culture**	**Smear**	**Culture**	**Smear**	**Culture**	**Smear**
S	Georgia	31	+	2+	+	Scanty	+	Scanty
S	Georgia	58	+	Scanty	*Unavailable**	-	+	-
S	Madagascar	45	+	3+	-	1+	+	-
S	Paraguay	24	+	3+	-	-	+	*Unavailable***
S	Paraguay	29	+	3+	+	-	+	*Unavailable***

Footnotes: T0: baseline. T1: T0 + 2 months. T2 : end of treatment. S: drug-susceptible. LTFU: lost to follow-up. + : positive. - : negative. *contamination during culture. **: not enough sputum.

Supplementary Table 6. Receiver Operating Curve (ROC) analysis.

Clinical parameters at baseline	AUC	Sensitivity	Specificity	Optimal threshold
Absolute WBC counts (cells/mm^3)	0.788 (0.664-0.912)	1 (0.8-1)	0.74 (0.57-0.84)	11435 (10105-12072.5)
Lymphocyte proportions (% of WBC)	0.807 (0.671-0.943)	1 (0.8-1)	0.68 (0.58-0.93)	16.0 (10.5-16.5)
Absolute WBC counts (cells/mm^3) + lymphocyte proportions (%)	0.841 (0.723-0.959)	1 (0.8-1)	0.74 (0.62-0.94)	-

Footnotes: WBC: white blood cells. AUC: Area Under the Curve. AUC are given with the 95% confidence interval.

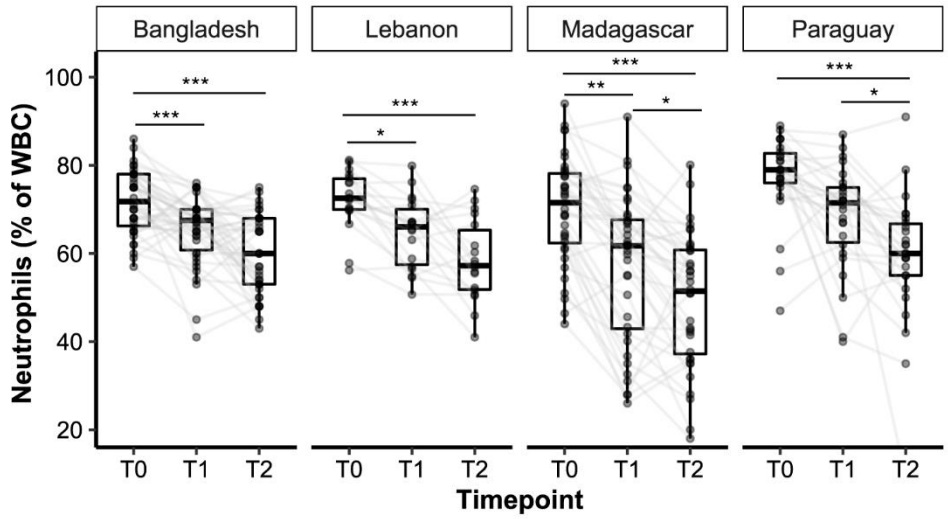

Supplementary Figure 1. Neutrophil proportions of total white blood cells during treatment.
Data are given as median + interquartile range (total n = 129). Each dot represents one patient at one timepoint. Grey lines connect data points from a same patient. T0: baseline. T1: baseline + 2 months. T2: end of treatment. Data were analyzed using Friedman's test, with the Wilcoxon-Nemenyi-McDonald-Thompson test as a post-hoc correction for pairwise multiple comparisons. *: p<0.05. **: p<0.01. ***: p<0.001.

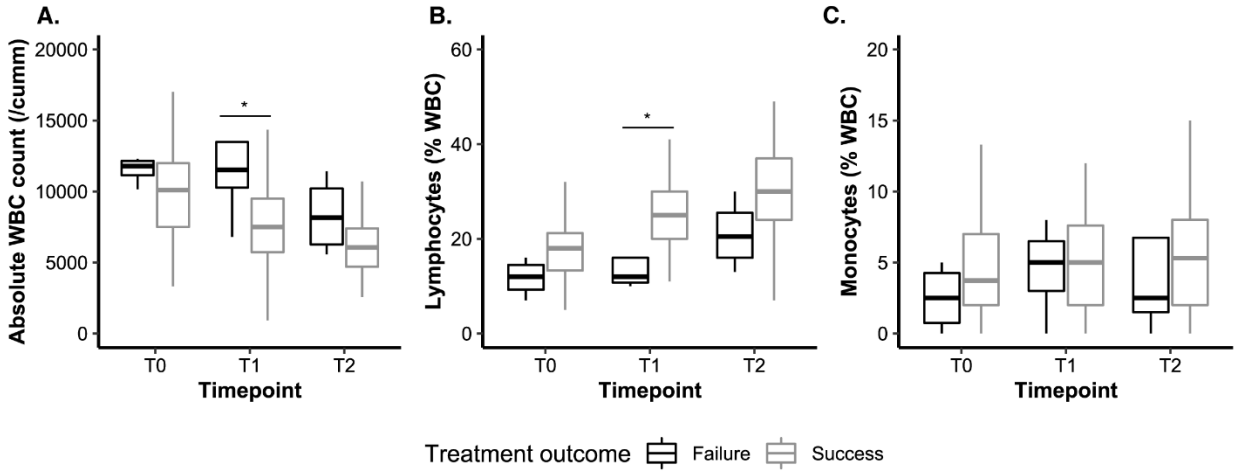

Supplementary Figure 2. Evolution of the main white blood cell types during treatment in patients with high baseline sputum smear microscopy grades.
White blood cell (WBC) absolute counts (**A.**), lymphocyte percent of WBC (**B.);** and monocyte percent of WBC (**C.**) were assessed over time in 74 patients with sputum smear microscopy grades of 2+ or 3+ (success, n = 70; failure, n = 4). Data are given as median + interquartile range. T0: baseline. T1: baseline + 2 months. T2: end of treatment. Data were analyzed using the Mann-Whitney U test. *: p<0.05.

1.2 Annex 2 – Supplementary data from publication 2

Supplementary Table 1. Sociodemographic characteristics of the cohort, stratified by country.

	Bangladesh	**Georgia**	**Lebanon**	**Madagascar**	**Paraguay**	***p***
N	38	31	7	36	20	
Patient demographics						
Age (years), median (IQR)	22 (18.25-28)[G,P]	34 (28-43) [B,M]	23 (20.5-28.5)	26 (19.75-36.75)	28.5 (22.5-38.25)[B]	***>0.001***
Sex (male), % (N)	65.8% (25/38)	77.4% (24/31)	42.9% (3/7)	55.6% (20/36)	55% (11/20)	*0.23*
Drug resistance, % (N)	44.7% (17/38) [M,P]	32.3% (10/31) [M]	0	0[B]	5% (1/20)[B]	***>0.001***
Treatment failure, % (N)	2.6% (1/38)	6.5% (2/31)	0	2.8% (1/36)	0	*0.72*
BMI at inclusion, median (IQR)	17.6 (16.3-20.7)[G,L,P]	20.3 (18.8-23.8)[B,M]	20.9 (20.2-21.2)[B,M]	17.1 (16.3-18.2)[G,L,P]	20.8 (18.5-22.7)[B,M]	***>0.001***
White blood cell absolute count at inclusion (/cumm)	9500 (8050-10975)	9800 (7000-12050)	8610 (6780-12450)	9370 (5802.5-12002.5)	11180 (8690-13567.5)	*0.52*
Lymphocyte proportion at inclusion (% of WBC)	20 (18-26.75)[L]	18 (15-21.5)	13.4 (12.55-15.6)[B]	17.6 (12.6-24.28)	18.5 (15.5-23)	***0.041***
Number of household contacts, median (IQR)	4.5 (3-7)	4 (3-4.75)	5 (4-5.5)	5 (4-6)	4 (4-6)	*0.18*
BCG vaccination, % (N)	84.2% (32/38)	38.7% (12/31)	14.3% (1/7)*	91.7% (33/36)	94.1% (16/17)	***>0.001***
Risk factors and comorbidities						
Smoking, % (N)	84.2% (32/38)	38.7% (12/31)	14.3% (1/7)	91.7% (33/36)	50% (10/20)	*0.49*
Alcohol abuse, % (N)	44.7% (17/38)[M]	58.1% (18/31)[M,P]	28.6% (2/7)	38.9% (14/36)[B,G]	35% (7/20)[G]	***0.0010***
Injectable drug use, % (N)	13.2% (5/38)	6.5% (2/31)	0	41.7% (15/36)	5% (1/20)	*0.10*
Jail detention history, % (N)	10.5% (4/38)	0	0	0	25% (5/20)	*0.064*
Chronic HCV infection, % (N)	5.3% (2/38)	6.5% (2/31)	14.3% (1/7)	2.9% (1/34)	0	*0.69*
Other disease[1], % (N)	0	3.2% (1/31)	0	2.8% (1/36)	16.7% (3/18)	*0.060*
History of TB						
Previous TB, % (N)	29.7% (11/37)	10.3% (3/29)	14.3% (1/7)	13.9% (5/36)	20% (4/20)	*0.10*
Prior exposure to active TB patients, % (N)	28.9% (11/38)	6.7% (2/30)	42.9% (3/7)	36.1% (13/36)	45% (9/20)	*0.36*
Previous TB outcome						
Cured and completed, % (N)	42.9% (3/7)	0	0	0	75% (3/4)	*1*
Treatment completed, % (N)	28.6% (2/7)	0	0	0	0	*1*
Outcome not evaluated or unknown, % (N)	0	66.7% (2/3)	0	0	25% (1/4)	*1*
Treatment failure, % (N)	0	33.3% (1/3)	0	33.3% (1/3)	0	*1*

Footnotes: BMI: body mass index. IQR: interquartile range. TB: tuberculosis. WBC: white blood cells.
1: asthma, hypertension, inflammation.
Data were compared with Kruskal-Wallis' test with Dunn's post-hoc, or Fisher's test with Bonferroni's post-hoc when significant.
[B, G ,L, M, P]: initial of study sites that are different from each other ($p<0.05$). *: different from all other sites.

Supplementary Table 2. QFT-P or HBHA IFN-y levels in the different study sites.

Parameter	Timepoint	All N = 132	Bangladesh N = 38	Georgia N = 31	Lebanon N = 7	Madagascar N = 36	Paraguay N = 20	*p (countries)*
TB1 [IFN-y] (IU/mL)	**T0**	0.52 (0.11-1.78)	0.49 (0.08-1.9)	1 (0.24-2.42)	0.74 (0.33-1.8)	0.25 (0.02-1.04)	0.36 (0.24-0.74)	*0.12*
	T1	0.53 (0.1-1.73)	0.55 (0.18-1.4)	0.94 (0.17-4.49)	1.53 (0.53-1.78)	0.26 (0.05-1.54)	0.35 (0.11-1.47)	*0.23*
	T2	0.62 (0.12-2.07)	0.85 (0.17-2)	0.46 (0.16-1.68)	0.72 (0.47-2.15)	0.6 (0.12-2.21)	0.53 (0.08-1.99)	*0.96*
TB2 [IFN-y] (IU/mL)	**T0**	0.64 (0.27-2.06)	0.55 (0.18-1.98)	1.51 (0.33-3.88)	0.62 (0.5-1.76)	0.56 (0.1-1.29)	0.53 (0.3-0.91)	*0.24*
	T1	0.66 (0.12-2.91)	0.84 (0.2-3.6)	0.77 (0.12-3.83)	0.92 (0.68-1.62)	0.48 (0.04-2.08)	0.37 (0.12-1.7)	*0.47*
	T2	0.82 (0.11-3.43)	0.9 (0.12-3.29)	0.61 (0.11-4.17)	0.87 (0.5-2.55)	0.8 (0.1-2.33)	0.59 (0.08-3.75)	*0.92*
MIT [IFN-y] (IU/mL)	**T0**	10 (6.47-10)	10 (7.43-10)	10 (10-10)^{M}	7.91 (5.12-10)	9.44 (1.98-10)^{G}	10 (5.41-10)	*0.0025*
	T1	10 (8.07-10)	10 (6.53-10)	10 (10-10)^{M}	10 (10-10)	9.54 (5.35-10)^{G}	10 (7.72-10)	*0.0075*
	T2	10 (8.59-10)	10 (7.72-10)^{G}	10 (10-10)^{B,M}	10 (9.75-10)	9.87 (7.42-10)^{G}	10 (7.09-10)	*0.0095*
HBHA [IFN-y] (IU/mL)	**T0**	0.08 (0.01-0.48)	0.16 (0.03-0.6)^{P}	0.54 (0.08-4.14)^{M,P}	0.04 (0.01-0.07)	0.05 (0.01-0.2)^{G}	0.05 (0.01-0.07)^{B}	*>0.001*
	T1	0.37 (0.09-1.78)	0.6 (0.19-1.72)^{M,P}	2.5 (0.48-8.71)^{L,M,P}	0.14 (0.07-1.28)^{G}	0.14 (0.03-0.31)^{B,G}	0.09 (0.02-0.45)^{B}	*>0.001*
	T2	1 (0.12-5.24)	5.05 (1.25-10) *	4.65 (1.46-10) *	0.36 (0.08-0.92)	0.08 (0.01-0.31)	0.5 (0.18-1.09)	*>0.001*

Footnotes: T0: baseline. T1: baseline + 2 months. T2: end of treatment. All values are given after subtraction of NIL [IFN-y]. $^{B, G, L, M, P}$: initial of study sites that are different from each other ($p<0.05$). *: different from all other sites. Data were compared using Kruskal-Wallis's non-parametric test with Dunn's post-hoc when significant.

Supplementary Table 3. Blood count thresholds for stratified IFN-γ analysis.

	T0		T1		T2	
	Q1	Q3	Q1	Q3	Q1	Q3
WBC (cells/mm^3)	7300	12000	5900	9500	4900	7400
Neutrophils (% of WBC)	70	80	60	70	50	70
Lymphocytes (% of WBC)	14	25	20	31	26	37

Footnotes: T0: baseline. T1: baseline + 2 months. T2: end of treatment. Q1: first quartile. Q3: third quartile. WBC: total white blood cells.

Supplementary Table 4. Assay performances of the QFT-P and rmsHBHA IGRAs compared to sputum culture.

Test	Thresholds	Timepoint	Sensitivity	Specificity	Accuracy
Smear microscopy	-	*T1*	81.1	50	76.6
		T2	92.9	33.3	91.5
QFT-P IGRA	TB1 ≥ 0.75 IU/mL and TB2 ≥ 0.71 IU/mL	*T1*	45.3	35.3	43.8
		T2	45.7	66.7	46.2
QFT-P TB2-TB1	≥ 0.03 IU/mL	*T1*	51.6	52.9	51.8
		T2	54.3	66.7	54.6
HBHA IGRA	≤ 0.22 IU/mL	*T1*	64.2	64.7	64.3
		T2	66.9	0	65.4
HBHA and QFT-P IGRA	-	*T1*	86.3	23.5	76.8
		T2	82.7	0	80.8
HBHA and TB2-TB1	-	*T1*	80	35.3	73.2
		T2	85	0	83.1

Footnotes: T0: baseline. T1: baseline + 2 months. T2: end of treatment.
For all IGRA variables, cutoffs adapted for this study on active TB patients were calculated using AUC analyses. Respective cutoffs are indicated in the "Threshold" column. The overall QFT-P test was considered positive if either TB1 or TB2 were above the indicated thresholds. The "HBHA and QFT-P IGRA" variable was defined as follows: positive when HBHA-IGRA results are negative and QFT-P results are positive; negative when HBHA-IGRA results are positive and/or QFT-P results are negative or indeterminate. The "HBHA and TB2-TB1" variable was defined as follows: positive when HBHA-IGRA results are negative and TB2-TB1 is strictly greater than the indicated threshold; negative when HBHA-IGRA results are positive and/or TB2-TB1 is equal to or lesser than the indicated threshold.

Supplementary Table 5. Associations between time to culture conversion and WBC counts.

		Successfully treated patients with available T1 culture results (n = 112)			
	Timepoint	**Fast converters**	**Slow converters**	**Failure or relapse**	***p***
N		92	16	4	
Absolute WBC count (per mm^3)	*T0*	9500 (7302.5-11425)	9385 (7822.5-14325)	12200 (12082.5-13400)	*0.077*
	T1	7535 (6247.5-9367.5)	8500 (6220-10900)	10780 (9470-11300)	*0.14*
	T2	6190 (4742.5-7812.5)	6750 (4387.5-7687.5)	6050 (5595-7247.5)	*0.97*
Neutrophil % of WBC	*T0*	75 (68-79)	75 (71.97-78.25)	84 (81.5-86.5)*	***0.022***
	T1	67.55 (60-72.17)	67.5 (61.1-75)	79 (75-81.75)*	***0.043***
	T2	60.15 (54.75-68)	58.5 (51.75-66.97)	64.5 (59-71.75)	*0.49*
Lymphocyte % of WBC	*T0*	19 (15-26)	17.5 (12.8-19.5)	12.5 (9.2-15.2)*	***0.017***
	T1	25 (20.7-31)	23 (16.2-28.0)	15.5 (11-21.2)*	***0.027***
	T2	30 (25.9-36)	29.5 (23.5-36.2)	21 (17.7-26.5)	*0.21*
High absolute WBC count (>3rd quartile)	*T0*	21.7% (20/92)	31.2% (5/16)	75% (3/4)	*0.050*
	T1	20.7% (19/92)	43.8% (7/16)	75% (3/4)*	***0.014***
	T2	29.3% (27/92)	25% (4/16)	25% (1/4)	*1*
High neutrophil % (>3rd quartile)	*T0*	22.8% (21/92)	18.8% (3/16)	100% (4/4)*	***0.0053***
	T1	23.9% (22/92)	31.2% (5/16)	75% (3/4)	*0.081*
	T2	28.3% (26/92)	31.2% (5/16)	50% (2/4)	*0.62*
Low lymphocyte % (<1st quartile)	*T0*	14.1% (13/92)	37.5% (6/16)	50% (2/4)*	***0.020***
	T1	19.6% (18/92)	37.5% (6/16)	50% (2/4)	*0.12*
	T2	22.8% (21/92)	31.2% (5/16)	75% (3/4)	*0.06*

Footnotes: Data are given as median (interquartile range) or % (N). WBC: white blood cells. T0: baseline. T1: baseline + 2 months. T2: end of treatment. Fast converters: culture conversion between T0 and T1. Slow converters: culture conversion between T1 and T2. Treatment failure: positive culture at T2 or T3 (end of treatment + 2 months). *: significantly different from both other groups (Kruskal-Wallis test + Dunn's post-hoc test).

Supplementary Table 6. Sociodemographic characteristics and culture conversion profile

N	Fast converters 92	Slow converters 16	Failure or relapse 4	*p*
Patient demographics				
Age (years), median (IQR)	26.5 (21-36.25)	33.5 (25.75-47.75)	38 (30.5-48.25)	*0.099*
Sex (male), % (N)	63% (58/92)	62.5% (10/16)	100% (4/4)	*1*
Drug resistance, % (N)	26.1% (24/92)	18.8% (3/16)	0	*0.76*
Country of origin, % (N)				
Bangladesh	38% (35/92)	18.8% (3/16)	0	*0.14*
Georgia	26.1% (24/92)	25% (4/16)	50% (2/4)	*0.93*
Lebanon	5.4% (5/92)	0	0	*0.34*
Madagascar	10.9% (10/92)*	56.2% (9/16)*	25% (1/4)	***>0.001***
Paraguay	19.6% (18/92)	0	25% (1/4)	*0.053*
BMI at inclusion, median (IQR)	19.7 (17.3-21.4)*	17.0 (16.2-18.6)*	17.5 (15.9-20.2)	***0.0088***
White blood cell absolute count at inclusion (/mm^3)	9500 (7302.5-11425)	9385 (7822.5-14325)	12200 (12082.5-13400)	*0.75*
Lymphocyte proportion at inclusion (% of WBC)	19 (15-26)	17.5 (12.8-19.55)	12.5 (9.25-15.25)	*0.099*
Number of household contacts, median (IQR)	4 (3-6)	3.5 (3-5.25)	5.5 (4.75-8)	*0.44*
BCG vaccination, % (N)	83.8% (62/74)	100% (13/13)	100% (2/2)	*0.19*
Risk factors and comorbidities				
Smoking, % (N)	42.4% (39/92)	43.8% (7/16)	100% (4/4)	*1*
Alcohol abuse, % (N)	17.4% (16/92)	12.5% (2/16)	50% (2/4)	*0.32*
Injectable drug use, % (N)	4.4% (4/91)	0	0	*1*
Jail detention history, % (N)	7.7% (7/91)	6.2% (1/16)	50% (2/4)	*1*
Chronic HCV infection, % (N)	1.4% (1/71)	8.3% (1/12)	0	*0.27*
Other disease[1], % (N)	5% (4/80)	8.3% (1/12)	0	*0.51*
History of TB				
Previous TB, % (N)	17.3% (16/92)	12.5% (2/16)	25% (1/4)	*0.73*
Prior exposure to active TB patients, % (N)	26.4% (24/91)	12.5% (2/16)	75% (3/4)	*1*

Footnotes: BMI: body mass index. IQR: interquartile range. TB: tuberculosis. WBC: white blood cells.
1: asthma, hypertension, inflammation. Data were compared with the Kruskal-Wallis test and Dunn's post hoc, or Fisher's test. *: groups significantly different from each other.

Supplementary Table 7. Associations between time to culture conversion and IFN-γ response.

Parameter	Timepoint	Univariate analysis		Multivariate analysis[1]			
		OR (95%CI)	*p*	aOR (95%CI)	*p*	C	AIC
TB1 IFN-γ	*T0*	0.87 (0.611 - 1.09)	*0.32*	0.914 (0.652 - 1.213)	*0.55*	0.62	67.1
	T1	0.879 (0.646 - 1.08)	*0.30*	1.051 (0.74 - 1.392)	*0.74*	0.61	67.4
	T2	1.01 (0.831 - 1.18)	*0.91*	1.365 (1.002 - 1.943)	*0.058*	0.66	63.6
TB2 IFN-γ	*T0*	0.81 (0.543 - 1.03)	*0.17*	0.856 (0.592 - 1.143)	*0.33*	0.65	66.4
	T1	0.874 (0.659 - 1.07)	*0.25*	0.992 (0.715 - 1.289)	*0.96*	0.62	67.5
	T2	0.99 (0.818 - 1.15)	*0.90*	1.162 (0.911 - 1.493)	*0.22*	0.62	66.0
HBHA IFN-γ	*T0*	0.336 (0.023 - 0.916)	*0.25*	0.241 (0.004 - 1.068)	*0.36*	0.68	64.8
	T1	0.989 (0.814 - 1.15)	*0.89*	1.068 (0.746 - 1.515)	*0.69*	0.61	67.3
	T2	0.843 (0.674 - 0.993)	*0.072*	0.983 (0.712 - 1.333)	*0.91*	0.64	67.5

Footnotes: T0: inclusion. T1: T0 + 2 months. T2: end of treatment. OR: odds ratio. aOR: adjusted odds ratio. CI: confidence interval. WBC: white blood cells. C: model C statistic. AIC: Akaike Information Criterion. Slow culture conversion was defined as a persistently positive culture result at T1 followed by a culture conversion at T2. TB1, TB2 and HBHA IFN-γ levels were measured in IU/mL. For continuous independent variables, associations were calculated for each unit increase. 1: models were adjusted for age, sex, country of origin, drug resistance strain, body mass index at inclusion, and BCG vaccination rate.

Supplementary Table 8. Associations between time to culture conversion and IFN-γ response, adjusted for neutrophil and monocyte proportions at baseline.

Parameter	Timepoint	Multivariate analysis[1]			
		aOR (95% CI)	*p*	C	AIC
TB1 IFN-γ	*T0*	0.939 (0.642 - 1.34)	*0.73*	0.62	68.0
	T1	0.957 (0.636 - 1.32)	*0.80*	0.61	68.0
	T2	1.42 (1.027 - 2.08)	*0.054*	0.68	63.6
TB2 IFN-γ	*T0*	0.844 (0.563 - 1.206)	*0.36*	0.64	67.2
	T1	0.928 (0.64 - 1.247)	*0.64*	0.62	67.8
	T2	1.19 (0.927 - 1.57)	*0.16*	0.67	66.1
HBHA IFN-γ	*T0*	0.341 (0.006 - 1.185)	*0.45*	0.66	66.4
	T1	1.133 (0.779 - 1.661)	*0.49*	0.62	67.6
	T2	1.004 (0.723 - 1.39)	*0.98*	0.62	68.1
MIT IFN-γ	*T0*	0.62 (0.391 - 0.857)	*0.013*	0.74	58.7
	T1	0.711 (0.498 - 0.954)	*0.034*	0.70	62.8
	T2	0.799 (0.555 - 1.122)	*0.19*	0.63	66.3
Positive QFT-P IGRA	*T0*	0.045 (0.002 - 0.404)	*0.022*	0.75	59.5
	T1	0.279 (0.036 - 1.631)	*0.17*	0.66	66.1
	T2	2.69 (0.462 - 21.2)	*0.29*	0.66	66.9
Positive HBHA IGRA	*T0*	0.551 (0.057 - 4.366)	*0.57*	0.61	67.8
	T1	0.075 (0.003 - 0.689)	*0.045*	0.72	62.7
	T2	0.623 (0.098 - 4.45)	*0.62*	0.61	67.8
Lymphocyte % of WBC	*T0*	0.89 (0.482 - 1.685)	*0.71*	0.61	67.9
	T1	0.898 (0.788 - 0.988)	*0.055*	0.66	63.0
	T2	1.00 (0.915 - 1.09)	*0.98*	0.61	68.1
Body mass index	*T0*	0.912 (0.578 - 1.35)	*0.66*	0.64	66.1

Footnotes: T0: inclusion. T1: T0 + 2 months. T2: end of treatment. aOR: adjusted odds ratio. CI: confidence interval. WBC: white blood cells. C: model C statistic. AIC: Akaike Information Criterion. Slow culture conversion was defined as a persistently positive culture result at T1 followed by a culture conversion at T2. TB1, TB2 and HBHA IFN-γ levels were measured in IU/mL. 1: models were adjusted for age, sex, country of origin, drug resistance strain, body mass index at inclusion, BCG vaccination rate, and neutrophil and monocyte proportion at baseline.

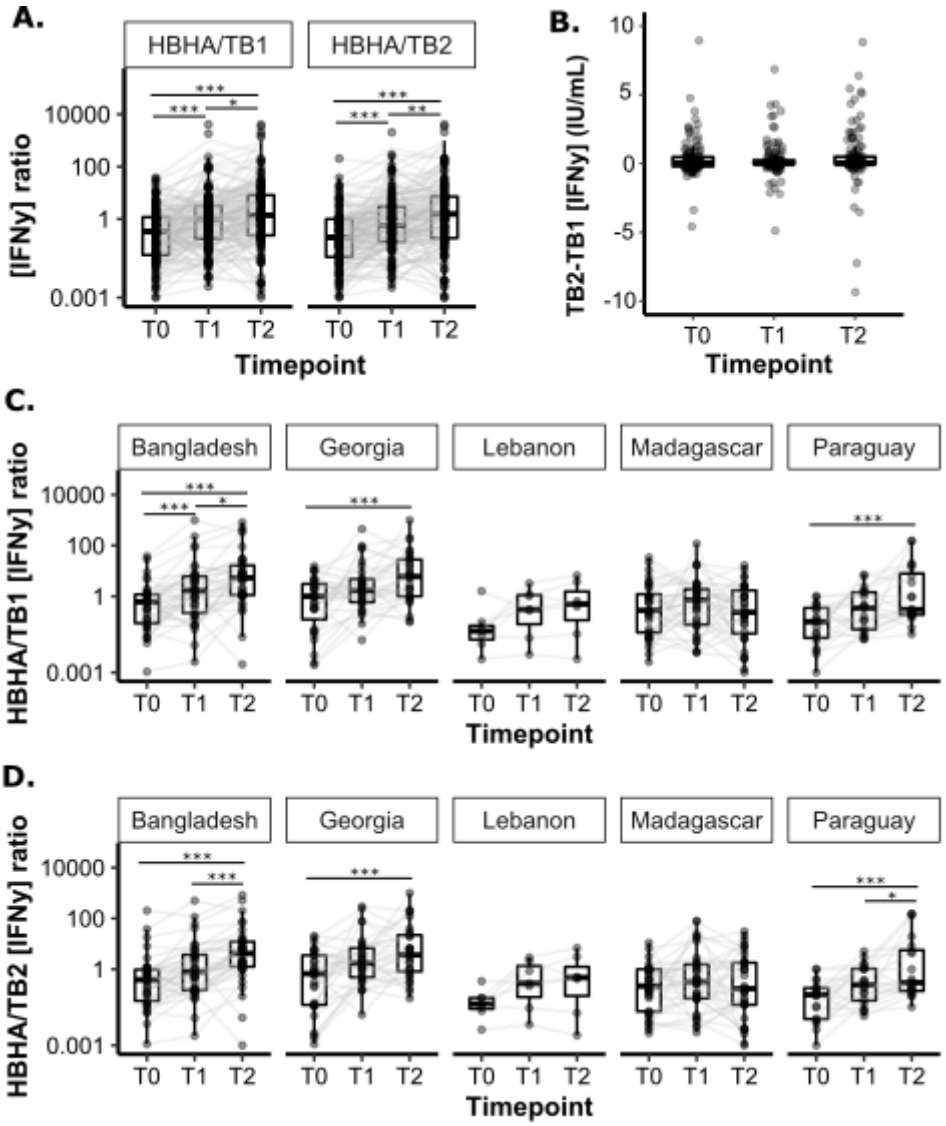

Supplementary Figure 1. Dynamics of plasmatic IFN-y response to QFT-P and HBHA stimulations over the course of TB therapy. Data are given as median + interquartile range. **A.** Evolution of the HBHA/TB1 and HBHA/TB2 IFN-y ratios throughout treatment. **B.** Evolution of the TB2-TB1 IFN-y response (QFT-P CD8+ T cell response) throughout treatment. Stratification per study site of the HBHA/TB1 (**C.**) and HBHA/TB2 (**D.**) ratios. Bangladesh (n = 38), Georgia (n = 31), Lebanon (n = 7), Madagascar (n = 36), Paraguay (n = 20). Each black dot represents one patient at one timepoint. Grey lines connect data points from a same patient. T0: baseline. T1: baseline + 2 months. T2: end of treatment. Data were compared using Friedman's Exact Test with the Wilcoxon-Nemenyi-McDonald-Thompson post-hoc, or the Mann-Whitney U test (panel B). *: p<0.05; **: p<0.01; ***: p<0.001.

1.3 Annex 3 – Supplementary data from publication 3

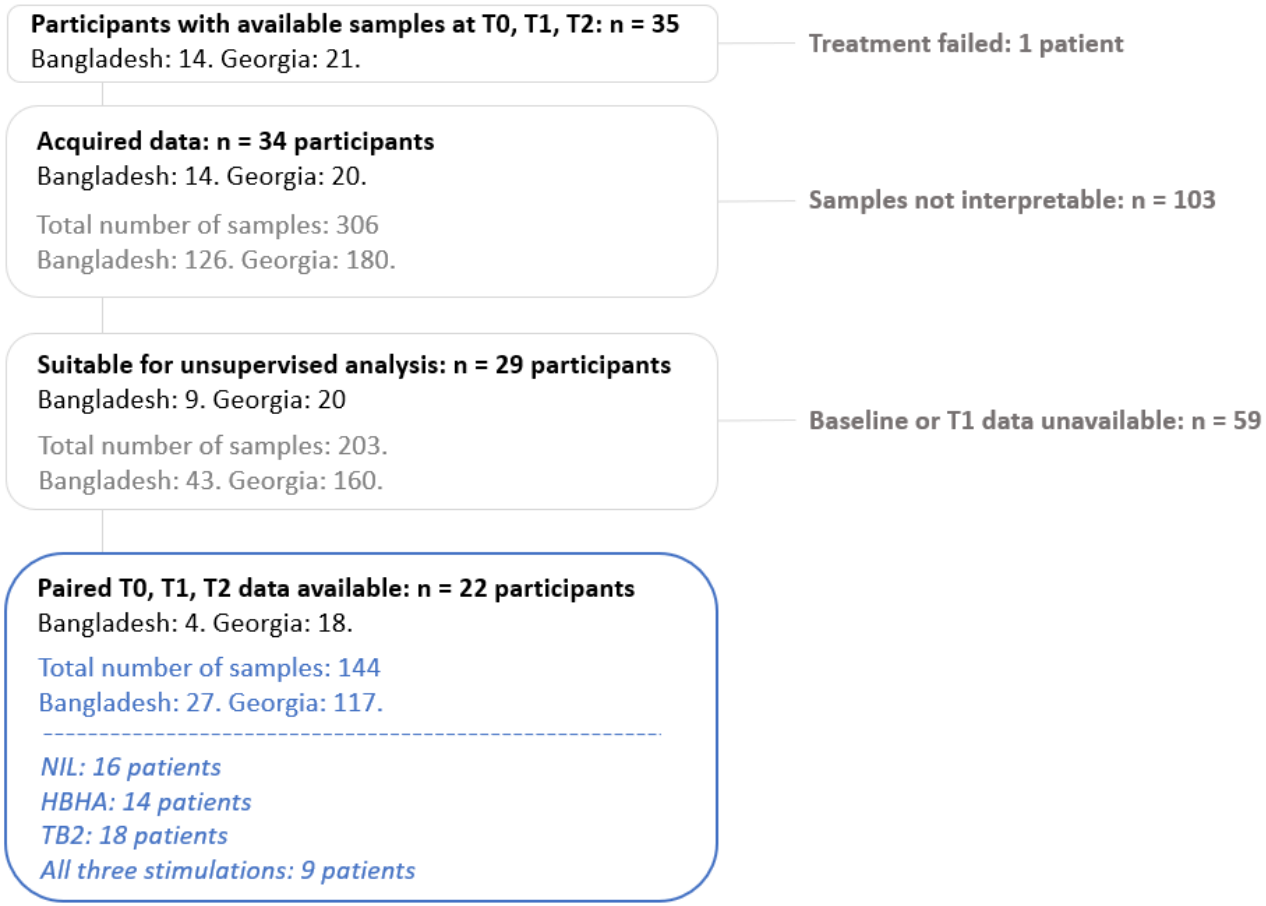

Supp. Figure 1. Flowchart of patient inclusions.

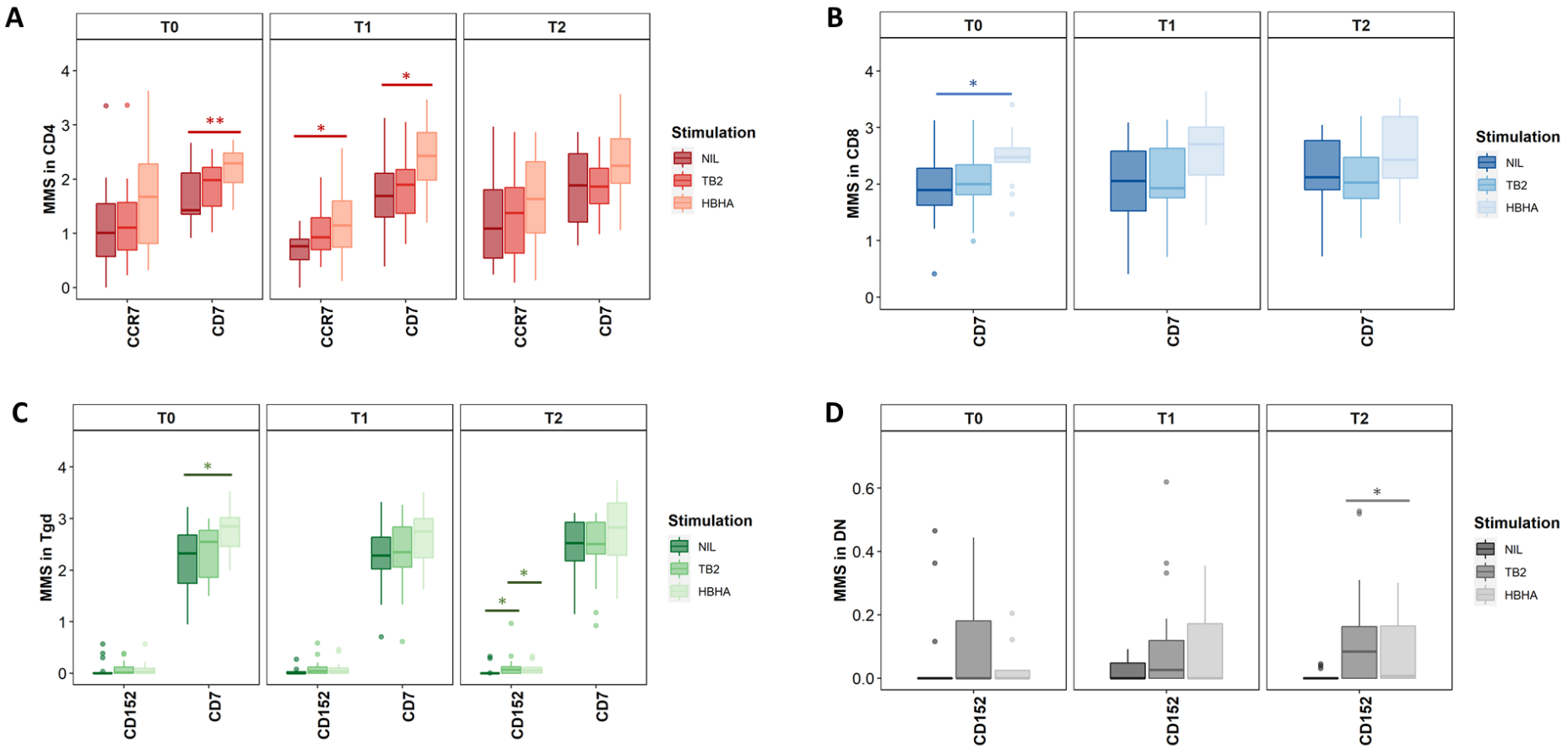

Supp. Figure. 2. Impact of *in vitro* whole blood stimulation with *Mtb* antigens on surface marker expression in the main T-cell subpopulations.

The surface expression of all panel markers was compared between the three stimulation conditions (unstimulated (NIL), TB2, and rmsHBHA) in $CD4^+$ (**A**), $CD8^+$ (**B**), gamma-delta (Tgd; **C**), or double negative (DN) T-cells (**D**). MMS: median mass signal. Only the markers for which a significant difference was observed were represented. Statistical analysis: two-sided Kruskal-Wallis test with Dunn's Kruskal–Wallis Multiple Comparisons post-hoc at T0, T1, and T2. *: p<0.05. **: p<0.01. Number of data points per timepoint for all panels: NIL: n = 16. TB2: n = 18. HBHA: n = 14. Exact p-values and test statistics are available in Supp. Table 2.

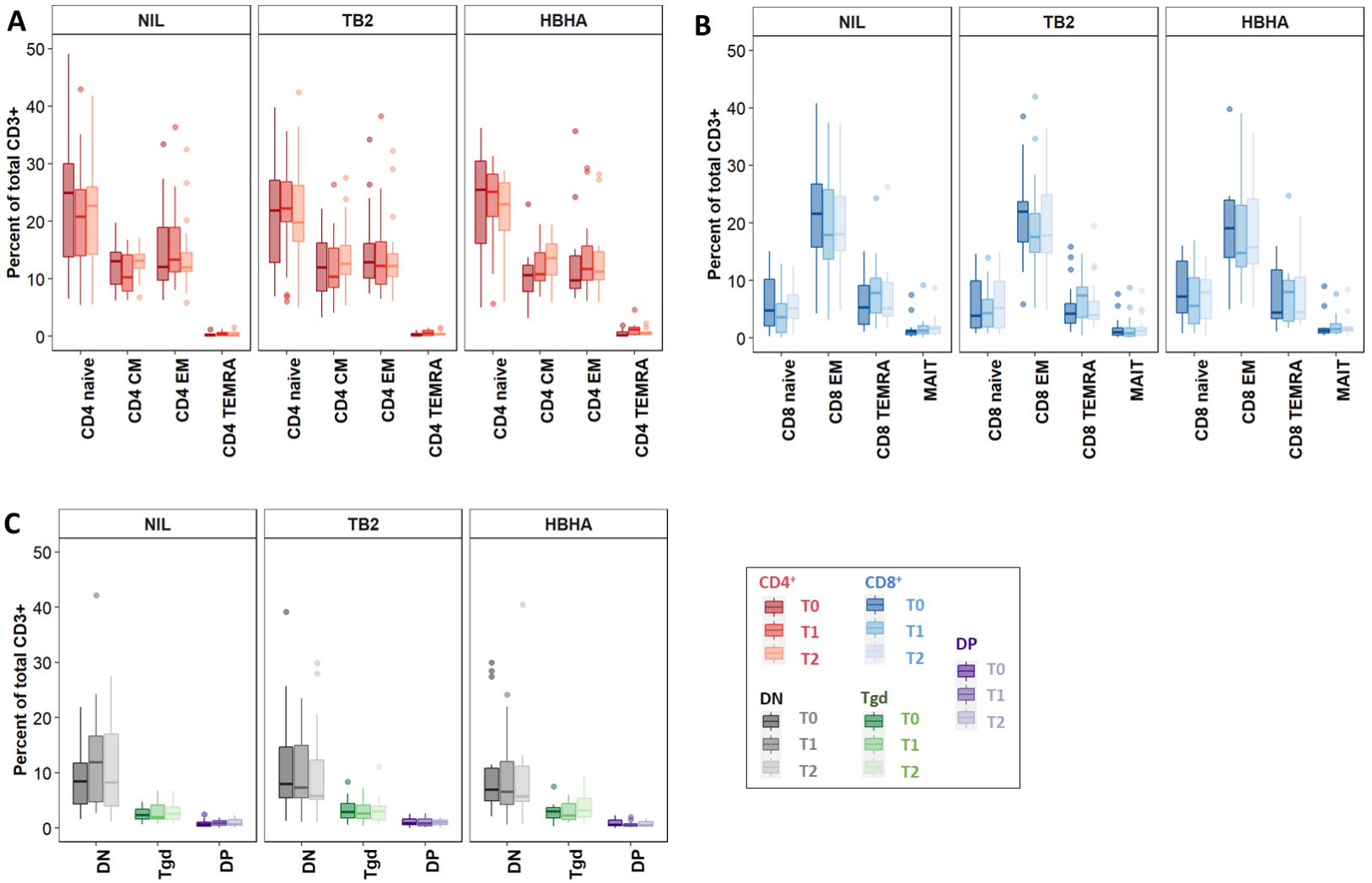

Supp. Figure. 3. Frequencies of the main peripheral T-cell subpopulations throughout anti-TB treatment.

Evolution of the frequency of canonical T-cell subsets identified through FlowSOM meta-clustering and corresponding respectively to $CD4^+$ phenotypes (**A**), $CD8^+$ phenotypes (**B**), or other cell subsets (**C**). Number of data points per timepoint for all panels: NIL: n = 16. TB2: n = 18. HBHA: n = 14. Data are given as median + interquartile range. Abbreviations: CM: central memory. DN: double-negative $CD4^-CD8^-$. DP: double-positive $CD4^+CD8^+$. EM: effector memory. HBHA: recombinant *M. tuberculosis* heparin-binding hemagglutinin. MAIT: mucosal associated invariant T-cells. NIL: unstained control. TB2: *M. tuberculosis* antigenic peptide pool. Tgd: gamma delta T-cells. Treg: T-regulators. TEMRA: terminally differentiated effectors re-expressing CD45RA. No statistically significant differences were detected (pairwise comparisons between non-sindependent observations at T0, T1, and T2: two-sided Friedman rank sum test and Wilcoxon-Nemenyi-Thompson post-hoc for pairwise comparisons between non-independent observations at T0, T1, and T2).

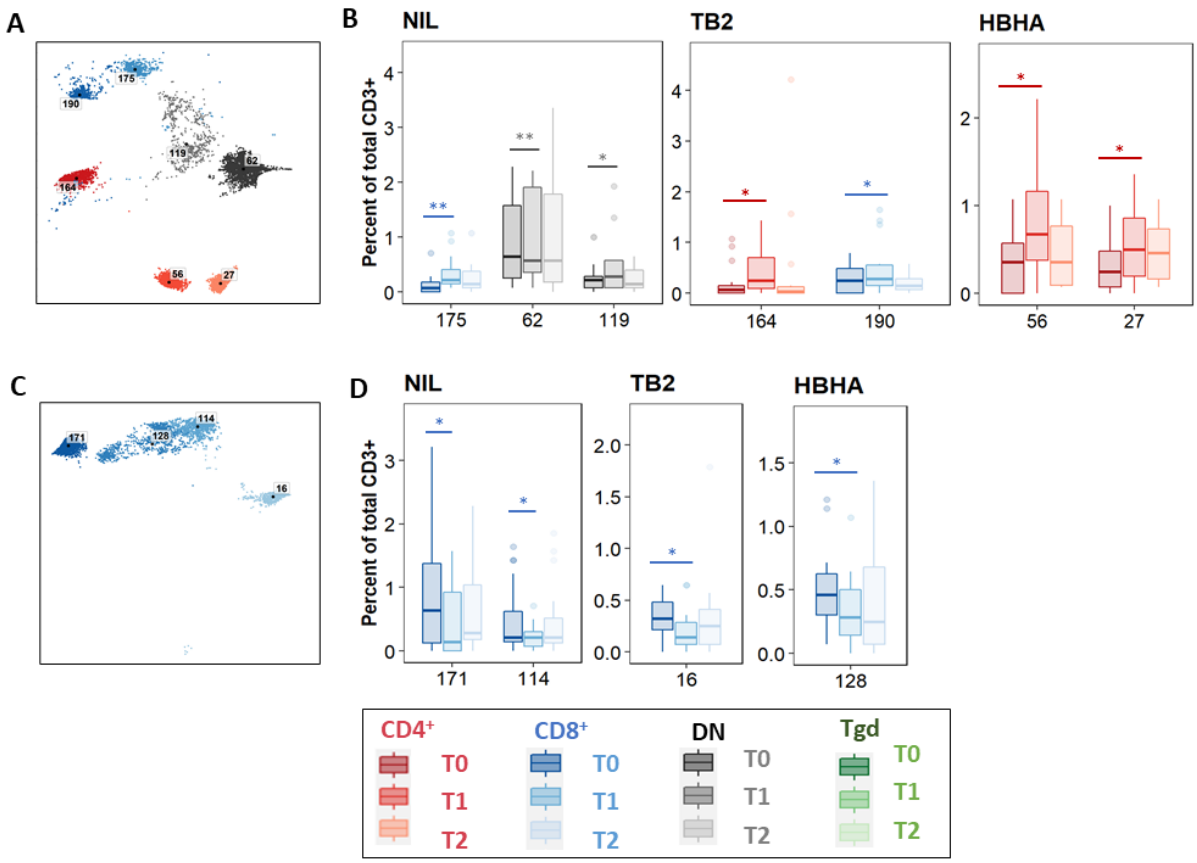

Supp Figure 4. Significant abundance changes in non-canonical T-cell subsets after the intensive phase of treatment. The evolution of FlowSOM cluster abundance was analyzed over time in unstimulated or *Mtb*-stimulated samples (TB2 or rmsHBHA), and only the clusters within which significant abundance changes were detected were displayed. $CD4^+$ clusters were represented in red, $CD8^+$ clusters in blue, γδ T-cell clusters in green, and $CD4^-$ $CD8^-$ clusters in grey. Number of matched data points per timepoint for all panels: NIL: n = 16. TB2: n = 18. rmsHBHA: n = 14. Data are given as median + interquartile range.

A and B. Significantly increased clusters at the end of the intensive phase of treatment (T1) compared to treatment initiation (T0). Clusters within which a significant increase was detected between T0 and T1 were first visualized on the reference UMAP (**A**). Cluster abundance quantification was then was performed in unstimulated, TB2-stimulated or rmsHBHA-stimulated samples (**B**).

C and D. Significantly decreased clusters at the end of the intensive phase of treatment (T1) compared to treatment initiation (T0). Mapping **(C)** and abundance quantification of clusters which decreased between T0 and T1 in unstimulated, TB2-stimulated, or rmsHBHA-stimulated samples (**D**).

Statistical analysis: two-sided Friedman rank sum test and Wilcoxon-Nemenyi-Thompson post-hoc for pairwise comparisons between non-independent observations at T0, T1, and T2. *: p<0.05. **: p<0.01. ***: p<0.001. Exact p-values and test statistics are available in Supp. Table 3 (associated Excel file).

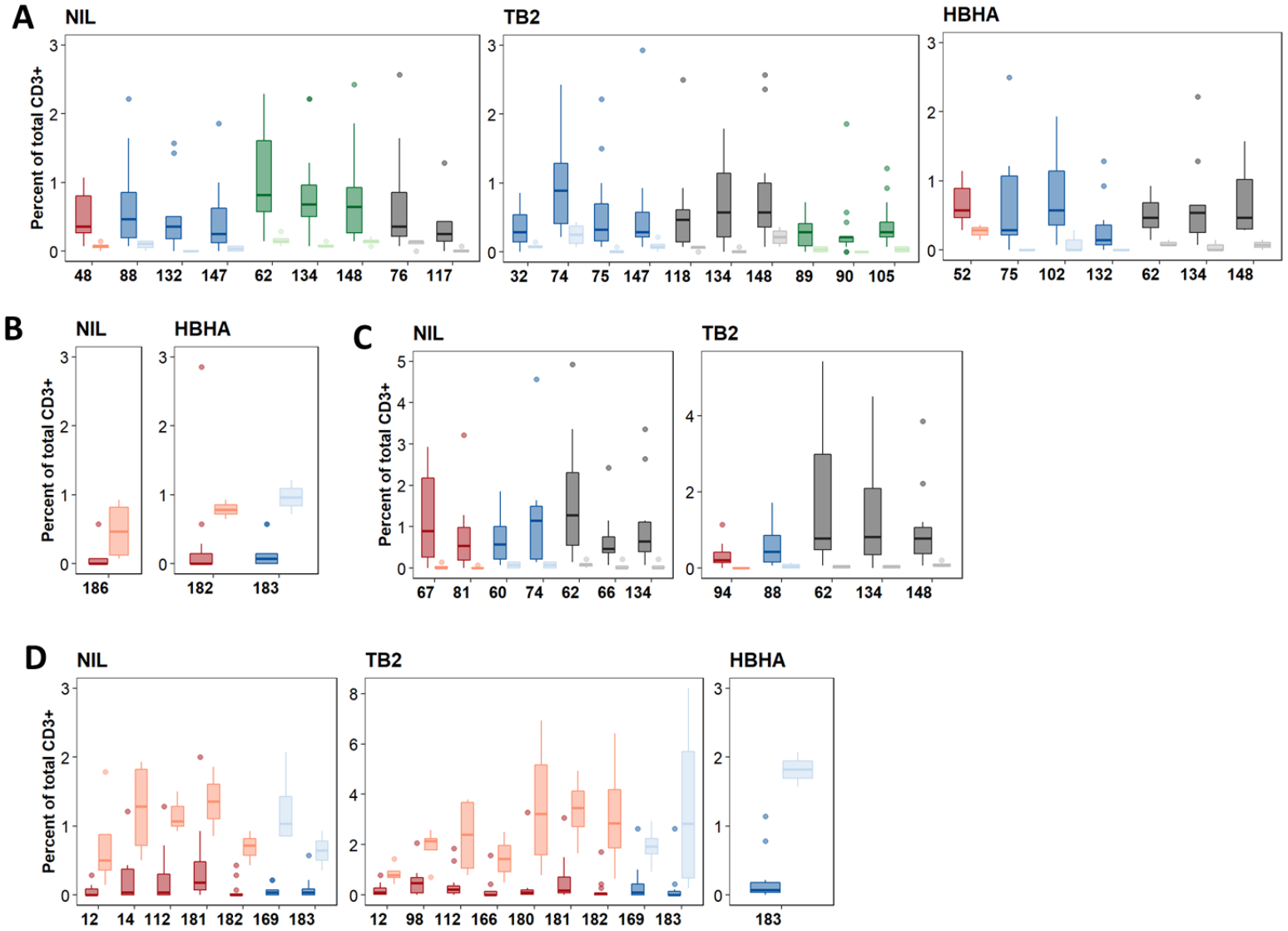
A
NIL
TB2
HBHA
Percent of total CD3+
48 88 132 147 62 134 148 76 117
32 74 75 147 118 134 148 89 90 105
52 75 102 132 62 134 148
B
NIL
HBHA
186
182 183
C
NIL
TB2
67 81 60 74 62 66 134
94 88 62 134 148
D
NIL
TB2
HBHA
12 14 112 181 182 169 183
12 98 112 166 180 181 182 169 183
183

Supp. Figure. 5. Patients with slow microbiological culture conversion show decreased CD8$^+$ and γδ and enriched CD4$^+$ naïve peripheral T-cell subsets during treatment. Clusters with differential abundance between patients with positive mycobacterial cultures at T1 (slow converters, n = 4) or with negative cultures at T1 (fast converters, n = 18). Data are shown as median + interquartile range.

A and B. At treatment initiation (T0). Clusters significantly decreased (**A**) and increased (**B**) in slow converters compared to fast converters.

C and D. At treatment completion (T2). Clusters significantly decreased (**C**) and increased (**D**) in slow converters compared to fast converters.

CD4$^+$ clusters are represented in red, CD8$^+$ clusters in blue, Tgd clusters in green, and DN clusters in grey. The lighter shade of each color code corresponds to data from the slow converters. Statistical analysis: two-sided Mann-Whitney U-test. For all represented clusters: $P<0.025$ at T0; $P<0.013$ at T2. Significance stars were not displayed for readability. Exact p-values and test statistics are available in Supp. Table 6 (associated Excel file).

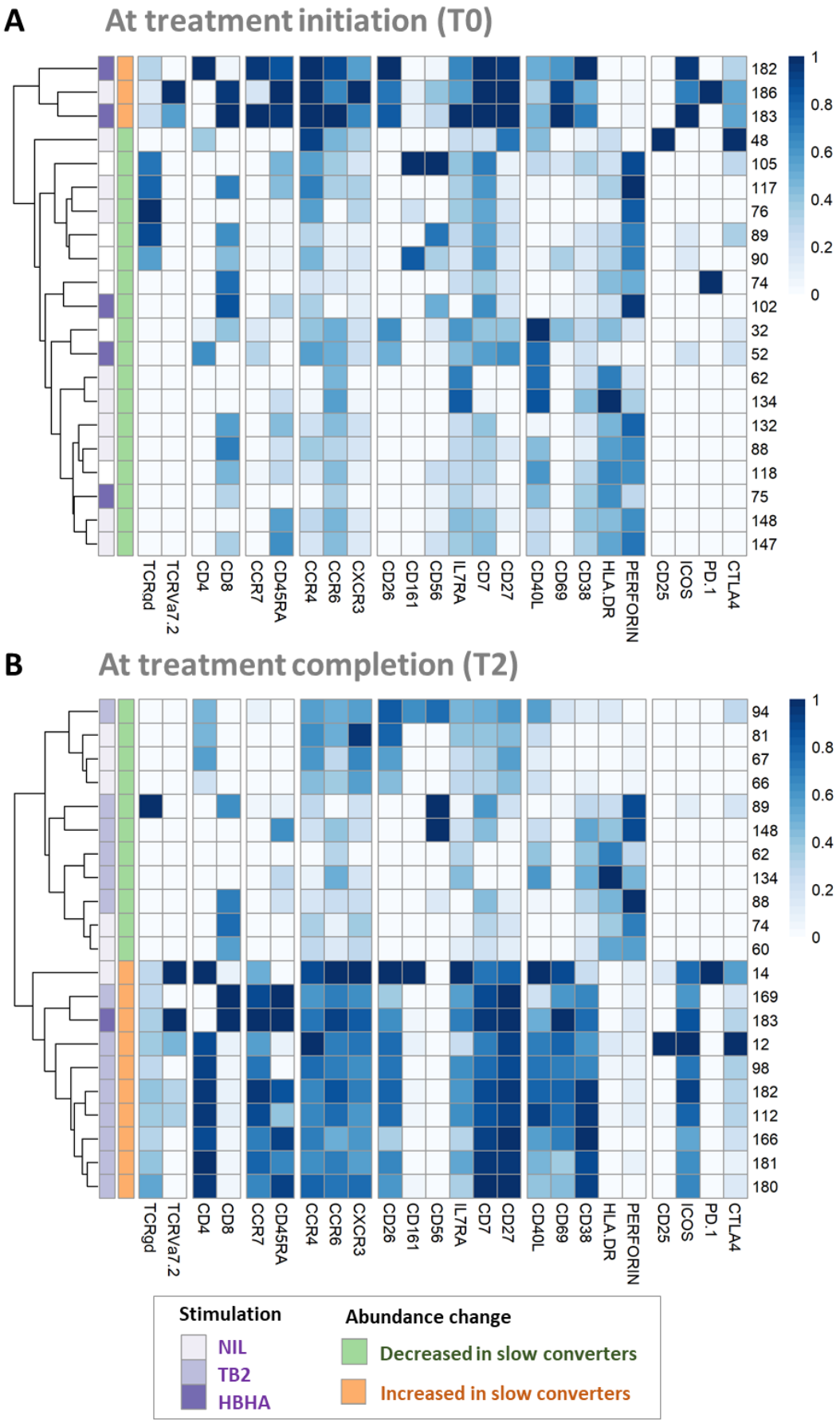
A
At treatment initiation (T0)
182
186
183
48
105
117
76
89
90
74
102
32
52
62
134
132
88
118
75
148
147
1
0.8
0.6
0.4
0.2
0
TCRgd
TCRVa7.2
CD4
CD8
CCR7
CD45RA
CCR4
CCR6
CXCR3
CD26
CD161
CD56
IL7RA
CD7
CD27
CD40L
CD69
CD38
HLA.DR
PERFORIN
CD25
ICOS
PD.1
CTLA4
B
At treatment completion (T2)
94
81
67
66
89
148
62
134
88
74
60
14
169
183
12
98
182
112
166
181
180
1
0.8
0.6
0.4
0.2
0
TCRgd
TCRVa7.2
CD4
CD8
CCR7
CD45RA
CCR4
CCR6
CXCR3
CD26
CD161
CD56
IL7RA
CD7
CD27
CD40L
CD69
CD38
HLA.DR
PERFORIN
CD25
ICOS
PD.1
CTLA4
Stimulation
NIL
TB2
HBHA
Abundance change
Decreased in slow converters
Increased in slow converters

Supp. Figure 6. Patients with slow microbiological culture conversion show decreased cytotoxic $CD8^+$ and γδ and enriched $CD4^+$ naïve T-cell subsets before treatment initiation and after treatment completion compared to fast converters. Fast converters (n = 18) were defined as patients with permanently negative *M. tuberculosis* culture after the intensive phase of treatment (T1), whereas slow converters (n = 4) were defined as patients with persistently positive cultures at T1. The abundance of all FlowSOM clusters at baseline was compared between fast and slow converters. Only clusters within which significant differences were detected were represented (T0: $p<0.026$. T2: $p<0.013$; two-sided Mann-Whitney U test; see Supp. Figure 5).

A. Before treatment initiation (T0). Clusters which were significantly decreased (green) or increased (orange) at T0 in slow converters compared to fast converters were represented. Normalized, arcsinh-transformed mean marker expression levels were visualized). Each line represents one cluster. Scales indicate normalized mass signal intensity.

B. After treatment completion (T2). Clusters which were significantly increased or decreased at T2 in slow converters compared to fast converters were represented and marker expression levels were visualized. All patients achieved microbiological cure at T2.

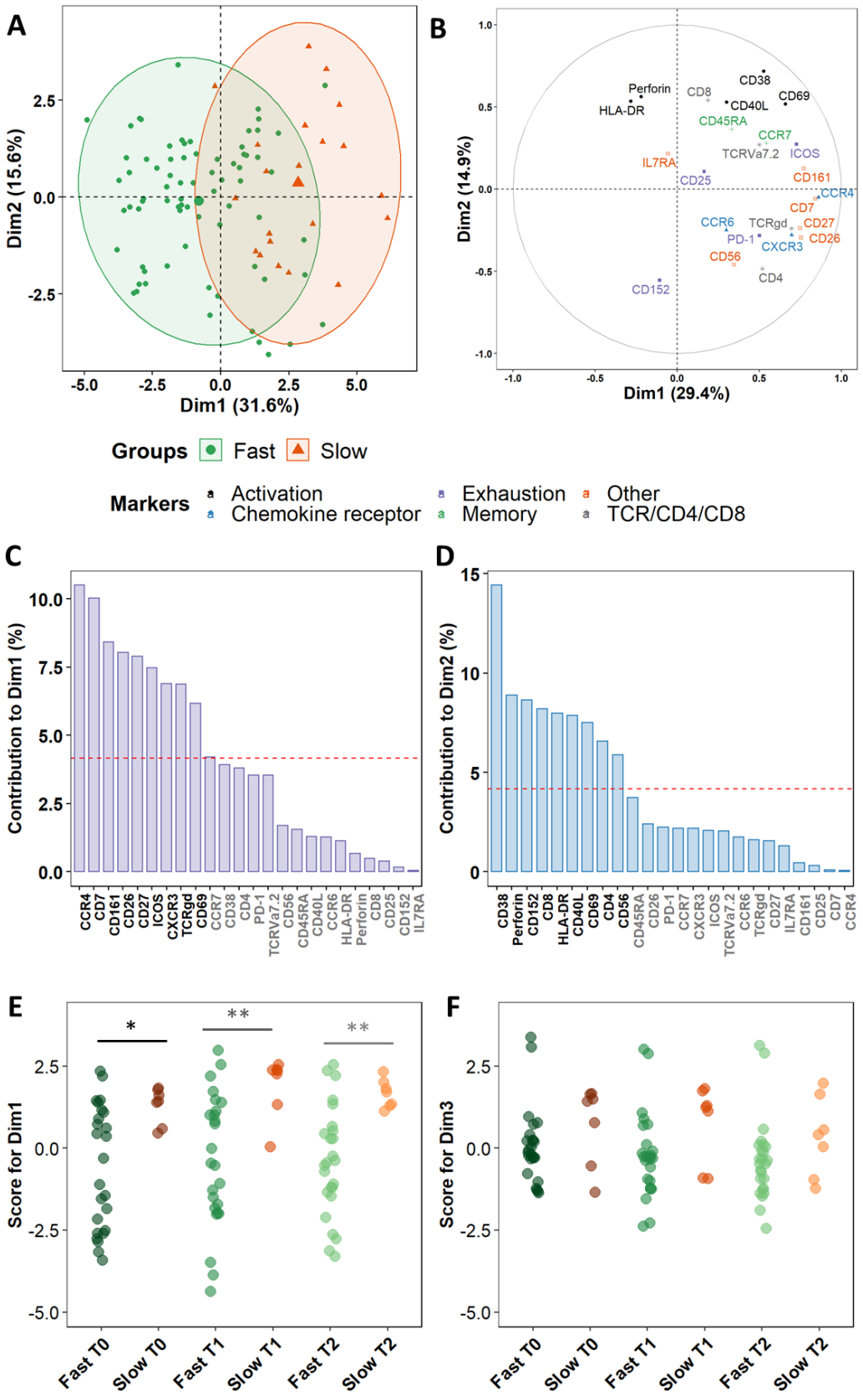
A
Dim2 (15.6%)
Dim1 (31.6%)
B
Dim2 (14.9%)
Dim1 (29.4%)
Perforin
CD8
CD38
CD69
HLA-DR
CD40L
CD45RA
CCR7
TCRVa7.2
ICOS
IL7RA
CD25
CD161
CCR4
CD7
CCR6
TCRgd
CD27
PD-1
CD26
CXCR3
CD56
CD4
CD152
Groups Fast Slow
Markers Activation Chemokine receptor Exhaustion Memory Other TCR/CD4/CD8
C
Contribution to Dim1 (%)
CCR4 CD7 CD161 CD26 CD27 ICOS CXCR3 TCRgd CD69 CCR7 CD38 CD4 PD-1 TCRVa7.2 CD56 CD45RA CD40L CCR6 HLA-DR Perforin CD8 CD25 CD152 IL7RA
D
Contribution to Dim2 (%)
CD38 Perforin CD152 CD8 HLA-DR CD40L CD69 CD4 CD56 CD45RA CD26 PD-1 CCR7 CXCR3 ICOS TCRVa7.2 CCR6 TCRgd CD27 IL7RA CD161 CD25 CD7 CCR4
E
Score for Dim1
*
**
**
Fast T0 Slow T0 Fast T1 Slow T1 Fast T2 Slow T2
F
Score for Dim3
Fast T0 Slow T0 Fast T1 Slow T1 Fast T2 Slow T2

Supp. Figure 7. Variance between fast and slow responders within all *Mtb*-stimulated CD3$^+$ T-cells. Principal Component Analysis (PCA) was performed on marker expression data within all CD3$^+$ T-cells from 96 *Mtb*-stimulated samples matched at T0, T1, and T2 (TB2: 54 samples; rmsHBHA: 42 samples).

A. Explanation of the variance between fast converters (25 samples at each timepoint) and slow converters (7 samples at each timepoint). Each dot represents one patient. The color code represents the culture conversion group. Axes represent the principal components 1 (Dimension 1, Dim1) and 2 (Dim2) and percentages indicate their contribution to the total observed variance. Axis values represent individual PCA scores. Concentration ellipses correspond to 90% data coverage.

B. Contribution of cellular markers to the variance described by Dim1 and Dim2. Axis values represent marker PCA scores. The color code represents broad marker functions.

C and D. Quantification of panel B. for Dim1 (**C**) and Dim2 (**D**). Contributions of each marker are expressed as a percentage of the dimensions. The red dashed line corresponds to the expected reference value if each marker contributed uniformly to the variance. Markers indicated in gray are below this reference value.

E and F. Distribution of individual PCA score values according to the culture conversion group and to the timepoint, for Dim1 (**E**) and Dim2 (**F**). Data were compared with the two-sided Wilcoxon Rank Sum Test. *: $p<0.05$; **: $p<0.01$. Exact p-values and test statistics are available in Supp. Table 7.

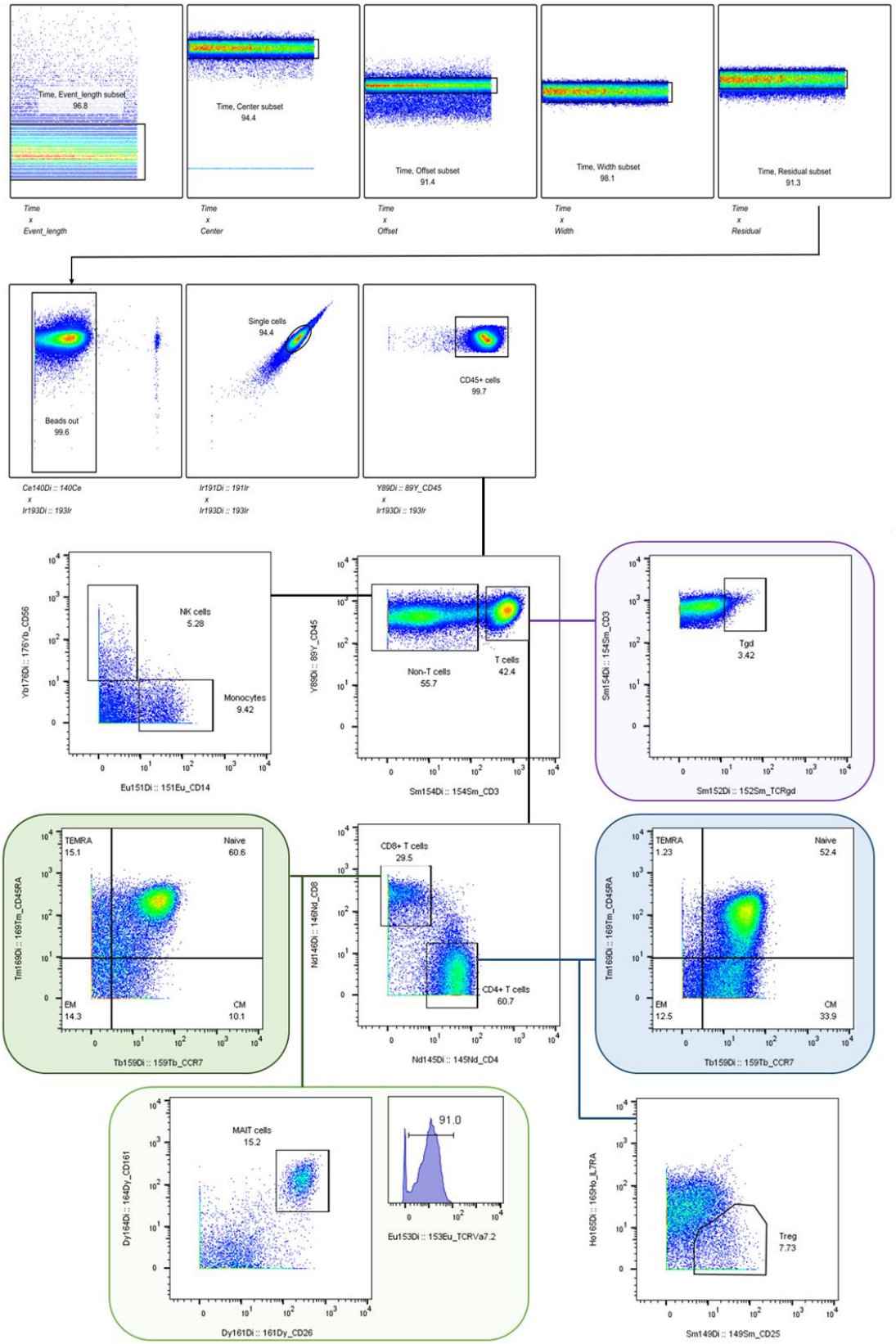

Supp. Figure 8. Main CD45^{+} non-granulocyte whole blood subpopulations and T-cell oriented gating strategy.

CM: central memory. EM: effector memory MAIT: mucosal-associated invariant T-cells. NK: natural killers. TEMRA: terminally differentiated effectors re-expressing CD45RA. Tgd: gamma delta T-cells. Treg: T regulators.

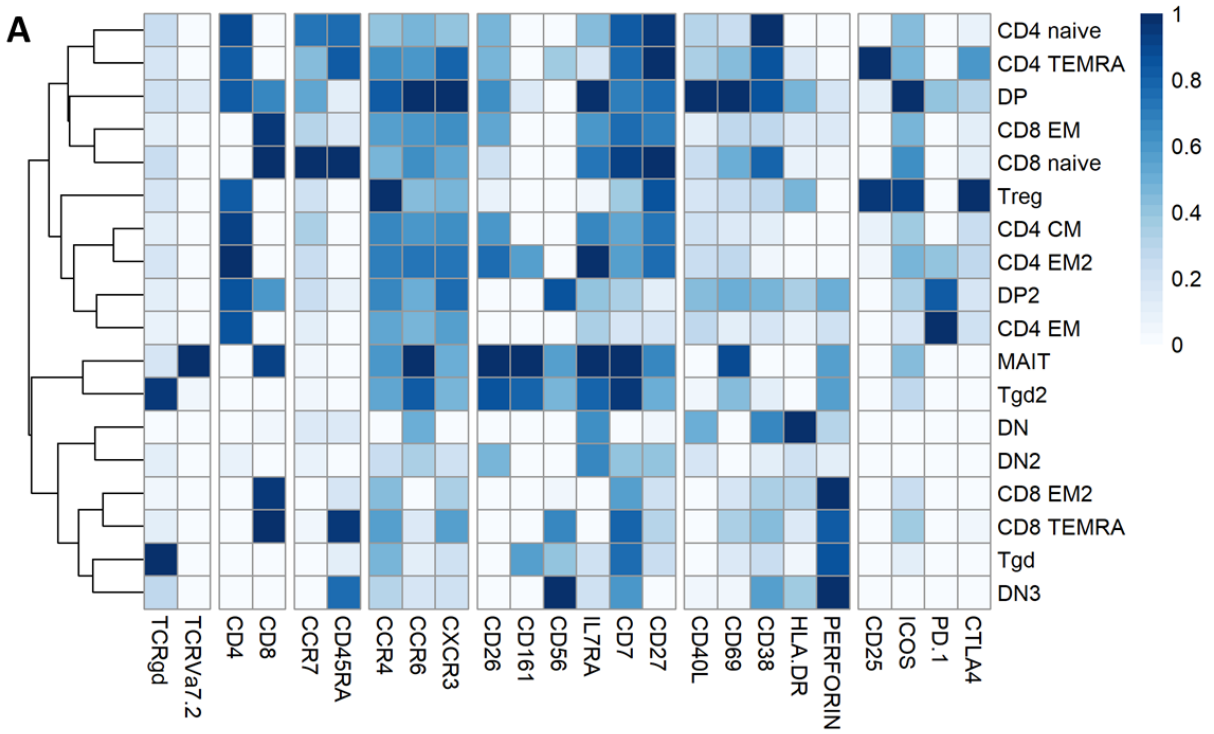

B.

Initial metacluster	Merged with
CD4 EM2	CD4 EM
Tgd2	Tgd
CD8 EM2	CD8 EM
DN2	DN
DN3	
DP2	DP
DN	CD8 EM

Supp. Figure 9. Control of automated FlowSOM metaclustering.

A. Expression of selected lineage markers in 18 automatically detected FlowSOM meta-clusters within total $CD3^+$ events. A higher number of meta-clusters than expected was chosen in order to detect all expected cell subpopulations (see Supp.Table 9). **B.** List of meta-clusters which were reassigned to other phenotypically similar meta-clusters. Abbreviations: CM: central memory. DN: double-negative $CD4^-CD8^-$. DN: double-positive $CD4^+$ $CD8^+$. EM: effector memory. HBHA: recombinant *M. tuberculosis* heparin-binding hemagglutinin. MAIT: mucosal associated invariant T-cells. NIL: unstained control. TB2: *M. tuberculosis* antigenic peptide pool. Tgd: gamma delta T-cells. Treg: T-regulators. TEMRA: terminally differentiated effectors re-expressing CD45RA.

Supplementary Table 1. Sociodemographic and clinical characteristics of the cohort.

	Nb of cell samples			Drug susceptibility		
ID	**NIL**	**TB2**	**HBHA**	**Phenotypic drug susceptibility**	**Treatment regimen**	**Country**
01DSGE	3	3	3	DS	2HRZE/4HRE	GEO
02DSGE	3	0	3	DS	2HRZE/4HRE	GEO
03DSGE	3	3	3	DS	2HRZE/4HR	GEO
04DSGE	3	0	0	DS	2HRZE/4HR	GEO
05DSGE	3	3	3	DS	2HRZE/4HR	GEO
06DSB	3	3	0	DS	2HRZE/4HR	BD
06DSGE	3	3	0	DS	2HRZE/4HRE	GEO
07DSGE	3	3	3	DS	2HRZE/4HRE	GEO
08DSB	3	3	0	DS	2HRZE/4HR	BD
08DSGE	3	3	3	DS	2HRZE/4HRE	GEO
21DSB	0	3	3	DS	2HRZE/4HR	BD
01DRGE	0	3	0	MDR	H+Z+Km+Lfx+cfz+Bdq / Z+Lfx+cfz+Bdq	GEO
02DRGE	3	3	3	MDR	Cm+Lfx+Pto+Cs+Cfz+H / Cm+Lfx+Cs+Bdq+Lzd / Lfx+Cs+Bdq+Lzd	GEO
03DRGE	3	0	3	Pre-XDR	(Z)+Lfx+Pto+Cfz+Bdq+Lzd / Cs+Cfz+Bdq+Lzd	GEO
04DRGE	0	3	0	Pre-XDR	Bdq+Cfz+Lfx+H+Pto+E+Z / Bdq+cfz+Lzd+H+E / Bdq+Cfz+Lfx+H+Z / Bdq+Cfz+Lfx+E+Z	GEO
05DRGE	3	3	0	Pre-XDR	H+Z+Km+Lfx+Cfz+Bdq / Z+Lfx+Cfz+Bdq	GEO
06DRGE	0	3	3	RR	H+E+Z+Km+Mfx+Pto+Cfz / Mfx+E+Z+cfz	GEO
07DRGE	3	3	3	XDR	Bdq+Lzd+cfz+Cs	GEO
09DRB	3	3	3	MDR	4-6 Km-Mfx-Pto-Cfz-Z-HHigh dose-E/5-6 Mfx-Cfz-Z-E3	BD
09DRGE	0	0	3	MDR	H+Z+Km+Lfx+Cfz+Bdq / Z+Lfx+Cfz+Bdq	GEO
10DRGE	0	3	0	MDR	H+Z+Km+Lfx+Cfz+Bdq / Z+Lfx+Cfz+Bdq	GEO
14DRGE	3	3	3	Pre-XDR	H+Z+Km+Lfx+Cfz+Bdq / Z+Lfx+Cfz+Bdq	GEO
Nb of patients:	*16*	*18*	*14*			
Number of samples:	48	54	42			
Total number of samples:	**144**					

Footnotes: Three samples per patient were collected in each stimulation condition, corresponding to each timepoint: T0: baseline. T1: T0 + 2 months. T2: end of treatment.Samples with < 1,000 $CD3^+$ events, and batches with missing samples from a given timepoint were removed from the analysis. Abbreviations: BD: Bangladesh. GEO: Georgia. DS: drug susceptible. MDR: multi-drug resistant. RR: rifampicin resistant. XDR: extensively drug resistant. Abbreviations for anti-TB drugs: E: Ethambutol. H: Isoniazid. R: Rifampicin. S: Streptomycin. Z: Pyrazinamide. Bdq: Bedaquiline. Cfz: Clofazimine. Cs: Cycloserine. Km: Kanamycin. Lfx: Levofloxacin. Lzd: Linezolid. Mfx: Moxifloxacin. Pto: Prothionamide. Numbers indicate months of treatment when the information was available

Supplementary Table 1 - continued

Baseline identification										Microbiological evolution						
ID	Gender	Age	Occupation	HIV	Diabetes	BCG	QFT-P	GeneXpert	GeneXpert RIFR	*Mtb* culture			AFB			Treatment response group
										T0	T1	T2	T0	T1	T2	
01DSGE	M	28	Small business	n	n		+	+	-	+	-	-	scanty	scanty	-	Fast
02DSGE	M	26	Student	n	n	y	+	+	-	+	-	-	-	-	-	Fast
03DSGE	M	37	Small business	n	n	y	+	+	-	+	-	-	-	-	-	Fast
04DSGE	M	24	Day Laborer	n	n	y	+	+	-	+	-	-	-	-	-	Fast
05DSGE	M	63	Unemployed / Retired	n	n		+	+	-	+	-	-	2+	2+	-	Fast
06DSB	M	16	Day Labour	n	n	y	+	+	-	+	-	-	2+	scanty	-	Fast
06DSGE	M	58	Unemployed / Retired	n	n		-	+	-	+	+	-	1+	1+	scanty	Slow
07DSGE	M	50	Unemployed / Retired	n	n		+	+	-	+	+	-	scanty	scanty	-	Slow
08DSB	M	60	Small business	n	n	y	-	+	-	+	-	-	1+	-	-	Fast
08DSGE	F	29	Small business	n	n	y	+	+	-	+	+	-	scanty	scanty	-	Slow
21DSB	F	20	Student	n	n	y	+	+	-	+	-	-	2+	-	-	Fast
01DRGE	M	42	Farmer	n	n		-	+	-	+	-	-	1+	-	-	Fast
02DRGE	F	34	Housewife	n	n	y	-	+	+	+	+	-	-	-	-	Slow
03DRGE	M	26	Business	n	n	y	+	+	-	+	-	-	2+	-	-	Fast
04DRGE	M	37	Private Service	n	n		+	+	-	+	-	-	-	1+	-	Fast
05DRGE	M	42	Unemployed	n	n		+	+	-	+	-	-	3+	scanty	-	Fast
06DRGE	F	33	Unemployed	n	n		+	+	+	+	-	-	2+	-	-	Fast
07DRGE	F	20		n	n	y	-	+	+	+	-	-	2+	-	-	Fast
09DRB	F	15	Garments worker	n	n	y	-	+	+	+	-	-	3+	-	-	Fast
09DRGE	F	28		n	n		+	+	-	+	-	-	2+	-	-	Fast
10DRGE	F	25		n	n		-	+	+	+	-	-	-	-	-	Fast
14DRGE	M	31		n	n		+	+	+	+	-	-	scanty	scanty	scanty	Fast

Footnotes: BCG: Bacille Calmette-Guérin vaccination. QFT-P: QuantiFERON-TB Gold Plus. AFB: Acid Fast Bacilli detection (sputum smear microscopy). BMI: body mass index. *Mtb: Mycobacterium tuberculosis*. Throughout the table, "+" and "-" indicate positive or negative results to the indicated test. For AFB results, 1+, 2+, or 3+ quantify the amount of bacilli observed.

Supplementary Table 1 - continued

Weight evolution							TB risk factors					
ID	Weight (kg)			BMI			Smoking	Alcohol	Intraveinous drug use	Prison	TB contact	Previous TB
	T0	T1	T2	T0	T1	T2						
01DSGE	72	72	73	20.8	20.8	21.1	n	n	n	n	n	n
02DSGE	59	61	64	20.1	20.8	21.8	n	n	n	n	n	n
03DSGE	65	66	71	24.1	24.5	26.3	y	n	n	n	n	n
04DSGE	59	60	64	19.9	20.2	21.6	y	n	n	n	n	n
05DSGE	66.7	67	68	24.2	24.3	24.6	n	n	n	n	n	n
06DSB	42.2	43.3	48.1	16.4	16.9	18.7	n	n	y	n	n	n
06DSGE	64.2			18.3			y		n	n	n	n
07DSGE	64	64	67	19.7	19.7	20.6	y	n	n	n	n	n
08DSB	52.5	57.5	59	18.1	19.8	20.4	y	n	n	n	n	n
08DSGE	60	61	67	24.3	24.7	27.1	n	n	n	n	n	y
21DSB	36.7	37	44.5	13.3	13.4	16.1	n	n	n	n	n	n
01DRGE	66	66	69	23.9	23.9	25.0	y	y	n	n	n	n
02DRGE	48	52	54	18.7	20.3	21.0	n	n	n	n	n	n
03DRGE	54	58	71	17.2	18.5	22.6	y	n	n	n	n	
04DRGE	71	72	73	20.5	20.8	21.1	y	n		n	n	n
05DRGE	60	62	65	19.8	20.4	21.4	y	n	n	n	n	y
06DRGE	48	52	56	18.7	20.3	21.8	n	n	n	n	n	n
07DRGE	54	57	61	19.5	20.6	22.1	n	n	n	n	n	n
09DRB	43.2	45.5	44.9	17.9	18.9	18.6	n	n	n	n	y	y
09DRGE		60	60				n	n	n	n	n	n
10DRGE	59	59	63	19.9	19.9	21.2	n	n	n	n		n
14DRGE	60	62	66	20.7	21.4	22.8	y	n	n	n	y	n

Footnotes: BMI: body mass index.

Supplementary Table 2. Exact p-values and test statistics for marker expression comparisons between stimulation conditions, presented in Supplementary Figure 2.

Population	Marker	Timepoint	Stimulation comparison	Kruskal p-value	Kruskal-Wallis Chi-Square	Degrees of freedom	Dunn's p-value	Dunn's statistic
$CD4^+$	CD7	T0	NIL-HBHA	0.012	8.75	2	0.0095	-2.95
$CD4^+$	CD7	T1	NIL-HBHA	0.029	7.03	2	0.031	-2.56
$CD4^+$	CCR7	T1	NIL-HBHA	0.036	6.62	2	0.035	-2.51
$CD8^+$	CD7	T0	NIL-HBHA	0.031	6.93	2	0.038	-2.49
Tgd	CD7	T0	NIL-HBHA	0.036	6.62	2	0.042	-2.45
Tgd	CD152	T2	NIL-TB2	0.016	8.26	2	0.045	-2.43
Tgd	CD152	T2	TB2-HBHA				0.033	2.54
DN	CD152	T2	TB2-HBHA	0.030	6.95	2	0.030	2.57

Footnotes: here, independent, non-normal continuous variables were analyzed with the two-sided Kruskal–Wallis test with Dunn's Kruskal–Wallis Multiple Comparisons post-hoc.

Supplementary Table 3. Exact p-values and test statistics for cluster abundance comparisons during treatment, presented in Figure 3 and Supplementary Figure 4.

Cluster	Timepoints	Friedman p-value	Friedman Chi-Square	Degrees of freedom	Post-hoc p-value	Post-hoc statistic
NIL (n = 16 at each timepoint)						
175	T0-T1	0.012	8.78	2	0.008	16
62	T0-T1	0.014	8.49	2	0.008	16
119	T0-T1	0.025	7.35	2	0.045	13
171	T0-T1	0.044	6.26	2	0.038	12.5
114	T0-T1	0.015	8.4	2	0.019	15
98	T0-T2	0.006	10.0	2	0.049	12
38	T0-T2	0.004	11.2	2	0.021	14.5
176	T0-T2	0.028	7.12	2	0.023	14
82	T0-T2	0.033	6.82	2	0.031	14
48	T0-T2	0.015	8.37	2	0.032	13.5
102	T0-T2	0.003	11.6	2	0.019	14.5
TB2 (n = 18 at each timepoint)						
164	T0-T1	0.015	8.41	2	0.024	14
190	T0-T1	0.002	12.5	2	0.013	16
16	T0-T1	0.055	5.81	2	0.046	13.5
38	T0-T2	0.007	9.94	2	0.025	15
70	T0-T2	0.001	13.7	2	0.016	14.5
28	T0-T2	0.013	8.68	2	0.012	16.5
37	T0-T2	0.007	9.81	2	0.009	16.5
137	T0-T2	0.001	14.9	2	0.005	18
74	T0-T2	0.012	8.82	2	0.015	16.5
102	T0-T2	0.022	7.61	2	0.024	15.5
77	T0-T2	0.014	8.57	2	0.015	16
HBHA (n = 14 at each timepoint)						
56	T0-T1	0.023	7.53	2	0.016	14
27	T0-T1	0.046	6.15	2	0.04	12.5
128	T0-T1	0.013	8.74	2	0.014	14
69	T0-T2	0.041	6.37	2	0.03	13
26	T0-T2	0.02	7.84	2	0.018	14
38	T0-T2	0.026	7.28	2	0.045	12.5
54	T0-T2	0.03	7.03	2	0.019	13.5
172	T0-T2	0.044	6.26	2	0.038	12.5
91	T0-T2	0.018	8.04	2	0.027	12.5
154	T0-T2	0.006	10.1	2	0.002	16.5
50	T0-T2	0.039	6.49	2	0.032	13
94	T0-T2	0.001	14.3	2	0,00	19
49	T0-T2	0.008	9.69	2	0.008	15
160	T0-T2	0.041	6.37	2	0.034	13
65	T0-T2	0.039	6.50	2	0.04	12

Footnotes**:** For pairwise comparisons between non-independent observations at T0, T1, and T2: the two-sided Friedman rank sum test was performed followed by the Wilcoxon-Nemenyi-Thompson post-hoc.Only clusters within which significant differences were detected were represented.

Supplementary Table 4. Pearson's correlation effect sizes (*r*) presented in Figure 5 for increased clusters.

	Clus 98	Clus 38	Clus 176	Clus 37	Clus 28	Clus 70	Clus 69	Clus 26	Clus 172	Clus 91	Clus 54
Clus 98	1	0.228	-0.203	0.643	0.045	0.803	0.353	-0.102	-0.239	-0.132	0.032
Clus 38	0.228	1	0.042	0.364	0.282	0.263	0.356	-0.043	-0.152	0.224	0.572
Clus 176	-0.203	0.042	1	-0.042	-0.049	-0.128	-0.131	-0.065	-0.116	0.018	-0.215
Clus 37	0.643	0.364	-0.042	1	0.261	0.444	0.114	-0.245	-0.183	0.135	-0.056
Clus 28	0.045	0.282	-0.049	0.261	1	0.214	0.184	0.483	0.374	0.367	0.39
Clus 70	0.803	0.263	-0.128	0.444	0.214	1	0.691	0.207	-0.259	0.048	0.279
Clus 69	0.353	0.356	-0.131	0.114	0.184	0.691	1	0.561	-0.154	0.068	0.647
Clus 26	-0.102	-0.043	-0.065	-0.245	0.483	0.207	0.561	1	0.543	0.157	0.471
Clus 172	-0.239	-0.152	-0.116	-0.183	0.374	-0.259	-0.154	0.543	1	-0.081	0.039
Clus 91	-0.132	0.224	0.018	0.135	0.367	0.048	0.068	0.157	-0.081	1	0.155
Clus 54	0.032	0.572	-0.215	-0.056	0.39	0.279	0.647	0.471	0.039	0.155	1

Footnotes**:** Values indicate Pearson's *r.* Correlations were calculated based on each cluster's abundance (percent of total $CD3^+$) in samples from all stimulation conditions at treatment initiation (T0). Clus: clusters. Clusters in bold indicate the clusters that were grouped together in Figure 5 for manual analysis. The associated *r* values are highlighted (orange: subgroup C corresponding to clusters, 37, 38, 70, 98; green: subgroup D corresponding to clusters 28, 54, 69).

Supplementary Table 5. Pearson's correlation effect sizes (*r*) presented in Figure 5 for decreased clusters.

	Clus 48	Clus 82	Clus 102	Clus 137	Clus 77	Clus 74	Clus 154	Clus 50	Clus 94	Clus 49	Clus 160	Clus 65
Clus 48	1	0.377	0.412	0.137	0.462	0.725	0.485	-0.093	0.711	0.565	0.286	0.372
Clus 82	0.377	1	-0.006	0.189	0.064	0.48	0.456	0.318	0.615	0.424	0.114	0.686
Clus 102	0.412	-0.006	1	-0.062	0.635	0.485	0.093	-0.365	0.206	-0.027	0.585	-0.087
Clus 137	0.137	0.189	-0.062	1	-0.072	-0.054	0.226	-0.113	0.066	0.237	-0.008	-0.076
Clus 77	0.462	0.064	0.635	-0.072	1	0.614	0.189	-0.239	0.352	0.076	0.6	-0.027
Clus 74	0.725	0.48	0.485	-0.054	0.614	1	0.261	-0.048	0.678	0.311	0.318	0.375
Clus 154	0.485	0.456	0.093	0.226	0.189	0.261	1	0.288	0.471	0.513	0.145	0.64
Clus 50	-0.093	0.318	-0.365	-0.113	-0.239	-0.048	0.288	1	0.124	0.263	-0.199	0.673
Clus 94	0.711	0.615	0.206	0.066	0.352	0.678	0.471	0.124	1	0.324	0.241	0.637
Clus 49	0.565	0.424	-0.027	0.237	0.076	0.311	0.513	0.263	0.324	1	-0.063	0.452
Clus 160	0.286	0.114	0.585	-0.008	0.6	0.318	0.145	-0.199	0.241	-0.063	1	-0.017
Clus 65	0.372	0.686	-0.087	-0.076	-0.027	0.375	0.64	0.673	0.637	0.452	-0.017	1

Footnotes: Values indicate Pearson's *r.* Correlations were calculated based on each cluster's abundance (percent of total $CD3^+$) in samples from all stimulation conditions at treatment initiation (T0). Clus: clusters. Clusters in bold indicate the clusters that were grouped together in Figure 5 for manual analysis. The associated *r* values are highlighted (green: subgroup A corresponding to clusters, 49, 50, 65, and 154; blue: subgroup B corresponding to clusters 74, 102, 160).

Supplementary Table 6. Exact p-values and test statistics for cluster abundance comparisons between fast and slow converters, presented in Figure 6 and Supplementary Figure 5.

Cluster	Timepoint	Stimulation	N (fast converters)	N (slow converters)	U statistic	p
T0 - significance threshold set at p < 0.026						
117	T0	NIL	12	4	45.5	0.0094
132	T0	NIL	12	4	46	0.0079
134	T0	NIL	12	4	45.5	0.0099
147	T0	NIL	12	4	43	0.023
148	T0	NIL	12	4	43.5	0.019
186	T0	NIL	12	4	3.5	0.0089
48	T0	NIL	12	4	44	0.017
62	T0	NIL	12	4	46	0.0087
76	T0	NIL	12	4	43.5	0.020
88	T0	NIL	12	4	43.5	0.020
105	T0	TB2	14	4	54	0.0061
118	T0	TB2	14	4	51.5	0.012
134	T0	TB2	14	4	52.5	0.010
147	T0	TB2	14	4	50	0.021
148	T0	TB2	14	4	49.5	0.025
32	T0	TB2	14	4	50	0.020
74	T0	TB2	14	4	49.5	0.025
75	T0	TB2	14	4	54.5	0.0053
89	T0	TB2	14	4	50	0.020
90	T0	TB2	14	4	52	0.010
102	T0	HBHA	11	3	32	0.018
132	T0	HBHA	11	3	31.5	0.021
134	T0	HBHA	11	3	31.5	0.023
148	T0	HBHA	11	3	33	0.012
182	T0	HBHA	11	3	2	0.015
183	T0	HBHA	11	3	0	0.010
52	T0	HBHA	11	3	31.5	0.023
62	T0	HBHA	11	3	32.5	0.015
75	T0	HBHA	11	3	31.5	0.021

Supplementary Table 6 - continued

T1 - significance threshold set at p < 0.031						
116	T1	NIL	12	4	43	0.023
120	T1	NIL	12	4	43.5	0.019
180	T1	NIL	12	4	6	0.023
75	T1	NIL	12	4	43.5	0.020
11	T1	TB2	14	4	7.5	0.031
117	T1	TB2	14	4	50	0.021
119	T1	TB2	14	4	49	0.027
125	T1	TB2	14	4	5.5	0.018
132	T1	TB2	14	4	49.5	0.025
134	T1	TB2	14	4	55	0.0047
146	T1	TB2	14	4	49.5	0.025
147	T1	TB2	14	4	53.5	0.0075
148	T1	TB2	14	4	52.5	0.010
166	T1	TB2	14	4	7.5	0.019
171	T1	TB2	14	4	6	0.021
178	T1	TB2	14	4	6	0.020
180	T1	TB2	14	4	7.5	0.028
4	T1	TB2	14	4	6	0.021
57	T1	TB2	14	4	5	0.016
62	T1	TB2	14	4	51	0.016
64	T1	TB2	14	4	49.5	0.025
76	T1	TB2	14	4	51	0.016
89	T1	TB2	14	4	49.5	0.023
117	T1	HBHA	11	3	33	0.011
12	T1	HBHA	11	3	1.5	0.022
147	T1	HBHA	11	3	31.5	0.021
180	T1	HBHA	11	3	1.5	0.020
34	T1	HBHA	11	3	31	0.028
62	T1	HBHA	11	3	32	0.018

Supplementary Table 6 - continued

T2 - significance threshold set at p < 0.013						
112	T2	NIL	12	4	2	0.0073
12	T2	NIL	12	4	2	0.0052
134	T2	NIL	12	4	46.5	0.0074
14	T2	NIL	12	4	2	0.0073
169	T2	NIL	12	4	0	0.0031
181	T2	NIL	12	4	3	0.012
182	T2	NIL	12	4	0.5	0.0021
183	T2	NIL	12	4	1	0.0049
60	T2	NIL	12	4	45	0.012
62	T2	NIL	12	4	47	0.0063
66	T2	NIL	12	4	45.5	0.010
67	T2	NIL	12	4	45	0.012
74	T2	NIL	12	4	47	0.0059
81	T2	NIL	12	4	45	0.012
112	T2	TB2	14	4	4	0.012
12	T2	TB2	14	4	3	0.0085
134	T2	TB2	14	4	52	0.012
148	T2	TB2	14	4	53	0.0088
166	T2	TB2	14	4	2	0.0045
169	T2	TB2	14	4	4	0.011
180	T2	TB2	14	4	2	0.0062
181	T2	TB2	14	4	1.5	0.0055
182	T2	TB2	14	4	1	0.0035
183	T2	TB2	14	4	3	0.0064
62	T2	TB2	14	4	55	0.0047
88	T2	TB2	14	4	52	0.012
94	T2	TB2	14	4	54	0.0059
98	T2	TB2	14	4	3.5	0.010
183	T2	HBHA	11	3	0	0.011

Footnotes**:** For comparisons between non-normal, independent continuous variables at T0, T1, and T2 separately, the two-sided Mann-Whitney U test was performed. For discovery of clusters with significantly different abundance, conservative corrections for multiple comparisons (*e.g*. Benjamini-Hochberg) were not used in order to minimize type II errors. Instead, all p-values were computed for each timepoint, and the p-value corresponding to the null hypothesis being rejected in 5% of all comparisons was used as the significance threshold instead of 0.05. This novel significance threshold enabled to control type I error while maintaining an exploratory approach. Only clusters within which significant differences were detected were represented.

Supplementary Table 7. Exact p-values and test statistics for comparison of PCA scores between fast and slow converters, presented in Figure 7 and Supplementary Figure 7.

Timepoint	N(fast converters)	N(slow converters)	U statistic	p-value
Figure 7 - within selected clusters				
Component 1				
T0	25	7	34	0.013
T1	25	7	28	0.0051
T2	25	7	25	0.0029
Component 2				
T0	25	7	130	0.0542
T1	25	7	72	0.503
T2	25	7	146	0.00602
Supp. Figure 7 - within all $CD3^+$ events				
Component 1				
T0	25	7	24	0.00247
T1	25	7	30	0.00709
T2	25	7	22	0.00166
Component 2				
T0	25	7	70	0.447
T1	25	7	101	0.562
T2	25	7	58	0.191

Footnotes: For comparisons between non-normal, independent continuous variables at T0, T1, and T2 separately, the two-sided Mann-Whitney U test was performed.

Supplementary Table 8. Mass cytometry panel components.

Cellular target	Clone	Metal tag	Volume for 10^6 cells in 100µL total
CD45	HI30	89Y	1,5
CD196/CCR6	11A9	141Pr	0,5
CD69	FN50	144Nd	1
CD4	RPA-T4	145Nd	1
CD8	RPA-T8	146Nd	0,7
CD7	CD7-6B	147Sm	1
CD278/ICOS	C398.4A	148Nd	0,7
CD25	2A3	149Sm	1
CD14	RMO52	151Eu	1,5
TCRgd	11F2	152Sm	1
TCRVa 7.2	3C10	153Eu	1,5
CD3	UCHT1	154Sm	1
CD279/PD-1	EH12.2H7	155Gd	1
CD183/CXCR3	G025H7	156Gd	1
CD194/CCR4	L291H4	158Gd	1
CD197/CCR7	G043H7	159Tb	1
CD26	BA5b	161Dy	1
CD27	L128	162Dy	1
CD161	HP-3G10	164Dy	1
CD127/IL-7Ra	A019D5	165Ho	0,7
CD38	HIT2	167Er	1
CD154/CD40L	24-31	168Er	1
CD45RA	HI100	169Tm	1
CD152/CTLA-4	14D3	170Er	1
CD185/CXCR5	RF8B2	171Yb	1
HLA-DR	L243	173Yb	0,7
Perforin	B-D48	175Lu	1
CD56	NCAM16.2	176Yb	1
CD16	3G8	209Bi	1

Footnotes: all antibodies were supplied by Fluidigm.

Supplementary Table 9. Definition of clustering channels and expected cell subpopulations for dimension reduction and automated clustering of $CD3^+$ T-cells.

Clustering channels	Expected cell subpopulations	Phenotype
CD4, CD8, CCR7, CD45RA, CD161, CD26, TCRgd, TCRVa7.2, CD25	Gamma delta T-cells	$CD3^+$ $TCR\gamma\delta^+$
	MAIT-cells	$CD3^+$ $CD4^-$ $CD8^+$ $CD26^+$ $CD161^+$ $TCRV\alpha7.2^+$
	Naive $CD8^+$ T-cells	$CD3^+$ $CD4^-$ $CD8^+$ $CCR7^+$ $CD45RA^+$
	Effector memory $CD8^+$ T-cells	$CD3^+$ $CD4^-$ $CD8^+$ $CCR7^-$ $CD45RA^-$
	Central memory $CD8^+$ T-cells	$CD3^+$ $CD4^-$ $CD8^+$ $CCR7^+$ $CD45RA^-$
	TEMRA $CD8^+$ T-cells	$CD3^+$ $CD4^-$ $CD8^+$ $CCR7^-$ $CD45RA^+$
	Naive $CD4^+$ T-cells	$CD3^+$ $CD4^+$ $CD8^-$ $CCR7^+CD45RA^+$
	Effector memory $CD4^+$ T-cells	$CD3^+$ $CD4^+$ $CD8^-$ $CCR7^-CD45RA^-$
	Central memory $CD4^+$ T-cells	$CD3^+$ $CD4^+$ $CD8^-$ $CCR7^+CD45RA^-$
	TEMRA $CD4^+$ T-cells	$CD3^+$ $CD4^+$ $CD8^-$ $CCR7^-$ $CD45RA^+$
	Treg	$CD3^+$ $CD4^+$ $CD25^+$ $IL7Ra^-$
	Double negative T-cells	$CD3^+$ $CD4^-$ $CD8^-$

Footnotes: only lineage-defining markers are presented in this table. MAIT: mucosal-associated invariant T-cells. TEMRA: terminally differentiated effectors re-expressing CD45RA. NK: natural killer cells. NKT: natural killer T-cells. Treg: T regulators.

Supplementary Table 10. Spectral flow cytometry panel components.

ANTIBODIES[1]		AURORA		
Cellular target	**Clone**	**Fluorochrome**	**Supplier**	**Single staining[2]**
CD45RA	HI100	BUV395	BD	Cells
CD8	RPA-T8	BUV496	BD	Cells
CD14[1]	RMO52	BUV563	BD	Cells
CD27	L128	BUV661	BD	Cells
CD56	NCAM16.2	BUV737	BD	Beads
CD4	RPA-T4	BUV805	BD	Cells
CD197/CCR7	G043H7	BV421	Biolegend	Cells
CD19[1]	HB19	SB436	Thermofisher	Cells
HLA-DR	L243	e450	Thermofisher	Beads
TCRgd	11F2	BV480	BD	Beads
TCRVa 7.2	3C10	BV510	Biolegend	Beads
CD16	3G8	BV570	Biolegend	Cells
CD194/CCR4	L291H4	BV605	Biolegend	Cells
CD183/CXCR3	G025H7	BV650	Biolegend	Cells
CD196/CCR6	11A9	BV711	BD	Beads
CD185/CXCR5	RF8B2	BV750	BD	Beads
CD279/PD-1	EH12.2H7	BV785	Biolegend	Cells
CD26	BA5b	FITC	Biolegend	Cells
CD3	UCHT1	A532	Thermofisher	Cells
CD45	HI30	PerCP	BD	Cells
Perforin	B-D48	PerCP-Cy5.5	Biolegend	Beads
CD69	FN50	PerCP-eFluor710	Thermofisher	Cells
CD25	2A3	PE	BD	Beads
CD278/ICOS	C398.4A	PE Dazzle594	Biolegend	Beads
CD154/CD40L	24-31	PE-Cy5	Biolegend	Cells
CD152/CTLA-4	14D3	PE-Cy7	Thermofisher	Cells
CD161	HP-3G10	APC	Biolegend	Cells
CD127/IL-7Ra	A019D5	AF647	Biolegend	Cells
CD7	CD7-6B	AF700	BD	Cells
CD38	HIT2	APC e780	Thermofisher	Cells

Footnotes:

[1] All CyTOF and Aurora antibody clones were the same except for anti-CD14 (Aurora: clone M5E2; only availability in this color), and anti-CD19, which was not included in the CyTOF panel.

[2] This column indicates which single stainings for unmixing reference controls were bright enough to be performed on fixed white blood cell samples, or had to be performed on UltraComp eBeads Plus compensation beads (ThermoFisher Scientific).

2. Other original publications

2.1 Annex 4 – MDR-TB surveillance in Haiti

Drug-resistant TB prevalence study in 5 health institutions in Haiti

Jonathan HOFFMANN, Carole CHEDID, Oksana Ocheretina, Chloé Masetti, Patrice Joseph, Marie-Marcelle Mabou, Jean-Edouard Mathon, Elie Maxime François, Juliane Gebelin, François-Xavier Babin, Laurent Raskine, Jean William Pape.

***PLoS ONE* 2021; 16(3); 1-12.**

PLOS ONE

RESEARCH ARTICLE

Drug-resistant TB prevalence study in 5 health institutions in Haiti

Jonathan Hoffmann[1☯]*, Carole Chedid[1,2☯], Oksana Ocheretina[3,4], Chloé Masetti[5], Patrice Joseph[4], Marie-Marcelle Mabou[4], Jean Edouard Mathon[4], Elie Maxime Francois[4], Juliane Gebelin[5], François-Xavier Babin[5], Laurent Raskine[5], Jean William Pape[4]

1 Fondation Mérieux, Direction Médicale et Scientifique, Lyon, France, **2** Département de Biologie, Ecole Normale Supérieure de Lyon, Lyon, France, **3** Division of Infectious Diseases, Department of Medicine, Center for Global Health, Weill Cornell Medical College, New York, New York, United States of America, **4** Les Centres GHESKIO, Port-au-Prince, Haiti, **5** Fondation Mérieux, Direction des Opérations Internationales, Lyon, France

☯ These authors contributed equally to this work.
* Jonathan.hoffmann@fondation-merieux.org

Citation: Hoffmann J, Chedid C, Ocheretina O, Masetti C, Joseph P, Mabou M-M, et al. (2021) Drug-resistant TB prevalence study in 5 health institutions in Haiti. PLoS ONE 16(3): e0248707. https://doi.org/10.1371/journal.pone.0248707

Editor: Shampa Anupurba, Institute of Medical Sciences, Banaras Hindu University, INDIA

Received: October 9, 2020

Accepted: March 4, 2021

Published: March 18, 2021

Peer Review History: PLOS recognizes the benefits of transparency in the peer review process; therefore, we enable the publication of all of the content of peer review and author responses alongside final, published articles. The editorial history of this article is available here: https://doi.org/10.1371/journal.pone.0248707

Data Availability Statement: The data underlying the results presented in the study have been uploaded with the manuscript as supplementary file (excel sheet 'Study dataset').

Abstract

Objectives

Tuberculosis (TB) is the leading infectious cause of death in the world. Multi-drug resistant TB (MDR-TB) is a major public health problem as treatment is long, costly, and associated to poor outcomes. Here, we report epidemiological data on the prevalence of drug-resistant TB in Haiti.

Methods

This cross-sectional prevalence study was conducted in five health centers across Haiti. Adult, microbiologically confirmed pulmonary TB patients were included. Molecular genotyping (*rpoB* gene sequencing and spoligotyping) and phenotypic drug susceptibility testing were used to characterize rifampin-resistant MTB isolates detected by Xpert MTB/RIF.

Results

Between April 2016 and February 2018, 2,777 patients were diagnosed with pulmonary TB by Xpert MTB/RIF screening and positive MTB cultures. A total of 74 (2.7%) patients were infected by a drug-resistant (DR-TB) *M. tuberculosis* strain. Overall HIV prevalence was 14.1%. Patients with HIV infection were at a significantly higher risk for infection with DR-TB strains compared to pan-susceptible strains (28.4% vs. 13.7%, adjusted odds ratio 2.6, 95% confidence interval 1.5–4.4, $P = 0.001$). Among the detected DR-TB strains, T1 (29.3%), LAM9 (13.3%), and H3 (10.7%) were the most frequent clades. In comparison with previous spoligotypes studies with data collected in 2000–2002 and in 2008–2009 on both sensitive and resistant strains of TB in Haiti, we observed a significant increase in the prevalence of the drug-resistant MTB Spoligo-International-Types (SIT) 137 (X2 clade: 8.1% vs. 0.3% in 2000–02 and 0.9% in 2008–09, p<0.001), 5 (T1 clade: 6.8% vs 1.9 in 2000–02 and 1.7% in

Funding: This project was supported by the SPHaïtiLab project financed by the European Commission via DEVCO under the Supporting Public Health Institutes Programme and by the Fondation Mérieux. The funders had no role in study design, data collection and analysis, decision to publish, or preparation of the manuscript.

Competing interests: The authors have declared that no competing interests exist.

2008–09, $P = 0.034$) and 455 (T1 clade: 5.4% vs 1.6% and 1.1%, $P = 0.029$). Newly detected spoligotypes (SIT 6, 7, 373, 909 and 1624) were also recorded.

Conclusion

This study describes the genotypic and phenotypic characteristics of DR-TB strains circulating in Haiti from April 2016 to February 2018. Newly detected MTB clades harboring multidrug resistance patterns among the Haitian population as well as the higher risk of MDR-TB infection in HIV-positive people highlights the epidemiological relevance of these surveillance data. The importance of detecting RIF-resistant patients, as proxy for MDR-TB in peripheral sites via molecular techniques, is particularly important to provide adequate patient case management, prevent the transmission of resistant strains in the community and to contribute to the surveillance of resistant strains.

Introduction

Tuberculosis (TB) is a communicable disease caused by *Mycobacterium tuberculosis* (MTB). It is the leading infectious cause of death worldwide. In 2018, the death toll for TB among HIV-negative people was estimated to be 1.2 million, with an additional 251 000 deaths among HIV-positive people. The estimated global burden for the same year was about 10 million new cases [1]. Currently, about a quarter of the global population is latently infected, and at risk of developing active TB.

Although the Americas accounted only for 3% of the global TB cases in 2018, Haiti is one of the countries with the highest TB incidence in the Western hemisphere. In 2018, the country reported an incidence of 176 cases per 100,000 population, of which approximately 15% were cases of TB/HIV coinfection [2]. In Haiti, the mortality due to TB is estimated to be 9.2 per 100 000 population for HIV-negative patients, and 7.7 per 100 000 population for HIV-positive patients [3]. The overall HIV prevalence is 2% and has remained stable in the past years, with 160,000 people living with HIV in 2018 including about 8,400 to 10,000 adolescents for whom tailored interventions are needed to improve retention in care [4,5].

The definition of Multi Drug Resistance TB (MDR-TB) refers to strains that show resistance to at least both Rifampicin (RIF) and Isoniazid (INH) two of the primary four drugs used in TB treatment, whilst Drug Resistant TB (DR-TB) is may refer to strains that are resistant to one or more drugs used in TB treatment. In Haiti, MDR-TB infections are a major public health issue as the treatment and the risk of poor outcomes are starkly increased [6,7]. The case management of such patients is costly for local healthcare systems and threatens to negatively impact of the progress made in the recent years in the fight against TB in Haiti [8]. In 2018 in Haiti, 94 patients were diagnosed with laboratory-confirmed MDR-TB or Rifampin Resistant TB (RR-TB) incidence of 5.1 per 100 000 population), and 91 were started on treatment [3]. There are two existing centers for the treatment of these patients in Haiti, and the capacity to perform Drug Susceptibility Testing (DST) to detect MDR-TB in Haiti remains limited outside the capital city of Port au Prince (Ouest department). However, since 2014, several peripheral laboratories have been equipped with GeneXpert® Systems (Cepheid, Sunnyvale, USA), enabling the molecular detection of rifampin resistant strains. Rifampin resistance serves as a proxy for MDR-TB diagnosis in low-resource settings. In December 2019, 27 public laboratories and subsidized health institutions across the country had access to GeneXpert machines.

In Haiti, the number of patients infected with Rifampin resistant MTB remains difficult to estimate [9]. Available studies on this topic mainly focus on the urban population of Port au Prince [6,10]. The present study was designed in collaboration with the National TB Program and the National Public Health Laboratory in 2014, and involved five health institutions located in the department of Ouest (GHESKIO INLR and GHESKIO IMIS), Nord (Hôpital Justinien du Cap Haïtien—HUJ), Sud (Hôpital Immaculée Conception des Cayes—HIC), and Centre (Hôpital Universitaire de Mirebalais—HUM). The general objective was to report the prevalence of DR-TB in these five study sites. For surveillance purposes, this study aimed to characterize the DR-TB strains circulating in Haiti from April 2016 to February 2018.

Materials and methods

Ethical statement

The study was approved by the Institutional Review Board of Weill Cornell Medical College (New York, USA), the Institutional Review Board of GHESKIO Centres (Port-au-Prince, Haiti) and the Haitian National Committee of Bioethics. Clinical and epidemiological data were extracted from patients' charts. As this was a retrospective clinical chart review, the requirement for informed consent was waived by the institutional review boards.

Study sites

Five health institutions were selected to participate in the present study, based on the availability of a functional GeneXpert® System (Cepheid, Sunnyvale, USA) on site and considered to have large catchment areas for the population. The geographic distribution of the sites allowed to cover four out of 10 departments: Ouest (GHESKIO INLR and GHESKIO IMIS), Nord (Hôpital Justinien du Cap Haïtien—HUJ), Sud (Hôpital Immaculée Conception des Cayes—HIC) and Centre (Hôpital Universitaire de Mirebalais—HUM). Exclusion criteria included age under 15, negative smear microscopy, and signs of extrapulmonary TB.

Tuberculosis screening and diagnostic algorithm

In the five participating health institutions, social workers administered a symptom checklist enquiring about chronic cough lasting $\geq$ 2 weeks, as well as other TB symptoms. Individuals who reported chronic cough were separated from other patients and referred for same-day physician evaluation. In the peripheral sites (HIC, HUJ, HUM), three sputum samples were collected per TB suspect: two were collected during the first consultation, then a sterile container was given to the patient for collection of the third specimen the next morning. Smear microscopy (Ziehl-Neelsen staining) was conducted. The third sputum specimen was refrigerated upon collection and transported to the biosafety level-3 Rodolphe Mérieux Reference Laboratory in the GHESKIO IMIS (Port-au-Prince). Xpert MTB/RIF testing was done directly on an early-morning specimen, in accordance with guidelines from the Haitian Ministry of Health [11] and the manufacturer's instructions. A single positive result from the smear examination led to the initiation of anti-TB treatment. HIV testing was conducted using rapid antibody tests (Determine; Alere, Waltham, MA, USA). The protocol conducted by the GHESKIO centers (INLR and IMIS) was slightly different as only two sputum specimens were collected per patient, and no microscopy testing was performed. Following internal diagnostics protocol, a digital chest radiograph (CXR) was performed on-site combined with Xpert MTB/RIF testing. All sputum specimens collected in the present study were cultured on liquid media (BACTEC MGIT 960, Becton Dickenson, Franklin Lakes, NJ, USA) and solid media (Lowenstein-Jensen).

Phenotypic and genotypic drug-resistant TB assessment

DST to first- and second-line anti tuberculosis drugs was conducted for all samples with rifampin resistance detected by Xpert MTB/RIF. First-line DST was performed with BACTEC MGIT 960 SIRE and PZA kits as previously described [12]. Drug-resistant TB strains were further characterized using an in-house Luminex PCR-based spoligotyping assay and by *rpoB* gene sequencing as previously described [12,13]. Spoligotype International Type (SIT) patterns were assigned using the SITVIT2 database [14].

Data analysis

Sociodemographic information, TB diagnosis and HIV status were collected using standardized clinical report forms. Data were cleaned and analyzed in R studio software (version 3.6.2). As the sample size was small, discrete variables were analyzed using Fisher's Exact test with Bonferroni's post-hoc [15]. Normal, continuous variables were analyzed using Student's t-test. Non-normal, continuous variables were analyzed using the Mann-Whitney or Kruskal-Wallis rank tests with Dunn's post-hoc [16] when necessary. For logistic regression, if missing data exceeded 10% of the sample size, the variable was not considered. Otherwise, missing data were replaced by the most frequent group (categorical variables) or the mean (continuous variables). Predictors were first evaluated in univariate logistic analyses, then models were adjusted for sociodemographic factors.

Results

Sociodemographic and clinical characteristics of the participants

From April 2016 to February 2018, 2,777 microbiologically confirmed pulmonary TB patients were enrolled in five study sites across Haiti. Initially, the aim of the study was to enroll 1,000 new TB patients and 250 re-treatment cases, with equal sampling from each site. However, country-wide strike movements hindered patient recruitment in peripheral study sites, prompting increased recruitment in central GHESKIO clinical centers (IMIS and INLR), hence the unequal sample size per site. All study sites were comparable regarding the age, sex ratio, and HIV prevalence of recruited participants (Table 1). The prevalence of HIV was 14.1% (391/2764). The frequency of retreatment was unequal between sites, with a lower frequency in the HUJ and HUM centers (center and northern sites) compared to the remaining

Table 1. Sociodemographic and clinical characteristics of the cohort.

	ALL	INLR	HIC	HUJ	HUM	IMIS	*P*
	N_T = 2777	N_T = 2049	N_T = 148	N_T = 50	N_T = 75	N_T = 455	
Age (years), median (IQR)	31 (24–40)	31 (25–41)	28.5 (23–39)	27 (23–40.75)	31 (24.5–44.5)	30 (23–39)	*0.132*
Sex (male), % (N)	56.6% (1572/2777)	58.1% (1190/2049)	55.4% (82/148)	60% (30/50)	50.7% (38/75)	51% (232/455)	*0.060*
HIV positivity, % (N)	14.1% (391/2764)	14.2% (291/2044)	19.9% (29/146)	12% (6/50)	11.4% (8/70)	12.6% (57/454)	*0.272*
Treatment category							
New cases, % (N)	86.5% (2401/2777)	85.8% (1759/2049)	84.5% (125/148)	96% (48/50)	96% (72/75)	87.3% (397/455)	***0.014***
Relapse, % (N)	8.5% (236/2777)	8.5% (175/2049)	13.5% (20/148)	2% (1/50)	4% (3/75)	8.1% (37/455)	*0.058*
Treatment after interruption % (N)	4% (110/2777)	4.5% (92/2049)	1.4% (2/148)	NA	NA	3.5% (16/455)	***0.049***
Treatment after failure, % (N)	1.1% (30/2777)	1.1% (23/2049)	0.7% (1/148)	2% (1/50)	NA	1.1% (5/455)	*0.823*
Drug resistance, % (N)	2.7% (74/2758)	1.7% (34/2045)	0.7% (1/138)	4.1% (2/49)	4.2% (3/71)	7.5% (34/455)	***<0.001***

Data were analyzed using Fisher's Exact text or the Mann-Whitney U test (p-values given for all categories). Pairwise differences were assessed using Bonferroni or Dunn's post hoc. Stars indicate statistically different groups.

https://doi.org/10.1371/journal.pone.0248707.t001

three sites. Among the 2,777 TB patients diagnosed with the Xpert MTB/RIF molecular test, 74 (2.7%) had TB isolates displayed a concordant genotypic/phenotypic DR-TB profiles. The prevalence of detected DR-TB strains was higher in te IMIS center compared to the rest of the partner sites.

Phenotypic diversity of detected drug-resistant TB strains

Among the 74 drug-resistant TB strains identified by DST, 12 strains (16.2%) displayed a mono-resistance to at least 1 antibiotic (drug-resistant TB strain; DR-TB) and 62 strains (83.8%) displayed a multi-drug resistant (MDR-TB) profile (defined by resistance to at least rifampin and isoniazid). Resistance phenotypes to INH and RIF were predominant (87.8% and 91.9%, respectively).

Details of monoresistance and multi-drug resistant profiles are shown in S1 Table and S1 Fig. Sixty-two (83.8%) DR-TB strains were identified in new TB cases, 11 (14.9%) in relapse TB cases, and 1 (1.4%) in subjects under retreatment after failure (Table 2).

Comparison of clinical and sociodemographic factors between drug-susceptible and drug-resistant TB patients

We then compared the sociodemographic and clinical characteristics of DR-TB and DS-TB patients. Patient characteristics were comparable (age group, sex ratio, and treatment category), but HIV prevalence was significantly higher in DR-TB patients (28.4% vs. 13.7%, p = 0.002) (Table 2). Logistic regression analyses confirmed that HIV-positive patients recruited in this cohort were at higher risk for detection of DR-TB strains. After adjusting for age, sex, and study site of recruitment, HIV-positive patients were 2.5 times more likely to be diagnosed with DR-TB than HIV-negative patients.

Diversity of circulating drug-resistant MTB strains

The repartition of drug-resistant *M. tuberculosis* strains in Haiti during this study period was then assessed (Fig 1). T1, LAM9, LAM1 and H3 were the most frequently detected clades

Table 2. Comparison of drug-susceptible and resistant TB patients and evaluation of associated risk factors.

	Total	Drug sensitive	Drug resistant		Logistic regression—association with drug resistance								
					Univariate analysis				Multivariate analysis*				
	N_T = 2777	N_T = 2684	N_T = 74	*P*	OR	2.50%	97.50%	*P*	aOR	lower	upper	*P*	AIC
Sex (male)	56.6% (1572/2777)	56.9% (1526/2684)	51.4% (38/74)	*0.345*	0.855	0.616	1.188	*0.347*	-	-	-	-	-
HIV positivity	14.1% (391/2764)	13.7% (365/2672)	28.4% (21/74)	***0.002***	2.504	1.463	4.139	***0.001***	2.585	1.478	4.383	***0.001***	643.28
Age (years; median, IQR)	31 (24–40)	30.5 (24–40)	33 (24–43.75)	*0.313*	1.012	0.995	1.029	*0.162*	-	-	-	-	-
Treatment category													
New cases	86.5% (2401/2777)	86.7% (2328/2684)	83.8% (62/74)	*0.486*	0.79	0.437	1.553	*0.462*	0.756	0.152	13.737	*0.788*	650.37
Relapse	8.5% (236/2777)	8.2% (219/2684)	14.9% (11/74)	*0.052*	1.965	0.968	3.636	*0.043*	1.397	0.247	26.408	*0.756*	650.37
Treatment after interruption	4% (110/2777)	4.1% (109/2684)	0	*0.118*	0	0	5789.26	*0.981*	-	-	-	-	-
Treatment after failure	1.1% (30/2777)	1% (28/2684)	1.4% (1/74)	*0.547*	1.299	0.072	6.216	*0.798*	0	0	2529.87	*0.98*	650.37

Data were compared with Fisher's Exact Test. OR: odds ratio. aOR: Adjusted odds ratio. IQR: Interquartile range. AIC: Akaike Information Criterion.

*Models were adjusted for age, sex, and study site. Fifteen out of 2,777 smear-positive samples were tested GeneXpert MTB/RIF negative (MTB not detected) and 4 isolates could not be cultured for DST.

https://doi.org/10.1371/journal.pone.0248707.t002

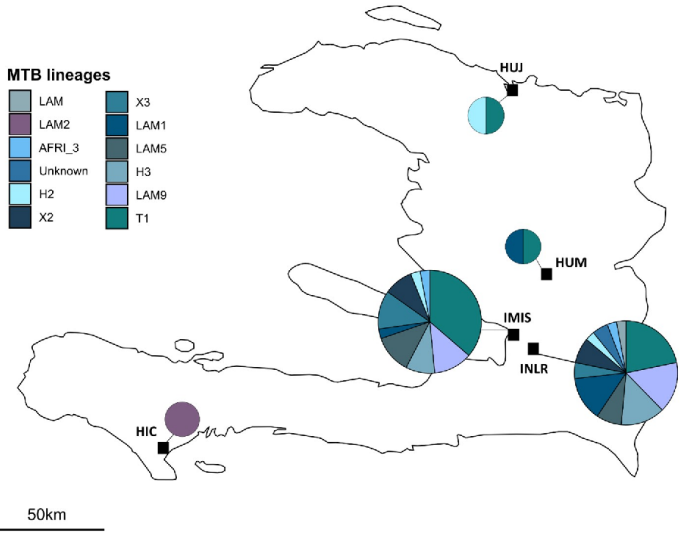

Fig 1. Repartition of drug-resistant M. tuberculosis clades in Haiti (n = 74). Geographic repartition of DR-TB clades in partner study sites. Data are given for all patients with known spoligotypes. Pie chart size correlates with sample size in each site (Gheskio: n = 34. IMIS: n = 34. HUM: n = 3. HUJ: n = 2. HIC: n = 1).

https://doi.org/10.1371/journal.pone.0248707.g001

among all DR-TB patients. In the two sites with the most recruited patients (GHESKIO IMIS and INLR), T1 was also the most frequently detected clade, however, a greater diversity of clades was observed in the INLR center. Frequencies of detected DR-TB clades and spoligotypes were compared with data collected in 2002 and in 2009 [13] (Table 3). The prevalence of X2 strains (SIT 137) significantly increased from 0.3% and 0.9% in 2002 and 2009, respectively, to 8.1% (6/74) in our study ($P < 0.001$). Three of these strains had the same resistance phenotype (STR+INH+RIF+EMB+ETH), the same *rpoB* mutation (S531L), and were detected in the same study site (GHESKIO INLR) (Table 4). A similar phenomenon was observed with T1 strains (SIT 5), carrying the D516V *rpoB* mutation, with the same resistance profiles (STR +INH+RIF+EMB), and detected in the same site (GHESKIO INLR). Moreover, we recorded rare occurrences of MDR-TB strains that were not detected in these previous studies (T1 SIT 373 and 7, LAM SIT 1624, EAI-SOM SIT 6 and SIT 909 with unknown clade) among new TB cases (S2 Table). Finally, some of the strains that were highly prevalent in previous works (LAM2) were less frequent in our study (1.4% vs. 5.8% in 2002 and 4.4% in 2009).

Relationship between *rpoB* mutation and lineage

rpoB sequencing was performed on DR-TB isolates (S2 Fig). S531L was the most frequently detected mutation (44/74, 59.4%) followed by S531W and D516V (7/74, 9.4% respectively). *rpoB* mutations were heterogeneously distributed within the detected clades (S3 Fig). As expected, the highest mutation diversity was observed in the most frequent lineage (T1), and the most frequent *rpoB* mutation (S531L) was detected in every lineage. Interestingly, S531L mutations were detected in at least 50% of isolates for every lineage except LAM9, in which

Table 3. Spoligotyping data of TB isolates in Haiti.

SIT	Clade	TB isolates N (%)			
		2000–2002*	2008–2009*	2016–2018	
		$N_T = 379$	$N_T = 758$	$N_T = 74$**	*P*
42	LAM9	27 (7.1)	54 (7.1)	10 (13.5)	*0.149*
53	T1	27 (7.1)	46 (6.1)	7 (9.5)	*0.433*
93	LAM5	15 (4)	33 (4.4)	7 (9.5)	*0.135*
20	LAM1	26 (6.9)	42 (5.5)	4 (5.4)	*0.693*
91	X3	29 (7.7)	31 (4.1)	5 (6.8)	*0.031*
137	X2	1 (0.3)	7 (0.9)	6 (8.1)	***<0.001***
5	T1	7 (1.9)	13 (1.7)	5 (6.8)	***0.034***
50	H3	37 (9.8)	79 (10.4)	2 (2.7)	*0.084*
455	T1	6 (1.6)	8 (1.1)	4 (5.4)	***0.029***
2	H2	37 (9.8)	72 (9.5)	3 (4.1)	*0.287*
77	T1	4 (1.1)	11 (1.5)	3 (4.1)	*0.149*
51	T1	17 (4.5)	26 (3.4)	2 (2.7)	*0.671*
294	H3	1 (0.3)	2 (0.3)	2 (2.7)	***0.039***
408	AFRI_3	- (-)	4 (0.5)	1 (1.4)	***0.019***
17	LAM2	22 (5.8)	33 (4.4)	1 (1.4)	*0.218*
373	T1	- (-)	- (-)	1 (1.4)	*1.000*
578	LAM1	3 (0.8)	7 (0.9)	1 (1.4)	*0.761*
714	H3	4 (1.1)	3 (0.4)	1 (1.4)	*0.189*
909	No clade	- (-)	- (-)	1 (1.4)	*1.000*
1624	LAM	- (-)	- (-)	1 (1.4)	*1.000*
6	EAI-SOM	- (-)	- (-)	1 (1.4)	*0.061*
7	T1	- (-)	- (-)	2 (2.7)	***0.003***

*Data from Ocheretina, O. *et al.* Journal of Clinical Microbiology 51, 2232–2237 (2013). Both studies include DS and DR-TB strains.

**4 samples failed to generate an interpretable pattern (SIT). SIT and Clades were retrieved from the SITVIT2 international database. Data were compared with Fisher's Exact Test.

https://doi.org/10.1371/journal.pone.0248707.t003

S531W was the most frequent mutation. No difference was observed when stratifying data according to HIV status (data not shown).

Discussion

In this study, we reported the occurrence of DR-TB infections in patient cohorts across five study sites in Haiti. We evaluated their distribution according to selected sociodemographic parameters, and we described the phenotypic and genotypic characteristics of isolated DR-TB strains.

First, we observed that patients living with HIV infection were at a significantly higher risk for infection with DR-TB strains compared to pan-susceptible strains (31% vs. 15%, aOR 2.5, 95%CI 1.5–4.1, $p < 0.001$). Comparatively, in Haiti, reported rates of HIV infection are of 16% in TB patients regardless of the drug-susceptibility status, and 2% in the general population [17]. Increased epidemiological interactions between HIV and MDR-TB infections compared to pan-susceptible TB infections have been described since the late nineties [18]. Data on this topic in Haiti are scarce, but a 2006 study reported significantly higher rates of MDR-TB in HIV-positive than in HIV-negative patients [7], which is corroborated by our results. The reason for the interactions between HIV and MDR-TB remains unclear: explanatory hypotheses available in the literature include increased anti-TB drug malabsorption in HIV-positive

Table 4. Description of DR-TB cases and characterization of genotypic and phenotypic drug-resistances by SIT.

SIT	CLADE	SITE	PID	AGE	SEX	TREATMENT CATEGORY	HIV status	*rpoB* mutation	Drug Susceptibility Testing					
									STR	INH	RIF	EMB	PZA	ETH
137	X2	GHESKIO	GH-0128	62	M	N	P	S531L	**R**	**R**	**R**	**R**	**S**	**R**
		GHESKIO	GH-0477	25	M	N	N	S531L	**R**	**R**	**R**	**R**	**S**	**R**
		GHESKIO	GH-0573	68	F	N	N	S531L	**R**	**R**	**R**	**R**	**S**	**R**
		IMIS	IMIS-040	71	M	N	N	S531L	S	R	R	S	R	R
		IMIS	IMIS-388	57	F	N	N	S531L	S	R	R	R	R	R
		IMIS	IMIS-420	19	M	R	I	S531L	S	R	R	S	R	S
5	T1	GHESKIO	GH-0235	17	M	N	P	D516V	**R**	**R**	**R**	**R**	**S**	**S**
		GHESKIO	GH-0269	29	M	N	N	D516V	**R**	**R**	**R**	**R**	**S**	**S**
		GHESKIO	GH-1017	21	F	N	N	D516V	**R**	**R**	**R**	**R**	**S**	**S**
		GHESKIO	GH-1980	45	M	N	N	D516V	**R**	**R**	**R**	**R**	**S**	**S**
		IMIS	IMIS-239	69	F	R	P	S531L	S	S	R	S	S	S
455	T1	GHESKIO	GH-0640	26	M	R	N	S531L	**S**	**S**	**R**	**S**	**S**	**S**
		IMIS	IMIS-344	29	M	N	P	S531L	**S**	**S**	**R**	**S**	**S**	**S**
		IMIS	IMIS-210	18	M	N	N	S531L	R	R	R	R	R	S
		HUM	PIH-005	30	M	R	N	S531L	R	R	R	R	S	R

SIT and clades were retrieved from the SITVIT2 international database. Sex: M = male, F = female; Treatment category: N = new case, R = Relapse; HIV status: P = positive; N = Negative; Drug susceptibility testing: R = Resistant; S = Susceptible; Drugs: STR = streptomycin, INH = isoniazid, RIF = Rifampin, EMB = ethambutol, PZA = Pyrazinamide), ETH = ethionamide. The shaded areas represent identical genotypic and phenotypic resistance profiles for the same SIT.

https://doi.org/10.1371/journal.pone.0248707.t004

patients, or enhanced fitness of MDR-TB strains compared to pan-susceptible strains in HIV-positive hosts [19]. However, current evidence points to an increase in the risk of primary MDR-TB infection in HIV-positive patients, rather than acquired drug-resistance [20].

Secondly, we studied the phenotypic and genotypic diversity of the DR-TB strains isolated from our cohort. Most strains with RIF resistance upon GeneXpert testing also displayed drug or multi-drug resistant phenotypes upon DST. The most frequent resistance phenotypes detected were resistance to Isoniazid and Rifampin, and resistance to all four first line anti-TB drugs. Sequencing analyses identified two high frequency *rpoB* mutations (S531L and S531W) and 12 low-frequency *rpoB* mutations on different loci. Five strains with discrepant phenotypic and genotypic results for resistance to RIF were isolated. Strains exhibiting these discrepancies have been described in previous works in Haiti as possibly harboring subcritical levels of resistance to RIF [12,21]. In our cohort, sequencing analyses identified either T508A or silent T508T *rpoB* mutations in these five discrepant strain isolates, and their SIT numbers were 20 and 50 respectively, which is consistent with earlier findings [12]. In addition, strains harboring a L511P *rpoB* mutation have been detected in our cohort; while this has been previously found in phenotypically RIF susceptible strains [12], they were phenotypically drug-resistant in our case.

Thirdly, we aimed to identify the MTB clades detected in the cohort's DR-TB patients. Indeed, molecular epidemiology is now an important tool to determine MTB transmission patterns, as it complements classic epidemiologic contact tracing and allows investigators to better characterize transmission dynamics. In this study, T1, LAM9, LAM1 and H3 were the most frequently detected clades among all DR-TB patients. In the two sites with the most recruited patients (GHESKIO IMIS and INLR), T1 was the most frequently detected clade as well, but increased diversity was observed in the INLR center. These observations are consistent with a review of MTB drug-resistance and associated genotypic clades observed in 3 French Departments of the Caribbean (Guadeloupe, Martinique and French Guiana) over a seventeen-year period (January 1995–December 2011) [22]. This review reports that T, LAM,

and H were the most common clades, respectively accounting for 29.9% (358/1199), 23.9% (286/1199), and 22.1% (265/1199) of all DR-TB isolates. Moreover, a previous spoligotyping study of 758 TB strains collected in patients presenting to the 6 largest TB centers in and around Port-au-Prince (2008-to-2009 MDR-TB survey [6]) revealed that H3 (10.4%, SIT 50), H2 (9.5%, SIT 2), LAM9 (7.1%, SIT42), T1 (6.1%, SIT 53) and LAM-1 (5.5%, SIT 20) were the 5 most prevalent clades circulating in Haiti during this period [13]. Other spoligotyping data from a project conducted by GHESKIO and Pasteur Institute Guadeloupe from 2000 to 2002 showed that H3 (9.8%, SIT 50), H2 (9.8%, SIT 2), LAM9 (7.1%, SIT42), T1 (7.1%, SIT 53) and LAM-1 (6.9%, SIT 20) were also the 5 most prevalent TB clades detected in 378 GHESKIO patients [13]. Here, a comparative analysis of DR-TB strains spoligotypes circulating in Haiti revealed a resurgence in the number of cases caused by strains with a previously low prevalence (i.e. SIT 137, 5, 455 and 294) or even unknown (SIT 373, 6, 7 909 and 1624). Phenotypic and genotypic analysis of individual MTB strains revealed several identical patterns of MDR-TB. These observations suggest that patients with genetically identical strains may have been infected by a common index case or may have been part of a larger cluster of cases.

The Luminex spoligotyping method currently used by GHESKIO in combination with the GeneXpert MTB/RIF was adapted as a first-line, high-throughput tool for MTB genotyping in resource-limited countries. Luminex spoligotyping allows real-time typing and can be used for multiple clinical and public health purposes in Haiti, such as epidemiological investigation through community-based active case finding (ACF), contact tracing, and MTB strain characterization during clinical trials of pulmonary MDR-TB treatments [23–27]. Data from a 2014–2015 retrospective cohort analysis using the GHESKIO ACF campaign revealed that the prevalence of TB and HIV in slums of Port-au-Prince was respectively four and five times higher than national estimates [23]. Active case finding for TB and HIV should be expanded to other slum populations in Haiti as part of routine programmatic activities to increase the detection rate of TB cases.

Conclusion

Overall, our study showed that people living with HIV in Haiti were particularly at risk for drug-resistant TB, which is a major public health issue on the island. The identified MTB clades were consistent with similar works conducted in the Caribbean, and several MTB clades harboring drug resistance patterns were either newly identified or increasingly detected among the Haitian population. These observations demonstrate that MTB strain genotyping, identification, and surveillance of specific *M. tuberculosis* SITs are essential to better understand the dynamics of DR-TB strain transmission, and to design adapted TB control measures in Haiti. The use of Xpert MTB/RIF testing increased the detection rate of patients with bacteriologically-confirmed TB, and an additional surrogate spoligotyping method is useful to identify MDR-TB clades among newly diagnosed TB cases, to differentiate reactivation from re-infection, to discover more virulent strains, and to monitor the spread of new types.

Supporting information

S1 Fig. Description of DR-TB strains phenotypes among all patients with available DST results. Total of 74 DR-TB strains including 12 mono-drug resistant strains and 62 multi-drug resistant TB strains. GHESKIO (INLR): n = 34. IMIS: n = 34. HUM: n = 3. HUJ: n = 2. HIC: n = 1. I: Isoniazid. R: Rifampin. S: Streptomycin. E: Ethambutol. PZA: Pyrazinamide. KM: Kanamycin.
(DOCX)

S2 Fig. *rpoB* genotypic diversity of DR-TB isolates (n = 74).
(DOCX)

S3 Fig. Frequency of detected rpoB mutation in each identified drug-resistant *M. tuberculosis* lineage (n = 74). Data are given for all patients with known spoligotypes.
(DOCX)

S1 Table. Summary of resistance profiles of DR-TB isolates identified in new TB cases, relapse, treatment after failure or treatment after interruption.
(DOCX)

S2 Table. Mono-resistance profile of DR-TB isolates identified in new TB cases, relapse, treatment after failure, treatment after interruption.
(DOCX)

S3 Table. Multi-resistant profile of DR-TB isolates identified in new TB cases, relapse, treatment after failure, treatment after interruption.
(DOCX)

S4 Table. Summary of resistance profiles of DR-TB isolates identified in new TB cases, relapse, treatment after failure, treatment after interruption.
(DOCX)

S5 Table. Distribution of DR-TB lineages (SIT) among new TB cases, relapse and treatment after failure.
(DOCX)

S1 Dataset.
(XLSX)

Acknowledgments

We are very grateful to the National Laboratory for Public Health (LNSP) and the National Programme for TB (PNLT) for their collaboration in the design of the study, and to the administrative and laboratory staff in the five participating sites for sample collection and processing.

Author Contributions

Conceptualization: Oksana Ocheretina, Chloé Masetti, Patrice Joseph, Marie-Marcelle Mabou, Jean Edouard Mathon, Elie Maxime Francois, Juliane Gebelin, François-Xavier Babin, Jean William Pape.

Data curation: Jonathan Hoffmann, Carole Chedid, Oksana Ocheretina, Patrice Joseph, Marie-Marcelle Mabou, Jean Edouard Mathon, Elie Maxime Francois, Laurent Raskine, Jean William Pape.

Formal analysis: Oksana Ocheretina.

Funding acquisition: Chloé Masetti, Juliane Gebelin, François-Xavier Babin, Jean William Pape.

Investigation: Jonathan Hoffmann, Carole Chedid, Oksana Ocheretina, Patrice Joseph, Marie-Marcelle Mabou, Jean Edouard Mathon, Elie Maxime Francois, Jean William Pape.

Methodology: Oksana Ocheretina, Patrice Joseph, Marie-Marcelle Mabou, Jean Edouard Mathon, Elie Maxime Francois, Jean William Pape.

Project administration: Chloé Masetti, François-Xavier Babin, Jean William Pape.

Software: Jonathan Hoffmann, Carole Chedid, Laurent Raskine.

Supervision: Oksana Ocheretina, Chloé Masetti, Juliane Gebelin, François-Xavier Babin, Jean William Pape.

Validation: Oksana Ocheretina, Patrice Joseph, Marie-Marcelle Mabou, Jean Edouard Mathon, Elie Maxime Francois, Juliane Gebelin, Laurent Raskine, Jean William Pape.

Visualization: Jonathan Hoffmann, Carole Chedid.

Writing – original draft: Jonathan Hoffmann, Carole Chedid, Chloé Masetti, Laurent Raskine.

Writing – review & editing: Jonathan Hoffmann, Carole Chedid, Oksana Ocheretina, Chloé Masetti, Patrice Joseph, Marie-Marcelle Mabou, Jean Edouard Mathon, Elie Maxime Francois, Juliane Gebelin, François-Xavier Babin, Laurent Raskine, Jean William Pape.

References

1. WHO | Global tuberculosis report 2019. In: WHO [Internet]. World Health Organization; [cited 25 May 2020]. http://www.who.int/tb/publications/global_report/en/.
2. Center for Disease Control and Prevention. Global HIV and TB_Haïti country profile. 2018. https://www.cdc.gov/globalhivtb/where-we-work/haiti/haiti.html.
3. WHO | Tuberculosis country profiles. In: WHO [Internet]. [cited 4 Oct 2017]. http://www.who.int/tb/country/data/profiles/en/.
4. UNICEF. For Every Child, End AIDS, Seventh Stocktaking Report, 2016. 2016. https://www.unicef.org/publications/files/Children_and_AIDS_Seventh_Stocktaking_Report_2016_EN.pdf.pdf.
5. Reif LK, Rivera V, Bertrand R, Rouzier V, Kutscher E, Walsh K, et al. Outcomes across the tuberculosis care continuum among adolescents in Haiti. Public Health Action. 2018; 8: 103–109. https://doi.org/10.5588/pha.18.0021 PMID: 30271725
6. Ocheretina O, Morose W, Gauthier M, Joseph P, D'Meza R, Escuyer VE, et al. Multidrug-resistant tuberculosis in Port-au-Prince, Haiti. Rev Panam Salud Publica. 2012; 31: 221–224. https://doi.org/10.1590/s1020-49892012000300006 PMID: 22569696
7. Joseph P, Severe P, Ferdinand S, Goh KS, Sola C, Haas DW, et al. Multidrug-resistant tuberculosis at an HIV testing center in Haiti. AIDS. 2006; 20: 415–418. https://doi.org/10.1097/01.aids.0000206505.09159.9a PMID: 16439875
8. WHO | WHO consolidated guidelines on drug-resistant tuberculosis treatment. In: WHO [Internet]. World Health Organization; [cited 25 May 2020]. http://www.who.int/tb/publications/2019/consolidated-guidelines-drug-resistant-TB-treatment/en/.
9. Ministère de la santé publique et de la population, République d'Haïti. Rapport statistique 2018. 2019. https://mspp.gouv.ht/site/downloads/Rapport%20Statistique%20MSPP%202018%20version%20web.pdf.
10. Charles M, Vilbrun SC, Koenig SP, Hashiguchi LM, Mabou MM, Ocheretina O, et al. Treatment outcomes for patients with multidrug-resistant tuberculosis in post-earthquake Port-au-Prince, Haiti. Am J Trop Med Hyg. 2014; 91: 715–721. https://doi.org/10.4269/ajtmh.14-0161 PMID: 25071001
11. Ministère de la Santé publique et de la Population. Programme National de Lutte contre la Tuberculose (PNLT): manuel de normes de la tuberculose en Haiti. 2010. https://mspp.gouv.ht/site/downloads/Manuel%20de%20normes%20PNLT.pdf.
12. Ocheretina O, Escuyer VE, Mabou M-M, Royal-Mardi G, Collins S, Vilbrun SC, et al. Correlation between Genotypic and Phenotypic Testing for Resistance to Rifampin in Mycobacterium tuberculosis Clinical Isolates in Haiti: Investigation of Cases with Discrepant Susceptibility Results. PLOS ONE. 2014; 9: e90569. https://doi.org/10.1371/journal.pone.0090569 PMID: 24599230
13. Ocheretina O, Merveille YM, Mabou M-M, Escuyer VE, Dunbar SA, Johnson WD, et al. Use of Luminex MagPlex Magnetic Microspheres for High-Throughput Spoligotyping of Mycobacterium tuberculosis Isolates in Port-au-Prince, Haiti. Journal of Clinical Microbiology. 2013; 51: 2232–2237. https://doi.org/10.1128/JCM.00268-13 PMID: 23658258
14. Couvin D, David A, Zozio T, Rastogi N. Macro-geographical specificities of the prevailing tuberculosis epidemic as seen through SITVIT2, an updated version of the Mycobacterium tuberculosis genotyping

database. Infection, Genetics and Evolution. 2019; 72: 31–43. https://doi.org/10.1016/j.meegid.2018.12.030 PMID: 30593925

15. Kim H-Y. Statistical notes for clinical researchers: Chi-squared test and Fisher's exact test. Restorative Dentistry & Endodontics. 2017; 42: 152. https://doi.org/10.5395/rde.2017.42.2.152 PMID: 28503482

16. Dunn OJ. Multiple Comparisons Using Rank Sums. Technometrics. 1964; 6: 241–252. https://doi.org/10.1080/00401706.1964.10490181

17. Center for Disease Control. Haiti Country Profile. 27 Aug 2019 [cited 26 May 2020]. https://www.cdc.gov/globalhivtb/where-we-work/haiti/haiti.html.

18. Ritacco V, Di Lonardo M, Reniero A, Ambroggi M, Barrera L, Dambrosi A, et al. Nosocomial spread of human immunodeficiency virus-related multidrug-resistant tuberculosis in Buenos Aires. J Infect Dis. 1997; 176: 637–642. https://doi.org/10.1086/514084 PMID: 9291309

19. Eldholm V, Rieux A, Monteserin J, Lopez JM, Palmero D, Lopez B, et al. Impact of HIV co-infection on the evolution and transmission of multidrug-resistant tuberculosis. Elife. 2016; 5. https://doi.org/10.7554/eLife.16644 PMID: 27502557

20. Suchindran S, Brouwer ES, Van Rie A. Is HIV infection a risk factor for multi-drug resistant tuberculosis? A systematic review. PLoS ONE. 2009; 4: e5561. https://doi.org/10.1371/journal.pone.0005561 PMID: 19440304

21. Ocheretina O, Shen L, Escuyer VE, Mabou M-M, Royal-Mardi G, Collins SE, et al. Whole Genome Sequencing Investigation of a Tuberculosis Outbreak in Port-au-Prince, Haiti Caused by a Strain with a "Low-Level" rpoB Mutation L511P—Insights into a Mechanism of Resistance Escalation. PLOS ONE. 2015; 10: e0129207. https://doi.org/10.1371/journal.pone.0129207 PMID: 26039194

22. Millet J, Baboolal S, Streit E, Akpaka PE, Rastogi N. A First Assessment of Mycobacterium tuberculosis Genetic Diversity and Drug-Resistance Patterns in Twelve Caribbean Territories. Biomed Res Int. 2014;2014. https://doi.org/10.1155/2014/718496 PMID: 24795893

23. Rivera VR, Jean-Juste M-A, Gluck SC, Reeder HT, Sainristil J, Julma P, et al. Diagnostic yield of active case finding for tuberculosis and HIV at the household level in slums in Haiti. Int J Tuberc Lung Dis. 2017; 21: 1140–1146. https://doi.org/10.5588/ijtld.17.0049 PMID: 29037294

24. Masur J, Koenig SP, Julma P, Ocheretina O, Durán-Mendicuti MA, Fitzgerald DW, et al. Active Tuberculosis Case Finding in Haiti. Am J Trop Med Hyg. 2017; 97: 433–435. https://doi.org/10.4269/ajtmh.16-0674 PMID: 28722608

25. Rivera VR, Lu L, Ocheretina O, Jean Juste MA, Julma P, Archange D, et al. Diagnostic yield of active case finding for tuberculosis at human immunodeficiency virus testing in Haiti. Int J Tuberc Lung Dis. 2019; 23: 1217–1222. https://doi.org/10.5588/ijtld.18.0835 PMID: 31718759

26. Walsh KF, Vilbrun SC, Souroutzidis A, Delva S, Joissaint G, Mathurin L, et al. Improved Outcomes With High-dose Isoniazid in Multidrug-resistant Tuberculosis Treatment in Haiti. Clin Infect Dis. 2019; 69: 717–719. https://doi.org/10.1093/cid/ciz039 PMID: 30698688

27. Ahmad N, Ahuja SD, Akkerman OW, Alffenaar J-WC, Anderson LF, Baghaei P, et al. Treatment correlates of successful outcomes in pulmonary multidrug-resistant tuberculosis: an individual patient data meta-analysis. The Lancet. 2018; 392: 821–834. https://doi.org/10.1016/S0140-6736(18)31644-1 PMID: 30215381

Supplementary data

Table 1S. Summary of resistance profiles of DR-TB isolates identified in new TB cases, relapse, treatment after failure or treatment after interruption.

Resistance profiles	New cases *N* (%)	Relapse *N* (%)	Treatment after failure *N* (%)	Treatment after interruption *N* (%)	*P*	Total N (%)
	N_T=2,401	N_T=236	N_T=30	N_T=110		N_T=2,777
Resistant to INH*	56 (2.3)	8 (3.4)	1 (3.3)	-	*0.148*	65 (2.3)
Resistant to RIF*	57 (2.4)	10 (4.2)	1 (3.3)	-	*0.053*	68 (2.4)
Resistant to EMB*	24 (1.0)	2 (0.8)	1 (3.3)	-	*1.000*	27 (1.0)
Resistant to STR*	15 (0.6)	3 (1.3)	-	-	*0.431*	18 (0.6)
Resistant to ETH*	11 (0.5)	1 (0.4)	-	-	*0.846*	12 (0.4)
Resistant to PAS*	1 (0.0)	-	-	-	*1.000*	1 (0.0)
Resistant to PZA*	23 (1.0)	2 (0.8)	-	-	*0.720*	25 (0.9)
Monoresistant to INH	2 (0.1)	1 (0.4)	-	-	*0.448*	3 (0.1)
Monoresistant to RIF	6 (0.2)	3 (1.3)	-	-	*0.084*	9 (0.3)
Monoresistant to EMB	-	-	-	-	*1.000*	-
Monoresistant to STR	-	-	-	-	*1.000*	-
Monoresistant to ETH	-	-	-	-	*1.000*	-
Monoresistant to PAS	-	-	-	-	*1.000*	-
Monoresistant to PZA	-	-	-	-	*1.000*	-
Resistant to 1 AB**	8 (0.3)	4 (1.7)	-	-	*0.067*	12 (0.4)
Resistant to 2 AB**	18 (0.7)	2 (0.8)	-	-	*0.893*	20 (0.7)
Resistant to 3 AB**	11 (0.5)	3 (1.3)	1 (3.3)	-	*0.172*	15 (0.5)
Resistant to 4 AB**	13 (0.5)	1 (0.4)	-	-	*1.000*	14 (0.5)
Resistant to 5 AB**	12 (0.5)	1 (0.4)	-	-	*1.000*	13 (0.5)

***Footnotes** : *comprises all drug-resistant isolates to the respective drugs (irrespective of other associated resistances). INH (isoniazid), RIF (Rifampin), EMB (ethambutol), STR (streptomycin), ETH (ethionamide), PAS (para-aminosalicylic acid) or PZA (Pyrazinamide), respectively.** Strains resistant to 1, 2, 3 or 4 of the tested antibiotics (AB)*

Table 2S. Mono-resistance profile of DR-TB isolates identified in new TB cases, relapse, treatment after failure, treatment after interruption.

TB strain resistance profile	Antibiotic resistance profile	New cases		Relapse		Treatment after failure		Treatment after interruption		TOTAL	
		N	*%*	N	*%*	N	*%*	N	*%*	N	*%*
Mono-drug resistant TB	INH	2	*25*	1	*25*	0	-	0	-	3	*25*
	RIF	6	*75*	3	*75*	0	-	0	-	9	*75*
	STR	0	*0*	0	*0*	0	-	0	-	0	*0*
	EMB	0	*0*	0	*0*	0	-	0	-	0	*0*
	PZA	0	*0*	0	*0*	0	-	0	-	0	*0*
Total mono-drug resistant isolates		**8**	*100*	**4**	*100*	**0**	-	**0**	-	**12**	*100*

Table 3S. Multi-resistant profile of DR-TB isolates identified in new TB cases, relapse, treatment after failure, treatment after interruption.

		New cases		Relapse		Treatment after failure		Treatment after interruption		TOTAL	
		N	*%*	N	*%*	N	*%*	N	*%*	N	*%*
Multi-drug resistant TB	INH + RIF	16	*29.6*	2	*28.6*	0	*0.0*	0	-	18	*29.0*
	INH + RIF + STR	0	*0.0*	2	*28.6*	0	*0.0*	0	-	2	*3.2*
	INH + RIF + EMB	2	*3.7*	0	*0.0*	1	*100.0*	0	-	3	*4.8*
	INH + RIF + EMB + PZA	5	*9.3*	1	*14.3*	0	*0.0*	0	-	6	*9.7*
	INH + RIF + EMB + PZA + ETH	3	*5.6*	0	*0.0*	0	*0.0*	0	-	3	*4.8*
	INH + RIF + PZA	6	*11.1*	1	*14.3*	0	*0.0*	0	-	7	*11.3*
	INH + RIF + ETH	2	*3.7*	0	*0.0*	0	*0.0*	0	-	2	*3.2*
	INH + RIF + STR + EMB	5	*9.3*	0	*0.0*	0	*0.0*	0	-	5	*8.1*
	INH + RIF + STR + EMB + ETH	3	*5.6*	1	*14.3*	0	*0.0*	0	-	4	*6.5*
	INH + RIF + PZA + KM	1	*1.9*	0	*0.0*	0	*0.0*	0	-	1	*1.6*
	INH + RIF + PZA + ETH	2	*3.7*	0	*0.0*	0	*0.0*	0	-	2	*3.2*
	INH + RIF + STR + EMB + PZA	6	*11.1*	0	*0.0*	0	*0.0*	0	-	6	*9.7*
	INH + ETH + PAS	1	*1.9*	0	*0.0*	0	*0.0*	0	-	1	*1.6*
	ETH + INH	1	*1.9*	0	*0.0*	0	*0.0*	0	-	1	*1.6*
	STR + INH	1	*1.9*	0	*0.0*	0	*0.0*	0	-	1	*1.6*
Total multi-drug-resistant isolates		**54**	*100.0*	**7**	*100.0*	**1**	*100.0*	**0**	-	**62**	*100.0*

Table 4S. Summary of resistance profiles of DR-TB isolates identified in new TB cases, relapse, treatment after failure, treatment after interruption.

	New cases		Relapse		Treatment after failure		Treatment after interruption		TOTAL	
	N	*%*	N	*%*	N	*%*	N	*%*	N	*%*
Mono-drug resistant TB	8	*12.9*	4	*36.4*	0	*0.0*	0	-	12	*16.2*
Multi-drug resistant TB	54	*87.1*	7	*63.6*	1	*100.0*	0	-	62	*83.8*
Total drug-resistant isolates	**62**	*100.0*	**11**	*100.0*	**1**	*100.0*	0	-	**74**	*100.0*

Table 5S. Distribution of DR-TB lineages (SIT) among new TB cases, relapse and treatment after failure.

SIT	New cases	Relapse	Treatment	
	N_T=62	N_T=11	N_T=1	*P*
2	1 (1.6)	1 (9.1)	1 (100.0)	*<0.001*
5	4 (6.5)	1 (9.1)	- (-)	*0.177*
6	**1 (1.6)**	- (-)	- (-)	*0.196*
7	**2 (3.2)**	- (-)	- (-)	*0.398*
17	1 (1.6)	- (-)	- (-)	*0.196*
20	4 (6.5)	- (-)	- (-)	*0.818*
42	8 (12.9)	2 (18.2)	- (-)	*0.381*
50	2 (3.2)	- (-)	- (-)	*0.398*
51	2 (3.2)	- (-)	- (-)	*0.398*
53	6 (9.7)	1 (9.1)	- (-)	*0.947*
77	2 (3.2)	1 (9.1)	- (-)	*0.648*
91	5 (8.1)	- (-)	- (-)	*0.595*
93	5 (8.1)	2 (18.2)	- (-)	*0.543*
137	5 (8.1)	1 (9.1)	- (-)	*0.950*
294	2 (3.2)	- (-)	- (-)	*0.398*
373	**1 (1.6)**	- (-)	- (-)	*0.196*
408	1 (1.6)	- (-)	- (-)	*0.196*
455	2 (3.2)	2 (18.2)	- (-)	*0.126*
578	1 (1.6)	- (-)	- (-)	*0.196*
714	1 (1.6)	- (-)	- (-)	*0.196*
909	**1 (1.6)**	- (-)	- (-)	*0.196*
1624	**1 (1.6)**	- (-)	- (-)	*0.196*
UKN	4 (6.5)	- (-)	- (-)	*0.196*

New SIT detected in the present study are in bold.

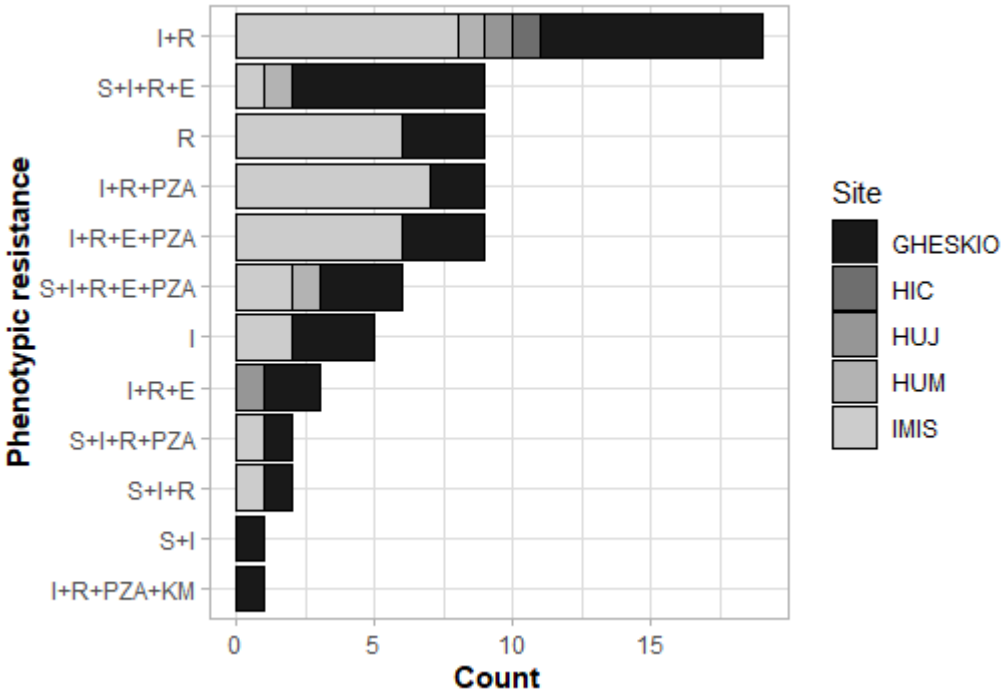

Figure 1S. Description of DR-TB strains phenotypes among all patients with available DST results. A total of 74 DR-TB strains were analyzed, including 12 mono-drug resistant strains and 62 multi-drug resistant TB strains. GHESKIO (INLR): n = 34. IMIS: n = 34. HUM: n = 3. HUJ: n = 2. HIC: n = 1. I: Isoniazid. R: Rifampin. S: Streptomycin. E: Ethambutol. PZA: Pyrazinamide. KM: Kanamycin.

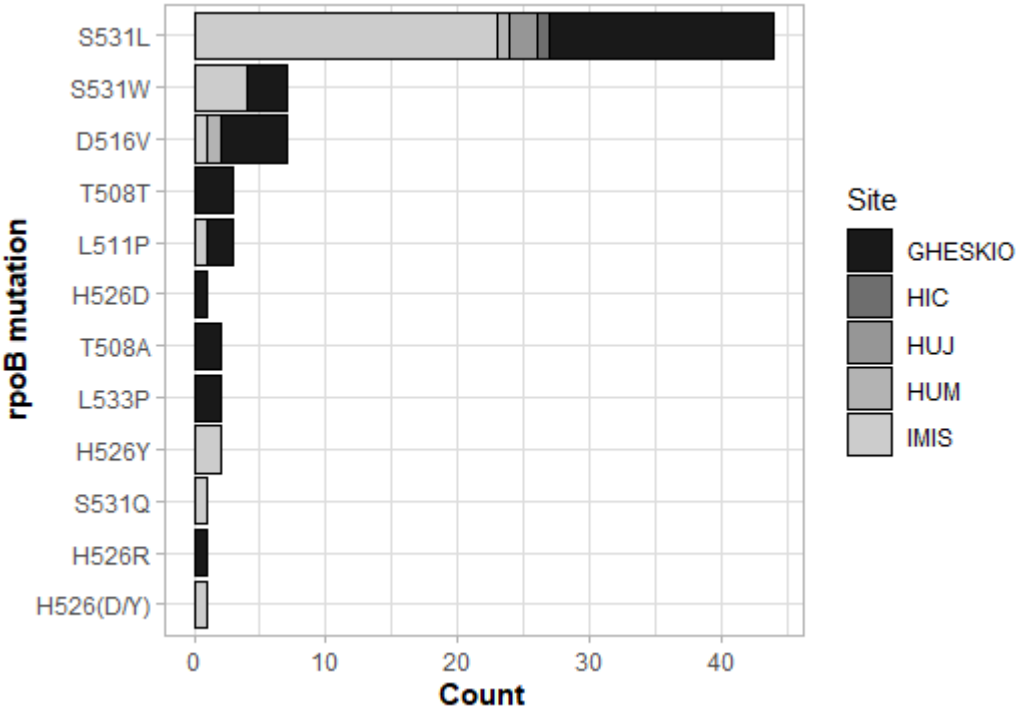

Figure 2S. *rpoB* genotypic diversity of DR-TB isolates (n = 74).

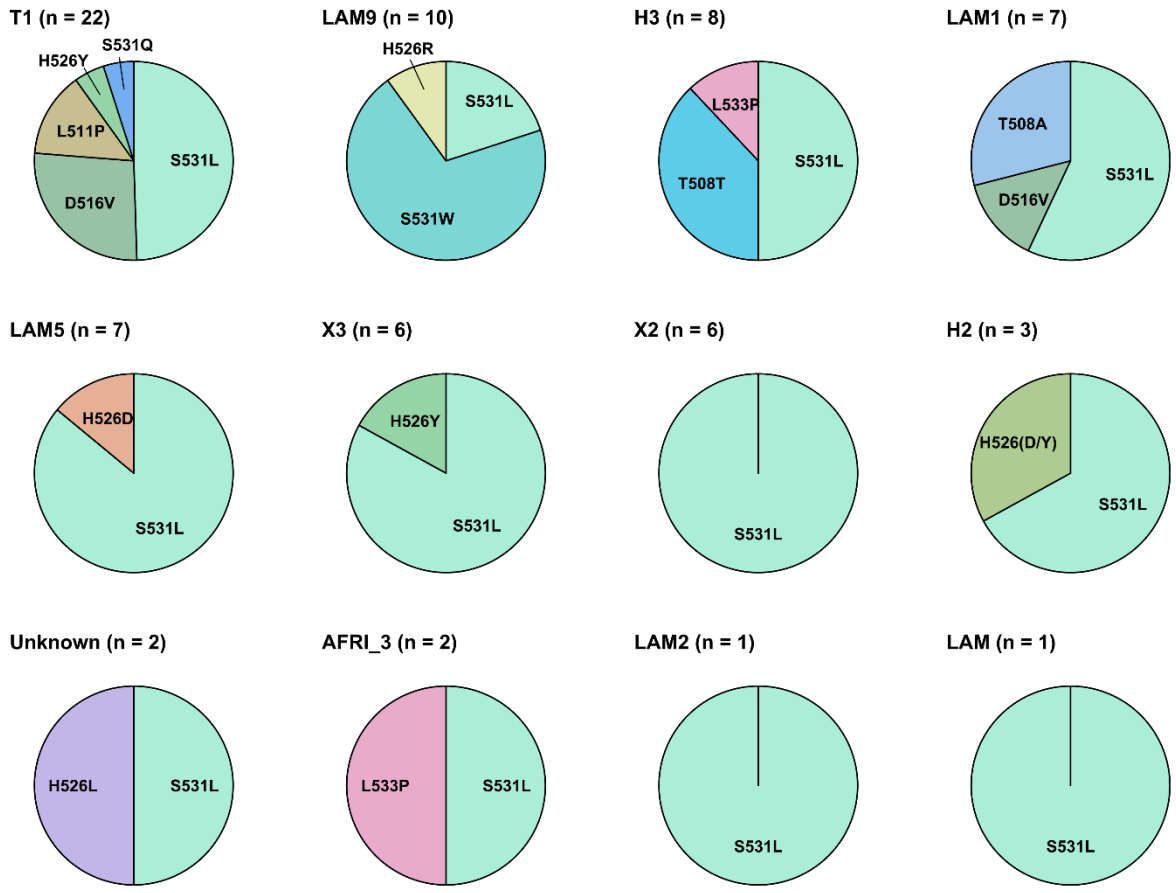

Figure 3S. Frequency of detected rpoB mutation in each identified drug-resistant *M. tuberculosis* lineage (n=74). Data are given for all patients with known spoligotypes.

2.2 Annex 5 – Multi-country evaluation of the blood transcriptomic signature RISK6

Multi-country evaluation of RISK6, a 6-gene blood transcriptomic signature, for tuberculosis diagnosis and treatment monitoring

Rim Bayaa, Mame Diarra Bousso Ndiaye, Carole Chedid, Eka Kokhreidze, Nestani Tukvadze, Sayera Banu, Mohammad Khaja Mafij Uddin, Samanta Biswas, Rumana Nasrin, Paulo Ranaivomanana, Antso Hasina Raherinandrasana, Julio Rakotonirina, Vohangy Rasolofo, Giovanni Delogu, Flavio De Maio, Delia Goletti, Hubert Endtz, Florence Ader, Monzer Hamze, Mohamad Bachar Ismail, Stéphane Pouzol, Niaina Rakotosamimanana, Jonathan Hoffmann.

Scientific reports **2021; 11(1); 1-12.**

scientific reports

Check for updates

OPEN

Multi-country evaluation of RISK6, a 6-gene blood transcriptomic signature, for tuberculosis diagnosis and treatment monitoring

Rim Bayaa[1,2,15✉], Mame Diarra Bousso Ndiaye[1,3,15], Carole Chedid[1,4,5], Eka Kokhreidze[6], Nestani Tukvadze[6], Sayera Banu[7], Mohammad Khaja Mafij Uddin[7], Samanta Biswas[7], Rumana Nasrin[7], Paulo Ranaivomanana[3], Antso Hasina Raherinandrasana[8], Julio Rakotonirina[8], Voahangy Rasolofo[3], Giovanni Delogu[9], Flavio De Maio[9], Delia Goletti[10], Hubert Endtz[11], Florence Ader[12], Monzer Hamze[2], Mohamad Bachar Ismail[2], Stéphane Pouzol[1], Niaina Rakotosamimanana[3,16], Jonathan Hoffmann[1,16✉] & The HINTT working group within the GABRIEL network*

There is a crucial need for non-sputum-based TB tests. Here, we evaluate the performance of RISK6, a human-blood transcriptomic signature, for TB screening, triage and treatment monitoring. RISK6 performance was also compared to that of two IGRAs: one based on RD1 antigens (QuantiFERON-TB Gold Plus, QFT-P, Qiagen) and one on recombinant *M. tuberculosis* HBHA expressed in *Mycobacterium smegmatis* (IGRA-rmsHBHA). In this multicenter prospective nested case–control study conducted in Bangladesh, Georgia, Lebanon and Madagascar, adult non-immunocompromised patients with bacteriologically confirmed active pulmonary TB (ATB), latent TB infection (LTBI) and healthy donors (HD) were enrolled. ATB patients were followed-up during and after treatment. Blood RISK6 scores were assessed using quantitative real-time PCR and evaluated by area under the receiver-operating characteristic curve (ROC AUC). RISK6 performance to discriminate ATB from HD reached an AUC of 0.94 (95% CI 0.89–0.99), with 90.9% sensitivity and 87.8% specificity, thus achieving the minimal WHO target product profile for a non-sputum-based TB screening test. Besides, RISK6 yielded an AUC of 0.93 (95% CI 0.85–1) with 90.9% sensitivity and 88.5% specificity for discriminating ATB from LTBI. Moreover, RISK6 showed higher performance (AUC 0.90, 95% CI 0.85–0.94) than IGRA-rmsHBHA (AUC 0.75, 95% CI 0.69–0.82) to differentiate TB infection stages. Finally, RISK6 signature scores significantly decreased after 2 months of TB treatment and continued to decrease gradually until the

[1]Medical and Scientific Department, Fondation Mérieux, Lyon, France. [2]Laboratoire Microbiologie, Santé et Environnement (LMSE), Doctoral School of Sciences and Technology, Faculty of Public Health, Lebanese University, Tripoli, Lebanon. [3]Institut Pasteur de Madagascar, Antananarivo, Madagascar. [4]Department of Biology, Ecole Normale Supérieure de Lyon, Lyon, France. [5]Equipe Pathogénèse des Légionelles, International Center for Research in Infectiology, INSERM U1111, University Lyon 1, CNRS UMR5308, École Normale Supérieure de Lyon, Lyon, France. [6]National Center for Tuberculosis and Lung Diseases (NCTLD), Tbilisi, Georgia. [7]International Centre for Diarrhoeal Disease Research, Bangladesh (icddr,b), Dhaka, Bangladesh. [8]Centre Hospitalier Universitaire de Soins et Santé Publique Analakely (CHUSSPA), Antananarivo, Madagascar. [9]Dipartimento di Scienze di Laboratorio e Infettivologiche, Fondazione Policlinico Universitario "A. Gemelli", IRCCS, Rome, Italy. [10]Translational Research Unit, Department of Epidemiology and Preclinical Research, "L. Spallanzani" National Institute for Infectious Diseases (INMI), IRCCS, Rome, Italy. [11]Erasmus MC, Medical Microbiology and Infectious Diseases, University Medical Center Rotterdam, Rotterdam, The Netherlands. [12]Service des Maladies Infectieuses et Tropicales, Hospices Civils de Lyon, Lyon, France. [15]These authors contributed equally: Rim Bayaa and Mame Diarra Bousso Ndiaye. [16]These authors jointly supervised this work: Niaina Rakotosamimanana and Jonathan Hoffmann. *A list of authors and their affiliations appears at the end of the paper. ✉email: bayaarim@gmail.com; jonathan.hoffmann@fondation-merieux.org

end of treatment reaching scores obtained in HD. We confirmed the performance of RISK6 signature as a triage TB test and its utility for treatment monitoring.

One fourth of the world population is estimated to be infected with *Mycobacterium tuberculosis* (*Mtb*) that causes approximately 10 million cases of tuberculosis (TB) yearly. This disease ranks among the leading causes of death worldwide, resulting in 1.4 million deaths in 2019[1]. Five to 10% of infected individuals develop the contagious, active form of TB (ATB) disease, while most of them (90%) control the infection and develop asymptomatic latent TB infection (LTBI). However, a small proportion (10%) of LTBI individuals will develop ATB during their lifetime[2]. TB can be treated with a regimen of several antibiotics for a minimum of 6 months. In most patients, TB therapy provides cure[3] but treatment failure and relapse can occur. These outcomes are associated with severe adverse effects and long treatment durations that induce a lack of patient adherence to the treatment regimen thus promoting the emergence of drug-resistance[4].

Current ATB diagnostic tests include sputum-based culture and acid-fast Bacillus (AFB) smear microscopy which are also used for monitoring TB treatment response[1,3]. Molecular tests like the GeneXpert MTB/RIF or ULTRA, are also performed using sputum samples[5]. Interferon (IFN)-γ release assays (IGRAs) such as QuantiFERON-TB Plus (QFT-P; Qiagen) are blood-based tests used for the detection of *Mtb* infection, yet cannot discriminate ATB from LTBI[6–9]. However, the combined use of QFT-P with the heparin-binding hemagglutinin antigen; HBHA-based IGRAs, that relies on the stimulation of whole blood with recombinant *Mtb* HBHA protein expressed in *Mycobacterium smegmatis* (IGRAs-rmsHBHA)[10], recently revealed the potential for the stratification of TB stages (e.g. ATB vs LTBI)[11–14].

Sputum-based TB tests are associated with several limitations including the long-time of culture and the lack of sensitivity and specificity of smear microscopy[15]. Besides, although molecular tests are more sensitive for diagnosing pulmonary TB, they still have limited sensitivity in paucibacillary pulmonary TB patients[16,17]. In addition, sputum samples may be difficult to obtain in some populations (e.g. children and HIV co-infected TB patients) as well as in ATB patients after symptom improvement[18]. In this context, the World Health Organization (WHO) has declared an urgent need for alternative non-sputum-based TB tests with a series of target product profiles (TPPs) which detailed the minimal and optimal criteria that should be met to diagnose and monitor TB treatment response[19–21]. Those new TB tests need to be based on accessible biological samples such as whole blood or urine, and must be practical for field applications[22].

Currently, there is much active research[23,24] on human blood transcriptomic TB biomarkers[25]. A six whole blood gene transcriptomic signature (RISK6) has been recently described and validated in 7 independent cohorts, demonstrating its utility to predict the risk of progression from TB infection to ATB disease, as a screening test for TB, and to monitor TB treatment response[19,26]. The present study aims: to evaluate the robustness of the RISK6 signature in four additional independent cohorts from different countries and ethnicities; to assess its performance for TB screening and triage; to compare its performance to that of two IGRAs (QFT-P and IGRAs-rmsHBHA); and to evaluate its utility for monitoring treatment outcome.

Results

Sociodemographic and clinical characteristics. A total of 141 patients with bacteriologically confirmed pulmonary ATB were included in the study. Their sociodemographic and clinical characteristics were compared at baseline. The median age was 28 years, 66% were male, and 51.8% were smokers. Among them, 48.2% had a positive sputum smear microscopy with a high grade at baseline (2+ or 3+). 97 of these patients were followed at least until the end of treatment and have been successfully treated for TB. The remaining participants included 26 individuals with LTBI and 71 healthy donors (Table 1).

Performance of the RISK6 signature as a screening and triage test for pulmonary TB disease. To investigate the use of RISK6 score as a screening and triage test for TB, we compared RISK6 scores between patients with ATB disease (n = 141), treated TB patients who have been successfully treated for TB (TREATED, n = 97, with negative sputum culture at T2 and/or T3), the individuals with LTBI (n = 26), and healthy donors (HD, n = 71). In all cohorts, RISK6 scores were significantly higher in ATB patients at baseline compared to HD ($p < 0.001$) and TREATED TB patients ($p < 0.001$) (Fig. 1a). Moreover, RISK6 score levels of TREATED patients became indistinguishable from HD. Remarkably, in the Madagascar cohort that includes the enrolled LTBI individuals, we observed a significant difference for the RISK6 scores between ATB and LTBI group ($p < 0.001$) but not between the LTBI group and the TREATED TB patients or the HD group. Remarkably, when we compared the RISK6 scores levels between study sites, we found that the RISK6 scores levels in ATB, TREATED TB patients and the HD recruited from Bangladesh were higher than the levels observed in the other study sites (Fig. 1a).

We then generated a receiver operating characteristic curve (ROC) and the respective areas under the curve (AUC) for each cohort to evaluate, by country, the performance of RISK6 signature as screening or triage test (Fig. 1b). First, we assessed the performance of RISK6 as a screening test for the discrimination between ATB patients and HD. Remarkably, the performance of the RISK6 signature was similar in the four different cohorts, with outstanding AUC values ranging from 90.1% (Bangladesh; 95% CI 80.7–99.4) to 96.4% (Georgia; 95% CI 90.5–100) (Fig. 1b). Secondly, ROC analysis was also performed to determine the potential of RISK6 signature as a triage test to discriminate between different stages of TB infection. Results demonstrated a powerful classifying potential to discriminate patients with ATB from LTBI or TREATED TB patients with an AUC of 92.8% (95% CI 85.6–100) and 96.1% (95% CI 91.7–100) respectively (Fig. 1b). Remarkably, we also found that the discrimination between ATB and HD was lowest in the cohort of Bangladesh when compared to other study sites (Fig. 1b).

	Georgia	Madagascar	Lebanon	Bangladesh	Total
ATB (N)	32	44	21	44	141
ATB patient demographics					
Age (years)	33.5 (26.75–44.5)	29.5 (21.75–43.25)	30 (22–37)	23.5 (20.75–30.5)	28 (22–39)
Gender (male)	81.2% (26/32)	59.1% (26/44)	47.6% (10/21)	70.5% (31/44)	66% (93/141)
BMI at baseline	20.06 (18.65–21.67)	17.19 (16.31–18.67)	20.94 (19.59–21.41)	18.28 (16.2–20.79)	18.68 (16.89–20.95)
Vaccination					
BCG vaccination	40.6% (13/32)	88.6% (39/44)	19% (4/21)	75% (33/44)	63.1% (89/141)
Risk factors					
Smoking habit	59.4% (19/32)	43.2% (19/44)	57.1% (12/21)	52.3% (23/44)	51.8% (73/141)
Alcohol consumption	9.7% (3/31)	45.5% (20/44)	9.5% (2/21)	11.4% (5/44)	21.4% (30/140)
Injecting drug users	–	–	–	9.3% (4/43)	2.9% (4/138)
Jail detention history	6.2% (2/32)	2.4% (1/42)	14.3% (3/21)	4.5% (2/44)	5.8% (8/139)
Other pathologies					
HCV positive	9.4% (3/32)	2.3% (1/44)	–	–	2.8% (4/141)
Other underlying disease	–	9.1% (4/44)	9.5% (2/21)	2.3% (1/44)	5.5% (7/127)
Sputum smear microscopy at baseline					
Low grade (1+ or scanty)	37.5% (12/32)	25% (11/44)	28.6% (6/21)	27.3% (12/44)	29.1% (41/141)
High grade (2+ or 3+)	25% (8/32)	54.5% (24/44)	38.1% (8/21)	63.6% (28/44)	48.2% (68/141)
Negative	34.4% (11/32)	20.5% (9/44)	19% (4/21)	9.1% (4/44)	19.9% (28/141)
Not evaluated	3.1% (1/32)	–	14.3% (3/21)	–	2.8% (4/141)
TB treatment					
Treated	26	33	15	23	97
LTBI (N)	–	26	–	–	26
Healthy donors (N)	7	23	25	16	77

Table 1. Baseline sociodemographic and clinical characteristics of ATB patients in the four cohorts. *TB* Tuberculosis, *BMI* Body Mass Index, *LTBI* latent TB infection, *IQR* interquartile range. Data were given as % (N) or median (IQR).

Performance of RISK6 signature benchmarked against the WHO TPP for a non-sputum based diagnostic test. Our findings were then benchmarked against the WHO TPP for a screening/triage test for TB that should have a minimum sensitivity of > 90% and specificity of ≥ 70%[19,27]. At a sensitivity set to > 90%, the performance of RISK6 signature as screening/triage test demonstrated specificity scores of > 70% in all cohorts, except for Bangladesh (Table 2). This shows that RISK6 signature achieves the minimal WHO TPP for non-sputum-based screening and triage tests discriminating patients with ATB from both HD and LTBI groups.

Performance of RISK6 as a confirmatory test for pulmonary TB disease. Our next aim was to evaluate the performance of RISK6 signature in sputum smear-negative and culture-confirmed TB individuals. Based on the TPP criteria set by the WHO as a reference[19,27], we found that RISK6 achieved the minimal sensitivity of > 60% with 100% specificity for an initial TB diagnostic test for sputum smear-negative TB to replace smear microscopy in the cohort from Georgia (Table 2). Similarly, in the same cohort, RISK6 signature also reached the minimum criteria of 65% sensitivity and 100% specificity for a confirmatory test. However, RISK6 signature detection failed to meet these WHO requirements in the other study sites (Table 2).

As most ATB patients had a positive sputum smear microscopy with a high grade at baseline, we wondered if RISK6 scores and mycobacterial loads were correlated. We therefore performed a sub-analysis on stratified sputum smear microscopy results among ATB patients, defined as follow: negative smears, low-grade positive smears (1+ or scanty) and high-grade positive smears (2+ or 3+). RISK6 scores in the negative smear group showed a significant difference ($p < 0.001$) compared to HD (Fig. 2). Moreover, RISK6 scores were significantly lower (median = 0.31, IQR 0.22–0.40) in negative smears than in individuals with low- or high-grade positive smears ($p < 0.001$). While not statistically different ($p > 0.05$), RISK6 scores in the high-grade smear group were higher (median = 0.5, IQR 0.40–0.56) than in the low-grade mycobacterial load group (median = 0.46, IQR 0.38–0.52).

Performance of RISK6 signature compared to IGRAs. Next, we assessed the performance of RISK6 signature compared to two assays based on IFN-γ release: the commercial QFT-P, and the non-commercial IGRAs-rmsHBHA. Compared to the QFT-P assay, the RISK6 signature achieved better performance in AUC (94.1% vs 57.2%), sensitivity (90.9% vs 50.9%) and specificity (87.8% vs 57.2%) to discriminate ATB patients from an asymptomatic population (LTBI + HD) (Table 3). However, a comparative sub-analysis indicated a lower positive (79.7%) and negative (50%) predictive values of the RISK6 signature when compared to QFT-P assay (100% and 63.9%, respectively) in detection of *Mtb*-infected individuals (ATB + LTBI) from uninfected ones (HD). Notably, the RISK6 signature showed a higher performance (AUC 90.9%, 95% CI 87.2–94.5), with 90.1% sensitivity and 72.2% specificity than the IGRAs-rmsHBHA (AUC 75.3%, 95% CI 68.6–82) that achieved

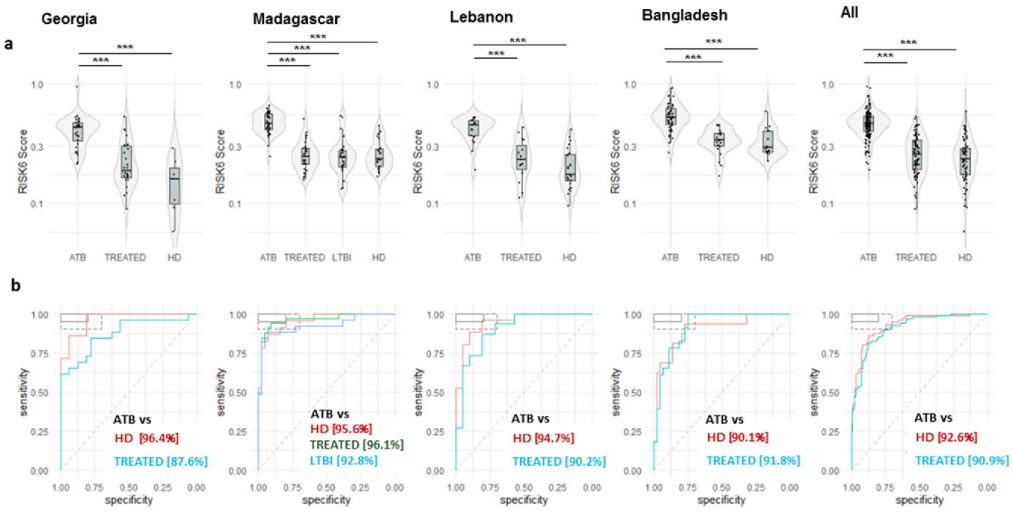

Figure 1. Validation of the performance of a multi-cohort 6-gene signature; RISK6 as a screening and triage test in patients with pulmonary TB. (**a**) Violin plots showing the differences in the levels of RISK6 signature scores from patients with active TB at baseline (ATB, n = 141), treated TB patients (TREATED, n = 97; patients with a negative sputum culture at T2 and/or T3), individuals with a latent TB infection (LTBI, n = 26), and healthy donors (HD, n = 71) from Georgia, Madagascar, Lebanon, Bangladesh and in all sites. Horizontal lines designate medians, boxes represent the inter-quartile ranges (IQR) and the ranges are represented by whiskers. Single patient results are represented by each dot in the graph. Statistical significance was calculated using Mann–Whitney U test. *Indicates a p-value < 0.05, **indicates a p-value < 0.01, and ***indicates a p-value < 0.001. (**b**) Receiver operating characteristic (ROC) curve analysis and the respective areas under the curve (AUC) with 95% confidence intervals showing the performance of the RISK6 signature to discriminate between ATB patients at baseline, HD and LTBI. In the top left box, the solid and dashed lines represent the respective optimal and minimum criteria set by the WHO in the target product profile (TPP) for a screening/triage test for TB.

lower sensitivity and specificity (83.8% and 59.8% respectively) to differentiate *Mtb*-infection status (i.e. ATB vs TREATED TB patients) (Table 3).

RISK6 as a biomarker for TB treatment monitoring. Patients with successful treatment (defined as negative sputum culture at T2) were selected to determine whether RISK6 signature was a clinically relevant biomarker for TB treatment monitoring. Overall, in all cohorts combined, we observed a significant drop in RISK6 scores after two months of treatment (T1, $p < 0.001$) and until treatment completion (T2, $p < 0.001$). Moreover, RISK6 scores were significantly higher in cured TB patients (T2, $p > 0.05$) when compared to HD, however, in each of the four cohorts, there were no significant difference between these two groups ($p > 0.05$) (Fig. 3a). Similarly, analytical performance demonstrated capacity of RISK6 signature to significantly discriminate patients at baseline and two months after treatment initiation (AUC 69.7%, 95% CI 57.1–79.6) (Fig. 3b and Supplementary Table 6). Noticeably, by the end of treatment, the majority of patients had lower RISK6 score levels, further enhancing the discriminatory power between ATB patients at T0 and T2 (AUC 87.1, 95% CI 77.6–94.3) and at T3 (AUC 90.4, 95% CI 82.6–96.6) (Fig. 3b and Supplementary Table 6).

Furthermore, we evaluated whether RISK6 allows the discrimination of cured TB patients (n = 104) from those with a treatment failure (defined as positive sputum culture at T2, n = 2). Thereafter, patients were stratified into drug-sensitive (DS) and drug-resistant TB (DR-TB) cases and the RISK6 signature scores were compared within these groups. We found that RISK6 scores decreased throughout treatment among DS-TB patients independently of treatment outcome (Supplementary Fig. 1). In contrast, the RISK6 score remained stable at baseline and during treatment in a DR-TB patient with a treatment failure. Importantly, RISK6 score levels during TB treatment seem to be higher in patients with treatment failure among both DS and DR-TB cases. However, in a univariate or multivariate analyses, no significant association of the RISK6 score at baseline with treatment failure was found (Supplementary Table 8).

TPP requirement		Cut-off	Sensitivity%	Specificity%	Cases, n	Controls, n	AUC	AUC 95%CI
Screening test (ATB vs HD)								
Georgia	Sensitivity > 90%	> 0.2583	90.6	85.7	32	7	96.4%	90.5–100%
Madagascar		> 0.3697	90.9	87	44	23	95.6%	90.9–100%
Lebanon		> 0.3171	90.5	88	21	25	94.7%	88.6–100%
Bangladesh		> 0.3625	90.9	68.8	44	16	90.1%	80.7–99.4%
All		> 0.3209	90.1	80.3	141	71	92.6%	88.8–96.3%
Triage test (ATB vs LTBI)								
Madagascar	Sensitivity > 90%	> 0.3697	90.9	88.5	44	26	92.8%	85.6–100%
Initial TB diagnostic test to replace smear microscopy (ATB (CLT^+ AFB^-) vs HD)								
Georgia	Sensitivity ≥ 60%	> 0.3514	63.6	100	11	7	94.8%	85.1–100%
Madagascar		> 0.4298	66.7	95.7	9	23	96.1%	90.1–100%
Lebanon		> 0.3217	75	88	4	25	90%	78.2–100%
Bangladesh		> 0.3541	75	68.8	4	16	79.7%	58.8–100%
All		> 0.3823	60.7	88.7	28	71	87.7%	80.6–94.8%
Confirmatory test (ATB (CLT^+ AFB^-) vs HD)								
Georgia	Sensitivity ≥ 65%	> 0.3131	72.7	100	11	7	94.8%	85.1–100%
Madagascar		> 0.4298	66.7	95.7	9	23	96.1%	90.1–100%
Lebanon		> 0.3217	75	88	4	25	90%	78.2–100%
Bangladesh		> 0.3541	75	68.8	4	16	79.7%	58.8–100%
All		> 0.3674	67.9	87.3	28	71	87.8%	80.6–94.8%

Table 2. Receiver operating characteristic curve analysis of the performance of the RISK6 signature to distinguish active TB cases (ATB) from healthy donors (HD) and from latent TB infected individuals (LTBI) in cohorts from Georgia, Madagascar, Lebanon, and Bangladesh. The performance of the signature is benchmarked against the WHO TPP for a non-sputum based screening/triage test (at a sensitivity of > 90%, the minimum specificity as set out in this TPP should be ≥ 70%), for an initial TB diagnostic test to replace sputum smear (at minimum 60% sensitivity, the minimum specificity as set out in this TPP should be > 98%) and for a confirmatory test (at minimum 65% sensitivity, the minimum specificity as set out in this TPP should be > 98%)[19]. *ATB* active TB, *LTBI* latent TB infection (were only recruited from Madagascar), *HD* healthy donors, CLT^+ positive sputum culture, AFB^- negative AFB smear microscopy, *AUC* area under the curve, *CI* confidence interval, *Vs* versus.

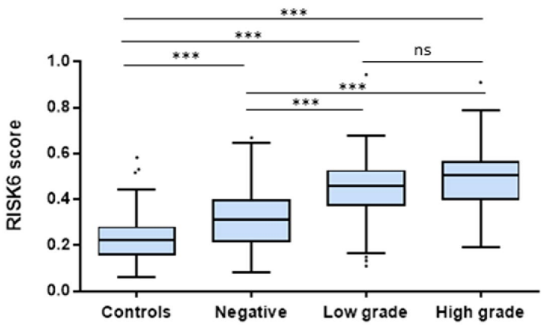

Figure 2. Correlation between RISK6 signature scores and mycobacterial loads determined by sputum smear microscopy in ATB patients. Boxplots comparing the RISK6 score levels stratified according to sputum smear grade: Negative smears, low grade positive smears (1+ or scanty) and high grade positive smears (2+ or 3+). Horizontal lines designate medians, boxes represent the inter-quartile ranges (IQR) and the ranges are represented by whiskers. Individual dots represent the results of patients with a RISK6 scores out of IQR. Statistical significance was calculated using Mann–Whitney U test. *Ns* non-significant, ***indicates a p-value < 0.001. *HD* Healthy donors.

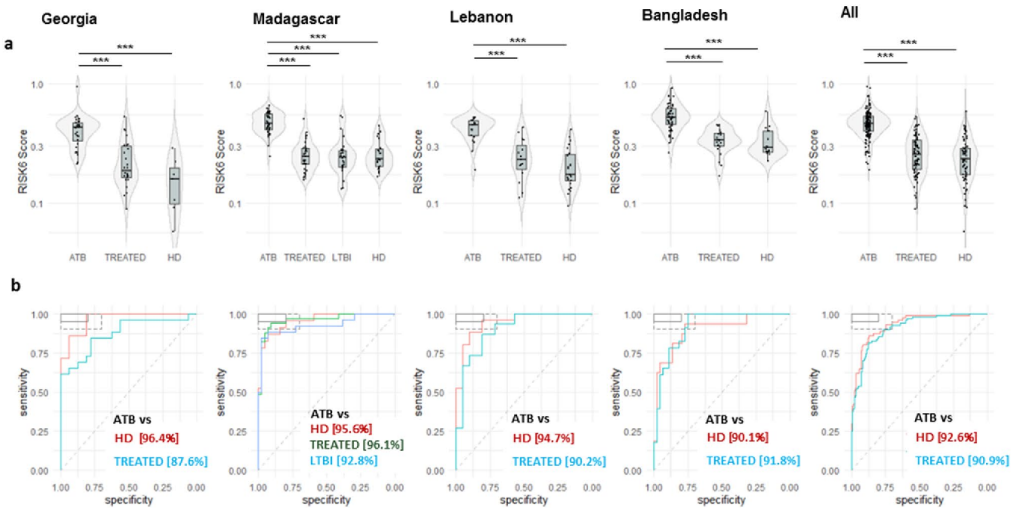

Figure 1. Validation of the performance of a multi-cohort 6-gene signature; RISK6 as a screening and triage test in patients with pulmonary TB. (**a**) Violin plots showing the differences in the levels of RISK6 signature scores from patients with active TB at baseline (ATB, n = 141), treated TB patients (TREATED, n = 97; patients with a negative sputum culture at T2 and/or T3), individuals with a latent TB infection (LTBI, n = 26), and healthy donors (HD, n = 71) from Georgia, Madagascar, Lebanon, Bangladesh and in all sites. Horizontal lines designate medians, boxes represent the inter-quartile ranges (IQR) and the ranges are represented by whiskers. Single patient results are represented by each dot in the graph. Statistical significance was calculated using Mann–Whitney U test. *Indicates a p-value < 0.05, **indicates a p-value < 0.01, and ***indicates a p-value < 0.001. (**b**) Receiver operating characteristic (ROC) curve analysis and the respective areas under the curve (AUC) with 95% confidence intervals showing the performance of the RISK6 signature to discriminate between ATB patients at baseline, HD and LTBI. In the top left box, the solid and dashed lines represent the respective optimal and minimum criteria set by the WHO in the target product profile (TPP) for a screening/triage test for TB.

lower sensitivity and specificity (83.8% and 59.8% respectively) to differentiate *Mtb*-infection status (i.e. ATB vs TREATED TB patients) (Table 3).

RISK6 as a biomarker for TB treatment monitoring. Patients with successful treatment (defined as negative sputum culture at T2) were selected to determine whether RISK6 signature was a clinically relevant biomarker for TB treatment monitoring. Overall, in all cohorts combined, we observed a significant drop in RISK6 scores after two months of treatment (T1, $p < 0.001$) and until treatment completion (T2, $p < 0.001$). Moreover, RISK6 scores were significantly higher in cured TB patients (T2, $p > 0.05$) when compared to HD, however, in each of the four cohorts, there were no significant difference between these two groups ($p > 0.05$) (Fig. 3a). Similarly, analytical performance demonstrated capacity of RISK6 signature to significantly discriminate patients at baseline and two months after treatment initiation (AUC 69.7%, 95% CI 57.1–79.6) (Fig. 3b and Supplementary Table 6). Noticeably, by the end of treatment, the majority of patients had lower RISK6 score levels, further enhancing the discriminatory power between ATB patients at T0 and T2 (AUC 87.1, 95% CI 77.6–94.3) and at T3 (AUC 90.4, 95% CI 82.6–96.6) (Fig. 3b and Supplementary Table 6).

Furthermore, we evaluated whether RISK6 allows the discrimination of cured TB patients (n = 104) from those with a treatment failure (defined as positive sputum culture at T2, n = 2). Thereafter, patients were stratified into drug-sensitive (DS) and drug-resistant TB (DR-TB) cases and the RISK6 signature scores were compared within these groups. We found that RISK6 scores decreased throughout treatment among DS-TB patients independently of treatment outcome (Supplementary Fig. 1). In contrast, the RISK6 score remained stable at baseline and during treatment in a DR-TB patient with a treatment failure. Importantly, RISK6 score levels during TB treatment seem to be higher in patients with treatment failure among both DS and DR-TB cases. However, in a univariate or multivariate analyses, no significant association of the RISK6 score at baseline with treatment failure was found (Supplementary Table 8).

and score changes over time despite the heterogeneity of both cohorts and study designs. In addition, marked technical differences are also apparent between our studies: we performed the RISK6 scores measurements on RNA manually isolated from whole blood collected directly in Tempus Blood RNA tubes and from blood samples first collected in lithium heparin tube and then transferred in Tempus Blood RNA Tubes, while this measurement was done by Penn-Nicholson et al. using RNA extracted manually or by an automated processes from whole blood collected in PAXgene Blood RNA tubes. Collectively, these results highlight the robustness of this PCR-based host-blood transcriptomic signature.

Besides, the higher RISK6 score levels detected in the cohort of Bangladesh compared to the other study sites was a remarkable result. We hypothesized that these RISK6 scores observed in Bangladesh may be influenced by the differing epidemiology, geographical locations as well as differences in gene expression levels between ethnic populations that may have contributed to a stronger transcriptomic signal in Bangladesh.

Our AUC data showed that RISK6 scores had a powerful ability to distinguish ATB from HD, with better or equal results to what was found with other transcriptomic signatures[28–34]. Moreover, while these previous signatures have shown promise as diagnostic tests, it should be noted that results of a three gene signature were not generalizable[28,34], while other signatures[33] require measurement of a high number of genes, thus limiting their possible application in resource-limited settings. Moreover, while RISK6 signature seems to meet or exceeded the TPP criteria based on each of our four cohorts, only two among the previous signatures (Sweeney3[28] and Sambarey10[32]) satisfied the sensitivity and specificity TPP criteria set by the WHO for a triage test[35]. However, it would be interesting to validate those signatures in other independent cohorts[28,36].

An important finding of our study is that RISK6 signature allowed to stratify TB patient's stages. Thus, when applied to the cohort of Madagascar, the only one including LTBI cases, the RISK6 signature demonstrated a significantly higher score in ATB individuals at baseline compared to those with LTBI. This is consistent with a previous study showing that a 3-gene transcriptomic signature was significantly higher in ATB patients versus LTBI[28] individuals, in addition to a 20-gene signature set that also discriminated ATB patients from LTBI and healthy controls[18]. In the same way, some gene-signatures were also evaluated[18] and showed high specificity and sensitivity to distinguish ATB patients from those with LTBI[23,28,31,33]. In our study, at > 90% sensitivity, RISK6 signature discriminated ATB from both LTBI and HD with a specificity > 70% which met the WHO TPP for a triage test for TB. Besides, no significant differences in the classification performance of RISK6 signature were observed between LTBI and HD, in line with recent transcriptomic studies demonstrating failure in discriminating LTBI from HD[18,28]. Moreover, while no previous studies has compared the levels of a transcriptomic signature between LTBI and treated TB patients, our data showed that the RISK6 signature reached the same score levels in treated TB patients when compared to LTBI individuals. Hence, it will be of interest to validate RISK6 signature in cohorts with larger number of latently infected individuals.

An additional finding of our study is that RISK6 signature also achieved the minimal WHO criteria in the Georgia cohort, for (i) an initial TB diagnostic test for sputum smear-negative TB to replace smear microscopy, using culture-confirmed TB as a gold standard (ii) and a non-sputum-based confirmatory test for sputum smear-negative TB. In this context, Turner et al.[37] reported a comparison of 27 signatures in cohorts of 181 patients for discriminating TB and no TB disease. They found that no previously published signatures achieved the minimal WHO sensitivity (65%) and specificity (98%) performance for a non-sputum-based confirmatory test for sputum smear-negative TB. Thus, our results are promising but further validation of RISK6 signature in larger cohorts will allow testing such performance. Furthermore, we found that ATB patients with low- or high-grade positive smears had significantly higher RISK6 scores compared with those with negative smears. Similarly to previous reported results with either Xpert MTB/RIF test or the C-reactive protein (CRP) concentration measurements[38,39], our findings suggest that RISK6 signature scores directly correlate with sputum smear grade, and may possibly represent a useful tool in the identification of patients with high transmission risk.

In the present study, we also attempted to compare the performance of different TB blood-based tests; RISK6 versus two IGRAs (QFT-P and IGRAs-rmsHBHA). Our results indicate that the performance of RISK6 was greater than that of QFT-P assay for ATB case-finding. Given that QFT-P was not recommended for the diagnosis of ATB but for LTBI diagnosis, we and others have shown that this assay is a better indicator for the detection of *Mtb* infection[12,40,41].

Our next aim was to evaluate variations in the RISK6 scores throughout successful treatment. We found that the RISK6 signature scores were significantly higher in ATB at baseline compared to HD, and continued to decrease progressively until the end of treatment reaching scores obtained in HD. Moreover, we also demonstrated that the RISK6 signature enables discrimination with high accuracy between untreated (T0), treated (T1 and T2), and post-treated (T3) TB patients who achieved a clinical cure. Taken together, these results showed the RISK6 genes might be modulated during anti-TB treatment as early as 2 months. Notably, the well-established data by Penn Nicholson et al.[26] also included additional earlier time points (week 1 and week 4) and found that RISK6 signature scores decrease over the course of successful treatment as early as 1 week. Data obtained with RISK6 is consistent with previous studies showing that transcriptomic signatures could be used as a powerful tool to monitor TB treatment response[30,42–46]. In this context, it has been previously reported that reduced gene expression levels occurred rapidly during the first and the second weeks of TB treatment[47,48]. An additional report showed that ATB gene set decreased after 4 months of anti-TB treatment, however, no tests were performed at earlier time points, or during TB treatment course[49]. To note, we showed that the RISK6 signature scores returned to normal levels (compared to HD) after 6 months of treatment, which confirmed previous data[26] but contrasted with another transcriptomic study showing that normal levels were reached 12 months after the treatment initiation[30]. Subsequently, these results indicate that RISK6 scores significantly stratified end of treatment from pre-treatment baseline. Taken together, our findings suggest that RISK6 signature could be used as a useful tool to monitor the response to anti-TB treatment. It may represent a potential alternative of the current tests used

to assess TB treatment efficacy and used comparing its result with those obtained by sputum culture that are crucial to evaluate drug resistance occurrence.

Remarkably, RISK6 relies on the use of qRT-PCR that could detect low levels of gene expression[50] and could be integrated into clinical poor settings in contrast to other complex methods. Besides, this signature requires the measurement of a small number of genes with subsequent reduced complexity and costs. Moreover, a key advantage of RISK6 is that it is a blood-based test, which is an easily accessible sample. Blood transcriptomic tests will improve the diagnosis of TB allowing faster treatment and thus reduction of transmission, especially in children, HIV co-infected TB patients and paucibacillary pulmonary TB patients. In such populations, microbiological tests are not always feasible due to the limited ability to produce good quality sputum samples or due to low bacterial loads in their samples. In the future, it will be of interest (i) to evaluate if RISK6 is able to predict the risk of progression to TB as demonstrated by the RISK11 signature[25] and (ii) to assess the diagnostic performance of RISK6 signature as a prototype cartridge assay as it has already been evaluated for the 3-gene signature against a microbiological reference standard[51].

This study was subject to several limitations. Indeed, the sample size was relatively small and LTBI individuals were recruited from only one country. Hence, validation of our findings in cohorts with larger number of LTBI individuals is required to better estimate specificities and sensitivities for a triage test. Moreover, only two patients had failed treatment. Therefore, further validation is required to better understand how RISK6 signature tracks with response to treatment. Additionally, we excluded diabetic and HIV-positive patients and immunosuppressed individuals in general and our study was restricted to adults. Thus, similar validation studies are needed for children and HIV-positive patients. Moreover, in future studies, it would be relevant to evaluate the specificity of the RISK6 scores in comparison to other respiratory diseases than TB, which is considered as most difficult to distinguish with.

In conclusion, data from this study provide strong proof that RISK6 can be applied as a non-sputum-based screening and triage test that met the WHO TPP benchmarks. This host response-based gene signature may be used for stratifying patients according to their TB infection status, as well as for monitoring patients over the course of treatment. RISK6 signature is applicable using a robust and simple qRT-PCR platform which facilitates its implementation in the clinical laboratories located in resource-poor settings. Our overall findings support the efforts to incorporate RISK6 signature into a point-of-care test ensuring rapid and accurate detection of ATB cases. Indeed, such simple tests are highly needed to reduce TB spread and transmission especially in areas with high TB burden that are usually disturbed with poverty.

Methods

Study design and population. This evaluation of the RISK6 signature was a nested case–control multicenter prospective cohort study evaluating the prognostic value of blood-based immunological biomarkers for monitoring TB treatment outcome. It was conducted within the GABRIEL Network[52] in four different countries including Bangladesh, Georgia, Lebanon and Madagascar.

In total, 238 participants were recruited and followed-up between August 2018 and September 2020. Participants included patients with ATB disease (n = 141), HD (n = 71) and individuals with LTBI (n = 26). Enrolled ATB patients aged ≥ 15 years old, newly diagnosed with pulmonary ATB: scoring positive for TB following bacteriological (culture positive and/or sputum smear microscopy positive) and/or molecular analysis (GeneXpert positive results) were recruited at primary healthcare TB clinics in each country: National Center for Tuberculosis and Lung Diseases (NCTLD) in Tbilisi, Georgia; Tuberculosis screening and treatment center (CHUSSPA) related to National Tuberculosis Programs (NTPs) in Antananarivo, Madagascar; NTP centers in Tripoli and Akkar, Lebanon and International Centre for Diarrhoeal Disease Research, Bangladesh (icddr,b) in Dhaka, Bangladesh. Clinically asymptomatic healthy donors; who do not have a previous TB history and who have no recent TB contacts were also recruited in all sites. In Madagascar, participants with positive QFT-P results (IFN-γ production ≥ 0.35 IU/mL) were defined as latently *Mtb* infected individuals. Patients with negative cultures at inclusion, ATB patients with Human Immunodeficiency Virus (HIV) or with diabetes mellitus comorbidities and patients under immunocompromising treatment were excluded (Fig. 4).

Enrolled ATB patients were followed-up during the treatment course at four different time points and classified as follow: (i) ATB at baseline T0: patients who didn't start TB treatment; (ii) treated active TB at T1 and T2: patients with ATB followed-up during the treatment and tested after 2 months of the start of the treatment (T1), and at the end of treatment (T2); (iii) treated active TB at T3: treated TB patients tested at 2 months after treatment completion.

Ethics statement. The study protocols were reviewed and approved by the human research ethics committees in each country; Georgia, the Institutional Review Board of the National Center for Tuberculosis and Lung Diseases (NTCLD) (Reference number: IORG0009467), Madagascar, the Ministry of Public Health and the Ethical Committee for Biomedical Research (Reference number: n°099-MSANP/CERBM), Lebanon, the institutional review board of NINI hospital (Reference number: IRB-F-01) and Bangladesh, the Research Review Committee and the Ethical Review Committee of International center for diarrheal diseases and research (icddr,b). All study participants provided written informed consent. All research was performed in accordance with relevant guidelines/regulations.

Diagnostic assessment and follow-up. ATB diagnosis was based on both bacteriological and molecular parameters. At least one sputum sample was collected at inclusion (T0) for culture testing (liquid culture media: MGIT mycobacterial growth indicator tube, BD BioSciences, NJ, USA and/or solid culture media: L–J (Lowenstein–Jensen) and also tested by microscopy for the presence of acid-fast bacilli (AFB) using the Ziehl–Neelsen

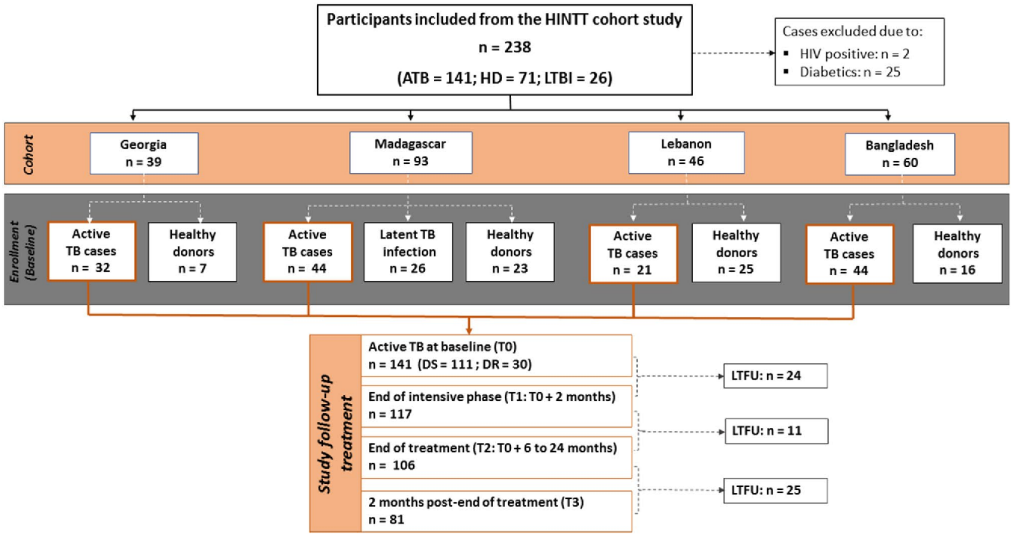

Figure 4. Flow diagram describing the enrollment and exclusion of participants with active TB, latent TB infection, and healthy donor participants from the different cohorts. ATB patients were followed-up at four different time points: at baseline (T0), ATB patients who didn't their TB treatment and followed throughout antibiotic therapy: at month 2 (T1), at the end of treatment (T2), and 2 months after treatment completion (T3). *TB* Tuberculosis, *ATB* active TB, *LTBI* Latent TB infection, *HD* healthy donors, *HIV* human immunodeficiency virus, *DS* drug-susceptible, *DR* drug-resistant, *LTFU* lost to follow-up.

staining method and/or Auramine O staining. In addition to positive culture, active TB status was defined by positive Xpert MTB/RIF (Cepheid). Patients were re-evaluated by sputum smear and culture during the intensive phase of treatment (T1) thereafter at the end of treatment (T2) and 2-months after treatment completion (T3) to confirm that they were successfully treated and cured. Drug susceptibility testing (DST) methods were performed according to standard protocols[53].

Demographic and clinical data collection. At enrollment and at each follow-up visit, medical history, clinical and demographic data were collected using standardized questionnaires to feed the cloud-based database system CASTOR (CASTOR Electronic Data Capture, Version 1.4, Netherlands).

Blood collection process. A minimum of 3 mL of whole blood for transcriptomic analysis and 5 mL for the Interferon-γ release assays were drawn from each participant. For transcriptomic analysis, specimens were directly collected in Tempus Blood RNA Tubes (Applied Biosystems, 4342792), vigorously shaken, and stored at − 80 °C. Of note, in Madagascar and Bangladesh, blood samples were first collected in lithium heparin tubes and then transferred in Tempus Blood RNA Tubes for transcriptomic analysis.

RNA extraction process and complementary DNA (cDNA) synthesis. Frozen Tempus Blood RNA tubes were thawed and RNA was manually extracted using the MagMAX™ for Stabilized Blood Tubes RNA Isolation Kit (Applied Biosystems by Thermo Fisher Scientific, 4451893) following the manufacturer's instructions. RNA elution was performed by adding 30 µL of Elution Buffer. The purified RNA was transferred to a nuclease-free tube, assessed for quantity and quality (Nanodrop spectrophotometer), and stored at − 80 °C until needed. The cDNA was synthetized using the Applied High Capacity RNA to cDNA kit (Applied Biosystems by Thermo Fisher Scientific, 4387406). The RT reaction mix was prepared as follows: 10 µL of 2xRT buffer mix, 1 µL of 20 × RT Enzyme, and 3 µL of nuclease-free water. Then 6 µL of purified RNA/negative control samples were added and proceeded using random hexamer primers (1 h 37 °C, 5 min 95 °C and hold 4 °C). cDNA was then 1:5 diluted (nuclease-free water) and stored at − 20 °C for long-term conservation.

Pre-amplification PCR. Prepared cDNA was pre-amplified using specific sequences of TaqMan primer-probes as previously described by Penn-Nicholson et al.[26]. 5 µL of 2 × PCR mix (TaqMan Universal PCR Master Mix 2×) (Applied Biosystems by Thermo Fisher Scientific, 4304437) with 2.5 µL of the specific primers-probes mix (PPM 0.6×), composed of primers of the 6 genes (listed in Supplementary Table 1) (Applied Biosystems by Thermo Fisher Scientific) was mixeded. Then 2.5 µL of the diluted cDNA/negative control samples were added and the mixture was incubated 10 min at 95 °C followed by 16 cycles of amplification at 95 °C for 15 s, 60 °C for

4 min, and hold at 4 °C. The pre-amplified PCR products were diluted 1:25 with nuclease-free water and stored at − 20 °C for long-term conservation.

Quantitative Real-Time PCR (qRT-PCR) assay and gene expression analysis. For every target to amplify, 4 µL of pre-amplified DNA was subjected to a real time nucleic acid amplification using 10 µL of TaqMan Universal PCR Master Mix (Applied Biosystems by Thermo Fisher Scientific), 1 µL of primers-probe mix (20×) and 4 µL of nuclease-free water using the following conditions: 2 min at 50 °C, 10 min at 95 °C, followed by 95 °C for 15 s and 60 °C for 1 min for 40 cycles. For analytical reasons, all the PCR reactions were performed in duplicate.

RISK6 score generation. Polymerase chain reaction signals were analyzed using CFX Manager Software version 3.1 (BioRad) in regression mode and expressed as cycle threshold (Ct) values. The step-by-step procedure for computing the 6-gene signature (RISK6) scores was performed as described by Penn-Nicholson et al.[26]. Briefly, the mean of Ct values was calculated for every targeted genes and combined to generate a score. The score was computed with R script available on https://bitbucket.org/satvi/risk6/src/master/.

QuantiFERON-TB Gold Plus and IGRAs-rmsHBHA assays. 1 mL of whole blood was collected directly into each of the QFT-P tubes (Qiagen, Hilden, Germany, 622526) (Nil: Negative Control, TB-Antigens (TB1/TB2) and Mitogen: Positive control) and an extra 1 mL of blood was collected in a heparin tube and stimulated with 10 µg/mL of rmsHBHA (UNICATT, Rome, Italy[10101010]). After 16–24 h incubation at 37 °C, plasma samples were harvested and stored at − 80 °C prior subjected to QFT-P ELISA (Qiagen, Hilden, Germany, 622120), following the manufacturer instructions. Briefly, 50 µL of plasma samples were tested, optical density results were compared to log-normalized values from freshly reconstituted IFN-γ kit standards. To account for potential immunomodulation phenomena unrelated with TB treatment, baseline IFN-γ level values (Nil tubes) were subtracted from antigen-stimulated IFN-γ values (TB1, TB2, Mitogen and rmsHBHA). According to the kit's sensitivity range, the maximum for IFN-γ level values was set at 10 IU/mL and negative values were rescaled to 0.

Statistical analysis. All statistical analyses were performed with R studio (version 4.0.3) software[54]. Graphs were created using the ggplot2 packages[55]. Statistical evaluation of the performance of RISK6 was done by calculating the Area Under the receiver operating characteristic curve (ROC AUC) and associated 95% confidence intervals (CI) using the pROC in R[56]. Discrete variables were analyzed using Fisher's Exact test with Bonferroni's post-hoc test. Normality was assessed using the Shapiro–Wilk Normality Test. Normal, continuous variables were analyzed with Student's t-test. Non-normal, continuous variables were analyzed with the Mann–Whitney test or the Kruskal–Wallis rank-sum test with Dunn's Kruskal–Wallis Multiple Comparisons post-hoc test. Repeated measures of non-independent continuous variables were analyzed using the Friedman rank-sum test, with Wilcoxon–Nemenyi–McDonald–Thompson's post-hoc test. Non-parametric data were presented as median ± IQR and the statistical significance cut-off was considered as a p value of < 0.05. For logistic regression analyses, variables were first evaluated in univariate analyses, then multivariate analyses were performed. Adjustment variables were selected as follows: sociodemographic variables of known clinical importance (e.g., sex, country of origin), TB risk factors (e.g., smoking), and additional sociodemographic variables that were at least moderately associated ($p < 0.10$) with the outcome in univariate analyses (e.g., prison). Irrelevant adjustment variables were then removed by backward model selection. The combination of variables that minimized the Akaike Information Criterion (AIC) for most tested predictors, while including important adjustment variables, was selected.

Data availability

The RISK6 scores and associated clinical data for all cohorts can be found in Supplementary Tables 2–7.

Received: 9 April 2021; Accepted: 21 June 2021
Published online: 01 July 2021

References

1. World Health Organisation. Global Tuberculosis Report. (2020).
2. Pai, M. *et al.* Tuberculosis. *Nat. Rev. Dis. Primers* **2**, 16076 (2016).
3. Goletti, D. *et al.* Can we predict tuberculosis cure? What tools are available?. *Eur. Respir. J.* **52**, 1801089 (2018).
4. World Health Organisation. Guidelines for treatment of drug-susceptible tuberculosis and patient care. (2017).
5. Parrish, N. M. & Carroll, K. C. Role of the clinical mycobacteriology laboratory in diagnosis and management of tuberculosis in low-prevalence settings. *J. Clin. Microbiol.* **49**, 772–776 (2011).
6. Goletti, D., Lee, M. R., Wang, J. Y., Walter, N. & Ottenhoff, T. H. M. Update on tuberculosis biomarkers: From correlates of risk, to correlates of active disease and of cure from disease. *Respirology* **23**, 455–466 (2018).
7. Petrone, L. *et al.* Evaluation of IP-10 in Quantiferon-Plus as biomarker for the diagnosis of latent tuberculosis infection. *Tuberculosis (Edinb)* **111**, 147–153 (2018).
8. Petruccioli, E. *et al.* Effect of HIV-infection on QuantiFERON-plus accuracy in patients with active tuberculosis and latent infection. *J. Infect.* **80**, 536–546 (2020).
9. Petruccioli, E. *et al.* Effect of therapy on Quantiferon-Plus response in patients with active and latent tuberculosis infection. *Sci. Rep.* **8**, 15626 (2018).
10. Delogu, G. *et al.* Methylated HBHA produced in *M. smegmatis* discriminates between active and non-active tuberculosis disease among RD1-responders. *PLoS One* **6**, e18315 (2011).

11. Chiacchio, T. *et al.* Immune characterization of the HBHA-specific response in *Mycobacterium tuberculosis*-infected patients with or without HIV infection. *PLoS ONE* **12**, e0183846 (2017).
12. Tang, J. *et al.* QuantiFERON-TB Gold Plus combined with HBHA-Induced IFN-gamma release assay improves the accuracy of identifying tuberculosis disease status. *Tuberculosis (Edinb)* **124**, 101966 (2020).
13. Sali, M. *et al.* Combined use of Quantiferon and HBHA-based IGRA supports tuberculosis diagnosis and therapy management in children. *J. Infect.* **77**, 526–533 (2018).
14. Chedid, C. *et al.* Relevance of QuantiFERON-TB gold plus and heparin-binding hemagglutinin interferon-gamma release assays for monitoring of pulmonary tuberculosis clearance: A multicentered study. *Front. Immunol.* **11**, 616450 (2020).
15. Davies, P. D. & Pai, M. The diagnosis and misdiagnosis of tuberculosis. *Int. J. Tuberc. Lung Dis.* **12**, 1226–1234 (2008).
16. Diagnostic Standards and Classification of Tuberculosis in Adults and Children. *Am. J. Respir. Crit. Care. Med.* **161**, 1376–1395 (2000).
17. Steingart, K. R. *et al.* Xpert(R) MTB/RIF assay for pulmonary tuberculosis and rifampicin resistance in adults. *Cochrane Database Syst. Rev.* **2014**, CD009593 (2014).
18. Singhania, A. *et al.* A modular transcriptional signature identifies phenotypic heterogeneity of human tuberculosis infection. *Nat. Commun.* **9**, 2308 (2018).
19. World Health Organisation. Foundation for Innovative New Diagnostics. Pipeline Report 2020 Tuberculosis Diagnostics. (2020).
20. Wallis, R. S. *et al.* Tuberculosis biomarkers discovery: Developments, needs, and challenges. *Lancet Infect. Dis.* **13**, 362–372 (2013).
21. Kik, S. V. *et al.* An evaluation framework for new tests that predict progression from tuberculosis infection to clinical disease. *Eur. Respir. J.* **52**, 1800946 (2018).
22. Denkinger, C. M. *et al.* Defining the needs for next generation assays for tuberculosis. *J. Infect. Dis.* **211**(Suppl 2), S29-38 (2015).
23. Zak, D. E. *et al.* A blood RNA signature for tuberculosis disease risk: A prospective cohort study. *Lancet* **387**, 2312–2322 (2016).
24. Esmail, H., Cobelens, F. & Goletti, D. Transcriptional biomarkers for predicting development of tuberculosis: Progress and clinical considerations. *Eur. Respir. J.* **55**, 1901957 (2020).
25. Scriba, T. J. *et al.* Biomarker-guided tuberculosis preventive therapy (CORTIS): A randomised controlled trial. *Lancet Infect. Dis.* **21**, 354–365 (2021).
26. Penn-Nicholson, A. & Mbandi, S. K. RISK6, a 6-gene transcriptomic signature of TB disease risk, diagnosis and treatment response. *Sci. Rep.* **10**, 8629 (2020).
27. World Health Organization. High-priority target product profiles for new tuberculosis diagnostics: report of a consensus meeting. (2014).
28. Sweeney, T. E., Braviak, L., Tato, C. M. & Khatri, P. Genome-wide expression for diagnosis of pulmonary tuberculosis: A multicohort analysis. *Lancet Respir. Med.* **4**, 213–224 (2016).
29. Blankley, S. *et al.* The application of transcriptional blood signatures to enhance our understanding of the host response to infection: The example of tuberculosis. *Philos. Trans. R. Soc. Lond. B Biol. Sci.* **369**, 20130427 (2014).
30. Berry, M. P. *et al.* An interferon-inducible neutrophil-driven blood transcriptional signature in human tuberculosis. *Nature* **466**, 973–977 (2010).
31. Maertzdorf, J. *et al.* Concise gene signature for point-of-care classification of tuberculosis. *EMBO Mol. Med.* **8**, 86–95 (2016).
32. Sambarey, A. *et al.* Unbiased identification of blood-based biomarkers for pulmonary tuberculosis by modeling and mining molecular interaction networks. *EBioMedicine* **15**, 112–126 (2017).
33. Kaforou, M. *et al.* Detection of tuberculosis in HIV-infected and -uninfected African adults using whole blood RNA expression signatures: A case-control study. *PLoS Med.* **10**, e1001538 (2013).
34. Laux da Costa, L. *et al.* A real-time PCR signature to discriminate between tuberculosis and other pulmonary diseases. *Tuberculosis (Edinb.)* **95**, 421–425 (2015).
35. Warsinske, H., Vashisht, R. & Khatri, P. Host-response-based gene signatures for tuberculosis diagnosis: A systematic comparison of 16 signatures. *PLoS Med.* **16**, e1002786 (2019).
36. Warsinske, H. C. *et al.* Assessment of validity of a blood-based 3-gene signature score for progression and diagnosis of tuberculosis, disease severity, and treatment response. *JAMA Netw. Open* **1**, e183779 (2018).
37. Turner, C. T. *et al.* Blood transcriptional biomarkers for active pulmonary tuberculosis in a high-burden setting: A prospective, observational, diagnostic accuracy study. *Lancet Respir. Med.* **8**, 407–419 (2020).
38. Beynon, F. *et al.* Correlation of Xpert MTB/RIF with measures to assess *Mycobacterium tuberculosis* bacillary burden in high HIV burden areas of Southern Africa. *Sci. Rep.* **8**, 5201 (2018).
39. Miranda, P. *et al.* Sustained elevated levels of C-reactive protein and ferritin in pulmonary tuberculosis patients remaining culture positive upon treatment initiation. *PLoS One* **12**, e0175278 (2017).
40. Sane Schepisi, M. *et al.* Immune status and serial quantiferon-TB gold in-tube screening for latent *Mycobacterium tuberculosis* infection among HIV-infected persons in a country with a low tuberculosis incidence. *J. Infect. Dis.* **211**, 1852–1853 (2015).
41. Won, D., Park, J. Y., Kim, H. S. & Park, Y. Comparative results of QuantiFERON-TB gold in-tube and QuantiFERON-TB gold plus assays for detection of tuberculosis infection in clinical samples. *J. Clin. Microbiol.* **58**, e01854-e1919 (2020).
42. MacLean, E. & Broger, T. A 10-gene signature for the diagnosis and treatment monitoring of active tuberculosis using a molecular interaction network approach. *EBioMedicine* **16**, 22–23 (2017).
43. Sambarey, A. *et al.* Meta-analysis of host response networks identifies a common core in tuberculosis. *NPJ Syst. Biol. Appl.* **3**, 4 (2017).
44. Thompson, E. G. *et al.* Host blood RNA signatures predict the outcome of tuberculosis treatment. *Tuberculosis (Edinb.)* **107**, 48–58 (2017).
45. Darboe, F. *et al.* Detection of tuberculosis recurrence, diagnosis and treatment response by a blood transcriptomic risk signature in HIV-infected persons on antiretroviral therapy. *Front. Microbiol.* **10**, 1441 (2019).
46. Satproedprai, N. *et al.* Diagnostic value of blood gene expression signatures in active tuberculosis in Thais: A pilot study. *Genes Immun.* **16**, 253–260 (2015).
47. Cliff, J. M. *et al.* Distinct phases of blood gene expression pattern through tuberculosis treatment reflect modulation of the humoral immune response. *J. Infect. Dis.* **207**, 18–29 (2013).
48. Bloom, C. I. *et al.* Detectable changes in the blood transcriptome are present after two weeks of antituberculosis therapy. *PLoS One* **7**, e46191 (2012).
49. Francisco, N. M. *et al.* Diagnostic accuracy of a selected signature gene set that discriminates active pulmonary tuberculosis and other pulmonary diseases. *J. Infect.* **75**, 499–510 (2017).
50. van Rensburg, I. C. & Loxton, A. G. Transcriptomics: The key to biomarker discovery during tuberculosis?. *Biomark. Med.* **9**, 483–495 (2015).
51. Sodersten, E. *et al.* Diagnostic accuracy study of a novel blood-based assay for identification of TB in people living with HIV. *J. Clin. Microbiol.* **4**, 213 (2020).
52. Komurian-Pradel, F. *et al.* Enhancing research capacities in infectious diseases: The GABRIEL network, a joint approach to major local health issues in developing countries. *Clin. Epidemiol. Glob. Health* **1**, 40–43 (2013).
53. World Health Organisation. WHO Consolidated Guidelines on Tuberculosis, Module 4: Treatment - Drug-Resistant Tuberculosis Treatment. (2020).
54. R Core Team. *R: A Language and Environment for Statistical Computing*. R Foundation for Statistical Computing, (2021).

55. Wickham, H. *ggplot2: Elegant Graphics for Data Analysis* (Springer, 2016).
56. Robin, X. *et al.* pROC: An open-source package for R and S+ to analyze and compare ROC curves. *BMC Bioinform.* **12**, 77 (2011).

Acknowledgements
We are grateful for the inventors of a patent on RISK6 signature, the SATVI Clinical and Laboratory Team. This work was supported by Fondation Mérieux. We thank the patients and volunteer participants, as well as the local healthcare staff in each clinical site for their excellent assistance. We would like to thank Dr. Matthieu SCHOENHALS head of the immunology of infectious diseases unit of IPM for his assistance.

Author contributions
J.H. conceived and designed the study, and initiated this project in partnership with N.R., M.H., N.T., S.Ba. and D.G. Patient recruitment, follow-up and data collection was done by E.K., M.U., S.Bi., R.N., P.R., C.R., P.H., J.R., A.R. and R.B. The experiments were performed by R.B., M.N. and S.P. and J.H. performed statistical analysis with contribution from C.C. Data analysis and interpretation of results was implemented by R.B., M.N., J.H. and S.P. The manuscript was written by R.B., and all authors have read, reviewed and approved the final manuscript.

Competing interests
The authors declare no competing interests.

Additional information
Supplementary Information The online version contains supplementary material available at https://doi.org/10.1038/s41598-021-93059-1.

Correspondence and requests for materials should be addressed to R.B. or J.H.

Reprints and permissions information is available at www.nature.com/reprints.

Publisher's note Springer Nature remains neutral with regard to jurisdictional claims in published maps and institutional affiliations.

The HINTT working group within the GABRIEL network

Graciela Russomando[13], Chyntia Carolina Díaz Acosta[13] & Rossana Arenas[14]

[13]Instituto de Investigaciones en Ciencias de la Salud, National University of Asunción, Asunción, Paraguay. [14]Hospital General de San Lorenzo, MSPyBS, Asunción, Paraguay.

Supplementary data

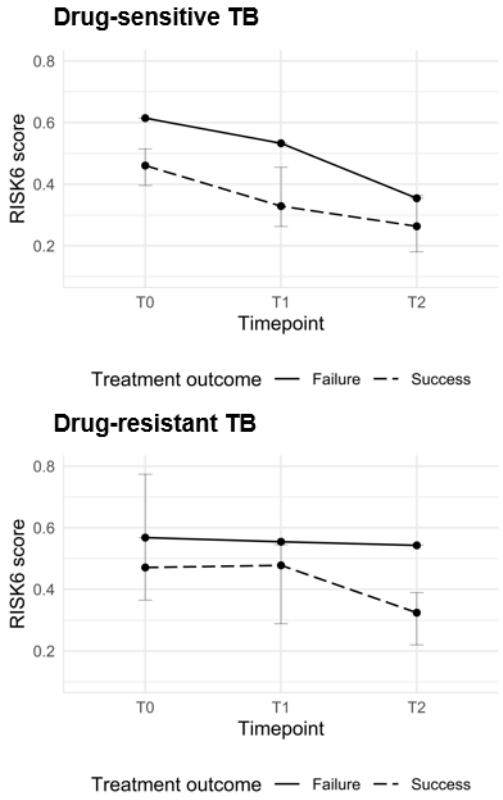

Supplementary Figure 1. Ability of RISK6 signature to stratify TB patients according to ultimate treatment outcome. Longitudinal kinetics of RISK6 signature scores across TB treatment time (T0: baseline; T2: 2 months after initiation and T2: at the end of treatment) in patients with cure and those with a treatment failure, stratified into drug-susceptible (n= 95) and drug-resistant TB cases (n= 11). Dots depict medians and error bars represent the IQR.

3. Oral communications

July 11, 2021: 31st ECCMID (European Congress of Clinical Microbiology & Infectious Diseases; virtual).

January 19, 2021: CYTEK User Meeting, Europe-Middle East-Asia region (virtual).

February 5 – 7, 2020: 2nd Swiss Cytometry Meeting (Ecole Polytechnique Fédérale de Lausanne, Switzerland).

January 21, 2020: Infectious Diseases Theme Day (Istituto Nazionale per le Malattie Infettive "Lazzaro Spallanzani", Rome, Italy).

April 25, 2019: DécrypThèse – PhD day of the E2M2 doctoral school (Lyon, France). Award for the best oral communication.

REFERENCES

1. World Health Organization Geneva. *Guidelines for treatment of drug-susceptible tuberculosis and patient care*. *WHO press* vol. 1 http://www.tandfonline.com/doi/full/10.1586/17476348.1.1.85 (2017).
2. World Health Organization Geneva. *WHO consolidated guidelines on drug-resistant tuberculosis treatment*. (2019).
3. Woimo, T. T., Yimer, W. K., Bati, T. & Gesesew, H. A. The prevalence and factors associated for anti-tuberculosis treatment non-adherence among pulmonary tuberculosis patients in public health care facilities in South Ethiopia: a cross-sectional study. *BMC Public Health* **17**, 1–10 (2017).
4. Munro, S. A. *et al.* Patient Adherence to Tuberculosis Treatment: A Systematic Review of Qualitative Research. *PLoS Med.* **4**, (2007).
5. Volmink, J. & Garner, P. Directly observed therapy for treating tuberculosis (Review). (2012).
6. Law, S., Piatek, A. S., Vincent, C., Oxlade, O. & Menzies, D. Emergence of drug resistance in patients with tuberculosis cared for by the Indian health-care system : a dynamic modelling study. *Lancet Public Heal.* **2**, e47–e55 (2017).
7. Sharma, A. *et al.* Estimating the future burden of multidrug-resistant and extensively drug-resistant tuberculosis in India, the Philippines, Russia, and South Africa: a mathematical modelling study. *Lancet Infect. Dis.* **17**, 707–715 (2017).
8. World Health Organization Geneva. *Global Tuberculosis Report 2018*. (2018).
9. Parrish, N. M. & Carroll, K. C. Role of the clinical mycobacteriology laboratory in diagnosis and management of tuberculosis in low-prevalence settings. *J. Clin. Microbiol.* **49**, 772–776 (2011).
10. World Health Organization Geneva. *Early detection of Tuberculosis*. *WHO press* (2011).
11. Horne, D. J. *et al.* Sputum monitoring during tuberculosis treatment for predicting outcome : systematic review and meta-analysis. *Lancet Infect. Dis.* **10**, 387–394 (2010).
12. MacLean, E. *et al.* A sytematic review of biomarkers to detect active tuberculosis. *Nat. Microbiol.* (2017) doi:10.1038/s41564-019-0380-2.

13. Goletti, D. *et al.* Can we predict tuberculosis cure? Current tools available. *Eur. Respir. J.* 1801089 (2018) doi:10.1183/13993003.01089-2018.
14. Cave, A. J. E. The Evidence for the Incidence of Tuberculosis in Ancient Egypt. *Br. J. Tuberc.* 141–152 (1941).
15. Hershkovitz, I. *et al.* Detection and Molecular Characterization of 9000-Year- Old Mycobacterium tuberculosis from a Neolithic Settlement in the Eastern Mediterranean. *PLoS One* **3**, 1–6 (2008).
16. Rothschild, B. M. & Martin, L. D. Frequency of pathology in a large natural sample from Natural Trap Cave with special remarks on erosive disease in the Pleistocene. *Reumatismo* **55**, 58–65 (2003).
17. Rothschild, B. M. *et al.* Mycobacterium tuberculosis Complex DNA from an Extinct Bison Dated 17,000 Years before the Present. *Clin. Infect. Dis.* **44512**, 305–311 (2001).
18. Lee, O. Y. *et al.* Mycobacterium tuberculosis Complex Lipid Virulence Factors Preserved in the 17 , 000-Year-Old Skeleton of an Extinct Bison , Bison antiquus. *PLoS One* **7**, 1–9 (2012).
19. Faksri, K., Xia, E., Tan, J. H., Teo, Y. & Ong, R. T. In silico region of difference (RD) analysis of Mycobacterium tuberculosis complex from sequence reads using RD-Analyzer. *BMC Genomics* **17**, 1–10 (2016).
20. Comas, I. *et al.* Out-of-Africa migration and Neolithic coexpansion of Mycobacterium tuberculosis with modern humans. *Nat. Genet.* **1**, 1–9 (2013).
21. Rodriguez-Campos, S., Smith, N. H., Boniotti, M. B. & Aranaz, A. Overview and phylogeny of Mycobacterium tuberculosis complex organisms : Implications for diagnostics and legislation of bovine tuberculosis. *Res. Vet. Sci.* (2014) doi:10.1016/j.rvsc.2014.02.009.
22. Barberis, I., Bragazzi, N. L., Galluzzo, L. & Martini, M. The history of tuberculosis : from the first historical records to the isolation of Koch ' s bacillus. *J Prev Med Hyg* **58**, 9–12 (2017).
23. Daniel, T. M. & Iversen, P. A. Hippocrates and tuberculosis. *Int J Tuberc Lung Dis* **19**, 373–374 (2015).
24. Sepkowitz, K. A. Tuberculosis and the Health Care Worker : A Historical Perspective. *Ann. Intern. Med.* **120**, 71–79 (1994).

25. Murray, J. F., Rieder, H. L. & Finley-croswhite, A. The King's Evil and the Royal Touch : the medical history of scrofula. *Int J Tuberc Lung Dis* **20**, 713–716 (2016).
26. Daniel, T. M. The history of tuberculosis. *Respir. Med.* 1862–1870 (2006) doi:10.1016/j.rmed.2006.08.006.
27. Pezzella, A. T. History of Pulmonary Tuberculosis. *Thorac Surg Clin* **29**, 1–17 (2019).
28. Schatz, A., Bugle, E. & Waksman, S. A. Streptomycin, a Substance Exhibiting Antibiotic Activity Against Gram-Positive and Gram-Negative Bacteria. *Exp. Biol. Med.* **55**, 66–69 (1944).
29. Murray, J. F., Schraufnagel, D. E. & Hopewell, P. C. Treatment of Tuberculosis: A Historical Perspective. *Ann Am Thorac Soc* **12**, 1749–1759 (2015).
30. Fox, W., Wiener, A., Mitchison, D. A., Selkon, J. B. & Sutherland, I. The Prevalence of Drug-Resistant Tubercle Bacilli in Untreated Patients with Pulmonary Tuberculosis : A National Survey, 1955-56. *Tubercle, London* **38**, 71–77 (1956).
31. Keshavjee, S. & Farmer, P. E. Tuberculosis, Drug Resistance, and the History of Modern Medicine. *N. Engl. J. Med.* **367**, 931–936 (2012).
32. Cohen, A., Mathiasen, V. D. & Wejse, C. The global prevalence of latent tuberculosis : a systematic review and meta-analysis. *Eur. Respir. J.* **54**, 1–14 (2019).
33. Organization., G. W. H. *Global Tuberculosis Report 2020*. (2020).
34. Gordon, S. V & Parish, T. Microbe Profile: Mycobacterium tuberculosis: Humanity's deadly microbial foe. *Microbiology* **164**, 437–439 (2018).
35. Pieters, J. Mycobacterium tuberculosis and the Macrophage: Maintaining a Balance. *Cell Host Microbe* **3**, 399–407 (2008).
36. Gygli, S. M., Borrell, S., Trauner, A. & Gagneux, S. Antimicrobial resistance in Mycobacterium tuberculosis: mechanistic and evolutionary perspectives. *Fems Microbiol. Lett.* **41**, 354–373 (2017).
37. Smith, T., Wolff, K. A. & Nguyen, L. Molecular Biology of Drug Resistance in Mycobacterium tuberculosis. *Curr. Top. Microbiol. Immunol.* **374**, 53–80 (2012).
38. Heemskerk, D., Caws, M., Marais, B. & Farrar, J. *Tuberculosis in Adults and Children*. (2015).
39. Padmaja, G., Srujana, K. & Sadhana, C. Comparison of Ziehl-Neelsen's stain, fluorescent stain with CBNAAT of sputum for the diagnosis of pulmonary tuberculosis. *J. Dr. NTR Univ. Heal. Sci.* **8**, 238 (2019).

40. Calver, A. D. *et al.* Emergence of increased resistance and extensively drug-resistant tuberculosis despite treatment adherence, South Africa. *Emerg. Infect. Dis.* **16**, 264–271 (2010).
41. Andersson, D. I. & Hughes, D. Microbiological effects of sublethal levels of antibiotics. *Nat. Rev. Microbiol.* **12**, 465–478 (2014).
42. World Health Organization (WHO). *Companion Handbook to the WHO Guidelines for the Programmatic Management of Drug-Resistant Tuberculosis. World Health Organization* (2014). doi:WHO/HTM/TB/2014.11.
43. Mitchison, D. & Davies, G. The chemotherapy of tuberculosis: Past, present and future. *Int. J. Tuberc. Lung Dis.* **16**, 724–732 (2012).
44. WHO. WHO guidelines for treatment of drug-susceptible TB and patient care: factsheet. *WHO Press* (2017).
45. Gillespie, S. H. *et al.* Four-Month Moxifloxacin-Based Regimens for Drug-Sensitive Tuberculosis. *N. Engl. J. Med.* **371**, 1577–1587 (2014).
46. WHO. WHO treatment guidelines for drug-resistant tuberculosis: 2016 update. *WHO Press* 56 (2016) doi:WHO/HTM/TB/2016.04.
47. Aung K.J.M. *et al.* Successful '9-month Bangladesh regimen' for multidrugresistant tuberculosis among over 500 consecutive patients. *Int. J. Tuberc. Lung Dis.* **18**, 1180–1187 (2014).
48. World Health Organization (WHO). *Definitions and reporting framework for tuberculosis - 2013 revision (updated December 2014 and January 2020)*. *European communicable disease bulletin* vol. 18 (2013).
49. Olaru, I. D., Heyckendorf, J., Grossmann, S. & Lange, C. Time to culture positivity and sputum smear microscopy during tuberculosis therapy. *PLoS One* **9**, 8–13 (2014).
50. Friedrich, S. O. *et al.* Assessment of the sensitivity and specificity of Xpert MTB/RIF assay as an early sputum biomarker of response to tuberculosis treatment. *Lancet Respir Med* **1**, 462–470 (2013).
51. Denkinger, C. M. *et al.* Defining the needs for next generation assays for tuberculosis. *J. Infect. Dis.* **211**, S29–S38 (2015).
52. Lienhardt, C. *et al.* Translational Research for Tuberculosis Elimination: Priorities, Challenges, and Actions. *PLoS Med.* **13**, 1–11 (2016).

53. Drain, P. K. *et al.* Urine lipoarabinomannan to monitor antituberculosis therapy response and predict mortality in an HIV-endemic region: a prospective cohort study. *BMJ Open* **5**, e006833 (2015).
54. Oramasionwu, G. E. *et al.* The utility of stool cultures for diagnosing tuberculosis in people living with the human immunodeficiency virus. *Int J Tuberc Lung Dis* **17**, 1023–1028 (2016).
55. Mahapatra, S. *et al.* A metabolic biosignature of early response to anti-tuberculosis treatment. *BMC Infect. Dis.* **14**, 53 (2014).
56. Scriba, T. J., Coussens, A. K. & Fletcher, H. A. Human immunology of tuberculosis. *Microbiol Spectr.* **5**, 213–237 (2017).
57. Hmama, Z., Peña-Díaz, S., Joseph, S. & Av-Gay, Y. Immunoevasion and immunosuppression of the macrophage by Mycobacterium tuberculosis. *Immunol. Rev.* **264**, 220–232 (2015).
58. Andersson, J., Samarina, A., Fink, J., Rahman, S. & Grundström, S. Impaired expression of perforin and granulysin in CD8+ T cells at the site of infection in human chronic pulmonary tuberculosis. *Infect. Immun.* **75**, 5210–5222 (2007).
59. Lin, P. L. & Flynn, J. L. CD8 T cells and Mycobacterium tuberculosis infection. *Semin Immunopathol.* **37**, 239–249 (2015).
60. Wong, E. A. *et al.* Low levels of T cell exhaustion in tuberculous lung granulomas. *Infect. Immun.* **86**, (2018).
61. Ehlers, S. & Schaible, U. E. The granuloma in tuberculosis: Dynamics of a host-pathogen collusion. *Front. Immunol.* **3**, 1–9 (2012).
62. D'Avila, H. *et al.* Mycobacterium bovis Bacillus Calmette-Guérin Induces TLR2-Mediated Formation of Lipid Bodies: Intracellular Domains for Eicosanoid Synthesis In Vivo. *J. Immunol.* **176**, 3087–3097 (2006).
63. Pagán, A. J. & Ramakrishnan, L. Immunity and immunopathology in the tuberculous granuloma. *Cold Spring Harb. Perspect. Med.* **5**, 1–19 (2015).
64. Ramakrishnan, L. Revisiting the role of the granuloma in tuberculosis. *Nat. Rev. Immunol.* **12**, 352–366 (2012).
65. Ong, C. W. M., Elkington, P. T. & Friedland, J. S. Tuberculosis, pulmonary cavitation, and matrix metalloproteinases. *Am. J. Respir. Crit. Care Med.* **190**, 9–18 (2014).

66. Delogu, G. & Goletti, D. The spectrum of tuberculosis infection: New perspectives in the era of biologics. *J. Rheumatol.* **41**, 11–16 (2014).

67. Lin, P. L. & Flynn, J. L. The End of the Binary Era: Revisiting the Spectrum of Tuberculosis. *J. Immunol.* **201**, 2541–2548 (2018).

68. Walzl, G., Ronacher, K., Hanekom, W., Scriba, T. J. & Zumla, A. Immunological biomarkers of tuberculosis. *Nat. Rev. Immunol.* **11**, 343–354 (2011).

69. Panteleev, A. V. *et al.* Severe Tuberculosis in Humans Correlates Best with Neutrophil Abundance and Lymphocyte Deficiency and Does Not Correlate with Antigen-Specific CD4 T-Cell Response. *Front. Immunol.* **8**, 1–16 (2017).

70. Pai, M. *et al.* Tuberculosis. *Nat. Rev. Dis. Prim.* **2**, (2016).

71. Comas, Ĩ. *et al.* Human T cell epitopes of Mycobacterium tuberculosis are evolutionarily hyperconserved. *Nat. Genet.* **42**, 498–503 (2010).

72. Yang, J. D. *et al.* Mycobacterium tuberculosis-specific CD4(+) and CD8(+) T cells differ in their capacity to recognize infected macrophages. *Plos Pathog.* **14**, 30 (2018).

73. Behar, S. M. Antigen-Specific CD8+ T Cells and Protective Immunity to Tuberculosis. *Adv Exp Med Biol* **783**, 141–163 (2013).

74. Goletti, D. *et al.* Can we predict tuberculosis cure? What tools are available? *Eur. Respir. J.* **52**, (2018).

75. Meier, N. R., Jacobsen, M., Ottenhoff, T. H. M. & Ritz, N. A Systematic Review on Novel Mycobacterium tuberculosis Antigens and Their Discriminatory Potential for the Diagnosis of Latent and Active Tuberculosis. *Front. Immunol.* **9**, 1–22 (2018).

76. Rakotosamimanana, N. *et al.* Biomarkers for risk of developing active tuberculosis in contacts of TB patients: a prospective cohort study. *Eur. Respir. J.* **46**, 1095–1103 (2015).

77. Lowe, D. M. *et al.* Neutrophilia independently predicts death in tuberculosis. *Eur. Respir. J.* **42**, 1752–1756 (2013).

78. Roy Chowdhury, R. *et al.* A multi-cohort study of the immune factors associated with M. tuberculosis infection outcomes. *Nature* **560**, 644–648 (2018).

79. Goletti, D. *et al.* Region of difference 1 antigen-specific CD4+ memory T cells correlate with a favorable outcome of tuberculosis. *J. Infect. Dis.* **194**, 984–992 (2006).

80. Day, C. L. *et al.* Functional Capacity of Mycobacterium tuberculosis -Specific T Cell Responses in Humans Is Associated with Mycobacterial Load. *J. Immunol.* **187**, 2222–2232 (2011).

81. Axelsson-Robertson, R. *et al.* Frequency of Mycobacterium tuberculosis-specific CD8+ T-cells in the course of anti-tuberculosis treatment. *Int. J. Infect. Dis.* **32**, 23–29 (2015).
82. Kamada, A. & Amishima, M. QuantiFERON-TB Gold Plus as a potential tuberculosis treatment monitoring tool. *Eur. Respir. J.* **49**, 1601976 (2017).
83. Petruccioli, E. *et al.* Effect of therapy on Quantiferon-Plus response in patients with active and latent tuberculosis infection. *Sci. Rep.* **8**, 15626 (2018).
84. Sali, M. *et al.* Combined use of Quantiferon and HBHA-based IGRA supports tuberculosis diagnosis and therapy management in children. *J. Infect.* **77**, 526–533 (2018).
85. Agrawal, S. *et al.* Efficacy of T regulatory cells, Th17 cells and the associated markers in monitoring tuberculosis treatment response. *Front. Immunol.* **9**, 1–16 (2018).
86. Sada, I., Carrillo-Alduenda, J. L., Chavez-Galan, L., Skold, M. & Salazar-Lezama, M. A. Polyfunctional T cell responses to ESAT-6 and PPD after treatment in multidrugresistant tuberculosis patients. *J. Immunol.* **188**, (2012).
87. Latorre, I. *et al.* Study of CD27 and CCR4 Markers on Specific CD4+ T-Cells as Immune Tools for Active and Latent Tuberculosis Management. *Front. Immunol.* **9**, 1–11 (2019).
88. Adekambi, T. *et al.* Distinct effector memory CD4 + T cell signatures in latent Mycobacterium tuberculosis infection, BCG vaccination and clinically resolved tuberculosis. *PLoS One* **7**, (2012).
89. Nikitina, I. Y. *et al.* Th1, Th17, and Th1Th17 Lymphocytes during Tuberculosis: Th1 Lymphocytes Predominate and Appear as Low-Differentiated CXCR3 + CCR6 + Cells in the Blood and Highly Differentiated CXCR3 +/− CCR6 − Cells in the Lungs. *J. Immunol.* **200**, 2090–2103 (2018).
90. Adekambi, T., Ibegbu, C., Cagle, S., Ray, S. & Rengarajan, J. Monitoring the response to TB treatment using T cells biomarkers in TB/HIV patients undergoing ART. *J. Immunol.* **198**, 125.14 (2017).
91. Ahmed, M. I. M. *et al.* Phenotypic Changes on Mycobacterium Tuberculosis-Specific CD4 T Cells as Surrogate Markers for Tuberculosis Treatment Efficacy. *Front. Immunol.* **9**, 2247 (2018).
92. Day, C. L. *et al.* PD-1 Expression on Mycobacterium tuberculosis-Specific CD4 T Cells Is Associated With Bacterial Load in Human Tuberculosis. *Front. Immunol.* **9**, 1995 (2018).

93. Hassan, S. S., Akram, M., King, E. C., Dockrell, H. M. & Cliff, J. M. PD-1, PD-L1 and PD-L2 gene expression on t-cells and natural killer cells declines in conjunction with a reduction in PD-1 protein during the intensive phase of tuberculosis treatment. *PLoS One* **10**, e0137646 (2015).
94. Ferrian, S. *et al.* A combination of baseline plasma immune markers can predict therapeutic response in multidrug resistant tuberculosis. *PLoS One* **12**, e0176660 (2017).
95. Riou, C. *et al.* Effect of Standard Tuberculosis Treatment on Plasma Cytokine Levels in Patients with Active Pulmonary Tuberculosis. *PLoS One* **7**, e36886 (2012).
96. Bloom, C. I. *et al.* Detectable Changes in The Blood Transcriptome Are Present after Two Weeks of Antituberculosis Therapy. *PLoS One* **7**, 13 (2012).
97. Zak, D. E. *et al.* A blood RNA signature for tuberculosis disease risk: a prospective cohort study. *Lancet (North Am. Ed.* **387**, 2312–2322 (2016).
98. Penn-Nicholson, A. *et al.* RISK6, a 6-gene transcriptomic signature of TB disease risk, diagnosis and treatment response. *Sci. Rep.* **10**, 1–21 (2020).
99. Pai, M. *et al.* Gamma interferon release assays for detection of Mycobacterium tuberculosis infection. *Clin. Microbiol. Rev.* **27**, 3–20 (2014).
100. Doan, C. A. & Sabin, F. R. The Relation of the Tubercle and the Monocyte-Lymphocyte Ratio to Resistance and Susceptibility in Tuberculosis. *J. Exp. Med.* **52**, 113–152 (1930).
101. Morris, C. D. W., Bird, A. R. & Nell, H. The haematological and biochemical changes in severe pulmonary tuberculosis. *Qjm* **73**, 1151–1159 (1989).
102. La Manna, M. P. *et al.* Quantitative and qualitative profiles of circulating monocytes may help identifying tuberculosis infection and disease stages. *PLoS One* **12**, e0171358 (2017).
103. Pethe, K. *et al.* The heparin-binding haemagglutinin of M. tuberculosis is required for extrapulmonary dissemination. *Nature* **412**, 190–194 (2001).
104. Delogu, G. *et al.* Methylated HBHA produced in M. smegmatis discriminates between active and non-active tuberculosis disease among RD1-responders. *PLoS One* **6**, (2011).
105. Locht, C., Hougardy, J. M., Rouanet, C., Place, S. & Mascart, F. Heparin-binding hemagglutinin, from an extrapulmonary dissemination factor to a powerful diagnostic and protective antigen against tuberculosis. *Tuberculosis* **86**, 303–309 (2006).

106. Corbiere, V. *et al.* Risk Stratification of Latent Tuberculosis Defined by Combined Interferon Gamma Release Assays. *PLoS One* **7**, e43285 (2012).
107. Hougardy, J. M. *et al.* Heparin-binding-hemagglutinin-induced IFN-γ release as a diagnostic tool for latent tuberculosis. *PLoS One* **2**, (2007).
108. Tang, J. *et al.* QuantiFERON-TB Gold Plus combined with HBHA-Induced IFN-γ release assay improves the accuracy of identifying tuberculosis disease status. *Tuberculosis* **124**, (2020).
109. Masungi, C. *et al.* Differential T and B cell responses against Mycobacterium tuberculosis heparin-binding hemagglutinin adhesin in infected healthy individuals and patients with tuberculosis. *J. Infect. Dis.* **185**, 513–520 (2002).
110. Smits, K. *et al.* Immunological Signatures Identifying Different Stages of Latent Mycobacterium tuberculosis Infection and Discriminating Latent from Active Tuberculosis in Humans. *J. Clin. Cell. Immunol.* **06**, 1–9 (2015).
111. Aerts, L. *et al.* HBHA-Induced Polycytotoxic CD4+ T Lymphocytes Are Associated with the Control of Mycobacterium tuberculosis Infection in Humans. *J. Immunol.* **202**, 421–427 (2019).
112. Wen, H. L. *et al.* Involvement of methylated HBHA expressed from Mycobacterium smegmatis in an IFN-γ release assay to aid discrimination between latent infection and active tuberculosis in BCG-vaccinated populations. *Eur. J. Clin. Microbiol. Infect. Dis.* **36**, 1415–1423 (2017).
113. Mahnke, Y. D., Brodie, T. M., Sallusto, F., Roederer, M. & Lugli, E. The who's who of T-cell differentiation: Human memory T-cell subsets. *Eur. J. Immunol.* **43**, 2797–2809 (2013).
114. Shanmugasundaram, U. *et al.* Pulmonary Mycobacterium tuberculosis control associates with CXCR3- And CCR6-expressing antigen-specific Th1 and Th17 cell recruitment. *JCI Insight* **5**, (2020).
115. Marriott, I. *et al.* Active Tuberculosis Is Characterized by Highly Differentiated Effector Memory Th1 Cells. *Front. Immunol.* **9**, 2127 (2018).
116. Chiacchio, T. *et al.* Polyfunctional T-cells and effector memory phenotype are associated with active TB in HIV-infected patients. *J. Infect.* **69**, 533–545 (2014).
117. Wang, X. *et al.* Association of mycobacterial antigen-specific CD4(+) memory T cell subsets with outcome of pulmonary tuberculosis. *J Infect* **60**, 133–139 (2010).

118. Goletti, D. *et al.* Response to M. tuberculosis selected RDI peptides in Ugandan HIV-infected patients with smear positive pulmonary tuberculosis: a pilot study. *Bmc Infect. Dis.* **8**, 13 (2008).
119. Petruccioli, E. *et al.* IFNγ/TNFα specific-cells and effector memory phenotype associate with active tuberculosis. *J. Infect.* **66**, 475–486 (2013).
120. Nyendak, M. R. *et al.* Mycobacterium tuberculosis Specific CD8(+) T Cells Rapidly Decline with Antituberculosis Treatment. *PLoS One* **8**, e81564 (2013).
121. Jiang, H. *et al.* Decreased expression of perforin in CD8+ T lymphocytes in patients with Mycobacterium tuberculosis infection and its potential value as a marker for efficacy of treatment. *J. Thorac. Dis.* **9**, 1353–1360 (2017).
122. Riou, C., Berkowitz, N., Goliath, R., Burgers, W. A. & Wilkinson, R. J. Analysis of the phenotype of Mycobacterium tuberculosis-specific CD4+ T cells to discriminate latent from active tuberculosis in HIV-Uninfected and HIV-Infected individuals. *Front. Immunol.* **8**, (2017).
123. Young, J. M., Adetifa, I. M. O., Ota, M. O. C. & Sutherland, J. S. Expanded polyfunctional T cell response to mycobacterial antigens in TB disease and contraction post-treatment. *PLoS One* **5**, (2010).
124. Harari, A. *et al.* Dominant TNF-α+ Mycobacterium tuberculosis-specific CD4+ T cell responses discriminate between latent infection and active disease. *Nat. Med.* **17**, 372–377 (2011).
125. Lyadova, I. V & Panteleev, A. V. Th1 and Th17 Cells in Tuberculosis: Protection, Pathology, and Biomarkers. *Mediators Inflamm.* 854507 (2015) doi:10.1155/2015/854507.
126. Nikitina, I. Y. *et al.* Mtb-specific CD27low CD4 t cells as markers of lung tissue destruction during pulmonary tuberculosis in humans. *PLoS One* **7**, e43733 (2012).
127. Riou, C., Jhilmeet, N., Rangaka, M. X., Wilkinson, R. J. & Wilkinson, K. A. Tuberculosis antigen-specific T cell responses during the first 6 months of antiretroviral treatment. *J. Infect. Dis.* **221**, 162–167 (2020).
128. Moguche, A. O. *et al.* Antigen Availability Shapes T Cell Differentiation and Function during Tuberculosis. *Cell Host Microbe* **21**, 695-706.e5 (2017).
129. Zhao, Y. *et al.* IP-10 and RANTES as biomarkers for pulmonary tuberculosis diagnosis and monitoring. *Tuberc.* **111**, 45–53 (2018).

130. Hoel, I. M. *et al.* IP-10 dried blood spots assay monitoring treatment efficacy in extrapulmonary tuberculosis in a low-resource setting. *Sci. Rep.* **9**, 3871 (2019).
131. Miranda, P. *et al.* Sustained elevated levels of C-reactive protein and ferritin in pulmonary tuberculosis patients remaining culture positive upon treatment initiation. *PLoS One* **12**, e0175278 (2017).
132. Sigal, G. B. *et al.* Biomarkers of Tuberculosis Severity and Treatment Effect: a Directed Screen of 70 Host Markers in a Randomized Clinical Trial. *Ebiomedicine* **25**, 112-121 (2017).
133. Sweeney, T. E., Braviak, L., Tato, C. M. & Khatri, P. Genome-wide expression for diagnosis of pulmonary tuberculosis: A multicohort analysis. *Lancet Respir. Med.* **4**, 213–224 (2016).
134. Thompson, E. G. *et al.* Host blood RNA signatures predict the outcome of tuberculosis treatment. *Tuberculosis* **107**, 48–58 (2017).
135. Liechti, T. & Roederer, M. OMIP-060: 30-Parameter Flow Cytometry Panel to Assess T Cell Effector Functions and Regulatory T Cells. *Cytom. Part A* **95**, 1129–1134 (2019).
136. Bandura, D. R. *et al.* Mass cytometry: Technique for real time single cell multitarget immunoassay based on inductively coupled plasma time-of-flight mass spectrometry. *Anal. Chem.* **81**, 6813–6822 (2009).
137. Bendall, S. C., Nolan, G. P., Roederer, M. & Chattopadhyay, P. K. A deep profiler's guide to cytometry. *Trends Immunol.* **33**, 323–332 (2012).
138. Baumgart, S., Peddinghaus, A., Schulte-Wrede, U., Mei, H. E. & Grützkau, A. OMIP-034: Comprehensive immune phenotyping of human peripheral leukocytes by mass cytometry for monitoring immunomodulatory therapies. *Cytom. Part A* **91**, 34–38 (2017).
139. Dusoswa, S. A., Verhoeff, J. & Garcia-Vallejo, J. J. OMIP-054: Broad Immune Phenotyping of Innate and Adaptive Leukocytes in the Brain, Spleen, and Bone Marrow of an Orthotopic Murine Glioblastoma Model by Mass Cytometry. *Cytom. Part A* **95**, 422–426 (2019).
140. Takahashi, C. *et al.* Mass cytometry panel optimization through the designed distribution of signal interference. *Cytom. Part A* **91**, 39–47 (2017).
141. Nolan, J. P. & Condello, D. Spectral flow cytometry. *Curr. Protoc. Cytom.* 1–18 (2013) doi:10.1002/0471142956.cy0127s63.

142. Park, L. M., Lannigan, J. & Jaimes, M. C. OMIP-069: Forty-Color Full Spectrum Flow Cytometry Panel for Deep Immunophenotyping of Major Cell Subsets in Human Peripheral Blood. *Cytom. Part A* **97**, 1044–1051 (2020).
143. Chattopadhyay, P. K. & Roederer, M. A mine is a terrible thing to waste: High content, single cell technologies for comprehensive immune analysis. *Am. J. Transplant.* **15**, 1155–1161 (2015).
144. Gossez, M. *et al.* Proof of concept study of mass cytometry in septic shock patients reveals novel immune alterations. *Sci. Rep.* **8**, 1–12 (2018).
145. Kourelis, T. V *et al.* Mass cytometry dissects T cell heterogeneity in the immune tumor microenvironment of common dysproteinemias at diagnosis and after fi rst line therapies. *Blood Cancer J.* **9**, (2019).
146. Brummelman, J. *et al.* High-dimensional single cell analysis identifies stemlike cytotoxic CD8+T cells infiltrating human tumors. *J. Exp. Med.* **215**, 2520–2535 (2018).
147. Brodie, T. M., Tosevski, V. & Medová, M. OMIP-045: Characterizing human head and neck tumors and cancer cell lines with mass cytometry. *Cytom. Part A* **93**, 406–410 (2018).
148. Turner, J. S. *et al.* Human germinal centres engage memory and naive B cells after influenza vaccination. *Nature* **586**, 127–132 (2020).
149. Silvin, A. *et al.* Elevated Calprotectin and Abnormal Myeloid Cell Subsets Discriminate Severe from Mild COVID-19. *Cell* **182**, 1401-1418.e18 (2020).
150. Komurian-Pradel, F. *et al.* Enhancing research capacities in infectious diseases: The GABRIEL network, a joint approach to major local health issues in developing countries. *Clin. Epidemiol. Glob. Heal.* **1**, 40–43 (2013).
151. Bonilla, D. L., Reinin, G. & Chua, E. Full Spectrum Flow Cytometry as a Powerful Technology for Cancer Immunotherapy Research. *Front. Mol. Biosci.* **7**, 1–10 (2021).
152. Juvet, S. C. & Zhang, L. Double negative regulatory T cells in transplantation and autoimmunity: Recent progress and future directions. *J. Mol. Cell Biol.* **4**, 48–58 (2012).
153. Myers, J. A. Can tuberculosis be eradicated? *Dis. Chest* **43**, 327–329 (1963).
154. World Health Organization. End TB by 2030. *World Heal. Organ. Reg. Off. Africa* 1–28 (2017).
155. Fukunaga, R. *et al.* Epidemiology of Tuberculosis and Progress Toward Meeting Global Targets — Worldwide, 2019. *MMWR Surveill. Summ.* **70**, 427–430 (2021).

156. Bartalesi, F. *et al.* The role of Quantiferon-TB Gold in-Tube in the diagnosis and treatment monitoring of active tuberculosis. *Infect. Dis. (Auckl).* **49**, 474–477 (2017).
157. Denkinger, C. M., Pai, M., Patel, M. & Menzies, D. Gamma Interferon Release Assay for Monitoring of Treatment Response for Active Tuberculosis : an Explosion in the Spaghetti Factory. *J. Clin. Microbiol.* **51**, 607–610 (2013).
158. Kamada, A. & Amishima, M. QuantiFERON-TB Gold Plus as a potential tuberculosis treatment monitoring tool. *Eur. Respir. J.* **49**, 10–12 (2017).
159. Li, G. *et al.* Anti-tuberculosis (TB) chemotherapy dynamically rescues Th1 and CD8+ T effector levels in Han Chinese pulmonary TB patients. *Microbes Infect.* **22**, 119–126 (2020).
160. Chegou, N. N. *et al.* Africa-wide evaluation of host biomarkers in QuantiFERON supernatants for the diagnosis of pulmonary tuberculosis. *Sci. Rep.* **8**, 2675 (2018).
161. Mpande, C. A. M. *et al.* Immune profiling of Mycobacterium tuberculosis-specific T cells in recent and remote infection. *EBioMedicine* **64**, (2021).
162. Roy Chowdhury, R. *et al.* A multi-cohort study of the immune factors associated with M. tuberculosis infection outcomes. *Nature* (2018) doi:10.1038/s41586-018-0439-x.
163. Feng, J.-Y. *et al.* Depressed Gamma Interferon Responses and Treatment Outcomes in Tuberculosis Patients: a Prospective Cohort Study. *J. Clin. Microbiol.* **56**, 1–9 (2018).
164. Lyadova, I. & Nikitina, I. Cell differentiation degree as a factor determining the role for different T-helper populations in tuberculosis protection. *Front. Immunol.* **10**, 1–10 (2019).
165. World Health Organization Geneva. *Global Tuberculosis Report 2020*. *WHO press* vol. 1 (2020).
166. Robinson, J. P. Spectral flow cytometry—Quo vadimus? *Cytom. Part A* **95**, 823–824 (2019).
167. Kim, C. H. *et al.* Rules of chemokine receptor association with T cell polarization in vivo. *J. Clin. Invest.* **108**, 1331–1339 (2001).
168. Acosta-Rodriguez, E. V. *et al.* Surface phenotype and antigenic specificity of human interleukin 17-producing T helper memory cells. *Nat. Immunol.* **8**, 639–646 (2007).
169. Lindestam Arlehamn, C. S. *et al.* Memory T Cells in Latent Mycobacterium tuberculosis Infection Are Directed against Three Antigenic Islands and Largely Contained in a CXCR3+CCR6+ Th1 Subset. *PLoS Pathog.* **9**, (2013).

170. Pandya, J. M. *et al.* Circulating T helper and T regulatory subsets in untreated early rheumatoid arthritis and healthy control subjects. *J. Leukoc. Biol.* **100**, 823–833 (2016).
171. Klemann, C., Wagner, L., Stephan, M. & von Hörsten, S. Cut to the chase: a review of CD26/dipeptidyl peptidase-4's (DPP4) entanglement in the immune system. *Clin. Exp. Immunol.* **185**, 1–21 (2016).
172. Oshikawa, K. & Sugiyama, Y. Elevated soluble CD26 levels in patients with tuberculous pleurisy. *Int. J. Tuberc. Lung Dis.* **5**, 868–872 (2001).
173. Ohnuma, K., Dang, N. H. & Morimoto, C. Revisiting an old acquaintance: CD26 and its molecular mechanisms in T cell function. *Trends Immunol.* **29**, 295–301 (2008).
174. Sharma, P. K. *et al.* High expression of CD26 accurately identifies human bacteria-reactive MR1-restricted MAIT cells. *Immunology* **145**, 443–453 (2015).
175. Chen, H. H. *et al.* Effects of dipeptidyl peptidase-4 inhibitor treatment doses on tuberculosis in patients with diabetes: A long-term nationwide population-based cohort study. *Ann. Palliat. Med.* **9**, 2817–2825 (2020).
176. Ahmed, M. I. M. *et al.* Phenotypic Changes on Mycobacterium Tuberculosis-Specific CD4 T Cells as Surrogate Markers for Tuberculosis Treatment Efficacy. *Front. Immunol.* **9**, 2247 (2018).
177. Groom, J. R. & Luster, A. D. CXCR3 in T cell function. *Exp. Cell Res.* **317**, 620–631 (2011).
178. Bertolini, T. B. *et al.* CCR4-dependent reduction in the number and suppressor function of CD4+ Foxp3+ cells augments IFN-γ-mediated pulmonary inflammation and aggravates tuberculosis pathogenesis. *Cell Death Dis.* **10**, (2019).
179. Vickers, M. A. *et al.* Monitoring Anti-tuberculosis Treatment Response Using Analysis of Whole Blood Mycobacterium tuberculosis Specific T Cell Activation and Functional Markers. *Front. Immunol.* **11**, 1–13 (2020).
180. Adekambi, T. *et al.* Biomarkers on patient T cells diagnose active tuberculosis and monitor treatment response. *J. Clin. Invest.* **125**, 1827–1838 (2015).
181. Cliff, J. M. *et al.* Excessive cytolytic responses predict tuberculosis relapse after apparently successful treatment. *J. Infect. Dis.* **213**, 485–495 (2016).
182. Morgan, J. *et al.* Classical CD4 T cells as the cornerstone of antimycobacterial immunity. *Immunol. Rev.* **301**, 10–29 (2021).

183. De Albuquerque, A. C. *et al.* Association of polymorphism +874 A/T of interferon-γ and susceptibility to the development of tuberculosis: Meta-analysis. *Eur. J. Clin. Microbiol. Infect. Dis.* **31**, 2887–2895 (2012).
184. Tientcheu, L. D. *et al.* Immunological consequences of strain variation within the Mycobacterium tuberculosis complex. *Eur. J. Immunol.* **47**, 432–445 (2017).
185. Genestet, C. *et al.* Rifampicin exposure reveals within-host Mycobacterium tuberculosis diversity in patients with delayed culture conversion. *PLOS Pathog.* **17**, e1009643 (2021).
186. Marchese, A. Endocytic trafficking of chemokine receptors. *Curr Opin Cell Biol* **27**, 72–77 (2014).
187. WHO. The End TB Strategy. *WHO Press* (2015).
188. Erkens, C. G. M. *et al.* Monitoring latent tuberculosis infection diagnosis and management in the Netherlands. *Eur. Respir. J.* **47**, 1492–1501 (2016).
189. Behr, M. A., Edelstein, P. H. & Ramakrishnan, L. Revisiting the timetable of tuberculosis. *BMJ* **362**, 1–10 (2018).
190. Mpande, C. A. M. *et al.* Antigen-specific T-cell activation distinguishes between recent and remote tuberculosis infection. *Am. J. Respir. Crit. Care Med.* **203**, 1556–1565 (2021).
191. Bayaa, R., Ndiaye, M. D. B., Chedid, C. & Kokhreidze, E. Multi-country evaluation of RISK6, a 6-gene blood transcriptomic signature, for tuberculosis diagnosis and treatment monitoring. *Sci. Rep.* **11**, 1–12 (2021).
192. Achkar, J. M. *et al.* Host Protein Biomarkers Identify Active Tuberculosis in HIV Uninfected and Co-infected Individuals. *EBioMedicine* **2**, 1160–1168 (2015).
193. Bark, C. M. *et al.* Identification of Host Proteins Predictive of Early Stage Mycobacterium tuberculosis Infection. *EBioMedicine* **21**, 150–157 (2017).
194. Simmons, J. D., Stein, C. M., Seshadri, C., Campo, M. & Kizza, H. M.-. Immunological mechanisms of human resistance to persistent Mycobacterium tuberculosis infection. *Nat. Rev. Immunol.* **18**, 575–589 (2018).
195. Gutierrez, J., Kroon, E. E., Möller, M. & Stein, C. M. Phenotype Definition for “Resisters” to Mycobacterium tuberculosis Infection in the Literature—A Review and Recommendations. *Front. Immunol.* **12**, (2021).

List of abbreviations

APD: avalanche photodiode (cytometry detector)

ATB: active tuberculosis

AUC: area under the curve (see: “ROC”)

BCG: Bacille Calmette-Guérin

BMI: body mass index

CBC: complete blood counts

CCD: Charge Coupled Device (cytometry detector)

CD: cluster of differentiation

CFP-10: 10kDa culture filtrate protein

COVID-19: Coronavirus disease 2019

CT-scan: computed tomography scan

CyTOF: cytometry by time of flight

DR-TB: drug-resistant tuberculosis (includes all resistance phenotypes)

DS-TB: drug-susceptible tuberculosis

ELISA: enzyme-linked immunosorbent assay

ELISPOT: enzyme-linked immunosorbent spot assay

EPTB: extrapulmonary tuberculosis

ESAT-6: 6kDa early secreted antigenic target

HBHA: heparin-binding hemagglutinin

IFN-γ: interferon gamma

IGRA: Interferon gamma release assay

IL-2: interleukin 2

LMIC: lower-middle-income countries

LTBI: latent tuberculosis infection

LTFU: lost to follow-up

MDR-TB: multi-drug resistant tuberculosis

Mtb or *M. tuberculosis*: *Mycobacterium tuberculosis*

MTBC: *Mycobacterium tuberculosis* complex

PBMC: peripheral blood mononucleated cells

PCA: principal components analysis

PMT: photomultiplier tube (cytometry detector)

PTB: pulmonary tuberculosis

QFT-GIT: QuantiFERON-TB Gold In-Tube

QFT-P: QuantiFERON-TB Gold Plus

ROC: Receiver Operating Curve

RR-TB: rifampicin-resistant TB

TB: tuberculosis

TCR: T-cell receptor

TNF: tumor necrosis factor

WBC: white blood cells

WHO: World Health Organization

XDR-TB: extensively drug-resistant TB

Abbreviations for TB drugs

First line drugs:

E: Ethambutol.

H: Isoniazid.

R: Rifampicin.

S: Streptomycin.

Z: Pyrazinamide.

Second line drugs:

Bdq: Bedaquiline.

Cfz: Clofazimine.

Cs: Cycloserine.

Km: Kanamycin.

Lfx: Levofloxacin.

Lzd: Linezolid.

Mfx: Moxifloxacin.

Pto: Prothionamide.

List of figures

List of tables

Résumé en français

Contexte : La tuberculose (TB) est une des maladies infectieuses les plus meurtrières au monde, avec plus d'un million de morts en 2020. Délaissée dans les politiques sanitaires internationales, elle touche principalement les pays en voie de développement et les personnes en situation de précarité. Son traitement nécessite des multithérapies antibiotiques aux effets secondaires toxiques. Concernant la TB pulmonaire en particulier, il existe un besoin clinique pour de nouveaux tests de suivi du traitement plus rapides et adaptés à des échantillons accessibles plus régulièrement que les crachats. Dans ce contexte, les biomarqueurs sanguins immunologiques représentent des options prometteuses.

Objectifs : L'objectif principal de cette thèse était d'évaluer la pertinence clinique de tests immunologiques sanguins pour le suivi du traitement anti-TB par rapport à l'évolution microbiologique mesurée par la culture de *Mycobacterium tuberculosis* (Mtb). Pour ceci, une étude prospective multicentrique a été menée dans cinq pays à forte incidence de TB (Bangladesh, Géorgie, Liban, Madagascar, Paraguay). Elle comportait un volet d'évaluation de deux outils simples (une numération sanguine et deux tests plasmatiques), et un volet exploratoire utilisant des techniques de cytométrie à hautes dimensions.

Résultats : Nous avons recruté 152 patients adultes atteints de TB pulmonaire sensible ou résistante aux antibiotiques et prélevé des échantillons de sang et de crachats à l'inclusion, après deux mois (T1), et à la fin du traitement (6 à 24 mois). Nous avons observé qu'un nombre de leucocytes élevé et une faible proportion de lymphocytes à l'inclusion, mesurés lors de numérations sanguines de routine, avaient une valeur prédictive de l'échec du traitement. Puis, une combinaison de deux *IFN-γ release assays* (QuantiFERON-TB Gold Plus et *heparin-binding hemagglutinin* ; HBHA) a été évaluée. Chez un sous-groupe de patients dont les cultures étaient restées positives à T1, un schéma clinique commun à l'inclusion a été observé (neutrophilie, lymphopénie, faible indice de masse corporelle, faibles réponses QFT-P IFN-γ) ainsi qu'une faible réponse IFN-γ à HBHA pendant le traitement. Enfin, dans un sous-groupe de 22 patients, la diversité phénotypique des lymphocytes T (LT) dans le sang a été caractérisée par cytométrie de masse et de flux spectral. La comparaison des immuno-profils des patients ayant une culture négative à T1, par rapport à ceux dont les cultures

étaient restées positives, a révélé chez ces derniers une sous-représentation de LT $CD8^+$ cytotoxiques différenciés et une sur-représentation de LT $CD4^+$ naïfs après deux mois de traitement. Ceci suggère un lien entre le stade de différenciation de certaines sous-populations de LT et la clairance mycobactérienne au cours du traitement. Un phénotypage détaillé des sous-populations concernées a permis d'isoler les marqueurs cellulaires permettant la meilleure différenciation des patients en fonction de leur culture de Mtb.

Perspectives : Ces travaux ont documenté la pertinence clinique de deux tests de suivi simples et rapides, adaptés aux zones à forte incidence de TB. Ils ont généré de nouvelles données sur l'immunobiologie des lymphocytes T lors de l'infection tuberculeuse, chez des patients représentatifs des populations les plus touchées. Ceci a permis de faire émerger de nouvelles cibles cellulaires pour le suivi du traitement. Ces résultats pourront avoir des applications directes dans d'autres enjeux majeurs de la prise en charge de la TB, notamment la détection de l'infection tuberculeuse latente, l'identification des patients les plus susceptibles de progresser vers une TB active, et la prédiction des risques de rechute post-traitement.